Lakehead University

Geology and geochemistry of Midcontinent Rift-related igneous rocks

Robert Cundari

A thesis submitted to the Department of Geology in partial fulfillment of the requirements for the Degree Masters of Science

August 2012

Abstract

This study is focussed on the geology and geochemistry of Midcontinent Rift-related intrusive and extrusive rocks present in northern Ontario, Canada. The study focuses on three sections in order to elucidate the geochemical characteristics of Midcontinent Rift-related rocks and investigate geochemical evolutionary signatures through time. The Coubran Lake basalts, the rocks of the Logan Basin and the intrusive rocks of the Nipigon Embayment were all included in this study to provide a sound spatial representation of Midcontinent Rift (MCR) intrusive and extrusive rocks present within Canada.

The Coubran Lake basalts within the Coldwell Complex, have provided new representation of Midcontinent Rift-related volcanism along the northeast shore of Lake Superior. Physical features, including proximity to surrounding syenites, as well as alteration features, suggest that the Coubran Lake basalts represent a pre-existing sequence into which the Coldwell Complex intruded. Geochemical evidence has linked the Coubran Lake basalt to the Two Duck Lake gabbro (TDLG) suggesting the basalts may represent the volcanic expression of the TDLG. Trace element and Nd isotope data suggest the Coubran Lake basalts are akin to the basalt type I composition, linking the unit to the Lower Siemens Creek volcanics, the basal units in the Ely's Peak and Grand Portage areas of the North Shore Volcanics, and to the lower suite of the Osler Group. The geochemical data presented here is consistent with the available paleomagnetic data suggesting the basalts were erupted early in the history of the Midcontinent Rift.

A re-evaluation of 2397 spatially referenced samples with associated whole-rock geochemistry has yielded previously unrecognized variation within the Midcontinent Rift-related Nipigon sills of the Nipigon Embayment. The whole rock major and trace element geochemistry of 796 Nipigon sill samples was re-examined to investigate the origin of the sills. This investigation revealed three distinct Nipigon sill types based on Th/Yb_{pm} ratios and ε_{Nd1100} values: 395 Nipigon type I sill samples (Th/Yb_{pm} = 1.97 to 3.4; $\varepsilon_{Nd(t=1100Ma)}$ = -0.5 to -1.5), 171 Nipigon type II sill samples (Th/Yb_{pm} = 3.4 to 5.0; $\varepsilon_{Nd(t=1100Ma)}$ = -1.5 to -3.0), and 55 Nipigon type III sill samples (Th/Yb_{pm} = 5.0 to 6.5; $\varepsilon_{Nd(t=1100Ma)}$ = -5.0 to -7.0). Spatially, the distribution of the more contaminated Nipigon sill types II and III suggest centres which are inferred to represent zones of more contamination.

Field work in the Logan Basin has delineated the following timing requence between the various units present in the Logan Basin: the Riverdale sill, the Devon Volcanics, the Logan sills, the Pigeon River dykes, the Cloud River dykes, the Mount Mollie dyke and the Crystal Lake gabbro. Geochemical

source characteristics support this timing relationship as the Riverdale sill, the Devon volcanic and the Logan sills are geochemically similar to the ultramafic intrusions of the Nipigon Embayment which were emplaced early in MCR history. The three dyke sets of the Logan Basin have been determined to be emplaced in the following order: Pigeon River dykes, the Cloud River dykes and the Mount Mollie dyke. All three dyke sets display similar source characteristics yet show stronger crustal contamination signatures (i.e., higher Th/Yb_{pm} and more negative $\varepsilon_{Nd(t=1100Ma)}$) through time consistent with each dyke set having spent more time in the magma chamber through the duration of the emplacement sequence.

Based on the plots of Th/Yb_{pm} versus Nb/Th_{pm} and Th/Yb_{pm} versus Nb/Yb_{pm}, previously unrecognized relationships between units have allowed for inferences into the timing and geochemical evolution of the Midcontinent Rift. The progression of magmatism for both the Logan Basin and the Nipigon Embayment suggests that source characteristics became more depleted through time. Evidence of a link between the magmatism of the Logan Basin and the Nipigon Embayment is also indicated by the relationship between the Riverdale sill, the Devon Volcanics and the Logan sills with the mafic and ultramafic units of the Nipigon Embayment (excluding the Nipigon sills). Furthermore, the spatial link between the two magmatically endowed areas is bridged as the dykes of Sibley Peninsula showing evidence to be potential feeders to Nipigon sills.

Acknowledgements

I would like to thank Pete Hollings for his guidance, insight and support through the course of this project. I am grateful for all you have done for me. I would also like to thank Mark Smyk for the opportunities he has granted me over the past two years as well as technical insight and much appreciated revisions. The staff of MNDM deserves a big thank you for assistance with field and GIS work as well as moral support: Gerry White, John Scott, Dorothy Campbell, Neal Bennett and Gen Dorland. Jack Parker and Mike Easton at the Precambriam Geoscience Centre as well as Dave Good and the staff of Stillwater Mining made this project possible, and deserve a debt of gratitude. To Tassia, you have been a mountain of support for me over the past year, acting interested when I dragged on about my findings of the day, even when I know you are not. Thanks for everything. Thank you to Richard Ernst and Simon Jowitt for discussion and insight on the interpretation of the results of this study. To my pals, Steve Flank, Steve Siemieniuk, Jay Seals, Bre Beh, Victoria Stinson and Matt Zago, couldn't have done it without you guys, thanks. Special thanks to my parents, Rock and Denise and my brother Raph. Your encouragement and love kept my spirits and motivation high throughout, thanks always.

Table of contents

List of Figures

List of Tables

CHAPTER 1

INTRODUCTION AND SCOPE

1.1 Background

Recent geochronologic and geochemical studies conducted on the Midcontinent Rift (MCR) as part of the Lake Nipigon Region Geoscience Initiative (Heaman et al., 2007; Hollings et al., 2007a,b,c; Hollings et al., 2010; Hollings et al., 2011) as well as mapping and sampling programs conducted by the Ontario Geological Survey, have uncovered new insights into the geochemical and geodynamic evolution of the MCR. These studies have elucidated the nature of magmatism in the northern part of the MCR and have been used to augment and refine our previous understanding of these magmatic events. A large amount of whole-rock geochemical data has been produced throughout the course of these studies, currently comprising 2400 spatially referenced data points. Details regarding the compilation of this dataset are outlined in Section 2.3. Furthermore, an increase in exploration for the Ni-Cu-PGE deposits associated with Midcontinent Rift-related rocks has provided new insights into the emplacement mechanisms of intrusive rocks emplaced early in MCR history. The majority of this study focuses on the re-evaluation of the existing dataset in an attempt to reconcile relationships between units as well as determine the geochemical evolution of the Midcontinent Rift and comparing it to new data collected in the Logan Basin.

1.2 Objective

The objectives of this thesis are subdivided into three sections. Firstly, to provide a geochemical profile of the Coubran Lake basalts, a Midcontinent Rift-related volcanic sequence located in the centre of the Coldwell Complex, northwest of Marathon, Ontario. This work was undertaken to complement a paleomagnetic study carried out at Michigan Technological University (Kulakov, in progress). The goal is to characterize the geological, petrographical, and geochemical characteristics of the unit, as well as put the unit into context with the Coldwell Complex and the MCR. Secondly, a field-based study was carried out to determine a timing relationship of MCR-related intrusive units located within the Logan Basin south of Thunder Bay, Ontario. Recent geochemical, geochronological and paleomagnetic work in the study area (Hollings et al., 2010, Hollings et al., 2011) has revealed enigmatic results suggesting that magmatism was relatively long-lived (~60 m.y.). Furthermore, geochemical results show that units emplaced during this period display indistinguishable geochemical characteristics and arguable paleomagnetic polarities. Field work was required to determine cross-cutting relationships so as to pin-point a relative timing relationship for the study area. From field relationships, inferences into the geochemical characteristics of each unit were made. Lastly, a publically available, geochemical database

compriseing 2400 spatially referenced data points was re-evaluated to detect subtle variations within units, as well as to make inferences into the relationship between units and into the magmatic evolution of the Nipigon Embayment.

1.3 Structure of Thesis

The thesis is organized into seven chapters consisting of: 1) introduction and scope, 2) methodology, 3) regional geology, 4) Coubran Lake basalts, 5) petrogenesis and crustal contamination of the Nipigon sills, 6) Logan Basin emplacement sequence and 7) geochemical implications for the magmatic evolution of the Midcontinent Rift and conclusions. The methodology chapter outlines the location of the study areas as well as access and previous work, most notably that associated with the Lake Nipigon Regional Geoscience Initiative (LNRGI). Compilation of the existing geochemical database as well as sampling procedures and analytical techniques are also included in this chapter. The regional geology chapter reviews the current literature regarding Midcontinent rift system and its associated intrusive and extrusive igneous rocks. In addition, the Archean basement lithologies and Paleoproterozoic sedimentary cover are summarized. The Coubran Lake basalt chapter includes the results and discussion of the Coubran Lake basalts. Described within are the geological, petrographical and geochemical characteristics of the unit as well as inferences into its relationship with the Coldwell Complex and the Midcontinent Rift system. The chapter on the petrogenesis and crustal contamination of the Nipigon sills focuses on the variable crustal contamination signatures detected in Nipigon sills and makes inferences into their source characteristics and emplacement histories. The Logan basin chapter presents the results of a reconnaissance field initiative to evaluate a timing relationship of Midcontinent rift-related intrusive units located within the Logan Basin, most notably, the dyke sets of variable orientation. Furthermore, it attempts to reconcile some of the current geochemical issues surrounding the dyke sets. The chapter regarding the Midcontinent Rift geochemistry and implications for the magmatic evolution of the Midcontinent Rift outlines new discrimination parameters useful in delineating subtle geochemical variations within and between units. Using new methodology combined with the current understanding of the Midcontinent Rift, new relationships are proposed between units and inferences into the magmatic evolution of the Nipigon Embayment. This final chapter summarizes the results of the three-fold study and discusses implications for the Midcontinent Rift system, as well as suggesting directions for future work.

CHAPTER 2
METHOLODOGY

2.1 Location, Previous Work and Access

2.1.1 Overview

Midcontinent Rift-related rocks included within this study are found within three areas present along the north shore of Lake Superior; the Coldwell Complex, the Nipigon Embayment and the Logan Basin. Reference will be made to units present within other areas around Lake Superior (i.e. Duluth complex, the Northshore Volcanics, the Siemens Creek Volcanics), but as field work, data acquisition and subsequent data analysis wwere carried out within Canada, the detailed locations of each study area are provided below.

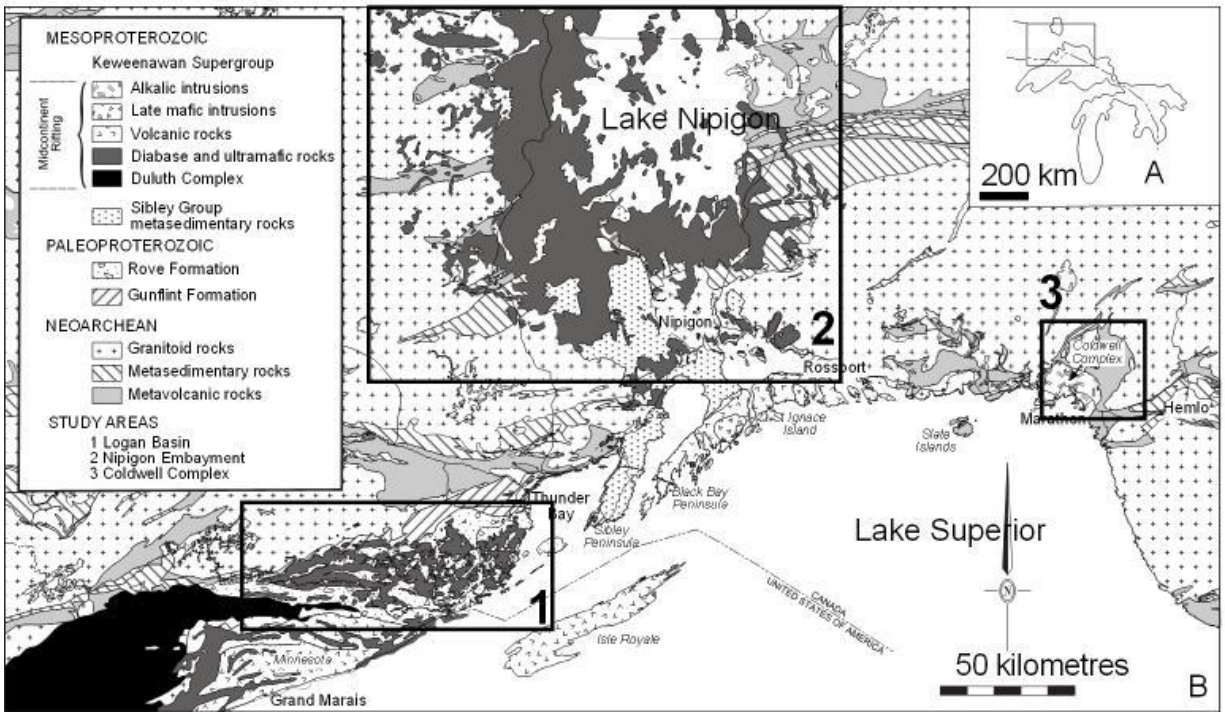

Figure 2.1: (A) Map of the upper Great Lake region showing the location of the study area. (B) Regional geology map showing the three study areas; 1= Logan Basin, 2 = Nipigon Embayment and 3 = Coldwell Complex. Modified after Pye and Fenwick (1965) and Carter et al. (1973).

2.1.2 The Coldwell Complex

The Coldwell Alkalic Intrusive Complex (also termed the Port Coldwell Complex) is located east of Thunder Bay, Ontario on the north shore of Lake Superior near Marathon, Ontario (Fig. 2.1). The ~28 km wide (~580 km^2) complex is bounded by the Pic River to the east and Dead Horse Creek to the west with the town of Marathon, Ontario situated within the eastern part of the complex. The area is characterized by rugged topography defined by large syenite hills and deep-incised fault scars. Kerr (1910) produced the first report on the nepheline syenites located with the southern part of the Coldwell complex. Mapping by Puskas (1967) followed by compilation work by Currie (1980) provided detailed accounts of the geology of the complex and inferences into its genesis. Further work by Mitchell and Platt (1977, 1978) provided petrological and geochronological evidence that the complex developed from episodic magmatism defined by three centres. Mapping by Walker et al. (1993) confirmed these findings as well as provided a detailed account of the spatial position of units.

Access is possible by Highway 17 along the southern margin of the complex with a network of logging and exploration roads leading to the northern parts of the complex. The Coubran basalts lie 5.9 km north of Highway 17 and were accessed by ATV. Stillwater Canada Incorporated exposed a 350 m long, 3 to 5 m wide area of the Coubran Lake basalts during overburden stripping. Detailed sampling and descriptions of the unit were carried out totalling 20 samples taken every metre so as to investigate the characteristics of the multiple flows that comprise the unit.

2.1.3 The Nipigon Embayment

The Nipigon Embayment is centered around Lake Nipigon (Fig. 2.1) located north of the town of Nipigon, Ontario, approximately 100 km northeast of Thunder Bay, Ontario. The area is accessible by boat as well as Highway 527 to the west, Highway 11/17 to the south and east and an extensive network of logging and exploration roads. Bell (1870) of the Geological Survey of Canada conducted the first geological survey of the Lake Nipigon area. Further mapping was carried out by Coates (1972) and Sutcliffe (1981, 1982, 1986) and Sutcliffe and Greenwood (1985a, 1985b, 1985c). Interest in Ni-Cu-PGE mineralization associated with Proterozoic intrusions within the Nipigon Embayment prompted the implementation of the Lake Nipigon Regional Geoscience Initiative (LNRGI). Mapping programs conducted by the Ontario Geological survey as part of the LNRGI were carried out between 2003 and 2005 at a scale of 1:50 000. Detailed accounts of the geology of the northern (Hart and MacDonald, 2003; MacDonald et al., 2004a, 2004b; MacDonald and Tremblay, 2004; MacDonald, 2004) west-central (MacDonald et al., 2004a; MacDonald et al., 2005a, 2005b; 2005c; 2005d and MacDonald and Tremblay,

2005) southwestern Nipigon Embayment (Hart and MacDonald, 2003; Hart and Préfontaine, 2004a, 2004b; Hart and Magyarosi, 2004a, 2004b), southern (Hart, 2005a, 2005b; Hart and Tolson, 2005; Hart et al., 2005) areas of the Nipigon Embayment were carried out during this period. Findings associated with these studies are summarized in Hart and MacDonald (2007). As units located within the Nipigon Embayment were extensively sampled through these programs, further field work was not warranted aside from select localities around Silver Harbour and Pillar Lake. Compilation work undertaken on the existing data sets is described in detail in section 2.3.

2.1.4 The Logan Basin

The Logan Basin is located southwest of Thunder Bay, Ontario (Fig. 2.1) and is bound by the Pigeon River (i.e., United States border) to the south and Highway 11/17 to the north. It is located within the Southern Province of the Canadian Shield, an area termed the Logan Basin by North (2000). The Logan basin is characterized by large diabase sill-capped mesas and ridges and deep, incised valleys that cut into the underlying Paleoproterozoic Rove Formation of the Animikie Group. Archean granitoid rocks of the Quetico and Wawa-Abitibi Subprovinces underlie the Rove Formation and crop out northwest of the Logan Basin. Tanton (1936a,b) was the first to map and describe intrusive units of the Logan basin in a report published by the Geological Survey on Canada. Further work by the Ontario Department of Mines (Guel, 1970, 1973) produced maps from field work and air photo interpretation delineating Mesoproterozoic intrusive units of the Logan basin. In an Ontario Geological Survey Summary of Field Work, Smith and Sutcliffe (1989) provided detailed physical and petrographical account of individual mafic intrusive units present within the Logan Basin.

The majority of the mainland area is accessible by way of Highways 61, 593, 595, 608, 588 and smaller logging roads. Reconnaissance traverses were made along ridges of interest to investigate cross-cutting relationships between intrusive units, in particular those present towards the southeast corner of the Logan Basin. Work was also performed by boat along the Lake Superior shoreline at Finger Point and McKeller Point as well as on Victoria, Jarvis, Spar and Thomson islands. Sampling by helicopter was necessary to access localities that could not be reached on foot, in particular, detailed sampling of the Arrow River dyke as well as the Cloud Lake float east of Cloud Lake.

2.2 Analytical Procedures

2.2.1 Whole-rock geochemistry

Samples were cut, crushed and milled to ~200 mesh in an agate ring mill so as to reduce the risk of contamination of trace elements (Jenner, 1996). Tools and all working surfaces were cleaned with acetone between each sample. Samples were analyzed for major elements by X-ray fluorescence (XRF) and for trace and rare earth elements by inductively coupled plasma mass spectrometry (ICP–MS) at the Geoscience Laboratories (Geo Labs) of the Ministry of Northern Development and Mines in Sudbury, Ontario. Selected trace elements (e.g., Zr and Y) were analyzed by XRF using a pressed pellet to allow comparison with data generated by ICP–MS. Totals for major element oxide data were generally 100 ± 2% and have been recalculated to a 100% volatile-free basis. Detection limits for major elements are 0.01 weight % and relative standard deviations of duplicate analyses are within 5%. Trace elements, including the REE and HFSE analyzed at the Geoscience Laboratories were completed on a Perkin-Elmer Elan 9000 ICP–MS following a variation on the protocol described by Burnham and Schweyer (2004) and Tomlinson et al. (1998). Twenty four trace elements were determined using a 200 mg aliquots of powder digested by a two stage procedure involving an initial decomposition in a closed beaker by a mixture of HF with lesser HCl and $HClO_4$ followed by a second mixture of dilute HCl and $HClO_4$ as described by Burnham et al. (2002). Detection limits for some critical elements, defined as 3σ of the procedural blank, are as follows: Th (0.032 ppm), Nb (0.044 ppm), Hf (0.085 ppm), Zr (3.2 ppm), La (0.048 ppm) and Ce (0.08 ppm) (Burnham and Schweyer, 2004). All analyses performed during the course of this study utilized standards, duplicate samples and blanks, both in-house as part of the normal procedures of the analytical facilities, as well as standards submitted for replicate analyses. Chondrite-normalized (e.g., La/Sm_n) and primitive mantle-normalized ratios (e.g., Th/Nb_{pm}) are calculated from the values of Sun and McDonough (1989) as are the primitive mantle-normalized diagrams.

2.2.2 Isotope analysis

Samples were analysed for radiogenic isotopes (Sr and Sm-Nd) at the Isotope Geochemistry and Geochronology Research Centre at Carleton University, Ottawa, Ontario. Sr and REE were separated using Dowex AG50-X8 cation resin. Sr procedural blanks are < 250 picograms. Sr samples were loaded onto single Ta filaments with H_3PO_4 for analysis. Sr isotope ratios are normalised to $^{88}Sr/^{86}Sr = 8.375$ and the NIST SRM987 standard was used: $^{87}Sr/^{86}Sr = 0.710234 \pm 14$, n=22. Sm and Nd were separated on Eichrom Ln Resin chromatographic columns containing Teflon powder coated with HDEHP (di(2-ethylhexyl)) orthophosphoric acid (Richard et al., 1976). Total procedural blanks for Nd are < 50 picograms, and < 6 picograms for Sm. Samples are spiked with a mixed ^{148}Nd-^{149}Sm spike prior to

dissolution. Concentrations are precise to ± 1%, but $^{147}Sm/^{144}Nd$ ratios are reproducible to 0.5%. Sm and Nd samples are loaded with H_3PO_4 on one side of a Re double filament for analysis. Isotope ratios are normalized to $^{146}Nd/^{144}Nd = 0.72190$. Analyses of the USGS standard BCR-1 yielded Nd = 29.02 ppm, Sm = 6.68 ppm, and $^{146}Nd/^{144}Nd = 0.512668 \pm 20$ (n=4). The international La Jolla standard produced: $^{143}Nd/^{144}Nd = 0.511847 \pm 7$, n = 26 (Feb 2005 – June 2007) and an internal lab standard = 0.511818 ± 8, n = 28 (Feb 2005-June 2007) and 0.511819 ± 10 n = 94 (Feb 2005 – Aug 2009).

2.3 Data Acquisition

A significant portion of this study is focused on the re-evaluation of the existing data set for Midcontinent rift-related igneous rocks. Many studies have been carried out by previous authors to delineate and characterized Midcontinent rift-related intrusive and extrusive rocks. All publically available was compiled in this study for geochemical re-evaluation and spatial presentation totalling 2397 samples (Fig. 2.2). Only data that could be spatially referenced was included in this compilation. A brief summary of these publications is provided below.

Table 2.1: Summary of Miscellaneous Releases of Data (MRD's) used in this study.

Name	Units Included	Reference
MRD 114	Osler Group, Mamainse Point Formation, Nipigon Embayment intrusives	Hart (2002)
MRD 132	Nipigon sills, Sibley Group, Jackfish sills, English Bay Complex, Inspiration sill, Pillar Lake volcanics, Archean intrusive, metavolcanic and metasedimentary rocks	MacDonald and Tremblay (2004)
MRD 133	Nipigon sills, Disraeli Intrusion, Seagull Intrusion, , Sibley Group, Quetico Subprovince Archean rocks	Hart and Magyarosi (2004a)
MRD 146	Nipigon sills, Sibley Group, Jackfish sill, Inspiration sill, Pillar Lake volcanics, Archean intrusive, metavolcanic and metasedimentary rocks	MacDonald and Tremblay (2005)
MRD 147	Nipigon sills, Hele Intrusion, Disraeli Intrusion, Seagull Intrusion, Sibley Group, Quetico Subprovince Archean rocks	Hart (2005a)
MRD 190	Nipigon sills, McIntyre sill, Shillabeer sill, Seagull intrusion, Kitto intrusion, Sibley Group, Rove Formation, Quetico Subprovince Archean rocks	Fralick et al. (2006b)
MRD 194	Marathon, Molson and Abitibi dyke swarms	Ernst et al. (2006)
MRD 261-REV	Nipigon sills, Logan sills, Pigeon River dykes, Cloud River dykes, Mount Mollie dyke, Current Lake Intrusive Complex, Gunflint formation sedimentary and volcanic rocks, Rove Formation, Moss Lake intrusion, Devon Volcanics, Riverdale sill	Hollings et al. (2011a)

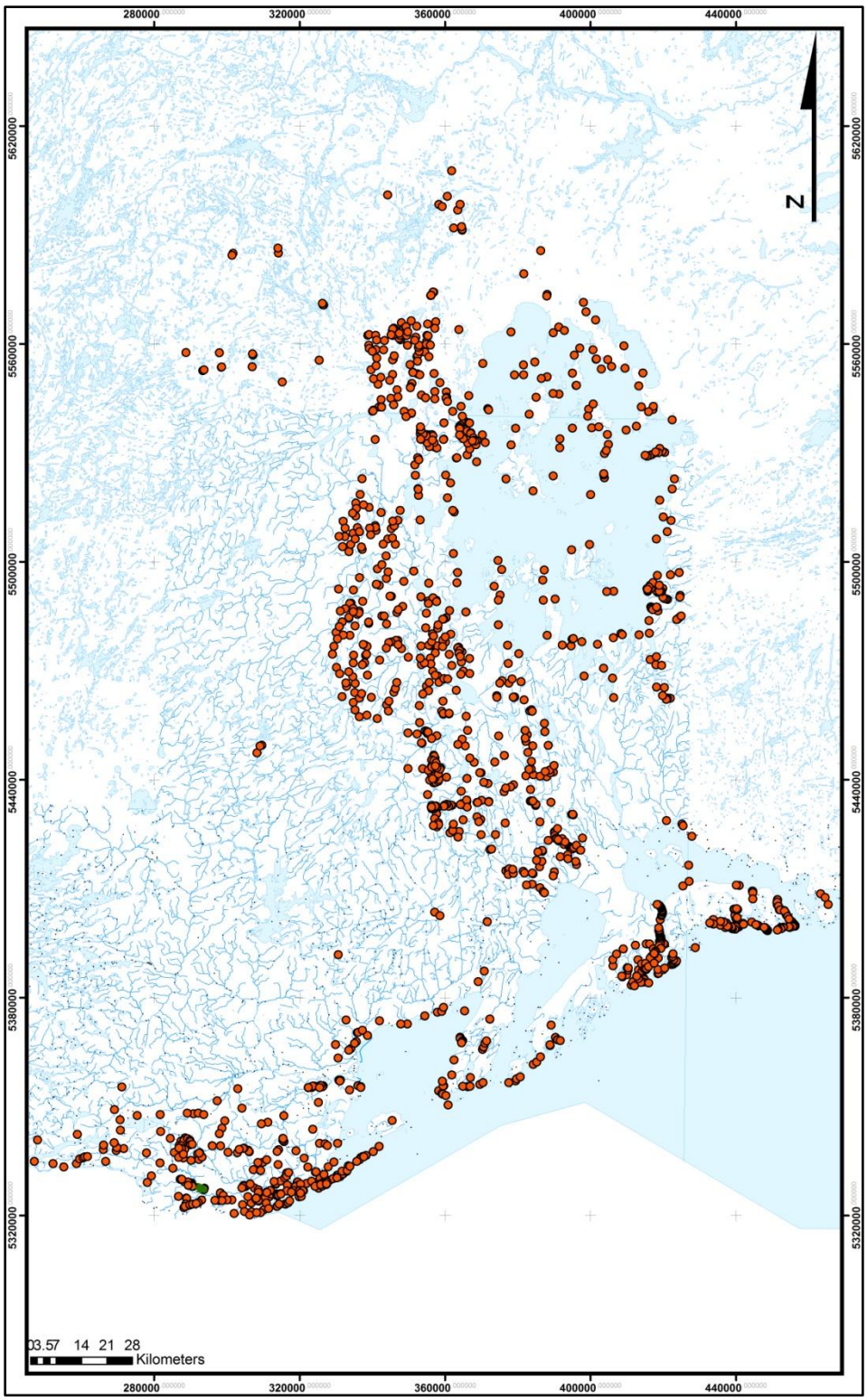

Figure 2.2: Map showing sample locations used in the Nipigon and Logan portions of this study.

Miscellaneous Release of Data 114 (Hart, 2002) combines geochemical data sampled for the accompanying report with the ERLIS geochemical database and open file reports including Sutcliffe (1986), Smith and Sutcliffe (1987), Lightfoot et al. (1989), Lightfoot (1995), Hill (1998), Lightfoot et al. (1999), and Hart et al. (2002). New analytical data presented in MRD 114 is concentrated in the Osler group volcanic rocks on Simpson Island and St. Ignace islands and the Black Bay Peninsula, as well as islands in Lake Superior in Crooks Township, south of Thunder Bay. Data taken from previous studies include those from the aforementioned studies as well as in intrusive rocks of the Nipigon Embayment and the volcanic rocks of the Mamainse Point Formation.

Miscellaneous Release of Data 132 (MacDonald and Tremblay, 2004) contains data gathered from the 2003 mapping program located in the northwest Nipigon Embayment as part of the Lake Nipigon Regional Geoscience Initiative (LNRGI). This data release accompanied Open File Report 6136 (MacDonald, 2004). Units included within this study are Nipigon sills, Sibley Group sedimentary rocks, the Jackfish sill, English Bay Complex, the Inspiration sill, Pillar Lake Volcanics and Archean intrusive, metavolcanic and metasedimentary rocks.

Miscellaneous Release of Data 133 (Hart and Magyarosi, 2004a) contains data gathered from mapping in the northern Black Stugeon River to Disraeli Lake area in the southwest Nipigon Embayment as part of the Lake Nipigon Regional Geoscience Initiative (LNRGI) in 2003. This data release accompanied Open File Report 6138 (Hart and Magyarosi, 2004b). Units included within this study are Nipigon sills, the Disraeli Intrusion, the Seagull Intrusion, Sibley Group sedimentary rocks and Archean rocks of the Quetico Subprovince.

Miscellaneous Release of Data 146 (MacDonald and Tremblay, 2005) contains data gathered from the 2004 mapping program in the west-central Nipigon Embayment as part of the Lake Nipigon Regional Geoscience Initiative (LNRGI). This data release accompanied Open File Report 6164 (MacDonald et al., 2005a). Units included within this study are Nipigon sills, Sibley Group sedimentary rocks, the Jackfish sill, the Inspiration sill, Pillar Lake Volcanics and Archean intrusive, metavolcanic and metasedimentary rocks.

Miscellaneous Release of Data 147 (Hart, 2005a) contains data gathered from mapping in the southern Black Sturgeon River area to the Seagull Lake area in the southwest Nipigon Embayment as part of the Lake Nipigon Regional Geoscience Initiative (LNRGI) in 2003. This data release accompanied Open File Report 6165 (Hart, 2005b). Units included within this study are Nipigon sills, the Hele intrusion, the

Disraeli intrusion, the Seagull intrusion, Sibley Group sedimentary rocks and Archean rocks of the Quetico Subprovince.

Miscellaneous Release of Data 190 (Fralick et al., 2006b) comprises the data released in tables and/or appendices in Open File Report 6174 (Rogala et al., 2005), Open File Report 6175 (Richardson et al., 2005) and Open File Report 6176 (Kissin et al., 2006). Units included within this release include Nipigon sills, the McIntyre sill, the Shillabeer sill, the Seagull intrusion, the Kitto intrusion, Sibley Group sedimentary rocks, Rove Formation sedimentary rocks and Archean rocks of the Quetico Subprovince,

Miscellaneous Release of Data 194 contains data gathered from dykes in the region west of the Nipigon Embayment (Ernst et al., 2006). This study yielded no dykes that could be directly linked to the Keweenawan Midcontinent Rift but some may be correlative to Paleoproterozoic Marathon and Molson swarms as well as the 1140 Ma Abitibi dyke (Ernst et al., 2006).

Miscellaneous Release of Data 261-REV (Hollings et al., 2011a) includes samples collected from Midcontinent Rift-related mafic rocks on Black Bay and Sibley peninsulas and around Thunder Bay, Ontario. Units included within this study are Nipigon sills, Logan sills, Pigeon River dykes, Cloud River dykes, the Mount Mollie dyke, the Current Lake Intrusive Complex, Gunflint Formation sedimentary and volcanic rocks, Rove Formation sedimentary rocks, the Moss Lake intrusion as well as from the newly recognized Devon Volcanics and the Riverdale sill.

Geochemical data for the intrusive rocks of the Coldwell Complex was also included in the compilation. Data was gathered from Good (1993) and includes samples from the Two Duck Lake Gabbro and the Geordie Lake Gabbro.

CHAPTER 3
REGIONAL GEOLOGY

3.1 Archean Superior Province

Rocks associated with the Mesoproterozoic Midcontinent Rift are underlain by Archean basement rocks of the Superior Province. The Superior Province represents 23% of the planet's exposed Archean crust (Thurston, 1991). The approximately 3.0 to 2.7 Ga Archean craton has been interpreted as the result of accretion of east-west trending belts during the Kenoran Orogeny whose effects extend to the far north (Percival, 2003). These belts or subprovinces are comprised of one of three assemblages: volcano-plutonic (granite-greenstone), metasedimentary, gneissic (plutonic), and high-grade gneiss, all of which have been metamorphosed to greenschist-granulite facies (Card and Ciesielski, 1986). The Superior Province is bounded by the Trans-Hudson Orogeny to the north and west, the New Quebec orogeny to the northeast, the Grenville orogeny to the southeast and the Penokean Orogeny to the south (Hoffman, 1989). Stott et al. (2010) most recently subdivided the Superior Province by building on the work of Card and Ciesielsk (1986) and adding the results of regional mapping and compilation programs as well as results from Lithoprobe and Natmap programs (Percival et al., 2006; White et al., 2003; Simard, 2008).

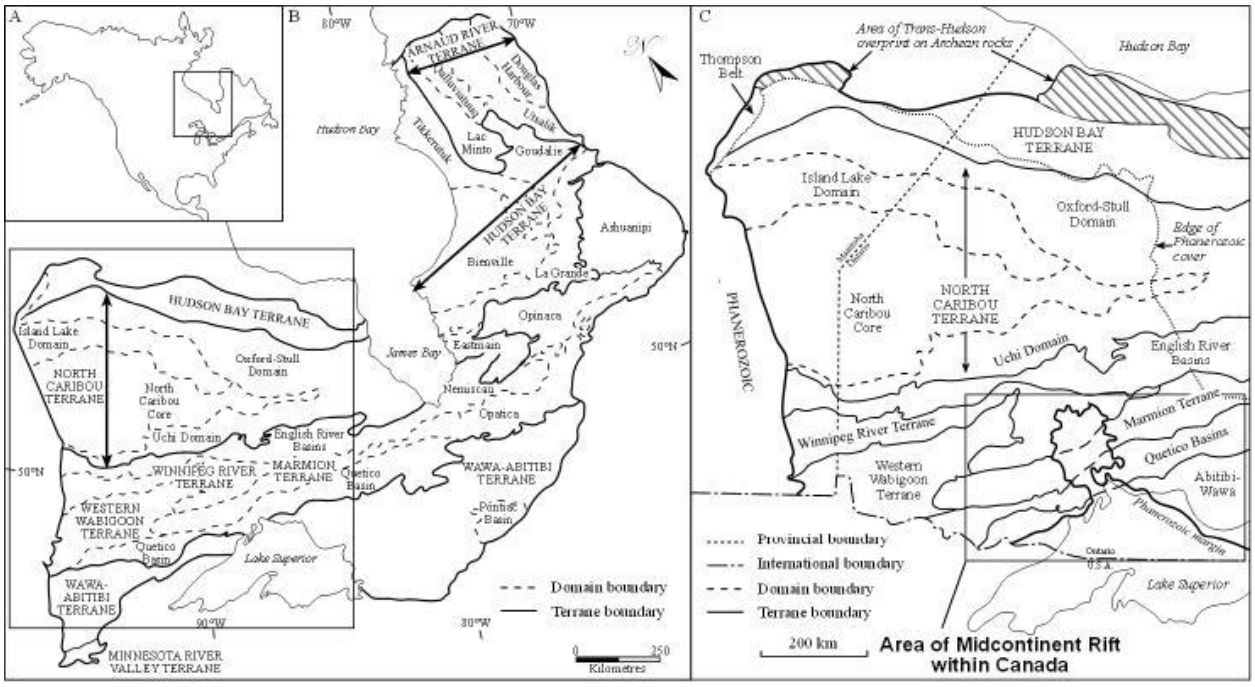

Figure 3.1: (A) Location of the Superior Province in Canada. (B) Generalized geological map of the Superior Province showing the location of northwestern Ontario. (C) Location of the Mesoproterozoic Midcontinent Rift within the Superior Province. Modified after Stott et al. (2010).

3.1.1 Wawa Subprovince

The Wawa Subprovince represents a supracrustal sequence of dominantly granitoid plutons with lesser greenstone belts comprising 20 to 30% of the subprovince (Williams et al., 1991). The subprovince is structurally bound to the north by overlying metasedimentary rocks of the Quetico Subprovince and to the south by the Great Lakes Tectonic Zone, which marks the boundary between the Minnesota River Valley gneiss terrane and the Wawa Subprovince (Fig. 3.1; Williams et al., 1991). To the east, the boundary is marked by the Montreal River Fault (Williams et al., 1991) but it is now widely accepted that the Wawa and Abitibi subprovinces are correlatable across the Kapuskasing uplift or structural zone (e.g. Percival, 2007).

Volcanism within the Wawa Subprovince began as early as 2.89 to 2.88 Ga with the Hawk assemblage followed by the 2.775 Ga Hemlo-Black River, the 2.745 Ga Wawa and the 2.72 Ga Greenwater and Manitouwadge assemblages (Williams et al., 1991; Percival, 2007). Late stage volcanism synchronous with deformation began at 2.689 Ga followed by the sanukitoid magmatism at 2.68 to 2.65 Ga (Percival, 2007). The Wawa Subprovince was sutured to the Quetico accretionary prism to the north, with pull-apart basins and associated late-stage alkaline (sanukitoid) magmatism occurring as a result of sustained compression after subprovince amalgamation (Williams et al., 1991).

3.1.2 Quetico Subprovince

The Quetico Subprovince, also termed the Quetico Basin, spans more than 1000 km from Minnesota in the southwest, through Ontario and into Quebec where it is referred to as the Opatica Subprovince (Stott et al., 2010). The Quetico Subprovince is dominated by supracrustal sedimentary sequences of mainly turbiditic wacke and pelite metamorphosed to schist, paragneiss and migmatite with abundant S-type granites and pegmatites derived from the anatexis of sedimentary rocks (Card and Ciesielski, 1986). The Quetico Subprovince is bordered to the north by the Marmion Terrane and the Winnipeg River Terrane and to the south by the Wawa Subprovince in Ontario and the Abitibi Subprovince in Quebec (Fig. 3.1). The boundaries between the Quetico Subprovince and the surrounding subprovinces are mapped as steeply dipping surfaces where a stark contrast in rock type is observed (Williams, 1990).

The sedimentary structure of the Quetico Subprovince is represented by wackes deposited in a submarine basin of considerable extent with rocks exhibiting sedimentary features akin to unstructured turbidite fans (Fralick et al., 2006a). No evidence of basement deposits has been reported (Williams, 1990). Kuzmich (2012) characterized the Dog Lake Granite chain composed of six magnetite-bearing, ovoid I-type granitic intrusions within the Quetico Basin. He concluded that these intrusions were derived from mafic

melts which underplated the Archean lithosphere where they evolved into granitic melts through fractionation. Timing of deposition of the Quetico Subprovince is constrained by the youngest zircon within the sediments at 2.698 Ga, and the oldest intrusion at 2.688 Ga (Davis et al., 1990).

3.1.3 Winnipeg River Terrane

The Winnipeg River Terrane is characterized as a plutonic domain located to the north and east of the western Wabigoon Subprovince (Percival et al., 2006). It is largely composed of two main elements (i) a >500km long terrane composed of Neoarchean plutonic rocks and (ii) a neoarchean plutonic domain formerly referred to as the central Wabigoon Subprovince. The Winnipeg River Subprovince is bordered to the north by the English River Basin, to the west by the Western Wabigoon Terrane and the south and east by the Marmion Terrane (Fig. 3.1).

The oldest rocks of the Winnipeg River Terrane are 3.32-3.04 tonalites with some showing older Nd isotopic signatures as well as zircon inheritance (Percival et al., 2006). Significant tonalite-granodiorite magmatism occurred at 2.716-2.705 Ga with later granitoid units emplaced at 2.70-2.69 Ga, all of which are now grouped into the Winnipeg River terrane (Percival et al., 2006). The eastern portion of the Winnipeg River Terrane is characterized by small, 3.075-2.703 Ga greenstone belts cut by 3.075-2.680 Ga granitoids (Davis et al., 1988). Some of the oldest rocks within this portion of the terrane have ε_{Nd} values of -1 to +1 which may have been derived from an older crustal source (Tomlinson et al., 2004). Extensive overprinting by Neoarchean magmatism and deformation, including five distinct generations of structures, make inferenences into the Mesoarchean history of the terrane difficult (Percival et al., 2006).

3.1.4 Marmion Terrane

The Marmion Terrane was formerly included as part of the south-central Wabigoon Subprovince but is now characterized as consisting of 3.01-2.999 Ga tonalite basement upon which 2.99-2.78 greenstone belts formed (Fig. 3.1; Pervical et al., 2006). The Marmion Terrane appears to be younger than the Winnipeg River terrane to the north and is interpreted to have either accreted to the Winnipeg River Terrane at ~2.92 Ga (Tomlinson et al., 2004) or formed by a magmatic addition to the Winnipeg River Terrane boundary at 3.0 Ga (Percival et al., 2006). Both the Marmion Terrane and the Winnipeg River Terrane are characterized by steeply dipping structures at surface a subhorizontal reflectivity at depth (Percival et al., 2006). Interpretations from Lithoprobe Line 1 show several 10 km scale, gently north dipping crustal panels as well as a high-velocity layer of mafic composition that terminates in the lower crust interpreted to be a subcreted fragment of oceanic crust (White et al., 2003).

3.2 Paleo-Mesoproterozoic Rocks and Sedimentary Basins

3.2.1 The Penokean Orogeny and Basin Formation

The Penokean Orogeny has been described as a period of mountain building in which an oceanic arc, the Pembine-Wausau terrane, collided with the Superior Craton from ~1880 Ma to ~1830 Ma (Schulz and Cannon, 2007). Development of the Animikie Basin is accepted to be the consequence of southward dipping subduction during the Penokean Orogeny, but two theories have been proposed as to the timing and subsequent emplacement of units. Many authors, including Morey and Southwick (1995), interpret the basin to be a foreland assemblage due to load-driven subsidence resulting from Penokean thrusting. The oldest volcanic rocks in the Wisconsin magmatic terrane are calc-alkaline and tholeiitic back-arc basin or arc-related basalts dated from 1860 Ma to 1889 Ma, which were thought to have collided with the Superior craton at ~1860 Ma (Sims et al., 1989). Based on dating relationships, the Animikie Basin must have been formed by way of back-arc extension, as a foreland setting would have developed much later in the orogeny. Hemming et al. (1995) and Kissin and Fralick (1994) proposed a theory of basin development due to extensionally driven subsidence in a back-arc basin environment. Fralick et al. (2002) dated volcaniclastic zircons from the Gunflint Formation at 1878.3±1.3 Ma which supports a back-arc extension model rather than a foreland setting. The Animikie basin comes from parts of Ontario, Minnesota, Wisconsin and Michigan. Deposition within this basin resulted in the formation of the Gunflint and overlying Rove Formations which together comprise the Animikie Group.

3.2.2 Gunflint Formation

The Gunflint Formation is a chemical-clastic sedimentary assemblage deposited on a south-facing shelf during a transgressive-regressive-transgressive cycle (Pufahl and Fralick, 2000). Due to cycling modes of deposition, the unit can be divided into two members. The lower member contains strand-proximal stomatolite bioherms, lagoonal ribbon chert-carbonates and offshore grainstone deposited by both tidal and storm activity, eroded from siliceous, iron oxide, and iron carbonate mud layers (Fralick and Barrett, 1995). The upper layer contains similar lithofacies to the lower layer with the addition of black shales and volcanic ash beds. In Ontario, the Gunflint Formation lies unconformably on Archean basement and is approximately 130 m thick, cropping out primarily around Thunder Bay

3.2.3 Rove Formation

Within the area of study, the Animikie group is represented by the Rove Formation. The rocks of the Rove Formation overlie the Gunflint Formation with a discontinuity marked by an ejecta layer from the Sudbury impact at 1850 Ma (Addison et al., 2005). The unit has an approximate thickness of 500m to

600m, thickens towards the south, and is primarily flat lying or gently dipping to the southeast (Smyk and Hollings, 2007). Amurawaiye (2001) described the unit as having been deposited in a submarine ramp system with low and high-density turbidity currents moving coarser sediments into the deeper parts of the basin. Amurawaiye (2001) also states that 70% of the Rove Formation consists of organic shale whose hydrocarbon content has been degraded over time.

The rocks of the Rove Formation are divided into two zones. The lower zone is correlative with the Virginia Formation in Minnesota and consists of 100m to 150m of alternating shale-siltstone and black pyritiferous shale, which Maric and Fralick (2005) describe as being indicative of fluctuations in sea level. Maric and Fralick (2005) describe the upper zone as a submarine fan system consisting of 100m of black shale and fine-grained sandstone coarsening upwards into 400m of dominantly medium-grained sandstone in stacked parasequences. Heaman and Easton (2006) reported a U-Pb detrital zircon age of 1790 Ma from a sandstone sample from the upper submarine fan zone.

3.2.4 The Sibley Group

The Mesoproterozoic Sibley group crops out in a ~175 km wide by 400 km long ovoid under Lake Superior extending north to the south and west of Lake Nipigon with a minimum thickness of 950 m inferred from drillcore (Rogala et al., 2007). The group is a predominantly flat-lying red-bed sequence which can be broken up into five lithological units; Pass Lake Formation, Rossport Formation, Kama Hill Formation, Outan Island Formation and the Nipigon Bay Formation.

The Pass Lake Formation consists of two members; the basal Loon Lake Member conglomerates and the overlying Fork Bay Member sandstones. The basal conglomerates are typically only a few metres thick with a maximum 15 m thickness and topographic lows within the basement rock. Conglomerates of the Loon Lake Member begin the large-scale, thinning-upward succession of the group and are dominantly composed of Archean basement material (Rogala et al., 2007). Sandstones of the Fork Bay Member are dominantly medium-grained, forming a large-scale, fining- and thinning-upward succession grading into the overlying siltstones of the Rossport Formation (Rogala et al., 2007).

The Rossport Formation consists of three members and has a maximum thickness of 100 m. Upsection, theses members include; the Channel Island Member dominated by cyclic siltstones-dolostones and –sandstones, the Middlebrun Bay Member comprises of stromatolite bearing chert-carbonate and the Fire Hill Member dominantly comprised of massive- to finely-laminated red siltstones to silty shales often underlain by a basal conglomerate (Rogala et al., 2007).

Wave-rippled and hummocky cross-stratified sandstones and mudstones of the ~50 m thick Kama Hill formation abruptly overlie the upper Fire Hill Member of the Rossport Formation (Rogala et al., 2007). Paleocurrent indicators suggest material comprising the Kama Hill Formation was derived from the south to southeast (Cheadle, 1986) with the unit being thickest in the central portion and thinning to toward the east. The Kama Hill Formation is dominated by horizontally laminated siltstone and fine-grained sandstones with interbeds of mudstone and ripple-laminated, fine-grained sandstone (Rogala et al., 2007). The Outan Island Formation consists of two members; the lower Lyon Member including and coarsening- and thickening-upward sandstone succession overlain by siltstone and ripple laminated sandstone and the Hele Member consisting of a fining-and thinning-upward sandstone succession overlain by mudcracked siltstone (Rogala et al., 2007). Erosively overlying the Outan Island Formation is the ~450m thick Nipigon Bay Formation comprising nearly half of the Sibley group. The Nipigon Bay succession is dominated by large-scale, planar cross-stratified sandstones indicative of an aeolian dune environment (Rogala et al., 2007).

Franklin et al. (1980) originally inferred the Sibley basin to be a result of subsidence caused from the ~1.1 Ga Midcontinent Rift System. Age constraints on the Sibley Group based on U-Pb geochronology of detrital zircons and stratigraphy are ~1770 Ma (Pass Lake Formation), ~1440 Ma (Kama Hill, Outan Island and Nipigon Bay Formations; Rogala et al., 2007) as well as the basal conglomerate of the Osler group erosively overlying the Nipigon Bay Formation giving a lower age constraint of 1109 Ma (Davis and Sutcliffe, 1985). Cheadle (1986) noted intercalation of English Bay Complex Rhyolites with Sibley Sandstones which together with geochronology, debunks the Sibley Group as being of MCR affinity and lends the notion that the succession was in fact 200-400 m.y. older than the MCR. The current model holds that the Sibley Group was deposited in a half graben controlled basin inferred to be a product of large-scale thermal subsidence following the ~1550 Ma thermal plume event which produced the English Bay Complex (Heaman et al., 2007).

3.2.5 Geon 15 Magmatism

Meso- to Paleoproterozoic magmatism in the northwest corner of the Nipigon Embayment is manifested by three units; the Pillar Lake Volcanic suite (see section 3.4.5), the Badwater intrusion and the English Bay Complex. The ~8 km in diameter, multiphase Badwater intrusion is composed of aphibolite, gabbro to diorite, syenite to monzonite, and quartz monzonite, with minor melagabbro to pyroxenite (MacDonald, 2004). High precision U-Pb dating shows the Badwater intrusion was emplaced between 1589.7 ± 1.1 Ma (gabbro) and 1590.7 0.8 ± Ma (syenite) (Hollings et al. 2004; Heaman et al., 2007).

The English Bay Complex was first mapped by Sutcliffe and Greenwood (1982, 1985a) with a more extensive map produced by MacDonald (2004). The 80 km^2 complex is an anorogenic granite-rhyolite suite composed of five main lithologies 1) crystal tuff to lapilli tuff, 2) fine tuff, 3) crystal lithic lapilli tuff, 4) massive crystal-rich tuff and/or intrusive porphyry, 5) pyroclastic breccias (MacDonald, 2004). U-Pb dating by Heaman et al. (2007) yielded an age of 1546.5 ± 3.9 Ma for a crystal tuff and 1536.7 $^{+10}_{-2.3}$ Ma for a felsic intrusive.

3.3 Midcontinent Rift-related Intrusive Units

3.3.1 Keweenawan Midcontinent Rift Overview and Tectonic Setting

The Midcontinent rift system (MCR) extends for more than 2000 km from Kansas, north through Minnesota to northwestern Ontario, southeast along Lake Superior and south through to Michigan (Fig. 3.2; Green, 1983). It represents a period of major magmatic activity producing volcanic, intrusive and sedimentary rocks known as the Keweenawan Supergroup. The rift system truncates several basement provinces ranging in age from 3.6 to 1.65 Ga including the Central Plains orogen, the Superior craton, the Penokean orogen, and the eastern Granite-Rhyolite province (Van Schmus, 1992). Large volumes of Keweenawan basalt, totalling ~1,500,000 cubic kilometers, were emplaced during rift related activity (Klewin and Shirey, 1992). The age of the MCR is ~1.1 Ga (ranging from 1150 Ma to 1094 Ma) with high precision U-Pb zircon geochronology with the majority of magmatism occurring from 1108 Ma to 1094 Ma (Heaman et al., 2007).

It is widely recognized by many workers, including Nicholson and Shirey (1990) that the most plausible explanation for magmatism is a rising mantle plume source resulting in the mixing of variable amounts of depleted and enriched mantle components. Intrusive rocks associated with the Keweenawan Midcontinent Rift fall within the Midcontinent Rift Intrusive Supersuite (Miller et al., 2002) with the intrusive rocks located north of Lake Superior being subdivided into the Logan Igneous Suite (Hollings et al., 2007a).

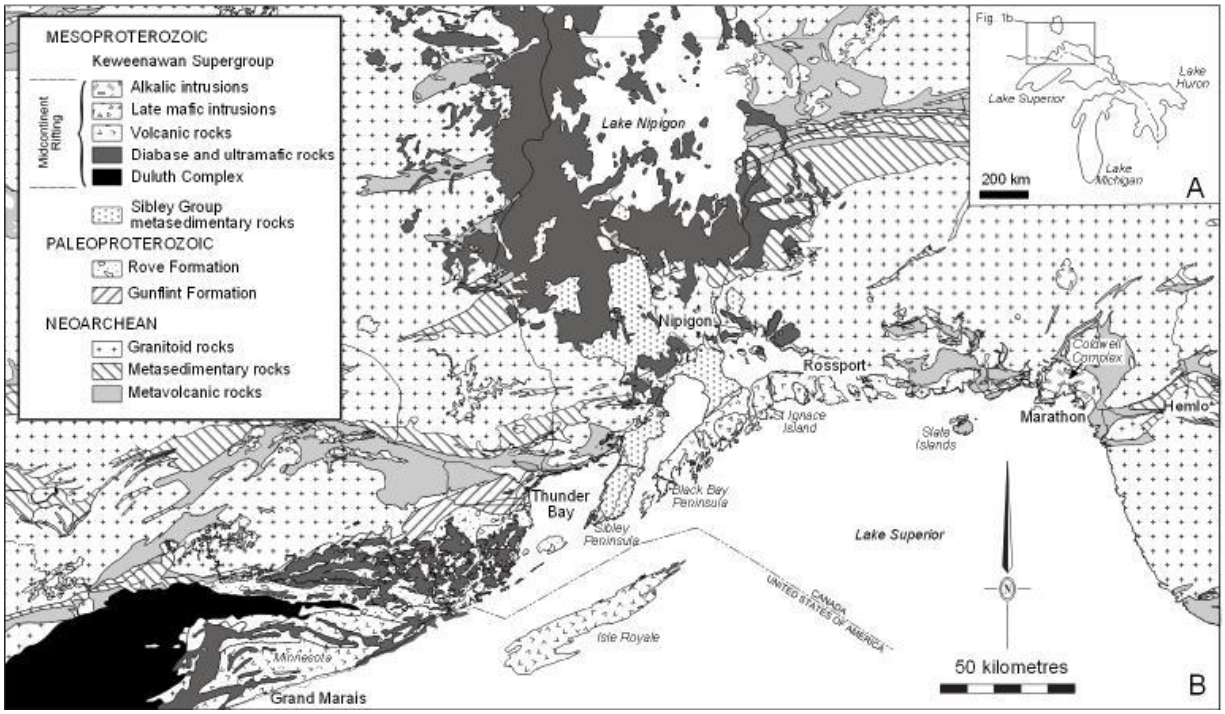

Figure 3.2: (A) Showing location of the Midcontinent Rift area in relation to the upper Great Lakes. (B) Generalized map of the Midcontinent Rift. Modified after Pye and Fenwick (1965) and Carter et al. (1973).

3.3.2 Coldwell Complex

The Coldwell Complex is a large (~28 km diameter) composite, alkaline intrusive complex associated with the Midcontinent Rift, located on the northeast corner of Lake Superior (Fig. 3.2; Heaman and Machado, 1992). The complex contains a diverse suite of rock types which were intruded into the Archean Abitibi and Wawa subprovinces and rapidly crystallized at 1108±1 Ma (Heaman and Machado, 1992) which confirms its association with the MCR. Field relationships described by Mitchell and Platt (1978) as well as Currie (1980) interpreted the complex to represent a ring structure with three intrusive centres younging to the west and south. Center 1, near Craddock Cove, occurs along the eastern part of the complex and is dominated by ferroaugite syenite and gabbro (termed the Eastern Gabbro). Centre 1 is intruded by the prominent north-south trending Two Duck Lake Gabbro which is host to significant Cu-PGE mineralization (Good, 1993). Centre 2 is marked by the presence of nepheline syenite which was emplaced as a hot, hydrous and relatively un-evolved magma (Mitchell and Platt, 1982). Center 3, also termed the Pic Island centre, is the youngest centre of the complex and intrudes most other phases of the

complex (Mitchell and Platt, 1978). Dominant lithologies within Centre 3 are nepheline syenite, amphibole syenite, quartz syenite and granite.

Hornfels basaltic material displaying relict volcanic features such as amygdules and relict primary textures have been noted throughout the Coldwell Complex (Sage, 1991). These rocks have been interpreted to represent down-drop blocks or roof pendants of roof material into which the alkaline complex was intruded. Alternatively, this volcanic material may represent the extrusive equivalent of the outer gabbro ring i.e., the Eastern Gabbro.

Based on U-Pb zircon/baddeleyite ages of 1108±1 Ma (Heaman and Machado, 1992) and a number of ages for mafic intrusive units of the Nipigon Embayment (cf. Heaman at al., 2007), tholeiitic and alkaline magmatism were contemporaneous during the Midcontinent rift. Heaman and Machado (1992) concluded that the alkaline magmatism associated with the MCR may correspond to the location of maximum lithospheric extension off-axis to the northeast of the central rift graben.

3.3.3 Duluth Complex

The Duluth Complex in northeastern Minnesota covers an arcuate area of over 5000 km^2 on the northwestern flank of Lake Superior constituting the second largest mafic intrusive complex in the world (Fig. 3.2; Miller et al., 2002). Intrusive and comagmatic rocks on the Duluth Complex were emplaced into Archean and Paleoproterozoic footwall rocks during a ~23 million year period defined by four distinct magmatic stages; early, latent, main and late (Miller and Vervoort, 1996). The early magmatic stage spans from 1109 to 1107 Ma and is characterized by early, primitive melts derived directly from the plume source (Miller et al., 2002). These rocks display reversed polarity and are of interest in targeting Ni-Cu-PGE mineralization. This was followed by a latent magmatic stage from 1107 to 1102 whereby volcanism was sparse aside from the production of rhyolitic volcanic rocks along the North Shore (Miller et al., 2002). This is inferred to be a time of plume upwelling and extensive crustal underplating and melting. The main magmatic stage followed from 1102 to 1094 Ma which produced a diverse suite of magma compositions comprises the majority of the Duluth Complex (Miller et al., 2002). Rocks produced during this period are thought to be a result of continued crustal separation, the emptying of crustal magma chambers and the continued melting of the mantle plume (Miller et al., 2002). From 1094 to 1986 Ma, volcanism waned, basin subsidence continued and rift-fill sediments were produced (Miller et al., 2002). The period likely represents a period where plate drift caused the plume to lose its heat source and the thermal collapse of the rift basin (Davis and Green, 1997).

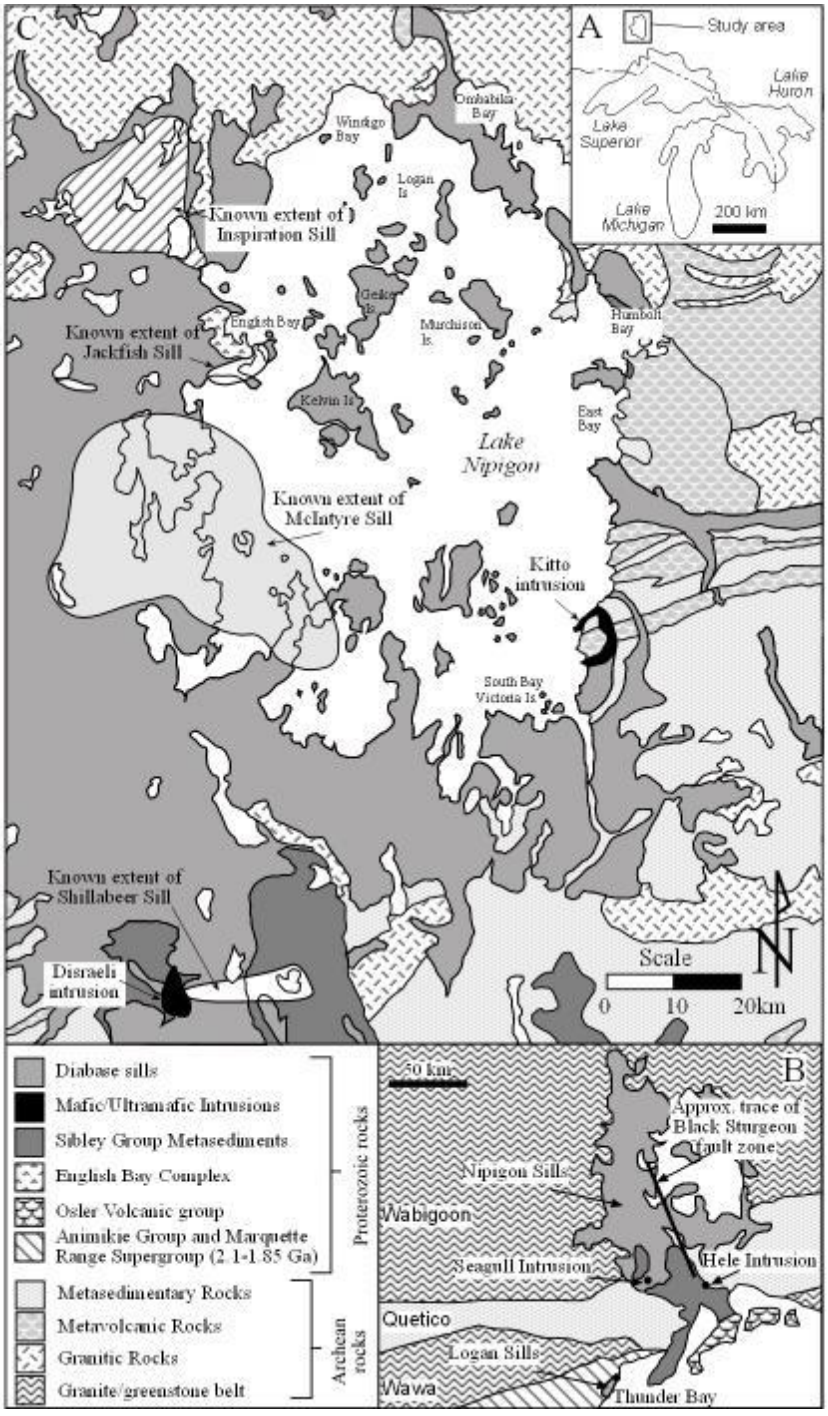

Figure 3.3: (A) Location of the Nipigon Embayment in relation to the Great Lakes. (B) Simplified geological map showing location of members of the Logan Igneous Suite. (C) Simplified geological map showing the main Proterozoic Midcontinent Rift-related intrusions. Unless otherwise indicated, the diabase sills are Nipigon sills. Modified after Sutcliffe (1986) and Hart and MacDonald (2007).

3.3.4 Ultramafic Intrusions

There are four major mafic-ultramafic intrusions associated with the MCR north of Thunder Bay; Disraeli, Seagull, Hele and Kitto. These intrusions crosscut Sibley Group sedimentary rocks and Archean basement to form sills, but no feeders have been recognized to date. They are composed of lherzolite and olivine websterite with irregular zones of olivine gabbro to gabbro along the margins (Hart and MacDonald, 2007) where the volume of ultramafic material roughly equals the volume of mafic material, with the exception of the Seagull intrusion (Hollings et al., 2007a)

3.3.4.1 Seagull

The 1112.8±1.4 Ma, ~750 m thick Seagull intrusion (Fig. 3.3) consists of a lower ultramafic unit (~650 m thick) composed of dunites, peridotites and pyroxenites with cumulate olivine and poikilitic clinopyroxene as the dominant textures (Heggie, 2005; Heaman et al., 2007). The upper section (<100 m) is variable in composition but is dominantly mafic composed of olivine gabbros and gabbros. Platinum, palladium, nickel and copper mineralization within the Seagull intrusion is found at the base of the ultramafic section and in three distinct horizons termed the RGB horizons, each separated by 2 m of unmineralized ultramafic rock (Heggie, 2005). The basal zone is interpreted to have formed during initial emplacement, whereas the RGB horizon was likely formed by secondary pulses of primitive magma refreshing the chamber and bringing the system back into sulphide saturation (Heggie, 2005).

3.3.4.2 Kitto

Located on the east side of Lake Nipigon (Fig. 3.3), the 1110.8±4.3 Ma Kitto intrusion is dominantly composed of lherzolite exhibiting cumulate to poikilitic textures dominated by olivine and lesser pyroxene (Heaman et al., 2007; Laarman, 2007). The intrusion was emplaced in two pulses as established from olivine mineral chemistry; an initial pyroxenite-melagabbro followed by a lherzolite-olivine websterite (Laarman, 2007). The Kitto intrusion likely exploited north-south trending Proterozoic and east-west trending Archean faults creating the ring-shaped form of the intrusion (Laarman, 2007).

3.3.4.3 Disraeli

The rocks of the 1109.0 ± 1.5 Ma Disraeli intrusion (Fig. 3.3) are commonly fine- to medium-grained ranging in composition from olivine gabbro to plagioclase-bearing olivine clinopyroxenite and wehrlite (Heaman at al., 2007; Hart and Magyarosi, 2004b). The overall zonation of the intrusion is similar to that of the Hele intrusion consisting of a massive to poikilitic textured pyroxene peridotite core grading into to an outer zone of fine- to medium-grained, massive olivine gabbro (Hart and Magyarosi, 2004b).

3.3.4.4 Hele

The 1106.6 ± 1.5 Ma Hele intrusion (Fig. 3.3) is an elliptically shaped ultramafic sill emplaced within the Kama Hill Formation of the Sibley Group (Heaman et al., 2007; Flank, 2011). The unit can be stratigraphically subdivided into five main lithologies: 1) the Upper Marginal Zone composed of varied-textured leucograbbo; 2) the Upper Gabbroic Zone consisting of a layered sequence of subophitic gabbro to cumulate melagabbronorite; 3) Ultramafic zone displaying cumulus olivine and pyroxenes; 4) Lower Gabbroic zone; and 5) the Lower Marginal Zone (Flank, 2011). The rocks of the Hele intrusion are interpreted to have formed from the fractionated ultramafic liquid which based on trace element abundances, correlate with the Middle Osler Group Volcanics (Flank, 2011).

3.3.5 Mafic and Mafic to Ultramafic Sills

The intrusive rocks of the Keweenawan Supergroup are represented by a series of mafic diabase sills and mafic to ultramafic intrusions. The sills around Thunder Bay can be subdivided into two informal groups; the Nipigon sills for those north of Thunder Bay and the Logan sills for those south of Thunder Bay (Hollings et al., 2007a). These intrusive units were emplaced in a short, magnetically reversed, interval between ~1115 Ma and 1100 Ma (Heaman et al., 2007).

3.3.5.1 Nipigon sills

Nipigon sills are commonly massive, medium- to coarse-grained, olivine-tholeiitic diabase/gabbros (Sutcliffe, 1986; Hart and MacDonald, 2007). Nipigon sills are dominantly present throughout the Lake Nipigon area but have also been recognized in the Thunder Bay area (Fig. 3.3; Hollings et al., 2007d; Magnus, 2010). Nipigon sills are characterized by a massive, subophitic to ophitic, plagioclase and clinopyroxene texture with trace to 3% olivine and 1-2% modal magnetite (Hart, 2005b).

Nipigon sills display a reverse magnetic polarity and generally form thick, columnar jointed sheets. Sills commonly intrude Sibley group sedimentary rocks but also can be found in contact with Archean rocks of the Quetico Subprovince and the Marmion and Winnipeg River Terranes. Sills often intrude earlier emplaced ultramafic units of the Nipigon Embayment as well as the 1129.0 ± 2.3 Ma Pillar Lake Volcanics and the 1546.5 ± 3.9 Ma English Bay Complex (Heaman et al., 2007) providing evidence for their emplacement during the second main phase of magmatism (Hart and MacDonald, 2007). The shallow dipping Nipigon diabase sills are estimated to cover an area in excess of 20 000 km^2 (Sutcliffe 1991) ranging in thickness from <5 m to >180 m (Hart and Macdonald, 2007). They are distinguishable from the Logan sills to the south based on lower abundances of TiO_2 and lower degrees of heavy rare-earth element fractionation (Hollings et al., 2007a).

3.3.5.2 Logan sills

Located in the Logan Basin south of Thunder Bay (Fig. 3.4; North, 2000) Logan sills are generally characterized as quartz tholeiitic diabase/gabbro with a fine to coarse-grained, ophitic to intergranular texture (Geul 1970, 1973; Smith and Sutcliffe 1987). The U/Pb date of 1114.7 ± 1.1 for a Logan sill on Mount McKay (Heaman et al., 2007) suggests that Logan sills are among the oldest Midcontinent rift-related intrusive rocks located within the Logan Basin.

Textural stratigraphy is variable through the sills ranging from a lower ophitic zone towards the base to an upper pegmatitic zone towards the top of the sills suggesting that the sills cooled as single units over a period of approximately 200 to 500 years (Smith and Sutcliffe, 1989). Coarse-grained, intergranular gabbro is common towards the centre of sills with as much as 60% phenocrysts present towards the upper plagioclase-porphyritic sections (Smyk and Hollings, 2007).The thickness and morphology of Logan sills are controlled by the relatively flat-lying Paleoproterozoic Rove Formation shales forming columnar-jointed, shallowly dipping sills with often pronounced chill margins. They cap prominent mesas and cuesas characteristic of the rugged topography of the Logan basin.

As many as six diabase sheets were emplaced within the area from the international border to Thunder Bay (Weiblen et al., 1972; Smith and Sutcliffe 1987, 1989). Smith and Sutcliffe (1989) reported sill thicknesses of up to 50m, whereas Jones (1984) noted four sills ranging from 50 to 160 m in thickness. Diamond drilling in Pardee Township conducted by Dumont Nickel reported 14 gabbroic sill intersections in a 705 m deep drill hole (Assessment Files, Thunder Bay South Resident Geologist's District, Thunder Bay). Rare exposures of feeder dykes to sills and preserved sill terminations have been noted. The Logan sills are distinguishable from the Nipigon sills to the north based on higher relative abundance of TiO_2 and a slightly greater degree of heavy rare-earth element fractionation (Hollings et al., 2007a).

3.3.5.3 Riverdale sill

The Riverdale sill was first characterized by Hollings et al. (2007d) as being geochemically and petrographically distinct from the surrounding Logan sills and the Nipigon sills to the north. Puchalski (2010) detailed the geochemical and petrographical characteristics of the Riverdale sill. The Riverdale sill lies within the southern city limits of Thunder Bay, Ontario close to the northern boundary of the Logan basin (Fig. 3.4). The unit displays a sill morphology exposed over an area approximately 6 km long and 2 km wide but the true thickness is unknown as the upper contact is not exposed (Puchalski, 2010). Exposures within a quarry on West Riverdale Road display a thickness of 10 m where detailed sampling

and subsequent geochemical and petrographical analyses were completed.

Rocks comprising the Riverdale sill are dominantly gabbro-norites with lesser olivine gabbro present towards the centre of the intrusion. The gabbro-norites are generally fine-grained and display no cumulate textures within any of the samples with plagioclase typically occuring as subhedral laths with euhedral orthopyroxene and lesser clinopyroxene and olivine (Puchalski, 2010). Minor alteration is present in most samples as chlorite replacing pyroxene and sericite replacing plagioclase. The olivine gabbro samples lying toward the centre of the unit are petrographically similar to the gabbro-norite samples except for a higher modal percentage of anhedral to euhedral olivine. Olivine grains are typically fine-grained but may range to medium-grained. Variable amounts of serpentine are found replacing olivine.

3.3.5.4 Crystal Lake Gabbro

The Crystal Lake Gabbro (Fig. 3.4) has been an exploration target for Ni-Cu-PGE mineralization for over a century. The deposit itself is referred to as the Great Lakes Nickel deposit after the Great Lakes Nickel Corporation who conducted the majority of work during the 1950's and 1960's. The 1097.6 ± 1.1 Ma Crystal Lake Gabbro is "Y-shaped" in plan view and takes the form of an inverted cone or lopolith (Smith and Sutcliffe, 1987; Heaman et al., 2007). The Crystal Lake Gabbro exhibits igneous layering with four distinct units mapped throughout the intrusion by Smith and Sutcliffe (1987, 1989) and Cogulu (1990): upper zone of sulphide barren troctolite, olivine gabbro, and anorthositic gabbro;
middle zone of cyclic layered anorthositic and olivine gabbros, chromite-spinel-bearing anorthosite, and olivine gabbro; lower zone of unlayered varied texture gabbro and leucotroctolite (hosts bulk of Ni-Cu sulphide deposit); and a basal zone of fine-grained, chilled melagabbro and hornsfelsed country-rock xenoliths.

3.3.5.5 Other Sills

Two mafic to ultramafic sills are recognized within the Nipigon Embayment: the 1112.4 ± 2.8 Ma Jackfish sill proximal to the English Bay Complex; and the Shillabeer sill which intrudes the ultramafic Disraeli intrusion (Fig. 3.3; Heaman et al., 2007). These sills are typically finer-grained and display higher modal olivine abundances compared to the surrounding Nipigon sills (Hollings et al., 2007a). In addition to the volumetrically dominant Nipigon sills, two other mafic sills are recognized in the Nipigon Embayment: the 1159 ± 33 Ma Inspiration sill in the northwest corner; and the 1100.8 ± 4.4 Ma McIntyre sill within the western portion of Lake Nipigon (Fig. 3.3; Heaman et al., 2007). The Inspiration and McIntyre sills can be distinguished from the surrounding Nipigon sills based on trace-element abundances whereby the Inspiration sill displays greater light rare-earth element enrichment and the McIntyre sill displays greater heavy rare-earth element fractionation (Hollings et al., 2007a). In Blake Township within

the Logan Basin (Fig. 3.4), a vari-textured, “taxitic” gabbro has been described by North (2000) and Beskar (2001) dated at 1091.1 ± 4.5 Ma (Heaman et al., 2007).

3.3.6 Logan Basin Dyke Sets

Three dyke sets are currently recognized within the Logan Basin based on geochronological data and orientation. The most abundant of these are the east-northeast to northeast trending Pigeon River dykes (Fig. 3.4). Two ages for the Pigeon River dykes have been determined based on U/Pb dating of baddelyite; 1141 ± 20 Ma and 1078 ± 4 Ma for dykes in Crooks and Devon Townships, respectively. Pigeon River dykes are commonly 50 m to 70 m in width ranging up to 150 m in Ontario (Smith and Sutcliffe, 1987) and up to 500 m in Minnesota (Green at al., 1987) and can be traced for up to 15 km along strike. They form prominent ridges within the south-eastern area of the Logan Basin and intrude sedimentary rocks of the Rove Formation commonly causing warping and deformation at contact zones. Typical composition for a non-porphyritic Pigeon River dyke is 60% plagioclase (zoned labrodorite, An_{55-70}), 20% augite ± hypersthene, up to 15% olivine and up to 5% magnetite, ilmeno-magnetite, and sulphides (Geul , 1970, 1973). Within the Pigeon River dyke suite is a prominent east-northeast trending dyke in southern Devon Township termed the Arrow River dyke (Smyk and Hollings, 2007). Pigeon River dykes display mostly N polarity with two dykes to the southeast of the basin displaying R polarity (Pesonen, 1978; Halls and Pesonen, 1982; Hollings et al., 2010).

The northwest trending Cloud River dykes were formerly termed the Arrow River dykes by Smith and Sutcliffe (1987) but have since been renamed by Smyk and Hollings (2007) due to the fact that this suite lies nowhere near the Arrow River (Fig. 3.4). This suite is composed of intergranular quartz diabase and is commonly plagioclase-phyric (Smith and Sutcliffe, 1989). The unit has been dated at 1109.3 ± 4.2 Ma (Hollings et al., 2010) and displays N polarity (Piispa et al., 2011) contradicting the previously recognized R polarity demonstrated by Hollings et al. (2010).

The Pine River-Mount Mollie dyke (hence forth referred to as the Mount Mollie dyke) is a 35 km long composite body that extends east from the Crystal Lake gabbro then northeast to form a string of islands in Lake Superior (Victoria Island, Spar Island, Thomson Island; Fig. 3.4; Smith and Sutcliffe, 1987). The unit consists of gabbroic, dioritic, and granophyric rocks with the mafic phases dominating the eastern end and the core of the intrusion (Smith and Sutcliffe, 1987). The Mount Mollie dyke has been dated at 1109.3±6.3 (Hollings et al., 2010) and displays a N polarity (Piispa et al., 2011) which is unusual as a R polarity is expected for rocks >1103 Ma (Halls and Pesonen, 1982).

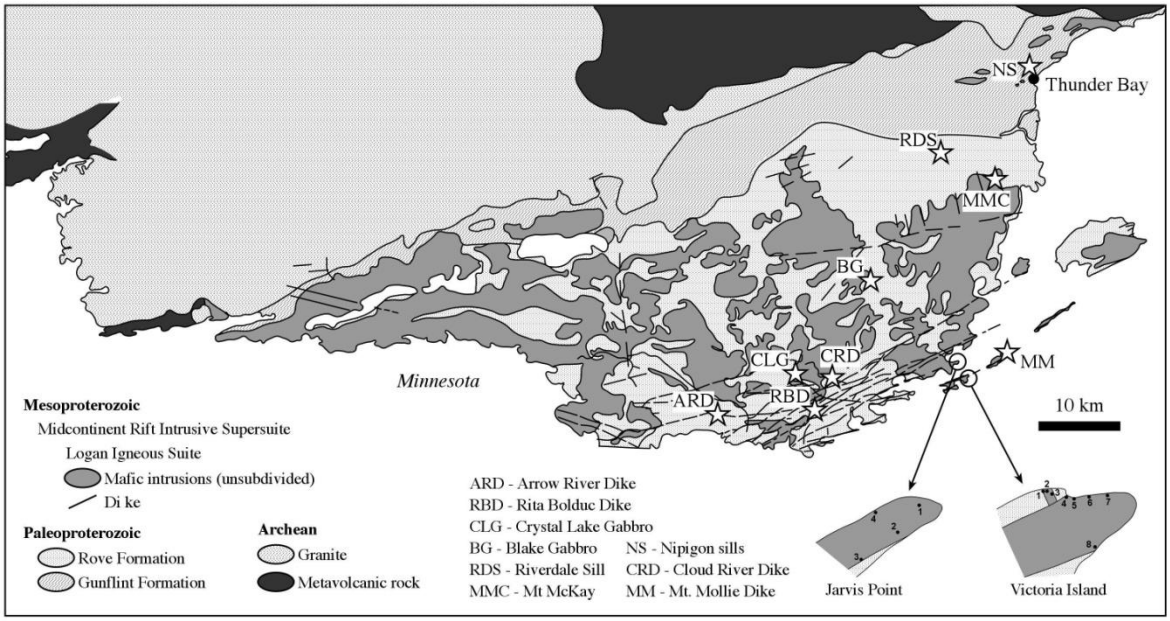

Figure 3.4: Geological map of the Logan Basin. Modified after Pye and Fenwick (1965).

3.4 Midcontinent rift-related extrusive units

3.4.1 Overview of Volcanic Assemblages

Volcanic units associated with the MCR can be correlated along the shores of Lake Superior and have been subdivided by Nicholson et al. (1997) into five distinct groups based on major element, trace element and Nd isotopic analysis. Furthermore, Nicholson et al. (1997) subdivided the five distinctions into two primary magmatic phases with a lull between them and a period of minor volcanism following. These successions are described in detail below and illustrated in Figure 3.5.

The first phase of magmatism from 1108 Ma to 1105 Ma produced three of the five basalt types as outlined by Nicholson et al. (1997). Basalt type I is found as flows at the base of the Keweenawan Supergroup as the basal units of Ely's Peak and Grand Portage areas of the North Shore Volcanic Group and as the lower suite of the Osler Group (Nicholson et al., 1997). The unit is commonly pillowed, augite-phyric, and overlies quartz sandstone except for the Osler on Black Bay Peninsula that overlies a thin conglomerate. Chemical distinctions are consistent throughout and are characterized by low Al_2O_3 and HREE as well as a smooth arcuate chondrite-normalized trace element pattern and consistent Nd isotopic composition (Nicholson et al., 1997).

Basalt type II is represented by the upper Siemens Creek basalts and is also correlative with basalts of the northeast limb of the North Shore Volcanic Group as well as the Osler group. This group is distinguished

from other MCR basalts by its broad range of $\varepsilon_{Nd(1100)}$ values (-1.4 to -6.9) and negative average $\varepsilon_{Nd(1100)}$ of -3.8 (Nicholson et al., 1997).

The third basalt type (basalt type III) as outlined by Nicholson et al. (1997) is represented by the Kallander Creek Volcanics and by rocks present in the Ely's Peak area. They have higher Al_2O_3 and TiO_2 and very low MgO with an $\varepsilon_{Nd(1100)}$ of about -0.6. No augite phenocrysts are observed but large tabular plagioclase phenocrysts are common within these units (Green, 1982). The period 1105 Ma to 1100 Ma was a time of minimal magmatic activity in western Lake Superior as determined from a compilation of high-precision U-Pb zircon ags for MCR rocks (Davis and Green, 1997). However, Nicholson et al. (1997) noted that localized systems such as the upper Kallander Creek Volcanics and the central to upper suites of the Osler Group may have been active during this time. Following the period of minimal volcanic activity, emplacement of flood basalts and intrusions increased dramatically. The Portage Lake flood basalts comprise the majority of what Nicholson et al. (1997) determined to be basalt type IV which is characterized by low TiO_2, high Al_2O_3 and low REE abundances with $\varepsilon_{Nd(1100)}$ values of +1.00 to -0.6 and average $\varepsilon_{Nd(1100)}$ of +0.4. Towards the top of the sequence lies a late volcanic sequence consisting of the Schroeder and Lutsen basalts of the North Shore Volcanic Group and possibly by some dykes and flows on the southern shore of Lake Superior on the Keweenaw Peninsula (Paces, 1998). This composition has been described as basalt type V and is more primitive than most of MCR basalts with the highest Al_2O_3 averages and lowest incompatible trace element abundances (Nicholson et al., 1997).

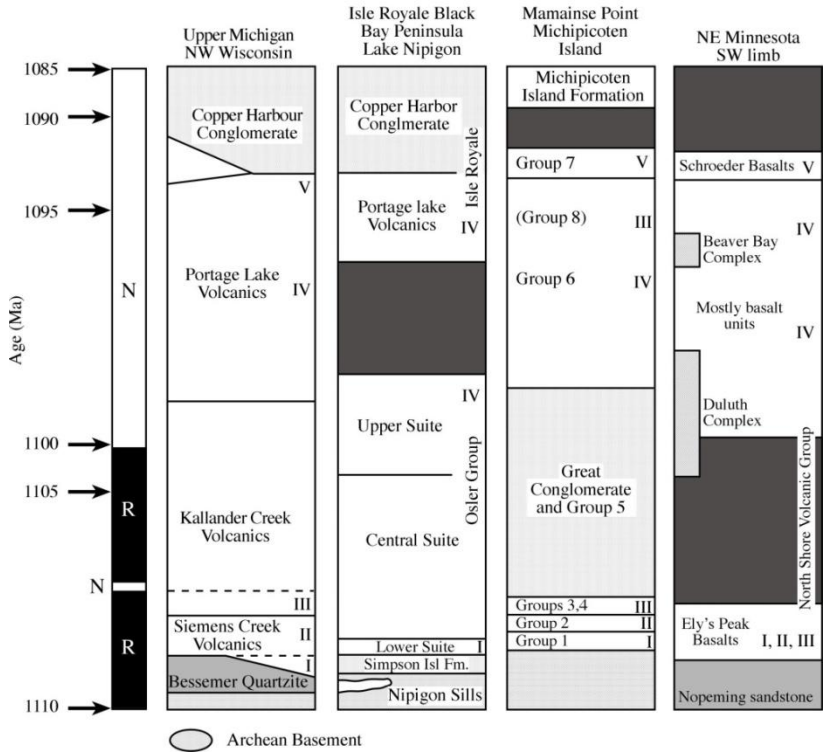

Figure 3.5: Stratigraphic column showing the succession of major Keweenawan volcanic units. After Nicholson et al. (1997).

3.4.2 Devon Volcanics

A unit of mafic rocks in Devon Township, south of Thunder Bay, was mapped by Tanton (1931) and was termed Rove Formation Basalts. Geul (1970) mapped this unit as a Logan diabase sill. The unit is exposed on a plateau 7 km long and 0.8 to 1.0 km wide (Fig. 3.4). The unit is 4 to 6 m thick and is in apparent conformable contact with the underlying shales of the Paleoproterozoic Rove Formation, where a pronounced chilled margin consists of variolitic material up to 20 cm thick. The flow-top also exhibits a variolitic texture ~15 cm thick. The presence of ropy flow top and amygdules as well as quench textures, support a volcanic origin (Cundari, 2010).

Major element chemistry reveals a tholeiitic, intermediate composition with samples plotting in the basaltic andesite to andesite fields as well as in the basaltic trachy-andesite to trachy-andesite fields on a total alkali versus silica (TAS) diagram (Cundari, 2010). The unit typically has an intergranular texture consisting of randomly oriented plagioclase laths with interstitial chlorite, an alteration product of primary augite. Most samples contain minor serpentine (after olivine), opaque minerals, secondary quartz, oxides, pyrite and calcite. Amygdules are present in most samples and are infilled with some combination of calcite, quartz, chlorite and pyrite. Lower flow contacts and flow-tops are typically glassy with abundant

spherulites that sometimes coalesce into bands (Cundari, 2010).

Rare-earth element geochemistry shows the unit to be relatively enriched in both HREEs and LREEs, similar to the ultramafic sills of the Nipigon Embayment as well as the Riverdale Sill (Hollings et al., 2007a, 2010). Incompatible element abundances and REE shows that the volcanic unit is characteristic of an Ocean-Island Basalt, but with a negative niobium anomaly, most likely the result of contamination by a lower crustal source. This evidence is further supported by an $\varepsilon_{Nd(t=1100Ma)}$ of -3.48, which also suggests contamination of the unit by a lower crustal source. The trace element characteristics of the volcanic unit suggest an origin in Keweenawan time as they are geochemically similar to volcanic units of the MCR (Hollings et al., 2007) rather than Paleoproterozoic volcanic units of the Gunflint Formation.

3.4.3 Osler Group Volcanics

The 1108 to 1105 Ma Osler Group represents a 3 km thick succession of basaltic flows and sedimentary units lying with angular unconformity on the underlying eolian and lacustrine deposits of the Sibley group (Hollings et al., 2007c). The volcanic and sedimentary succession is located on Black Bay and trends eastward forming an archipelago in Nipigon Bay, north Lake Superior. All units studied to date display a reverse magnetic polarity but work is on-going to develop precise measurements of polarity variations through stratigraphy (Swanson-Hysell et al., 2012). The sequence consists of a basal conglomerate overlain by felsic to mafic flows dominantly intercalated with sandstones with lesser conglomerate and limestone (Hollings et al., 2007c). Mafic units are commonly massive to amygdaloidal flows ranging in thickness from 5 cm to 30 m (Lightfoot et al., 1991) with locally developed ropey tops and pahoehoe textures (Sutcliffe and Smith, 1988). The basalts are characterized by plagioclase and clinopyroxene phenocrysts set in a fine-grained groundmass of plagioclase, augite and Fe-Ti oxides (Hollings et al., 2007c).

The Osler Group volcanics are characterized by basalts or basaltic andesites that show trends of broadly increasing SiO_2 and decreasing MgO with stratigraphic height above the Simpson Island formation (Hollings et al., 2007c). This is broadly consistent with the findings of Lightfoot et al. (1991) who identified three suites of volcanic rocks through the Osler Group on Black Bay (Table 3.1). General trends throughout the Osler Formation show general increases up section in SiO_2, Th, La/Sm_n, Th/La, and Th/Nb with corresponding decreases in MgO and Gd/Yb_n suggesting a increasingly shallow source of melting (Hollings et al., 2007c).

As the Osler Group represents a sequence of rocks deposited early in Midcontinent Rift history, Hollings

et al. (2007c) investigated the sedimentology within the pile as a means for evaluating rift axis orientation. They concluded that early phases of rifting took place along a north-south axis with later phases of rifting being subject to subsidence along an east-west axis characteristic of a shift in stress regime. This theory is consistent with the emplacement sequence of intrusive units within the Nipigon Embayment as well as the Logan Basin.

Table 3.1: Characterization of Osler Group Volcanic Suites (from Lightfoot et al., 1991).

Suite	**Lower**	**Central**	**Upper**
Height (m)	0-750	750-1900	1900-3000
Mg#	0.55-0.7	0.34-0.52	0.3-0.6
TiO_2	1.7-3.2	1.0-2.4	1.1-2.6
Al_2O_3	8-12	13-16	13-17
La/Sm	2.1-3.3	3.0-6.2	2.5-4.8
Gd/Yb	3.5-4.5	1.6-2.1	1.6-2.6

3.4.4 Mamainse Point Volcanics

The Mamainse Point volcanics are located on the eastern shore of Lake Superior and represent one of the most complete records of volcanism associated with the Midcontinent Rift (Shirey et al., 1994). The Mamainse Point lavas represent an approximately 5255 m thick sequence consisting of over 350 separate lava flows with interbedded conglomerate comprising 24% of the sequence (Klewin and Berg, 1990). Compositionally, the flows are dominantly basalt but display a range from picrite to basaltic andesite (Shirey et al., 1994) with minor rhyolite mapped dominantly inland from the shoreline of Lake Superior (Annels, 1973).

Geochemically, the Mamainse Point formation shows consistent variation through stratigraphy based on both major and trace element geochemistry. Shirey et al. (1994) defined eight groups for the Mamainse Point lavas with an overall trend of flows becoming less primitive up-section. Flows towards the base of the section display a typically higher Mg-number with the frequency of high Mg-number flows decreasing through stratigraphic height. This is believed to suggest lavas becoming less primitive up-section as a result of a decreased depth of melting through time (Klewin and Berg, 1990). It has been suggested that the Pukaskwa dyke swarm may represent the feeders to the Mamainse Point volcanics (Green et al., 1987).

The Mamainse point lavas are of particular interest with regards to paleomagnetism as they represent the most complete expression of volcanic activity through Keweenawan time. Furthermore, they are the only Midcontinent rift-related unit that displays multiple paleomagnetic reversals as first noted by Palmer (1970) who recorded three (reversed-normal-reversed-normal) reversals through Mamainse Point stratigraphy. Swanson-Hysell et al. (2009) carried out detailed paleomagnetic work through the Mamainse Point stratigraphy as a means of calculating rates of plate motion through Keweenawan time. They determined that the North American continent moved at a rate between 21.5 ± 7.1 cm yr^{-1} to 38.5 ± 4.4 cm yr^{-1} which is considerably faster than the typical modelled speed of 20 cm yr^{-1} suggesting that the period of Keweenawan magmatism was a time of significant motion of the North American continent.

3.4.5 Pillar Lake volcanic suite

The Pillar Lake volcanic suite was first mapped by MacDonald (2004) and was most recently characterized by Smyk et al. (2011). The volcanic rocks comprise a 20 to 40 m thick sequence of relatively flat-lying, pillowed to massive flows with autoclastic and hyaloclastic breccias covering an area of ~25 km^2 (Hart and MacDonald, 2007). Stratigraphically, rocks of the 1129.0 ± 4.6 Ma Pillar Lake Volcanic suite overlie Mesoproterozoic rocks of the Badwater gabbro (~1599 Ma) and the Badwater syenite (~1590 Ma) and are intruded by the Midcontinent rift-related Inspiration sill (1159 ± 33 Ma; Hart and MacDonald, 2007; Heaman et al., 2007). Based on alteration histories as well as stratigraphic relationships and geochemistry, Smyk et al. (2011) proposed the Pillar Lake basalts to be coeval with the Inspiration sill possibly representing a subvolcanic intrusion or a massive, ponded flow/lava lake erupted early in the MCR history.

3.5 Midcontinent Rift-related Mineralization

3.5.1 Overview

Intrusive rocks associated with the 1.1 Ga Midcontinent rift (MCR) surrounding the Lake Superior basin have long been an exploration target for Nickel-Copper-Platinum Group Element (Ni-Cu-PGE) deposits. Drawing comparisons to the Noril'sk deposit in Siberia, Naldrett (1992) suggested the area surrounding the Nipigon Embayment satisfied the geological criteria to host significant Ni-Cu-PGE mineralization. Since the early 2000s, the rising prices of platinum group elements (PGE's) have sparked exploration efforts surrounding the Lake Superior basin, with recent discoveries in northwestern Ontario, northeastern Minnesota and Michigan's Upper Peninsula (Fig. 3.6). Deposits are typically hosted in mafic to ultramafic intrusions with mineralization occurring as disseminated, semi-massive and massive magmatic sulphides (Miller et al., 2010). Two main styles of mineralization occur in MCR-related deposits; high-

tonnage, low-grade deposits (i.e. Duluth) and low-tonnage, high-grade conduit hosted Ni-Cu-PGE deposits (i.e. Thunder Bay North, Eagle and Tamarack). The locations, grades and tonnages of MCR-related Ni-Cu-PGE deposits are shown in Figure 3.6. The most recent exploration efforts have been guided towards the discovery of Noril'sk style conduit-hosted Ni-Cu-PGE sulphide deposits with discovery of the Eagle, Tamarack and Thunder Bay North deposits. The morphologies of these deposits are tube-shaped conduits in some cases representing the potential feeders to overlying voluminous flood-basalts. The model proposed by many authores (e.g., Nadrett, 1992) suggests that magma interacts with country rock, contaminating the melt with sulphur allowing for development of a sulphide melt. Sulphides then scavenge metals from the melt and settle towards the base of the intrusion and in depressions or areas of low-velocity.

3.5.2 Thunder Bay North

The Thunder Bay North deposit is located 50 km northeast of Thunder Bay, Ontario within the Nipigon Embayment. The deposit is hosted in the 1120 ± 23 Ma (Smyk and Hollings, 2009) Current Lake Intrusive Complex (CLIC) and is currently held and worked by Magma Metals Limited. The CLIC is a multi-phase, intermediate to ultramafic conduit or chonolith and is host to significant Pt-Pd-Cu-Ni sulphide mineralization (Heggie et al., 2012). The CLIC is highly variable in shape ranging from ≥30 metres in diameter to 50 metres in width and 70 metres in thickness with a 3.4 km long continuously mineralized body (Heggie et al., 2012). In addition to the CLIC, two other conduits have been identified within the 12 km by 6 km Thunder Bay North camp that are prospective for Pt-Pd-Ni-Cu mineralization; the Steepledge Lake and Lone Island Lake intrusive complexes (Heggie et al., 2012). Earliest phases of the CLIC are hybrid diorites to leucogabbros which are intruded by mineralized olivine melagabbro and lherzolite forming the main body of the CLIC (Heggie et al., 2012). Mineralization is dominantly disseminated and ranges from a few percent to >25% sulphides with mainly pyrrhotite, chalcopyrite, pentlandite, minor pyrite, and lesser cubanite and violarite (Heggie et al., 2012). Net-textured and massive sulphide mineralization has also been discovered and occurs towards the base of various zones within the complex (Heggie et al., 2012).

3.5.3 Tamarack Intrusion

The Tamarack intrusion is a tadpole shaped, cumulate, ultramafic intrusion or chonolith located approximately 80km west of Duluth (Goldner, 2011). Not exposed on surface, the Tamarack intrusion has been explored by Rio Tinto Exploration (formerly Kennecott Exploration) who conducted extensive drilling for the past decade. The 13 km long by 1-4 km wide intrusion was emplaced into black shales of the Animikie Basin at 1105.6 ± 1.2 Ma (Goldner, 2011) which likely acted as the source of sulphur

driving the system into sulphide saturation. The narrow tail portion of the intrusion is comprised exclusively of ultramafic lithologies and is thus the site of intense exploration drilling, whereas the body area of the intrusion is of mafic character with rock types ranging from lherzolite to granophyric gabbronorite (Goldner, 2011). Mineralization dominantly occurs as disseminated sulphides concentrated particularly towards the tail of the intrusion (Goldner, 2011).

3.5.4 Eagle Intrusion

The Eagle deposit is a small, but high grade Ni-Cu-PGE deposit located in Marquette County in the Upper Peninsula of Michigan (Ware, 2007). The Eagle deposit is hosted within the westernmost of two peridotite bodies within the Paleoproterozoic Baraga Basin collectively referred to as the Yellow Dog Peridotite, Three distinct type of mineralization are found in the Eagle deposit: blebby disseminations, semi-massive matrix, and massive (Ware, 2007). Nickel tenors are uniformly distributed throughout whereas platinum group metals and gold are correlative with more copper-rich massive sulphides as well as in the surrounding sediments (Ware, 2007). Sulphur saturation within the Eagle Intrusion was likely driven by the sequential emplacement and subsequent contamination by a lower, stratified magma chamber (Ware, 2007).

3.5.5 Marathon PGM

The Coldwell intrusive complex comprises three nested intrusive centres (Centres I, II, and II) (Mitchell and Platt, 1982) and is host to two late-stage, mineralized gabbroic intrusion. The Marathon platinum-group-mineral (PGM)-Cu deposit is hosted within the Two Duck Lake Gabbro and is part of a late phase multiple intrusive events which also formed the Eastern Gabbro. The intrusive complex lies towards the eastern portion of the Coldwell Complex within Centre 1 syenites. The Two Duck Lake Gabbro (TDLG) is a coarse-grained to pegmatitic intrusion approximately 6km in strike length and 50 to 250m wide, dipping from 5° to 45° to the west (Miller et al., 2010). The TDLG exhibits a fresh, relatively unaltered ophitic, clinopyroxene texture easily distinguishing it from the Layered Gabbro Series as well as the Eastern Gabbro (Miller et al., 2010). Mineralization within the Two Duck Lake Gabbro is akin to typical magmatic sulphide assemblages; chalcopyrite, pyrrhotite with minor amounts of pentlandite, cobaltite, bornite and pyrite occurring between primary silicates (Miller et al., 2010). The sulphide assemblage is variable up section through the TDLG with pyrrhotite dominating the basal portion and the relative proportion of chalcopyrite increasing towards the top of the unit (Miller et al., 2010). The Geordie Lake Cu-PGM deposit is similar to the Two Duck Lake Gabbro but is located to the west within Centre II syenites. It displays a very coarse-grained to pegmatitic texture and is composed of primarily troctolite and olivine gabbro.

3.5.6 Bovine Igneous Complex (BIC)

The Bovine Igneous Complex (BIC) is located within the Baraga Basin in the Upper Peninsula of Michigan. It is a small basin-shaped mafic/ultramafic intrusion or lopolith likely emplaced during the earliest phases of Midcontinent Rift magmatism, as geochronology has been unsuccessful to date (Foley, 2011). The prospect has undergone extensive exploration drilling yielding only weak mineralization of Ni-Cu-PGE sulphides with metal tenors less than 0.5% Cu and Ni and less than 350 ppb Pt and Pd (Rossell, 2008). From field mapping and core logging, the unit appears to be a layered mafic/ultramafic body composed of a basal wehrlite unit, overlain by a clinopyroxenite and a gabbro cap (Foley, 2011). Mineralization within the BIC is a product of three episodes of sulphur saturation caused the initial injection of magma into the country rock, a second pulse which recharged the chamber, and a last by progressive fractional crystallization of the system (Foley, 2011).

3.5.7 Crystal Lake Gabbro

The Crystal Lake gabbro has long been a target for Ni-Cu-PGE exploration. Since being worked in the 1970's by Great Lake Nickel Inc., the deposit has been referred to by locals as Great Lakes Nickel. Mineralization dominantly occurs within the 60m thick lower zone comprised of varied texture gabbro with abundant patches of gabbro pegmatite and blocks of leucotroctolite (Smyk and Hollings, 2007). Sulphides take form as abundant blebs and disseminations of chalcopyrite, pentlandite, and pyrrhotite with segregations within the upper part of the lower zone containing up to 5% disseminated chromite (Smith and Sutcliffe, 1987).

3.5.8 Duluth Complex

Mineralization within the Duluth complex is manifested in three distinct styles: disseminated copper-nickel-(PGE) sulphides hosted within the basal contact of mafic intrusions, massive sulphide mineralization hosted within the basal contact of mafic intrusion and in footwall rocks, and sulphide mineralization within feeder zones (Noril'sk, Voisey's Bay style; Miller et al., 2002). The bulk of mineralization associated with the MCR is hosted within the Duluth complex with the majority present as disseminated, high-tenor sulphides.

3.5.9 Rift Complexities and Exploration Models

Recent research and exploration efforts have revealed a number of discrepancies regarding mineralized intrusion associated with the 1.1 Ga Midcontinent Rift. Geochronological and geochemical analysis have demonstrated that rifting occurred over a period of time longer than previously thought and that associations between units are not well understood (e.g., Hollings et al., 2007, 2010; Heaman et al.,

2007). Primitive melts sourced from deep within the mantle plume are the desired host rock in targeting Ni-Cu-PGE deposits associated with the MCR (Fig. 3.6). An elevated Gd/Yb_n ratio indicating heavy rare-earth element (HREE) fractionation is characteristic of a deep-seated, primitive mantle melt sourced from below the garnet-spinel stablility field (>100 km; e.g. CLIC). Melts from this depth are often fertile having tapped a source potentially enriched in metals. Targeting rocks with this HREE signature is important in targeting potentially mineralized intrusions.

With the exception of the Duluth Complex, MCR-related Ni-Cu-PGE deposits (i.e., Tamarack, Eagle and Thunder Bay North) are older than ~1103 Ma suggesting that mineralized intrusions are emplaced within the early phases of rift development. As such, these units display a reverse paleomagnetic signature as they were emplaced prior to the 1103 Ma magnetic reversal. This allows for the targeting of reversely polarized intrusions using geophysical methods as well as verification by geochronology.
Structural interpretations are important as many of the desired host intrusions appear to be controlled by structures with ultramafic units present at the intersection of faults. These lithospheric scale faults allow for the tapping of deep seated plume material which as mentioned above, is the source for the desired host rock.

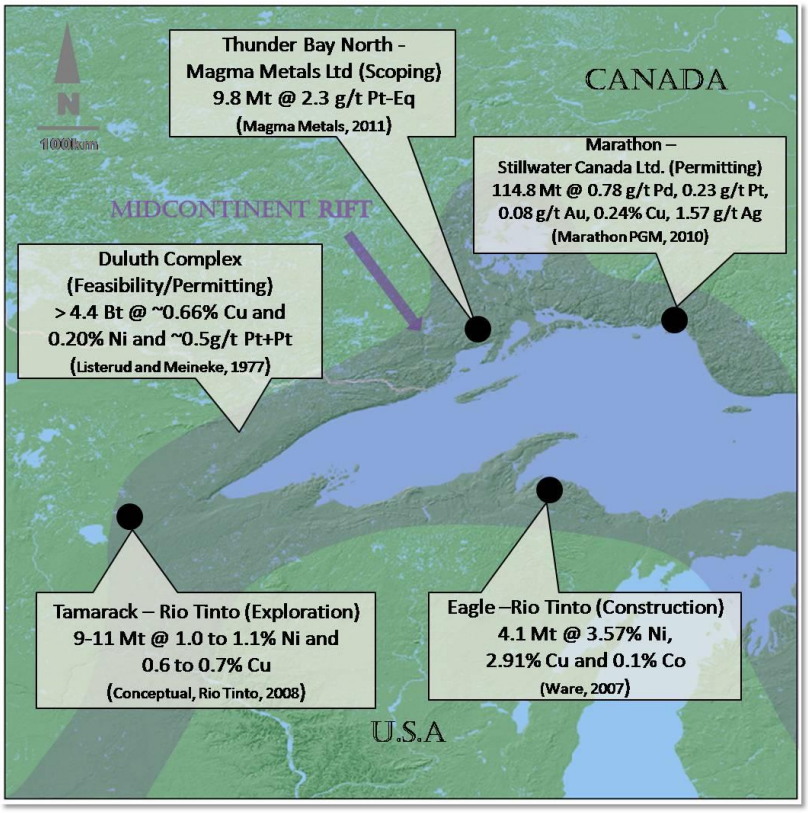

Figure 3.6: Location map of MCR-related Ni-Cu-PGE deposits around the Lake Superior region showing grades and tonnages.

CHAPTER 4
COUBRAN LAKE BASALTS

4.1 Results

4.1.1 Field Observations

Kilometre-scale basaltic xenoliths within Centre II syenites located in the centre of the Coldwell Complex were described by Puskas (1967) and Walker et al. (1993). They have been recently recognized by the staff of Stillwater Canada Incorporated who exposed them in the Geordie–Coubran lakes area during overburden stripping (Fig. 4.1). Basalt is exposed along a thin (3 to 5 m wide) approximately 350 m long stripped area trending roughly west and downslope. The volcanic sequence appears to be draped over the side of a hill with the material representing downslope flows. Large syenite mounds define prominent topographic highs to the northwest, southwest and southeast of the exposure. The basalts exhibit an amygdaloidal texture (Fig. 4.2 A and B) with several ropy flow tops (Fig. 4.3A and B) suggesting subaerial emplacement.

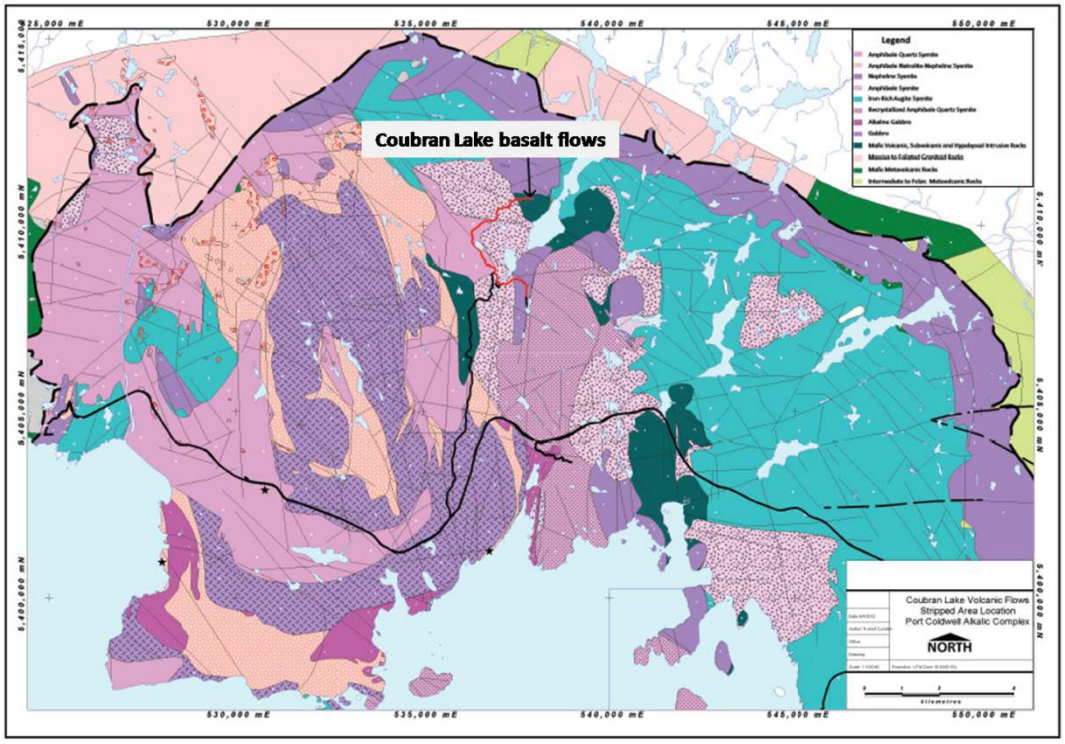

Figure 4.1: Map showing location of the Coubran Lake basalts within the Coldwell Complex (after Walker et al., 1993).

Distinguishing individual flows is difficult in most of the section as flow-top contacts are not always observed. Flow thickness was measured to be approximately 2 m, as determined from the vertical distance between flow tops and assuming flow thicknesses remain consistent for the majority of the sequence. Samples were taken from sites successively lower in the sequence in order to give a true representation of the volcanic pile. The basalt has a chalky white weathered surface, whereas fresh surfaces are dark blue-grey and aphanitic (Fig. 4.4B).

Sample site CL-RC-03 (Fig. 4.5A) shows volcanic material with what appears to be a veneer or reddish staining of alkalic material, likely due to metasomatism. Two ~2m wide syenite dykes are also present within the stripped area, one of which was measured to strike at 270°, with a dip of 60° to the north measured at one locality. The dykes exhibit relatively straight trends, although some undulating contacts were observed, possibly due to the re-heating of the basaltic material, which the syenite intruded. Reaction textures were also observed within the syenite dykes, which appear as wisps of mafic material radiating off the contact (Fig. 4.5B).

Ropy flow tops are evident in three localities within the stripped area. They are characterized as lava toes approximately 30 to 60 cm in length, generally, with no apparent preferred orientation (Fig. 4.3A and B). A contact between a ropy flow top and an overlying flow was noted at one location where the lava immediately above the underlying flow contains relatively large (~2 to 3 cm) amygdules (Fig. 4.3B). Mafic dykes, ranging from 10 to 50 cm in width and commonly displaying thin (<1 cm) chilled margins and plagioclase phenocrysts in their cores, may be feeder dikes to the overlying basalt flows (Fig. 4.4B).

Amygdules within the Coubran Lake basalts generally range in size from 0.2 to 4 cm and are dominantly round, but can also be ovoid in shape, the largest being 30 cm in length. The amygdule-filling assemblage includes quartz, calcite, actinolite, chalcopyrite and malachite. In the amygdaloidal flows near the base of the exposed sequence, there is a gradation from actinolite to calcite ± feldspar over a 20 cm section.

Photo 4.2: A) Ovoid-shaped amygdule infilled with quartz and calcite; location 16U 537785E 5410730N. B) Amygdule infilled with chalcopyrite with malachite rim; location 16U 537885E 5410733N.

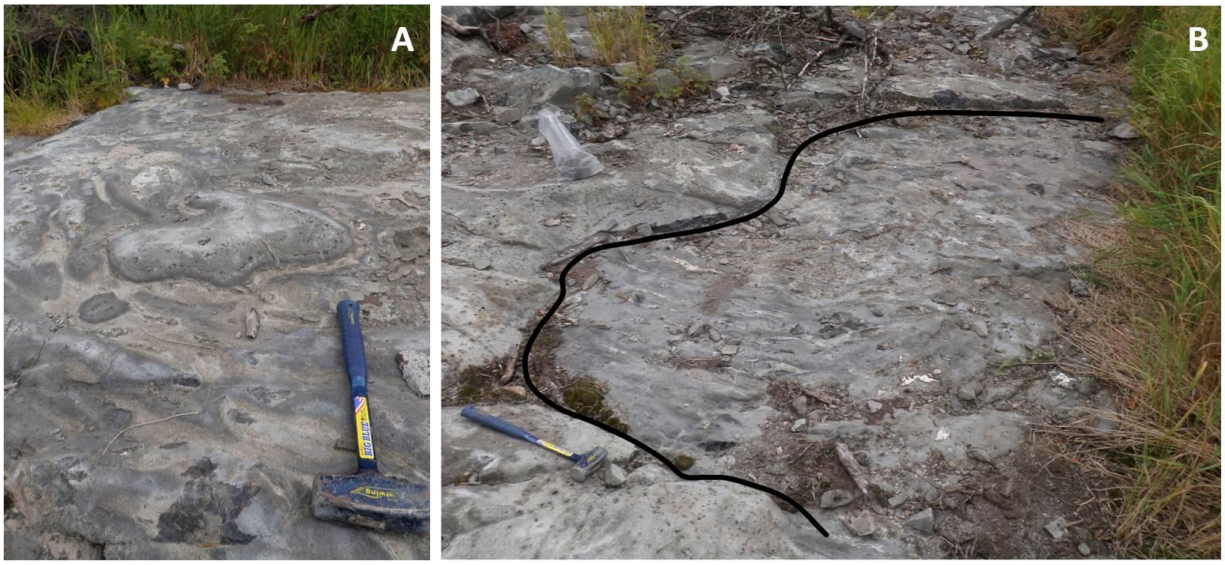

Photo 4.3: A) Ropy flow-top; location 537871E 5410734N. B) Contact (outlined) between ropy flow and overlying flow; location 16U 537885E 5410733N.

Photo 4.4: A) Massive flow showing chalk-white weathered surfaces and dark blue-grey fresh surfaces; location 537933E 5420730N. B) Feeder dike to overlying flow; location 16U 537921E 5410728N.

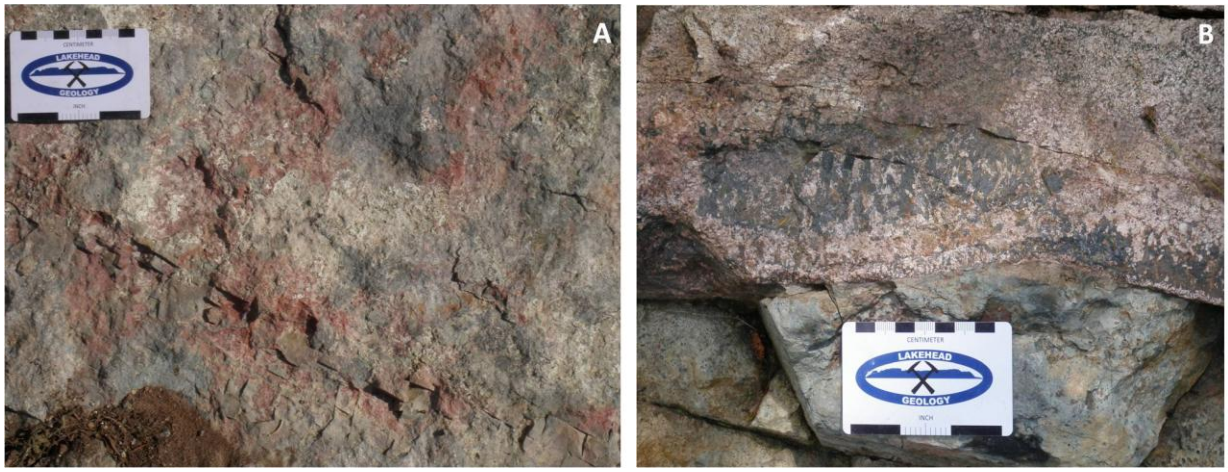

Photo 4.5: A) Metasomatized basalt; location 538017E 5410728N. B) Syenite dyke contact showing reaction rim; location 16U 537715E 5410725N.

4.1.2 Petrography

Petrographic descriptions were completed on select samples throughout the volcanic sequence to characterize the nature of the flows and make inferences into the alteration history. Flows within the unit primarily consist of an intergranular texture with slight grain-size variations observed between samples. Petrographic variations are also observed in the abundance and character of amygdules.

The majority of samples consist of an aphanitic, interstitial volcanic texture with mottled, randomly oriented plagioclase crystals (Fig. 4.6A). Interstitial material is fine-grained hornblende (actinolite) and chlorite, which are likely pseudomorphs of primary augite. Samples taken from thicker, more massive flows display textures similar to the bulk of the unit albeit with slightly larger grain-sizes (Fig. 4.6B). The more massive material displays an intergranular texture with plagioclase laths ranging from approximately 0.4 to 2 mm in length. Interstitial material is again dominanted by pseudomorphic actinolite and chlorite but coarser-grained, relict augite also is present. Brown to black subhedral oxide minerals are present in variable amounts but no greater than 1-2% of the rock. The opaque minerals present are magnetite and altered sulphide phases. An average composition for these rocks is 35-45% plagioclase, 15-20% actinolite, up to 20% chlorite, 2-5% primary augite, with the remainder being made up of variable amounts of quartz (both secondary and infilling amygdules), calcite, olivine and opaques.

Amygdules are present throughout all samples but in variable amounts. They are typically rounded ranging from 1mm up to 2-3cm in diameter and also occur as oblate or elongate blobs. Two major phase relationships are observed within the amgygules. The majority of amygdules are infilled with actinolite which has undergone a variable degree of alteration with more intensely altered actinolite amygdules present in samples taken towards the base of the sequence. Minor calcite was also noted to be associated with actinolite (Fig. 4.7B). Secondly, amygdules are filled with quartz and calcite, with calcite often appearing towards the rim of the amygdules (Fig. 4.7A). Minor epidote was also noted from petrographic observations but only comprised up to 5% of the total in-filling material. Field observations also showed amygdules in-filled with chalcopyrite and associated malachite (Fig. 4.2B) but no thin sections of these were cut. Samples taken towards the base of the sequence (CL-RC-18 and CL-RC-19) had a greater concentration of amygdules in-filled with actinolite compared to those higher in the sequence. Also, a greater degree of alteration is observed in samples taken towards the base of the unit when compared to those higher in the sequence displaying greater degrees of alteration to chlorite after actinolite. In some cases, the actinolite has been altered to biotite, although this was only observed in one instance.

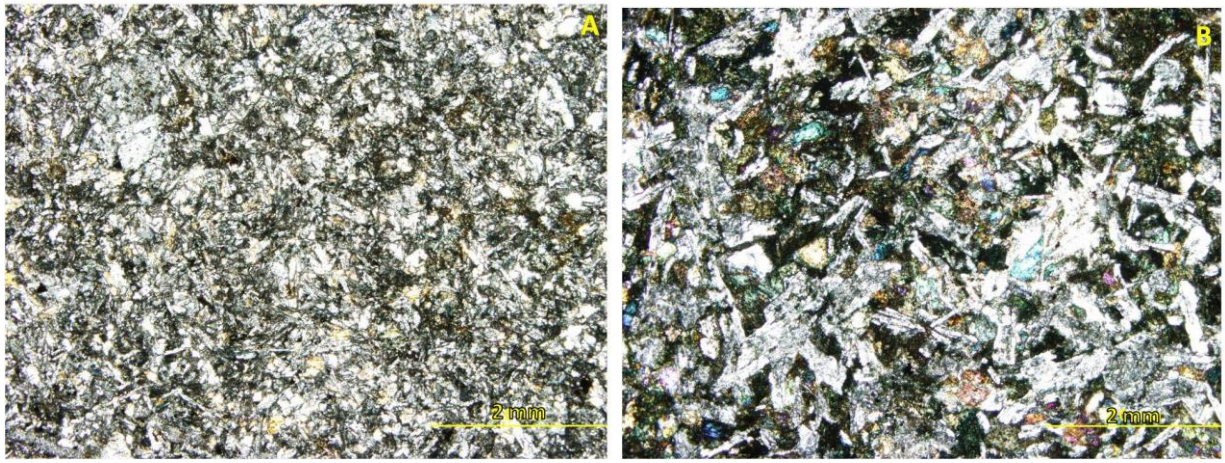

Figure 4.6: A) Sample CL-RC-01 showing typical intergranular, glassy texture. B) Sample CL-RC-06 from a more massive flow showing coarser-grained, intergranular texture. Both photomicrographs in XPL. Scale bar is 2mm.

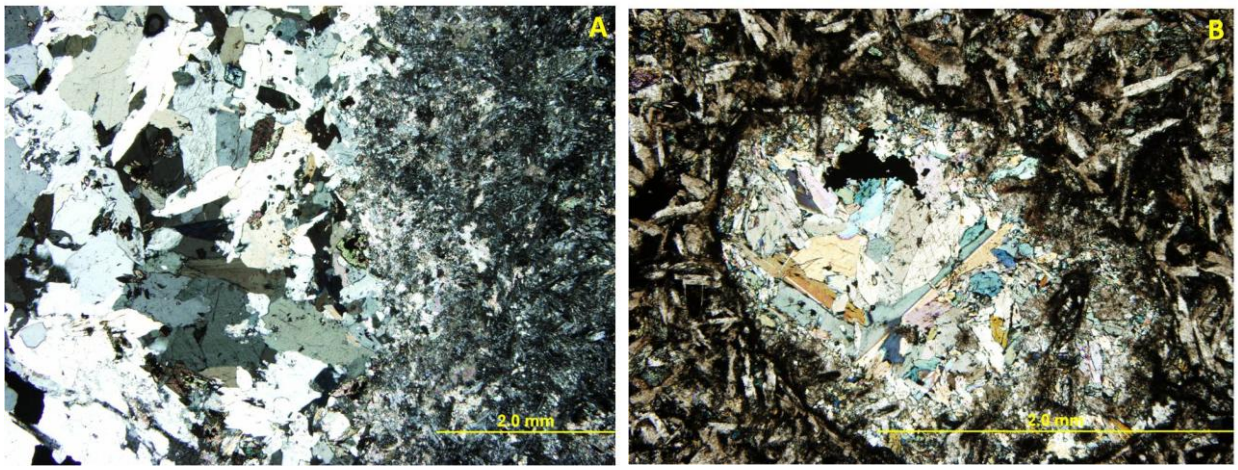

Figure 4.7: A) Edge of pipe-amygdule showing infilling of dominantly quartz with minor calcite and a calcite rim. B) Small 2mm amygdule showing infilling with actinolite and minor opaques and calcite. Both photomicrographs in XPL. Scale bar is 2mm.

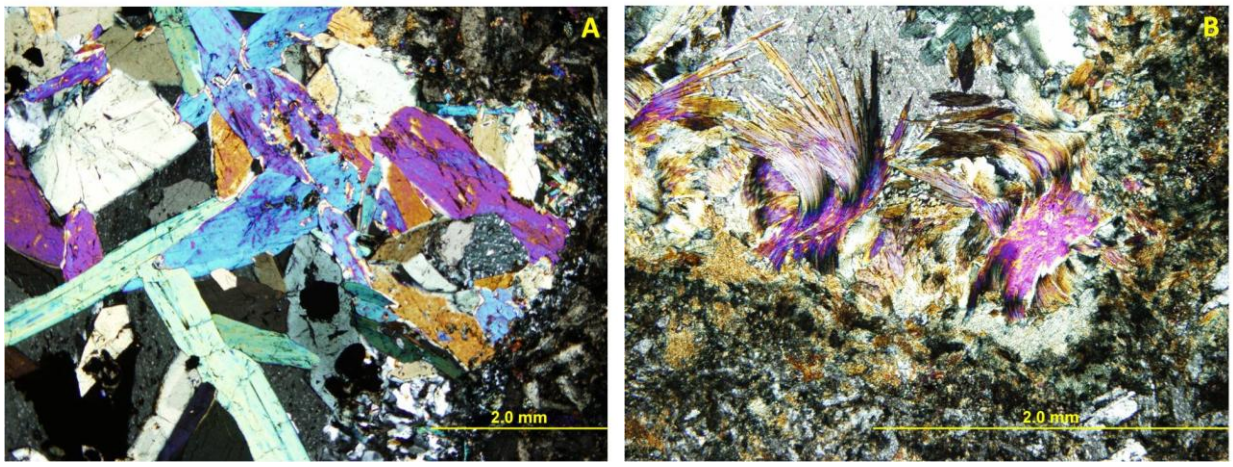

Figure 4.8: A) Amygdule infilled with primary, actinolite. B) amygdule infilled with primary actinolite being altered to chlorite. Sample CL-RC-018. Both photomicrographs in XPL. Scale bar is 2mm.

4.1.3 Whole-rock geochemistry

Nineteen samples were collected during this study. The samples are characterized by slight variation shown in major element chemistry. The suite as a whole showed SiO_2 ranging from 47% to 51%, TiO_2 ranging from 0.78% to 0.99%, MgO ranging from 4% to 7%, and total alkali content (Na_2O+K_2O) ranging from 3% to 5%. When SiO_2 was plotted against total alkali content (Na_2O+K_2O), the suite was shown to comprise three different rock types (Fig. 4.9). The results show the suite to be dominantly composed of basalt with samples with slightly higher alkali content plotting in the trachybasalt to trachyandesite fields (Fig. 4.9). The plot correlating depth within sequence and alkali content showed samples that were taken towards the base of the sequence contained higher alkali content (Fig. 4.10). Samples plotted on an AFM diagram (Na_2O+K_2O versus FeO versus MgO) show the unit to be dominantly calc-alkaline with two samples located in the middle of the sequence showing a tholeiitic nature (Fig. 4.11A). The calc-alkaline nature of the unit is confirmed by trace element data on the plot of LOG Nb/Y versus LOG Zr/Ti where the unit displays a tight population in the alkali basalt field (Fig. 4.11B).

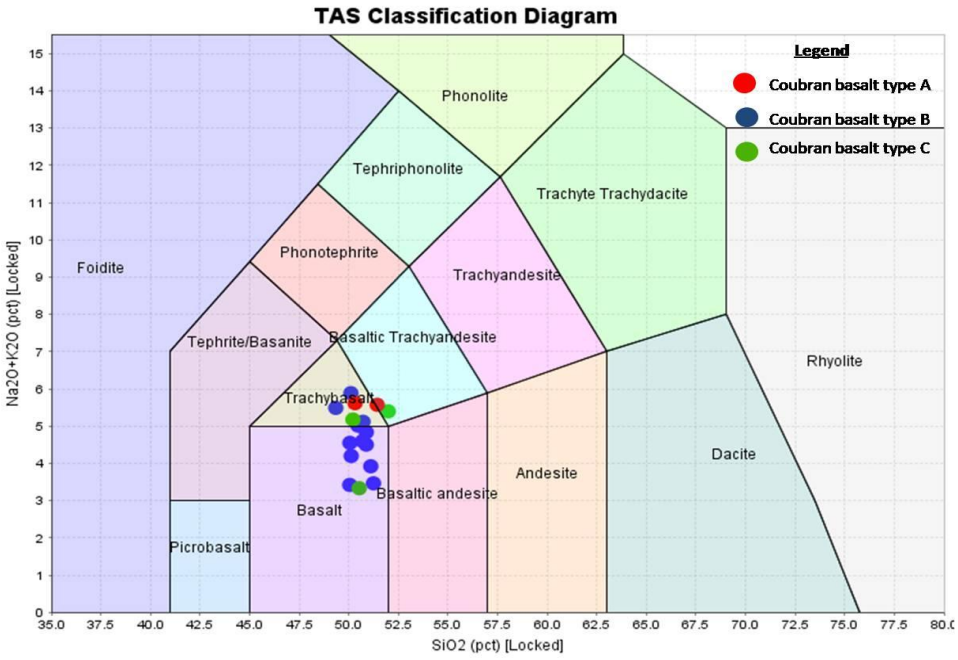

Figure 4.9: Silica versus total alkali diagram showing classification of the Coubran Lake basalts. Source of fields is Le Maitre et al. (1989).

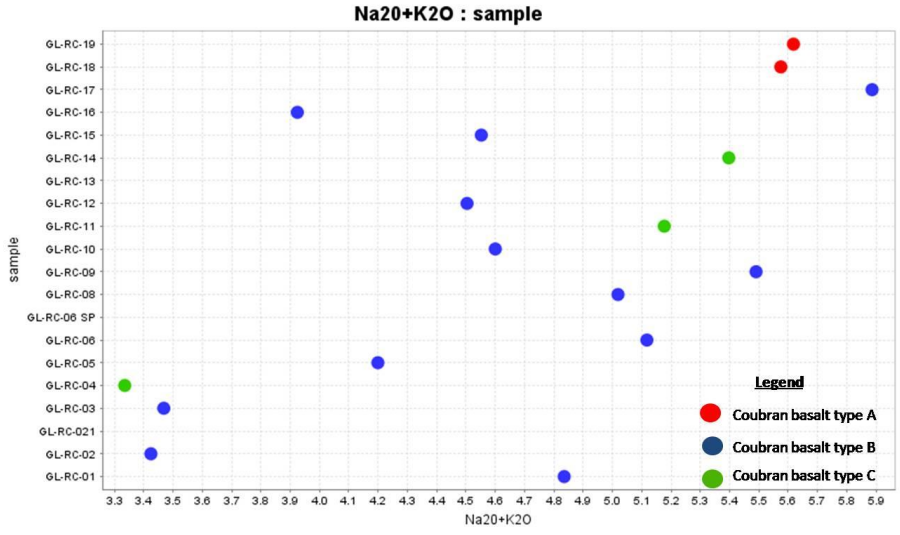

Figure 4.10: Total alkali content versus sample number. Higher numbered samples correlate to lower elevation (i.e., down stratigraphy).

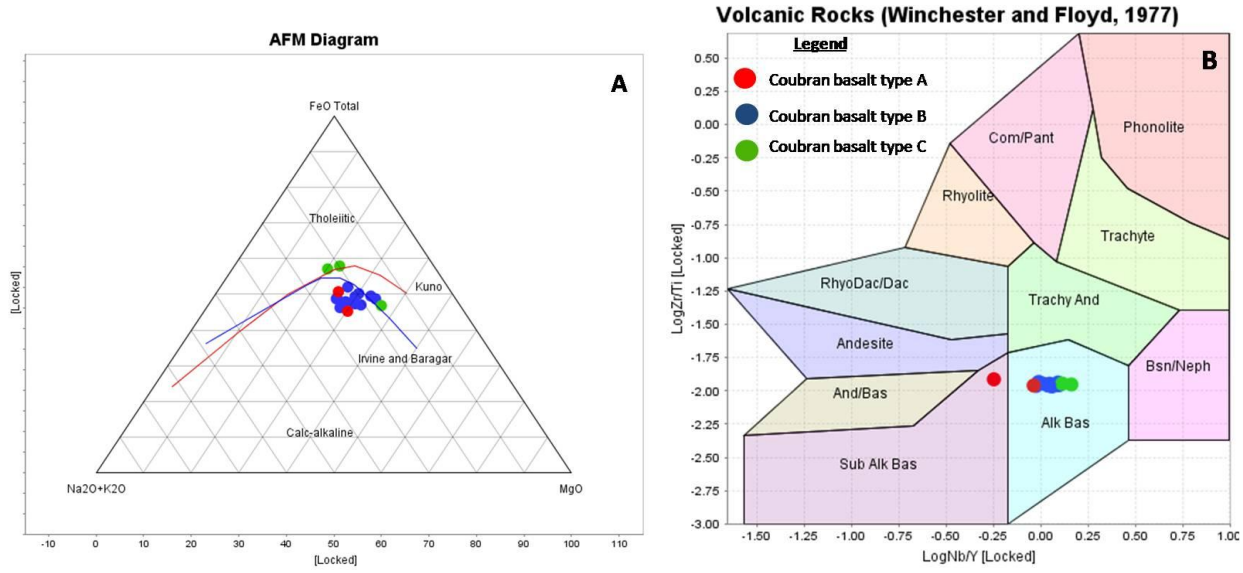

Figure 4.11: A) AFM diagram showing the dominantly calc-alkaline nature of the Coubran Lake basalts (division lines that of Irvine and Baragar (1971) and Kuno (1969); B) Winchester and Floyd (1977) diagram classifying the unit as alkaline based on trace element data.

The unit is comprised of three groups (types A, B, and C) distinguished by their incompatible element abundances displayed on primitive mantle normalized spider plots (Fig. 4.12). The distribution of basalt type A, B and C through stratigraphy is displayed in a cross-section Figure 4.13. The distribution of samples through the mapped exposure with primitive mantle normalized spider plots for each individual sample is shown is Figure 4.14.

Basalt type A lies towards the base of the unit, forming the lowermost 10% of the exposed sequence and displays strong light rare-earth element (LREE) enrichment (La/Sm_n 7.4 to 9.3) with heavy rare-earth element (HREE) ratios comparable to types B and C (Gd/Yb_n = 2.4 to 2.5). Rocks of this type are distinguishable from basalt types B and C by the pronounced enrichment in LREE (La, Ce, Pr , and Nd). Basalt type B dominates the succession and displays LREE enrichment (La/Sm_n = 2.4 to 4.7) and HREE fractionation (Gd/Yb_n = 1.9 to 2.3) totalling eleven samples through the sequence. Rocks of this type display LREE enrichment as well as pronounced high field-strength element (HFSE) anomalies displayed by relatively lower abundances of Nb, Zr, Hf, Ti, V and Sc. Basalt type C comprises only three samples sporadically located through the sequence. It displays LREE enrichment (La/Sm_n = 1.9 to 2.9) and HREE fractionation (Gd/Yb_n = 1.9 to 2.1). It is distinguishable from basalt type A and B based by the absence of a negative Nb anomaly and alternatively lower abundances of LREE (La and Ce). Also, samples, CL-RC-

11 and CL-RC-14 display the lowest magnesium numbers of all samples with values of 27.7 and 26.0 weight %, respectively. No appreciable geochemical differences were observed between the feeder dykes present in the sequence (Fig. 4.4) and overlying flows.

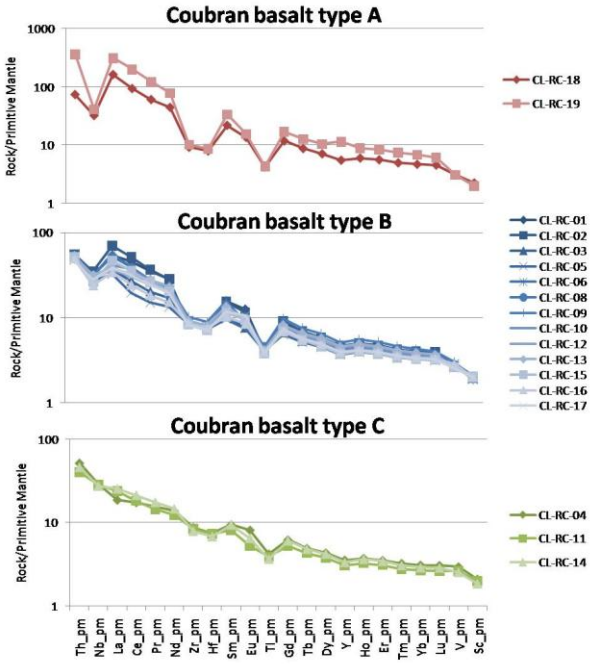

Figure 4.12: Primitive-mantle normalized spider plots showing Coubran Lake basalts type A, B and C. Normalizing values from Sun and McDonough (1989).

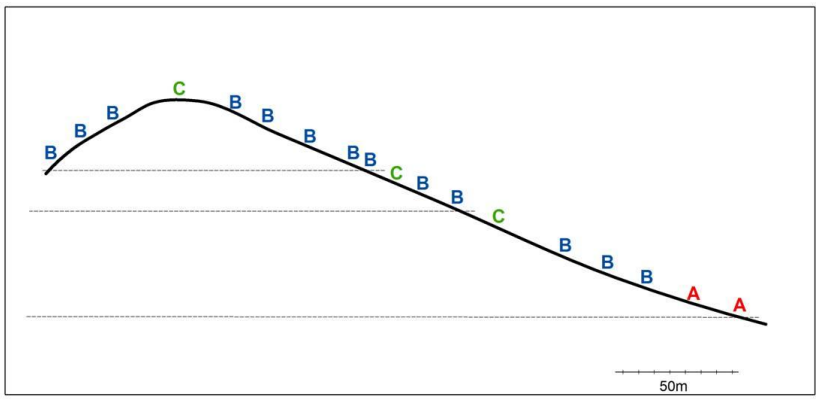

Figure 4.13: Generalized cross-section showing the distribution of basalt types through stratigraphy. Elevation enhanced to approximately 2x vertical exaggeration. View facing south.

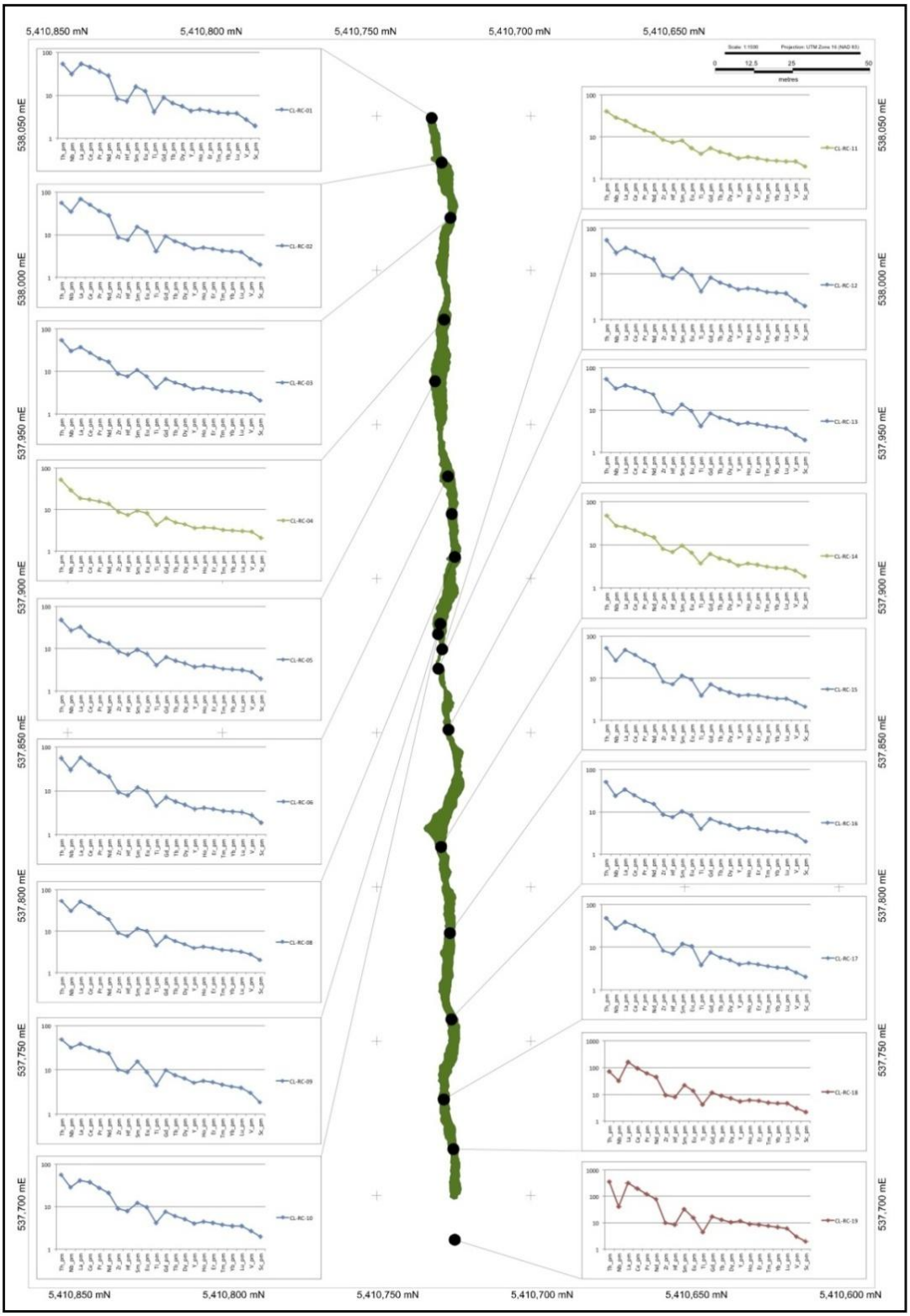

Figure 4.14: Primitive-mantle normalized spider plots showing Coubran Lake basalts through the sequence. Basalt type A = red, B = blue and C = green. Normalizing values from Sun and McDonough (1989).

4.1.4 Isotope results

Isotopic analyses were carried out on six samples from the Coubran Lake basalts. Samples were chosen to represent each of the three basalt types recognized by trace element chemistry; one sample from Basalt type A, one sample from basalt type B and four samples from basalt type C. The results of the isotope analyses are summarized in Table 4.1. All six samples show very similar $\varepsilon_{Nd(t=1100Ma)}$ values ranging from -0.5 to -1.0 with an average of -0.8. Plotting all six samples on a $^{143}Nd/^{144}Nd$ versus $^{87}Sr/^{86}Sr_i$ graph shows a negative slope with higher $^{143}Nd/^{144}Nd$ values correlating with lower $^{87}Sr/^{86}Sr_i$ values (Fig. 4.15). The basalts show a positive correlation between $\varepsilon_{Nd(t=1000Ma)}$ and $^{87}Sr/^{86}Sr_i$ (Fig. 4.16) with samples displaying more negative $\varepsilon_{Nd(t=1100Ma)}$ having lower $^{87}Sr/^{86}Sr_i$ values.

Table 4.1 Summary of isotope data for the Coubran Lake basalts.

Sample	**Basalt type**	**$\varepsilon_{Nd(t=1100Ma)}$**	**$^{87}Sr/^{86}Sr_i$**	**$^{143}Nd/^{144}Nd$**
CL-RC-01	B	-0.7	0.70442	0.511958
CL-RC-04	C	-0.9	0.70407	0.512139
CL-RC-09	B	-0.9	0.70386	0.512119
CL-RC-13	B	-0.7	0.70387	0.512020
CL-RC-17	B	-1.0	0.70356	0.512020
CL-RC-019	A	-0.5	0.70484	0.511799

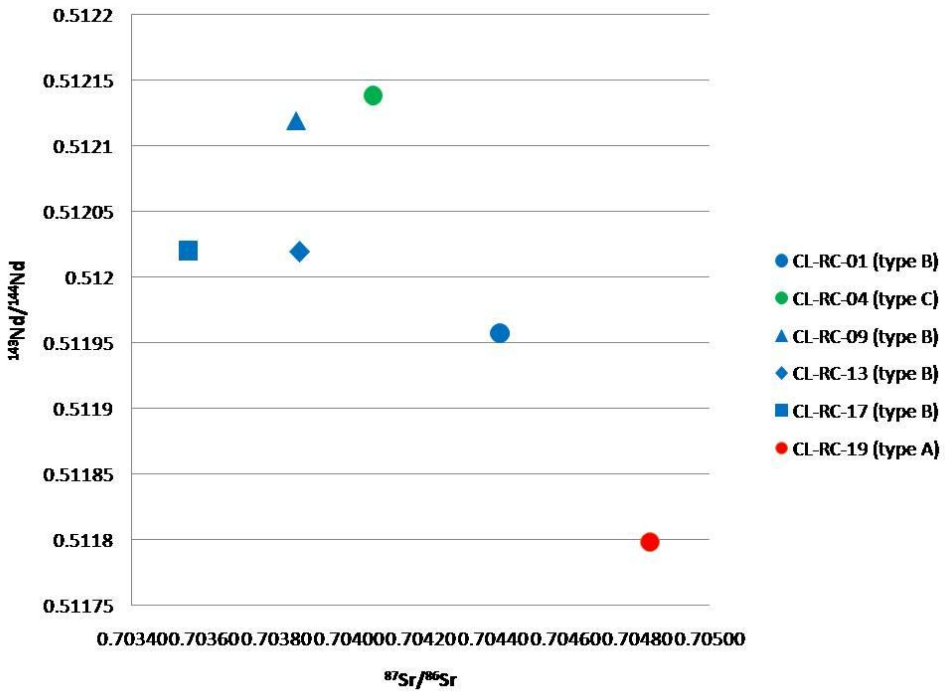

Figure 4.15: $^{87}Sr/^{86}Sr$ versus $^{143}Nd/^{144}Nd$ for the Coubran Lake basalts.

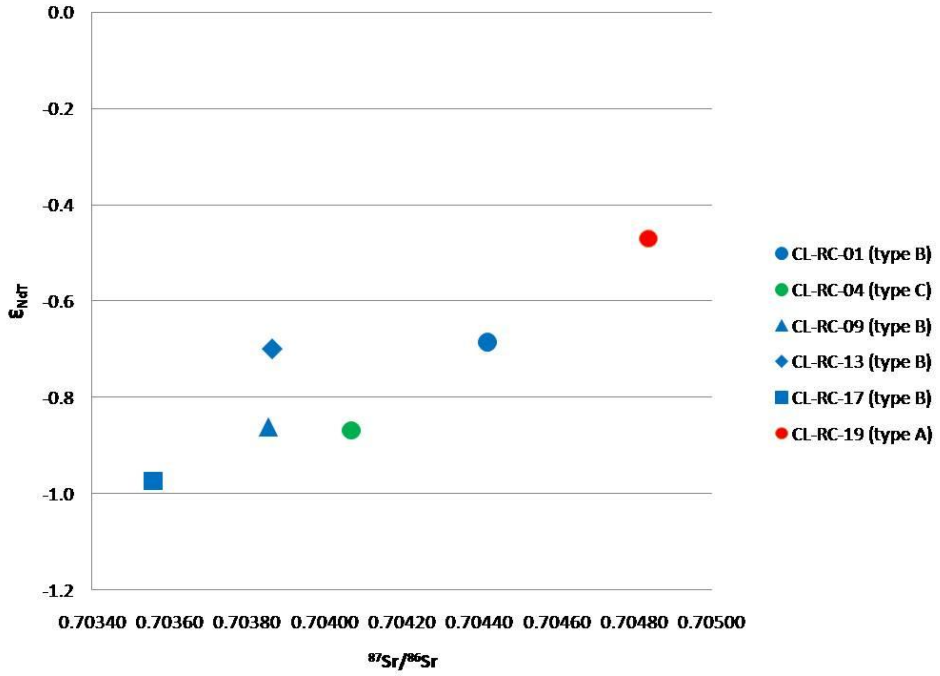

Figure 4.16: $^{87}Sr/^{86}Sr$ versus $\varepsilon_{Nd(t=1100Ma)}$ for the Coubran Lake basalts.

4.2 Discussion

4.2.1 Coubran Lake basalts as a roof pendant

The Coubran Lake roof pendant was first described by Puskas (1967) as being an extensive and centrally located metavolcanic roof pendant within the Coldwell complex. Puskas (1967) further noted that although many of the topographic highs throughout the Coldwell complex are capped by volcanic flows, the feldspathoidal syenites which occur in proximity to the Coubran Lake roof pendant consistently exhibit the highest elevations. The locality of the Coubran Lake roof pendant (hence forth referred to as the Coubran Lake basalts), as observed from field work in this study, confirms this association as the volcanic flows are situated at a lower elevation than the surrounding syenite. This implies that the Coubran Lake basalts were suspended in the magma chamber while intrusive syenite crystallized around it. No structural evidence suggests the volcanic block has shifted. The melting temperatures of basalt relative to that of syenite is consistent with this theory, as rocks of a typical basaltic composition melt at temperatures in excess of 1000°C whereas rocks of a typical syenitic composition typically melt at <1000 °C (Winter, 2001). This data suggest that it is plausible that the volcanic block was suspended in the magma without being completely destroyed. This association is further confirmed by the presence of syenite dykes within the volcanic flows denoting a timing relationship whereby indicating that the syenites are younger than the basalts.

Alkali alteration is present throughout the unit but is relatively more intense towards the base of the volcanic sequence in samples proximal to the underlying syenites. This can be explained by fluids radiating off the alkalic magma chamber altering the lower most flows in the sequence relative to the upper flows as denoted by the relative increase in abundance of alkali elements (Na_2O and K_2O) present in the lowermost samples (Fig. 4.10). Petrography also confirms this as the lowermost samples contain higher amounts of chloritized actinolite when compared to those higher up in the sequence.

The same alteration signatures should theoretically be present towards the top of the sequence if the volcanic block was in fact completely enveloped in the magma chamber with the top of the sequence covered. This is not consistent with the alteration signatures present throughout the sequence as the strongly altered material is only present towards the base. It is possible that the top of the volcanic sequence has been eroded away leaving only the middle to the base of the volcanic sequence preserved although, no direct field evidence confirms this.

4.2.2 Characterization of the Coubran Lake basalts

Based on major element analysis, the Coubran Lake volcanic rocks are dominantly basaltic with a few samples containing more alkali content ranging into the trachybasalt field (Fig. 4.9). The samples classified as trachybasalts are located towards the base of the sequence, proximal to the underlying syenites. The higher alkali content of the basal samples is attributed to alteration by alkali-rich fluids radiating off the intruding syenite. Based on AFM classification, the unit is dominantly calc-alkaline with only two samples ranging into the tholeiitic realm (Fig. 4.11a). Trace element chemistry shows the unit to dominantly be comprised of alkali basalt with only one sample plotting within the sub-alkali field (Fig. 411b). As trace element classifications are more reliable being impartial to alteration by fluids, the Coubran Lake basalts are likely to be inherently alkali basalts.

The REE geochemistry exhibits a relatively high abundance of incompatible elements with variable degrees of enrichment in LREE between basalt types and consistent, moderate HREE fractionation throughout the unit. The overall enrichment indicated by the negative trend of the primitive-mantle normalized patterns is comparable to many Keweenawan Midcontinent rift-related rocks, and similar to modern Ocean-Island Basalts of Hawaii, albeit at lower absolute abundances. The relatively lower trace element abundances may be a result of having formed from higher degrees of melting than typical OIB or variations in the composition of the source region (Hollings et al., 2007a). Nicholson and Shirey (1990) suggest that the main volume of rift basalt was produced from an enriched mantle plume with a chondrite-normalized La/Sm_n of 2 to 3. This is broadly consistent with the signature of the Coubran Lake basalts as the majority of samples lie within this range. Therefore, it is likely that the Coubran Lake basalts are in fact related to the Keweenawan Midcontinent Rift.

The Coubran Lake basalts exhibit slight negative $\varepsilon_{Nd(t=1100Ma)}$ values with an average of -0.8 calculated from six samples from all three basalt types. Furthermore, the Coubran Lake basalts exhibit consistent $\varepsilon_{Nd(t=1100Ma)}$ values throughout the sequence with little or no variation present between basalt type A, B and C. At 1100 Ma, depleted mantle would have had a positive ε_{Nd} up to a value of around +6 while an enriched plume source would have had an ε_{Nd} value less than that of depleted mantle (Nicholson and Shirey, 1990; Shirey et al., 1994). Based on the classification of Midcontinent Rift-related basalts by Nicholson et al. (1997), the slightly negative $\varepsilon_{Nd(t=1100Ma)}$ values of the Coubran Lake basalts suggest that they were derived from a plume source with possible interaction with the continental lithospheric mantle imparting the slightly negative $\varepsilon_{Nd(t=1100Ma)}$ on the rocks.

The variations present between the three basalt types comprising the Coubran Lake basalts is dominantly based on variable LREE enrichment signatures which conversely highlight negative HFSE anomalies. All

samples analyzed through the sequence, with the exception of basalt type C, display prominent negative HFSE anomalies. The negative Zr and Hf anomalies in basalt type C are obscured by the lower abundances of La, Ce, Pr and Nd but display relatively similar abundances of Nb, Zr, Hf, Sc and Ti to the other two basalt types.

The variable LREE enrichment observed through basalt type A, B and C may be attributed to variable degrees of contamination by Archean crustal rocks. Basalt type A is characterized by elevated Th values as well as the highest $^{87}Sr/^{86}Sr_i$ values, the former of which may be attributed to contamination by Archean crust. However, contamination by Archean crust is not supported by the Nd isotope data as all three basalt types display broadly similar $\varepsilon_{Nd(t=1000Ma)}$ values (-0.5 to -1.0). Vervoot and Green (1997) calculated that Archean tonalite-trondhjemite-granodiorite (TTG) suite underlying the MCR would have a $\varepsilon_{Nd(t=1100Ma)}$ values of -18 to -13. If LREE enrichment signatures (i.e. Th) are to be attributed to a greater degree of crustal contamination by an Archean crustal contaminant, one would expect to see more negative $\varepsilon_{Nd(t=1100Ma)}$ values in conjunction with LREE enrichment (e.g. Nicholson et al., 1997; Hollings et al., 2007b). As the LREE enrichment of basalt type A is not consistent with more negative $\varepsilon_{Nd(t=1100Ma)}$ values, the extreme LREE enrichment displayed by basalt type A cannot be attributed to contamination by Archean crustal rocks. Furthermore, it is likely that all three Coubran Lake basalt types experienced roughly the same, minor degree of crustal contamination by an Archean crustal source as denoted by their nearly homogenous $\varepsilon_{Nd(t=1100Ma)}$ values.

There is a correlation between the Sr and Nd isotope data with more negative $\varepsilon_{Nd(t=1100Ma)}$ correlating with lower $^{87}Sr/^{86}Sr_i$ values (Fig. 4.16). Conversely, the least negative $\varepsilon_{Nd(t=1100Ma)}$ values correlate to higher $^{87}Sr/^{86}Sr_i$ values as well as elevated Th abundances. Basalt type A, as represented by sample CL-RC-019, shows the highest $^{87}Sr/^{86}Sr_i$ as well as elevated Th values. It is therefore likely that the elevated Th and $^{87}Sr/^{86}Sr_i$ signatures displayed by basalt type A may be attributed to a contaminant with elevated Th and $^{87}Sr/^{86}Sr_i$ signatures albeit with a positive $\varepsilon_{Nd(t=1100Ma)}$ signature. No Sr isotope data is available for the underlying mafic volcanic rocks of the Archean Schreiber-Hemlo greenstone belt into which the Coldwell Complex intrudes. Positive $\varepsilon_{Nd(t=1000Ma)}$ signatures have been reported for Wabigoon Subprovince mafic volcanic rocks to north by Tomlinson et al. (2003) which may serve as an anologue for the underlying mafic volcanic rocks of the Schreiber-Hemlo greenstone belt. Unfortunately, no Sr isotope data is available for the Wabigoon rocks making this inference speculative.

Alternatively, the variable LREE enrichment signatures may be due to a phase concentrating Th and other LREE. Data from the Eastern gabbro in the Coldwell Complex has shown correlation between apatite and LREE and Th with concentrations of apatite controlling elevated LREE and Th abundances (Good, pers.

comm. 2011). Middle rare-earth elements (MREE) have a high partition coefficient for apatite (Rollinson, 1993). The relationship between MREE and apatite can be display on the plot of Gd versus P_2O_5 with MREE represented by Gd with apatite represented by P_2O_5 (Fig. 4.17). Data presented here shows a positive correlation between Gd and P_2O_5 suggesting that apatite maybe controlling Gd. The data also shows increased P_2O_5 in some samples suggesting an increased amount of apatite in those samples. The plot of Th versus P_2O_5 does not show any discernable correlation between Th and P_2O_5 suggesting that apatite is not controlling LREE enrichment in the Coubran Lake basalts.

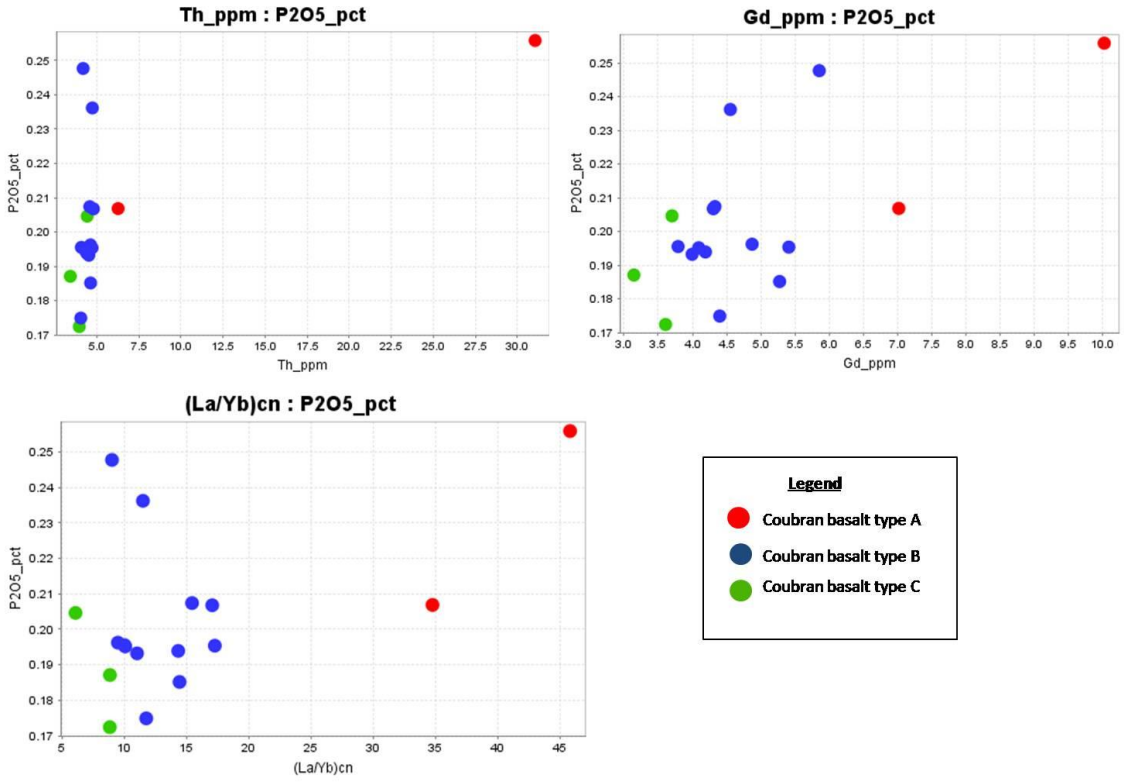

Figure 4.17: Variation diagrams showing control of apatite (P_2O_5) on elements and element ratios.

The strong Th enrichment present in basalt type A may be attributed to a greater abundance of hornblende in those samples. Th has a partition coefficient of 0.50 for hornblende compared to 0.03 for clinopyroxene and 0.10 for plagioclase (Fujimaki et al., 1984). The abundance of amygdules in-filled with hornblende towards the base of the sequence may explain the elevated Th abundances present in those samples. Furthermore, Rollinson (1993) states that the presence of hornblende in felsic liquids may account for extreme LREE enrichment relative to HREE. Although the Coubran Lake basalts were derived from a mafic liquid, the same principle can be applied.

4.2.3 Coubran Lake basalts within the context of the Coldwell Complex

As the Coubran Lake basalts lie within the centre of the Coldwell Complex (Fig. 4.1), it is likely that there is a genetic relationship with the mafic intrusive units that lie in the outer eastern ring (the Two Duck Lake gabbro) or in the centre of the complex (the Geordie Lake gabbro).

The Coubran Lake basalts exhibit very similar trace element patterns to those of the Two Duck Lake Gabbro (Fig. 4.18). The trace element pattern is characterized by strong LREE enrichment and moderate HREE fractionation as well as negative HFSE anomalies (Zr, Hf, and Ti). The Coubran Lake basalts exhibit similar abundances of Zr, Th and Nb to the Two Duck Lake Gabbro. This relationship is displayed in Figure 4.17 whereby relative abundances of Zr, Th and Nb are similar between the Coubran Lake basalts and the Two Duck Lake gabbro. The similar trace element abundances of the Two Duck Lake gabbro and the Coubran Lake basalts suggests the two units may be derived from the same source. Conversely, the higher abundances Zr, Th and Nb for the Geordie Lake gabbro compared to the Coubran Lake basalts implies the two units are not co-genetic.

All samples analyzed for the Coubran Lake basalts display prominent negative Ti and V anomalies. Ti and V are controlled by the fractionation of magnetite as it displays a partition coefficient of 7.5 for Ti and 26.0 for V (Rollinson, 1993). This may give weight to a genetic relationship with the Two Duck Lake Gabbro as the TDL gabbro contains massive magnetite which may account for the lack of magnetite in the Coubran Lake basalts. The magnetite may have fractionated out of the system and emplaced within the Two Duck Lake gabbro prior to the emplacement of the Coubran Lake basalts. The Two Duck Lake gabbro data presented here were reported by Good (1993) to contain no massive magnetite.

The plot of La/Sm_{cn} versus Gd/Yb_{cn} also shows similarities which further suggest a genetic relationship between the Coubran Lake basalts and the Two Duck Lake gabbro (Fig. 4.18). The majority of samples from the Coubran Lake basalts exhibit a La/Sm_{cn} ratio of 2.0 to 4.0, which the exception of basalts type A which have likely undergone significantly more crustal contamination than the majority of the sequence. Samples presented here from the Two Duck Lake gabbro show La/Sm_{cn} values within the same range implying that melts from which these two units largely underwent the same degree of crustal contamination. Alternatively, La/Sm_{cn} ratios may be explained by partial melting suggesting that the Two Duck Lake gabbro and the Coubran Lake basalts underwent the same degree of partial melting. The Gd/Yb_{cn} ratio for the Two Duck Lake gabbro shows a broad range between 2.37 and 4.63 whereas the Coubran Lake basalts display a tighter range between 1.96 and 2.52 with sample F31 from the Two Duck Lake gabbro plotting within the Coubran Lake field. Genetically, this could represent a progressively shallower depth of melting through the emplacement of the Two Duck Lake Gabbro denoted by a less

fractionated HREE signature (i.e., lower Gd/Yb_{cn} ratio) through time. As depth of melting became shallower, it is plausible that the depth of emplacement became shallower as well, resulting in a volcanic expression of the intrusive rocks of the Two Duck Lake gabbro manifested by the Coubran Lake Basalts. Thus, based on geochemical evidence, it is proposed that the Coubran Lake basalts represent the volcanic expression of the Two Duck Lake gabbro.

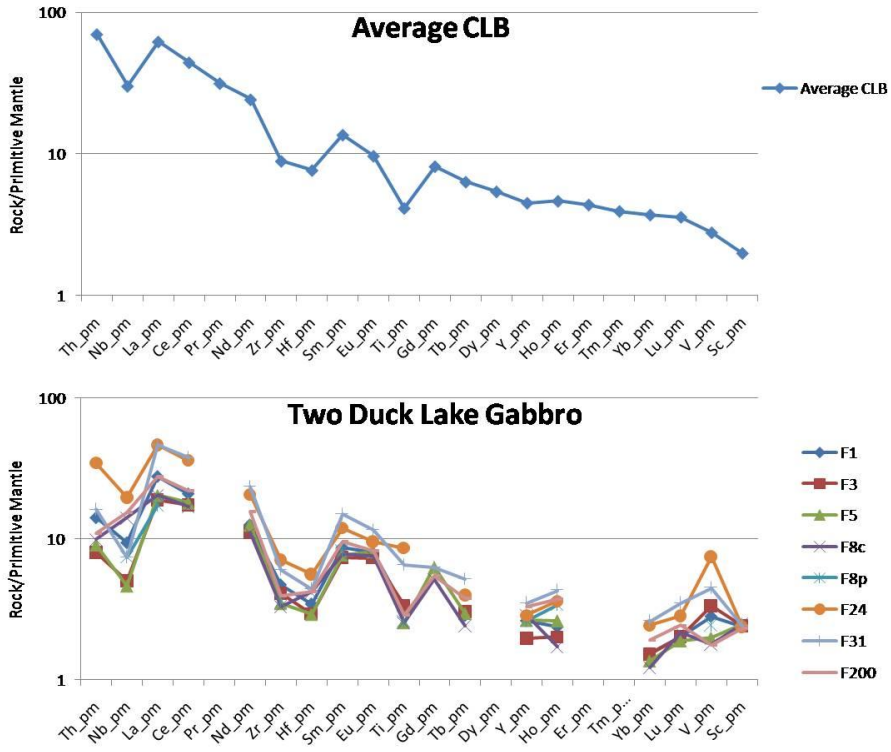

Figure 4.18: Primitive Mantle normalized plots showing average composition for the Coubran Lake Basalts (n=18; types A, B, and C) and the Two Duck Lake Gabbro. Two Duck Lake gabbro data from Good (1993), normalizing values from Sun and McDonough (1989).

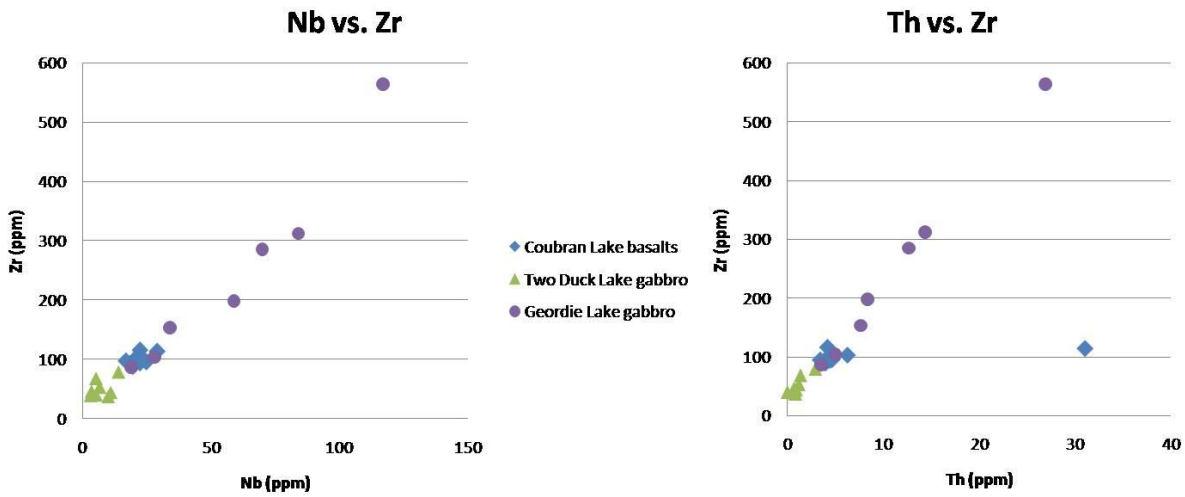

Figure 4.19: Plots of Nb vs. Zr and Th vs. Zr. Comparative data from Good (1993).

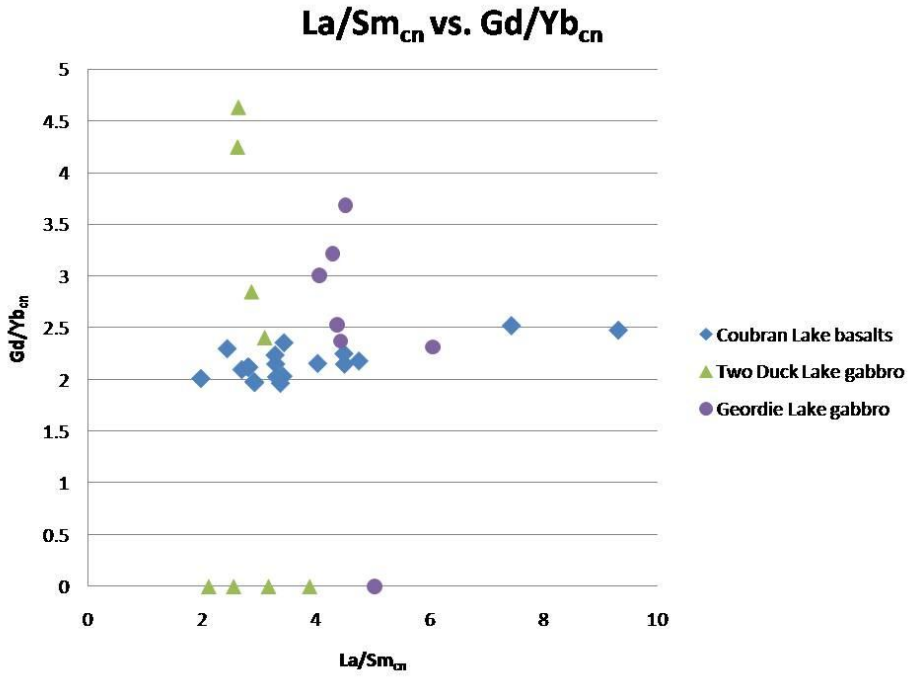

Figure 4.20: Plot of La/Sm_{cn} vs. Gd/Yb_{cn}. Comparative data from Good (1993), normalizing values from Sun and McDonough (1989).

4.2.4 Coubran Lake basalts within the context of the MCR

The Coubran Lake basalts exhibit an OIB-like primitive mantle normalized pattern akin to that of the majority of Midcontinent Rift-related rocks, it is likely that the unit is in fact related to the 1.1 Ga Keweenawan MCR. As such, it is imperative to place the unit in context with the system as a whole. Volcanic expressions of the MCR are sporadic along the north shore of Lake Superior with the Mamainse Point and Michipicoten volcanics northwest of Sault Ste. Marie, the Osler volcanics near Rossport and the Devon Volcanic outlier south of Thunder Bay representing the only recognized extrusive units. As such, there is a significant spatial gap between the Osler Group and the Mamainse Point volcanics. The Coubran Lake basalts provide a volcanic expression of the Midcontinent Rift which infills that gap and contributes to a more complete volcanic record of MCR-related volcanism north of Lake Superior.

Hollings et al. (2007c) noted high MgO, Ni and Cr indicative of the most primitive end members of the Osler Group present in the lower sequence on Vein and Wilson islands with ε_{Nd} values close to zero. Up section, the Osler basalts were characterized by lower MgO, Ni and Cr but higher SiO_2, Th and La/Sm_n with increasingly negative Nb and Ti anomalies and ε_{Nd} of -4 to -5. This trend was attributed to contamination of the central and upper sequences of basalts by an older lithospheric component characterized by significant LREE enrichment and high Th abundances but generally unfractionated HREE (Hollings et al., 2007c).

When comparing geochemical variations through stratigraphy within the Coubran Lake basalts to those observed in the Osler group, rocks displaying trends similar to those present in the lower suite are found. The lower-most flows in the Coubran Lake basalts (basalt type A) exhibit significantly greater LREE enrichment and high Th abundances than those in the upper flows. This may be attributed to the lower most flows being contaminated by an older lithospheric component, as outlined above. Shirey et al. (1994) and Nicholson et al. (1997) suggest that the earliest basaltic magmas underwent little interaction with the crust, whereas later magmas were forced to pond at the base of the crust thus assimilating crustal material. Lightfoot et al. (1991) inferred the lower suite to be sourced from an enriched asthenospheric upper mantle source distinct to those of the central and upper suites, which were sourced from a more depleted source contaminated with continental crust. Data from Hollings et al. (2007c) shows that sequences from Vein and Wilson islands below 400 m are comparable to those from the lower suite and samples above 400 m are similar to those from the central suite. Data presented here show the Coubran Lake basalts have similar geochemical trends and crustal contamination histories to those of the lower suite of the Osler group. Therefore it is suggested that the magmas forming the Coubran Lake basalts are

genetically similar to those of the lower suite of the Osler group having formed from a depleted mantle source slightly enriched in continental crustal material.

Nicholson et al. (1997) explains basalt type I melts are among the earliest preserved MCR-related volcanic rocks around Lake Superior erupted during the first phase of volcanism (>1105 Ma). These melts are manifested by the Lower Siemens Creek volcanics, the basal units in the Ely's Peak and Grand Portage areas of the North Shore Volcanics, and as the lower suite of the Osler Group. When comparing primitive mantle normalized plots of the Coubran Lake basalts to the average basalt type I composition (Fig. 4.21), they display broadly similar trends with LREE enrichment, moderate HREE fractionation. The only discrepancy with this association is the Coubran Lake basalts exhibit a negative Nb anomaly which may be attributed to the abundance of hornblende in the rocks most notably Coubran Lake basalt type A, as outlined above. Coubran Lake basalt type C does not display a negative Nb anomaly supporting a basalt type I composition. Furthermore, Basalt type I exhibits $\varepsilon_{Nd(1100Ma)}$ values of -0.7 to 0.7 with an average of -0.1 (n=10 samples). This supports the Coubran Lake basalts as being akin to basalt type I as they exhibit $\varepsilon_{Nd(1100Ma)}$ values ranging from -0.5 to -1.0 with an average of -0.8 with the slightly more negative values of some Coubran Lake basalt samples being attributed to slightly greater degrees of crustal contamination.

Kulakov et al. (2012) defined a reversed (R) polarity magnetization for the Coubran Lake basalts suggesting that they represent the earliest stage of Midcontinent rift-related volcanic activity. They report that the mean paleomagentic directions for the Coubran Lake basalts are statistically similar to those published for the reversely magnetized Lower North Shore Volcanics dated at 1107 ± 1.9 Ma (Halls and Pesonen, 1982; Davis and Green, 1997). This is consistent with the geochemical findings presented here as the basalt type I rocks are among the earliest volcanic products of the Midcontinent rift erupted between 1108 and 1105 and consistently display a reversed polarity (Nicholson et al., 1997). Therefore, based on geochemical and paleomagnetic evidence, it is proposed that the Coubran Lake basalts are classified as basalt type I based on the geochemical classification of Nicholson et al. (1997).

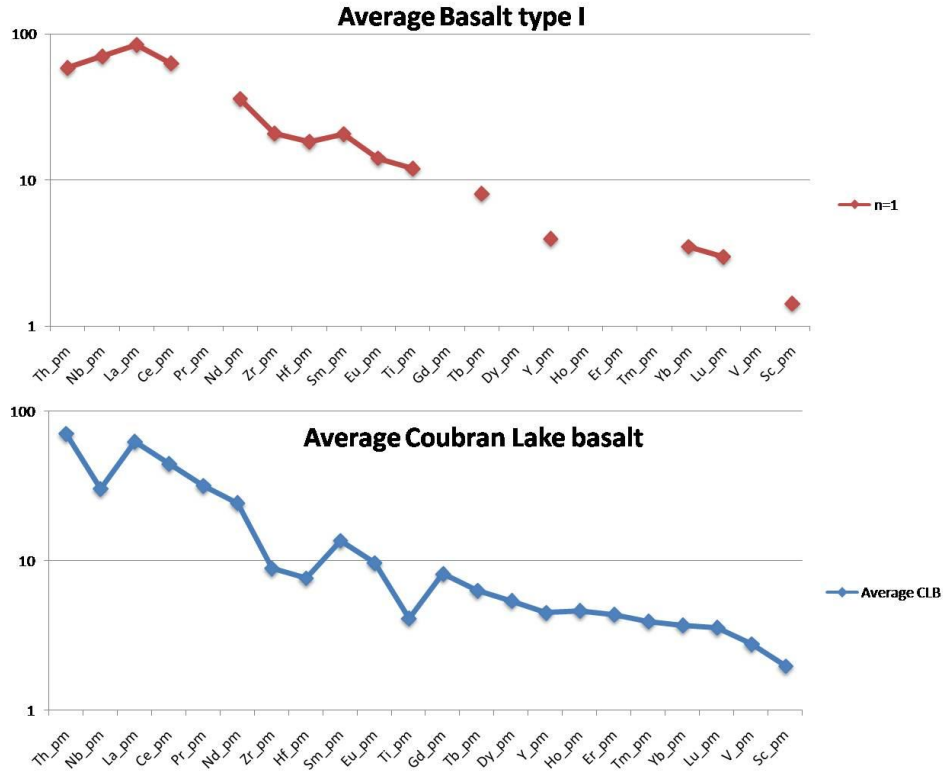

Figure 4.21: Primitive mantle normalized plots showing average Coubran Lake basalt data and average Basalt type II composition. Basalt type II data from Nicholson et al. (1997), normalizing values from Sun and McDonough (1989).

CHAPTER 5
PETROGENESIS OF THE NIPIGON SILLS

5.1 Results

A re-evaluation of 2397 spatially referenced samples with associated whole-rock geochemistry has yielded previously unrecognized variation within the Midcontinent Rift-related Nipigon sills of the Nipigon Embayment. The whole rock major and trace element geochemistry of 796 Nipigon sill samples was re-analysed in order to investigate the origin of the sills. This investigation revealed three distinct Nipigon sill types; 395 Nipigon type I sill samples, 171 Nipigon type II sill samples, and 55 Nipigon type III sill samples. Isotopic analyses were carried out on five Nipigon sill samples to supplement the existing isotope dataset of 22 Nipigon sill samples (Hollings et al., 2007b) in order to assess the degree of crustal contamination the three Nipigon sill types experienced. Analyses of Rb-Sr and Sm-Nd were carried out at Carleton University following the analytical procedure outlines in Chapter 2. Ranges for the three Nipigon sill types are summarized in Table 5.1.

5.1.1 Outliers and sampling biases

Populations comprising Nipigon sill types I, II and III were defined from the plot of Nb/Yb_{pm} versus Th/Yb_{pm} (Fig. 5.1). Outlier samples showing extremely elevated Th/Yb_{pm} were often reported to be taken from granophyric patches or country rock xenoliths and thus did not portray accurate geochemical characteristics of the magma. A total of 67 samples were noted to be taken from granophyric patches of xenoliths and were therefore eliminated from the classification. In some cases, as for the 80RHS-, 81RHS-, and 82RHS-series (MRD114), the Nipigon sill samples did not contain trace element data and thus were excluded from study. A total of 108 Nipigon sill samples were eliminated from the classification due to insufficient data.

As this study is a re-evaluation of an existing data set, sampling for the Nipigon sills was not carried out by the author, thus, the localities from which the Nipigon sill samples were not always described in full detail. The nature of the terrain in the Nipigon Embayment means that many of the sill outcrops are spatially restricted and do not always display prominent relief. As such, the sampler does not always know the position the sample is taken from within the sill (i.e. stratigraphic height). Sutcliffe (1986), Hart and Magyarosi (2004b), and MacDonald et al. (2005a) reported an idealized cross-section through a Nipigon sill which contains zones characterized by distinct textures and compositions from bottom to top: (1) chill, (2) fine-grained variably amygdaloidal, (3) pegmatitic diabase, (4) igneous layering, (5) magnetite-rich, (6) medium to coarse-grained, (7) coarse- to very coarse-grained, (8) fine-grained,

variable amygdaloidal, and (9) chill. However, these zones are not always present within any one section and the transitions between these zones are gradual and difficult to recognize in outcrop (Hart and MacDonald, 2007). The lack of textural, mineralogical and geochemical variations within the sills may inhibit the development of a complete stratigraphic succession (Hollings et al., 2007a; Hart and MacDonald, 2007). Therefore, the spatial re-evaluation of the existing dataset in geographic (i.e. XY) space is warranted as geochemical variations through stratigraphy (i.e. Z space) are not currently recognized within the mafic and mafic to ultramafic sills.

The distribution of samples within the Nipigon Embayment presents difficulty when interpreting the petrogenesis of units. A sampling gap is present within the west-central portion of the Embayment (Fig. 5.4) with a lack of Nipigon sills samples present relative to the sample density in the south-west portion of Embayment. Also, the samples present on the islands within Lake Nipigon provide a sound representation of the preserved rocks but leave considerable gaps where Lake Nipigon currently sits. Presumably, MCR-related rocks have been eroded away here leaving a gap in sample density throughout the immediate Lake Nipigon area. The best representation of Nipigon sill types is present in the south-western Nipigon Embayment which provides the highest sample density and the best distribution of Nipigon sill types allowing for the most accurate petrogenetic interpretation (Fig. 5.13).

5.1.2 Nipigon sill classification

Table 5.1 Summary of geochemical data for Nipigon sill types I, II, and III.

	Nipigon I	**Nipigon II**	**Nipigon III**
Number of samples	395	171	55
Th/Yb_{pm}	1.97 – 3.4	3.4 – 5.0	5.0 – 6.5
Nb/Yb_{pm}	0.75 – 1.65	1.2 – 1.8	1.5 – 2.2
Nb/Nb*	0.425 – 0.65	0.35 – 0.55	0.3 – 0.5
La/Sm_{pm}	1.2 – 1.8	1.60 – 2.0	2.2 – 2.6
Gd/Yb_{pm}	1.0 – 1.9	1.0 – 1.9	1.0 – 1.9
$\varepsilon_{Nd(t=1100Ma)}$	-0.5 to -1.5	-1.5 to -3.0	-5.0 to -7.0
$^{87}Sr/^{86}Sr_i$	0.70403 – 0.70556	0.70459 – 0.70681	0.70431 – 0.70761

Type I Nipigon sills form a relatively tight cluster on the plot of Nb/Yb_{pm} versus Th/Yb_{pm} displaying the lowest Th/Yb_{pm} values of the three sill types ranging from 1.97 to 3.4 and a Nb/Yb_{pm} range of 0.75 to 1.65 (Fig. 5.1). Type 1 sills also show relatively high Nb/Nb* values ranging from 0.42 to 0.65 as well as the lowest La/Sm_{pm} values of the three sill types ranging from 1.2 to 1.8. Type I sills show the least negative $\varepsilon_{Nd(t=1100Ma)}$ signatures ranging from -0.5 to -1.5 with $^{87}Sr/^{86}Sr_i$ values ranging from 0.70403 – 0.70556. Primitive mantle normalized plots (Fig. 5.2) for the average of 395 type I Nipigon sills show nearly flat trends with only slight LREE and enrichment and minor HREE fractionation with a distinct negative niobium anomaly.

Type II Nipigon sills display higher, but overlapping Th/Yb_{pm} values than type I sills ranging from 3.4 to 5.0 with a Nb/Yb_{pm} range of 1.2 to 1.8. Type II sills also show slightly lower Nb/Nb* values when compared to type I sills ranging from 0.35 to 0.55 as well as higher La/Sm_{pm} values ranging from 1.6 to 2.0.Type II sills display more negative $\varepsilon_{Nd(t=1100Ma)}$ values than type I sills ranging from -1.5 to -3.0 with $^{87}Sr/^{86}Sr_i$ values ranging from 0.70459 – 0.70681. Primitive mantle normalized plots (Fig. 5.2) for the average of 171 type II Nipigon sills show nearly flat trends with only slight LREE enrichment and weak

HREE fractionation with a distinct negative niobium anomaly. Type II sills show slightly higher thorium values when compared to type I sills as well as a slightly more pronounced negative niobium anomaly.

Type III Nipigon sills display the highest Th/Yb_{pm} values of all three sill types ranging from 5.0 to 6.5 with a Nb/Yb_{pm} range of 1.5 to 2.2. Type III sills display Nb/Nb* values of 0.3 to 0.5 with the highest La/Sm_{pm} range of all three sill types at 2.2 to 2.6. Type III sills display the most negative $\varepsilon_{Nd(t=1100Ma)}$ values of all three sill types with values from -5.0 to -7.0 and $^{87}Sr/^{86}Sr_i$ values ranging from 0.70431 – 0.70761. Primitive mantle normalized plots (Fig. 5.2) for the average of 55 type III Nipigon sills show a negative trend with LREE enrichment and slight HREE fractionation with a distinct negative niobium anomaly. Type III sills show the most pronounced negative niobium anomaly of all three sill types as well as a negative titanium anomaly.

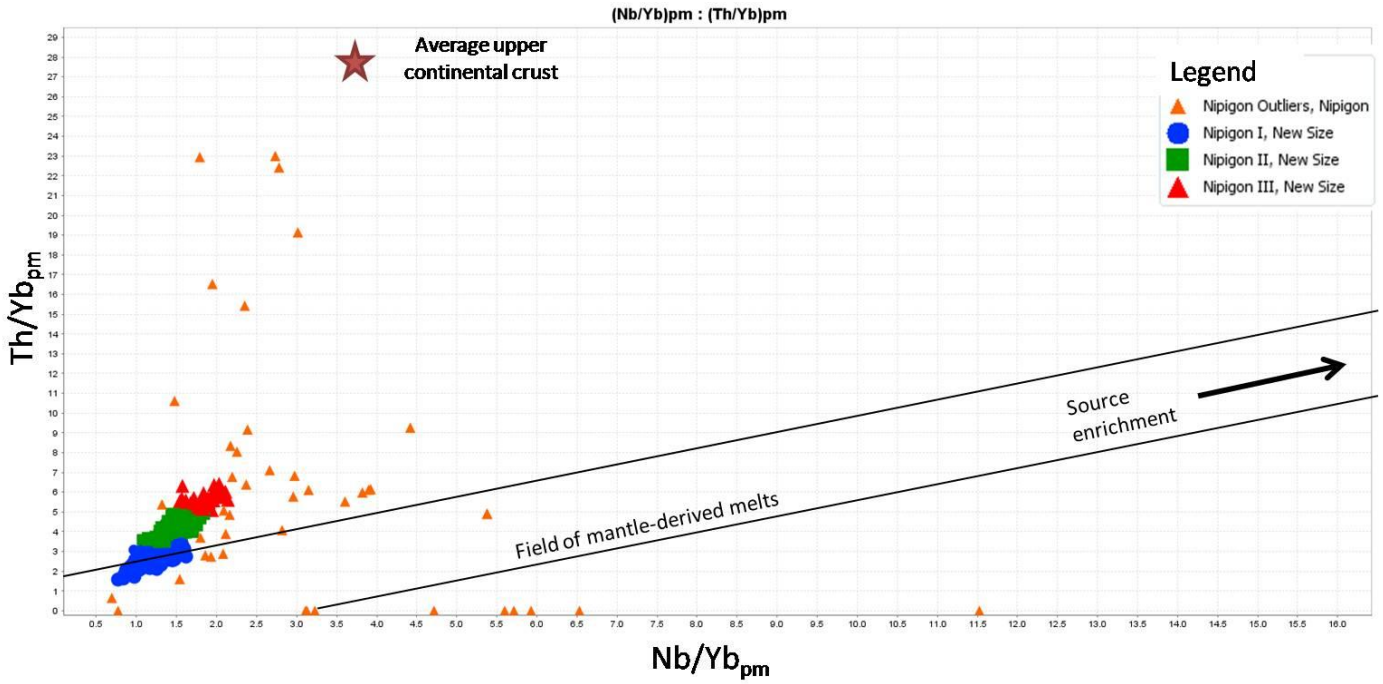

Figure 5.1: Plot of Nb/Yb_{pm} versus Th/Yb_{pm} showing all 796 Nipigon sill samples. Normalizing values from Sun and McDonough (1989). Average Upper Continental Crust value from Taylor and McLennan (1985). Field of mantle-derived melts from Jowitt and Ernst (in press).

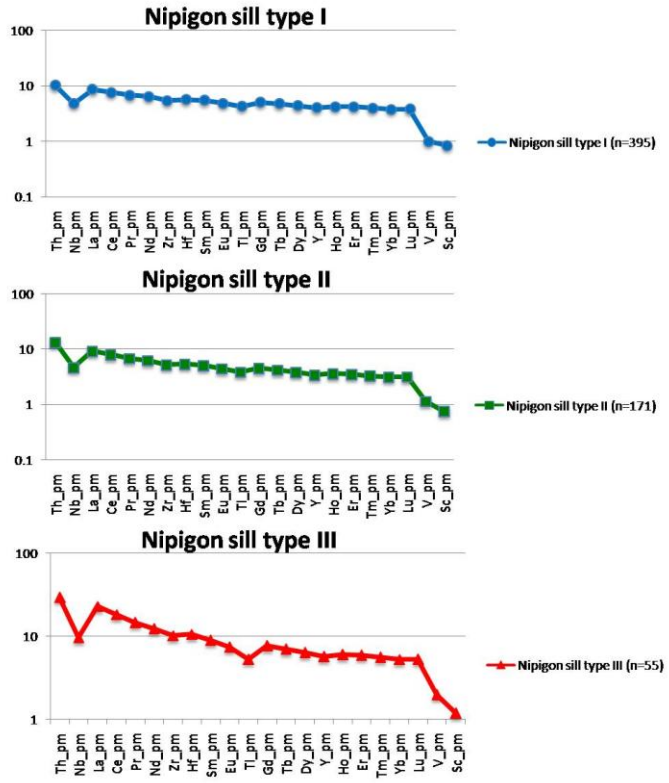

Figure 5.2: Primitive mantle normalized plots for averaged Nipigon sill types I (n=395), II (n=171) and III (n=55). Normalizing values from Sun and McDonough (1989).

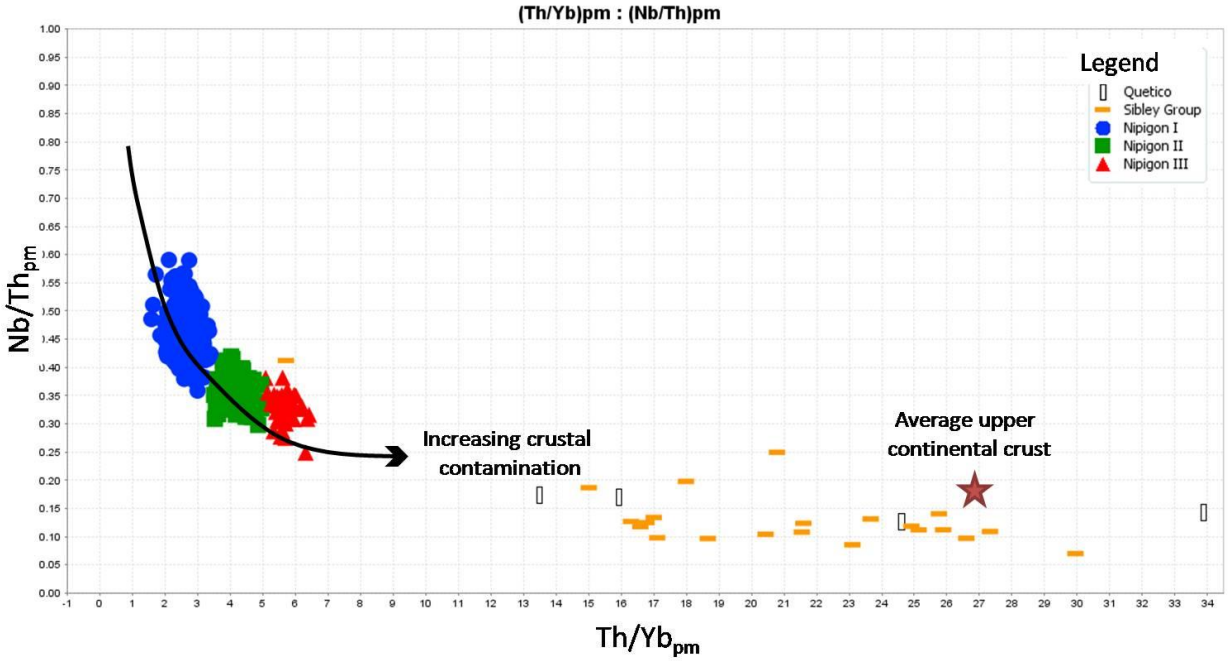

Figure 5.3: Plot of Th/Yb_{pm} versus Nb/Th_{pm}. Normalizing values from Sun and McDonough (1989).

5.1.3 Geochemistry of the country rock

Whole-rock and isotope geochemistry of samples of metasedimentary rocks of the Quetico Subprovince and Sibley Group sedimentary rocks were utilized to aid in the assessment of contamination of the Nipigon sills. Samples from both the Sibley Group and the Quetico Subprovince are assumed to be representative of the country rock proximal to the Nipigon sills. Whole-rock geochemical analyses of Quetico and Sibley rocks were gathered from a selection of MRD's as outlined in Chapter 2. All analyses are summarized in Table 5.2.

Rocks of the Quetico Subprovince display higher Th/Yb_{pm} values than the majority of MCR-related rocks ranging from 2.44 to 1321.72 with an average of 240.33 (n=15), Nb/Th_{pm} values lower than MCR-related rocks ranging from 0.14 to 0.17, Nb/Yb_{pm} values from 2.33 to 3.09 and Nb/Nb* values from 0.02 to 0.48 with an average of 0.23 (n=15). Rocks of the Sibley Group display similar trace element ratios to those of the Quetico rocks with Th/Yb_{pm} values from 5.71 to 86.59 with an average of 23.67 (n=23), Nb/Th_{pm} values from 0.07 to 0.25, Nb/Yb_{pm} values from 1.68 to 5.19 and Nb/Nb* values from 0.06 to 1.91 with an average of 0.46 (n=23).

Isotopic analyses from published and unpublished sources were also included and are assumed to be representative of the rock units. Isotope data for Quetico Subprovince rocks are from Pan et al. (1999) and Henry et al. (1998). Isotope data for Sibley Group rocks comprises only two representative samples (03RM4; siltstone and 03RM5; mudstone; Metsaranta, unpublished data). Both the Quetico and the Sibley samples produce negative $\varepsilon_{Nd(t=1100Ma)}$ values with the Quetico ranging from -16 to -23 and the two Sibley samples displaying values around -5. Initial $^{87}Sr/^{86}Sr$ for the Quetico displays values between 0.701678 and 0.715596 and the Sibley rocks displaying values between 0.71999 and 0.75039. All Sibley and Quetico samples were plotted on a $^{87}Sr/^{86}Sr$ versus $^{143}Nd/^{144}Nd$ graph (Fig. 5.4) for comparison. All three Nipigon sill types plot within a tight array towards the top left corner of the plot with the highest $^{143}Nd/^{144}Nd$ values and $^{87}Sr/^{86}Sr$ values similar to those of the Quetico rocks. The Sibley group metasedimentary rocks exhibit the highest $^{87}Sr/^{86}Sr$ values and $^{143}Nd/^{144}Nd$ values in between those of the Quetico and Nipigon samples. The Quetico samples exhibit the lowest $^{143}Nd/^{144}Nd$ with $^{87}Sr/^{86}Sr$ values similar to those of Nipigon sill types I, II and III.

Table 5.2 Summary of geochemical data for Quetico Subprovince and Sibley Group country rock. Quetico Subprovince data from Henry et al. (1998), Pan et al. (1999).Unpublished Sibley Group data from R. Metsaranta.

	Quetico Subprovince	Quetico Average	Sibley Group	Sibley Average
Th/Yb_{pm}	2.44 to 1321.72	240.33 (n=15)	5.71 to 86.59	23.67 (n=23)
Nb/Yb_{pm}	2.33 to 3.09	8.41 (n=15)	1.68 to 5.19	2.88 (n=23)
Nb/Nb*	0.02 to 0.48	0.23 (n=15)	0.06 to 1.91	0.46 (n=23)
Nb/Th_{pm}	0.14 to 0.17	0.12 (n=15)	0.07 to 0.25	0.14 (n=23)
$\varepsilon_{Nd(t=1000Ma)}$	-16 to -23		-5.20 and -5.38	
$^{87}Sr/^{86}Sr_i$	0.701678 to 0.715596		0.71999 to 0.75039	

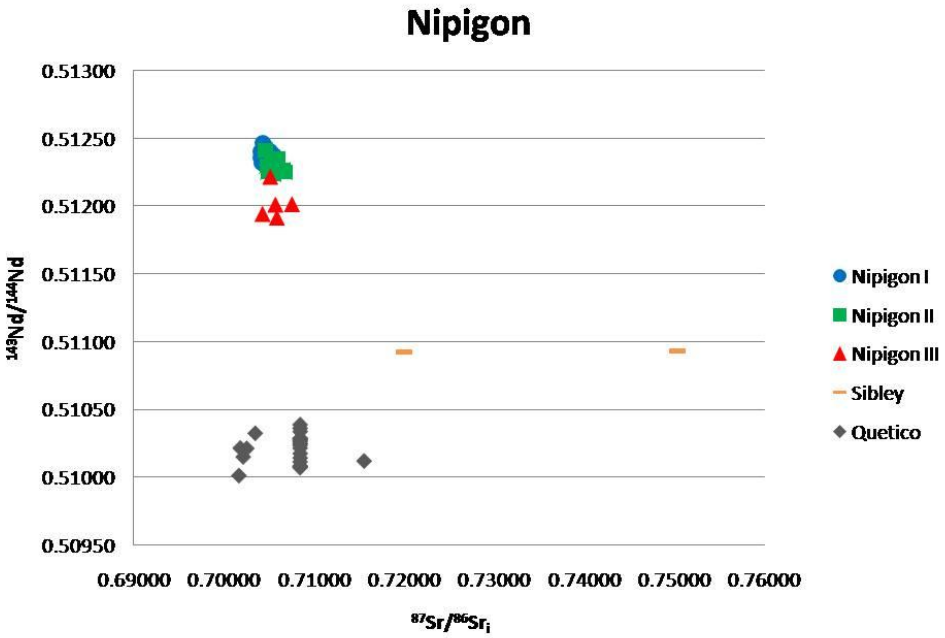

Figure 5.4: $^{87}Sr/^{86}Sr_i$ versus $^{143}Nd/^{144}Nd$ for Nipigon sill types I, II and III, Quetico Subprovince rocks and Sibley Group rocks. Additional data from Henry et al. (1998), Pan et al. (1999) and unpublished data from R. Metsaranta.

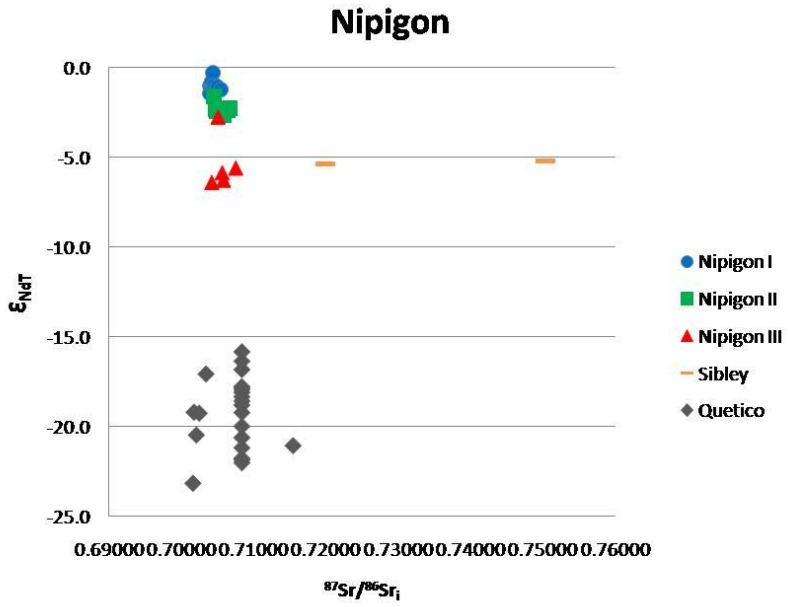

Figure 5.5: $^{87}Sr/^{86}Sr_i$ versus $\varepsilon_{Nd(t=1100Ma)}$ for Nipigon sill types I, II and III, Quetico Subprovince rocks and Sibley Group rocks. Additional data from Henry et al. (1998), Pan et al. (1999), and unpublished data from R. Metsaranta.

5.2 Discussion

As discussed in chapter 3, four geochemically distinct sill suites are currently recognized within the Nipigon Embayment: Nipigon, Inspiration, McIntyre, Jackfish-Shillabeer which in turn may be subdivided into a mafic suite including Nipigon, Inspiration and McIntyre and an ultramafic suite consisting of Shillabeer and Jackfish (Hollings et al., 2007a). Building on the current understanding of the intrusive rocks of the Nipigon Embayment, a re-evaluation of the existing dataset was undertaken to provide further insight into the source characteristics, contamination histories and emplacement processes these units underwent in an attempt to elucidate the magmatic evolution of the study area. Geochemical parameters developed by Pearce and Peate (1995) and Pearce (2008) and further refined by Jowitt and Ernst (in press) have been introduced to Midcontinent Rift-related rocks and have provided a more sensitive measure of crustal contamination as well as previously undetermined relationships between the sources of the various mafic and ultramafic units. The Th/Yb – Nb/Yb projection of Pearce (2008) demonstrates that rift-related rocks can lie along or be projected to a diagonal MORB-OIB array, as controlled be Nb/Yb. Variations along this array may be attributed to variable degrees of partial melting of a homogeneous source or variability within the source region. Scattering oblique to the source array,

towards continental crustal values, is indicative of crustal contamination of a source magma, as controlled by Th/Yb. The measures of source characteristics and contamination delineated by the Th/Yb – Nb/Yb projection will be substantiated with additional trace element and isotopic variables. The processes controlling the source characteristic of Midcontinent Rift-related units, as well as the sources and history of contamination of those magmas will be addressed in this chapter.

5.2.1 Nipigon sill source characteristics

It is widely accepted that Midcontinent Rift-related igneous rocks were derived from an upwelling mantle plume which produced large volumes of magma emplaced or erupted at approximately 1.1 Ga (e.g., Nicholson and Shirey, 1990). The high incompatible element abundances of Midcontinent Rift-related intrusive rocks displaying LREE enrichment and HREE fractionation are broadly comparable to modern plume-derived oceanic island basalts (OIB), albeit at lower abundances (Hollings et al., 2007a). The presence of an OIB-like mantle source signature is supported by the presence of OIB-like basalts throughout the MCR (Nicholson et al., 1997; Hollings et al., 2007a). The variability in incompatible element ratios between the sills and the ultramafic units has been interpreted to indicate that they were formed from different mantle sources, rather than variable degrees of melting of the same source (Hollings et al., 2007a). The fact that MCR-related rocks display lower absolute incompatible element abundances yet higher MgO contents, most notably the Jackfish, McIntyre and Shillabeer sills, may be due to them having formed at higher degrees of melting than typical OIB or variations in the composition of the source region (Hollings et al., 2007a). The majority of rocks of the Nipigon Embayment display prominent negative Nb anomalies, including the Nipigon sills, which is not consistent with typical OIB, but rather comparable to basalts formed in a supra-subduction environment (Hollings et al., 2007a). This is not consistent with the plume related source invoked for the MCR but rather has been interpreted to suggest that the magmas have been contaminated by continental crust. However, a number of units (i.e. the Hele intrusion, the basal flows of the Osler Group and the Seagull intrusion) display smaller negative or zero niobium anomalies with the later displaying $\varepsilon_{Nd(t=1100Ma)}$ value of 0 to -1.5. (Heggie, 2005; Hollings et al., 2007a; Hollings et al., 2007c). This data supports the ultramafic intrusions forming from a primary, uncontaminated magma derived from a mantle plume different to the source of Nipigon sills (Hollings et al., 2007a).

Elevated Nb/Yb_{pm} ratios are indicative of a changing mantle source from a more primitive mantle-like source region (Nb/Yb_{pm} closer to one) to more enriched mantle compositions (Nb/Yb_{pm} values >5) (Jowitt and Ernst, in press). Pearce (2007) states that N-MORB, E-MORB and OIB lie on the MORB-OIB array displaying progressively more enriched mantle source characteristics with progressively higher

Nb/Yb_{pm} values. Typically, each region has its own local array within which the more enriched samples and/or products of lower degrees of melting have the higher Nb/Yb_{pm} ratios, and the more depleted samples and/or products of higher degrees of partial melting, have the lower Nb/Yb_{pm} ratios (Pearce, 2007).

Nipigon sills display slight variability with types I, II, and III displaying progressively increased Nb/Yb_{pm} values as well as increased Th/Yb_{pm} ratios (Fig. 5.6). This implies that each sill type with a progressively more contaminated signature also displays a more enriched source signature. Theoretically, an elevated Nb/Yb_{pm} value should correlate with an elevated Gd/Yb_{pm}. The ratio of Gd/Yb_{pm} can be used as a means of evaluating depth of melting. Magmas containing a HREE fractionation signature (Gd/Yb_{pm}> ~2) are inferred to be sourced from below the garnet-spinel stability field (>90 km depth) whereby garnet is stable in the source region but melting occurred at low degrees of partial melting leaving garnet in the source (Rollinson, 1993). Contrary to the increasingly enriched source signature implied from the Nb/Yb_{pm} ratios, Nipigon sill types I, II and III all display Gd/Yb_{pm} values between 1.0 and 1.9 (Table 5.1; Fig.5.7). This suggests they did not undergo significant HREE fractionation and were all sourced from approximately the same depth, shallower than that of the ultramafic units and the Jackfish, McIntyre and Shillabeer sills. The slight variability in Nb/Yb_{pm} signatures observed between the three Nipigon sill types is likely a product of progressively lower degrees of melting as Pearce (2007) attributed local arrays towards higher Nb/Yb_{pm} values within source regions to lower degrees of melting. The Gd/Yb_{pm} values support this as all three Nipigon sills were sourced from the same depth arguing against the possibility for a different source region. The variability in Nb/Yb_{pm} observed between the Nipigon sills and the other intrusive units may in fact be attributed to different source regions which will be addressed in the final chapter.

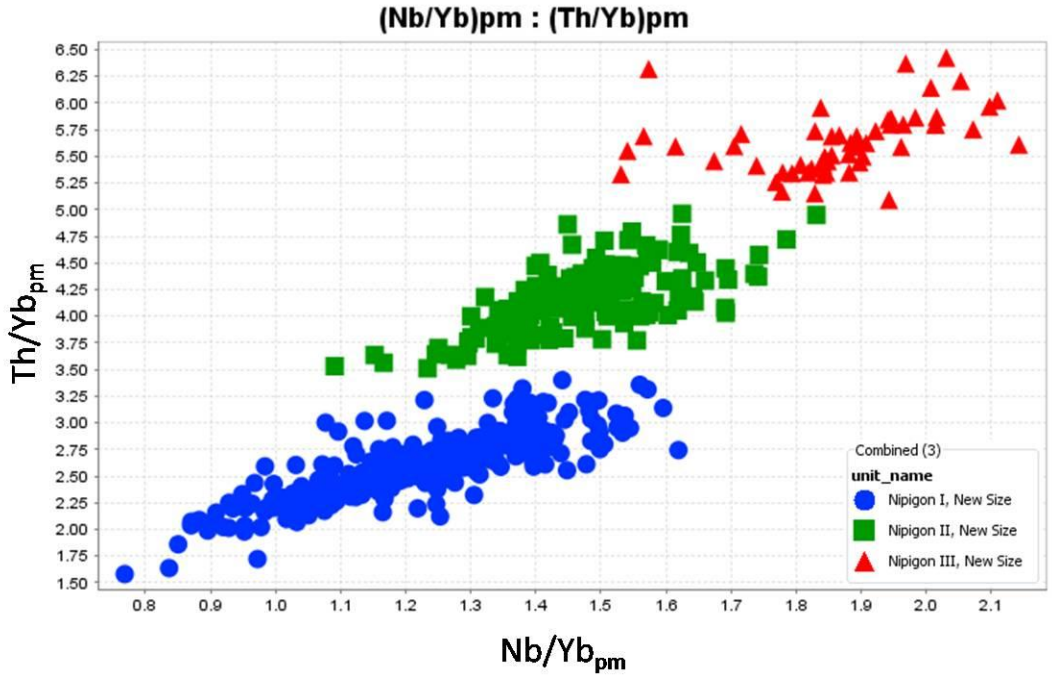

Figure 5.6: Plot of Nb/Yb_{pm} versus Th/Yb_{pm} showing Nipigon sill types I, II, and III. Close-up of Figure 5.1 with outliers eliminated. Normalizing values from Sun and McDonough (1989).

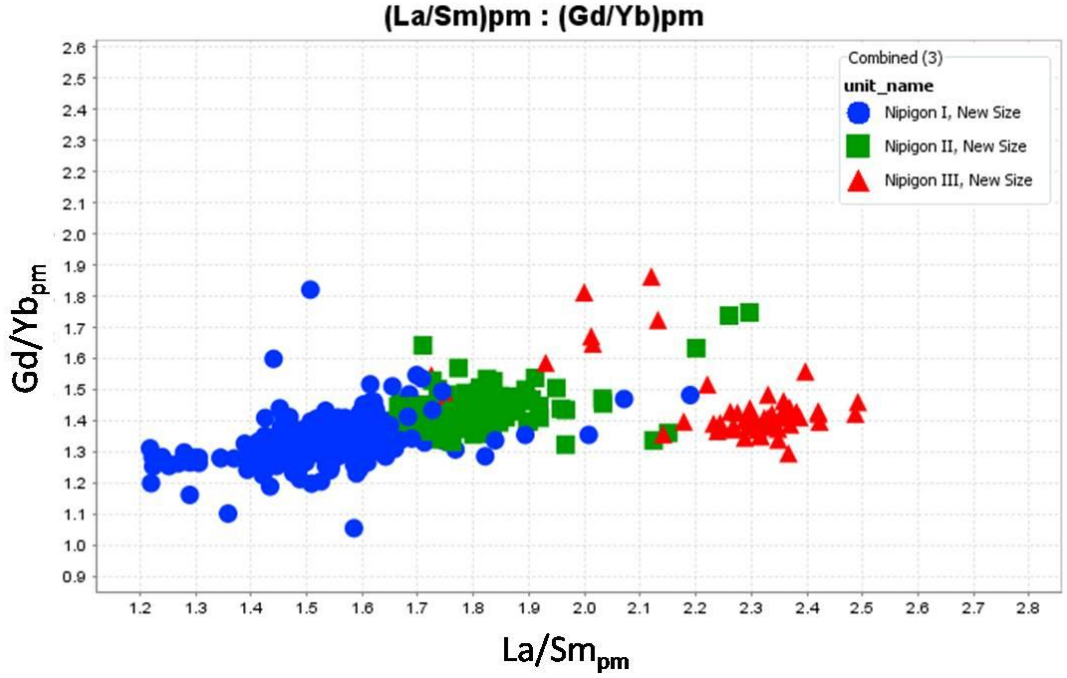

Figure 5.7: Plot of La/Sm_{pm} versus Gd/Yb_{pm} showing Nipigon sill types I, II, and III. Normalizing values from Sun and McDonough (1989).

5.2.2 Nipigon sill contamination

Many authors have proposed that the main volume of rift basalt was produced from an enriched mantle plume with a $\varepsilon_{Nd(t=1100Ma)}$ value close to 0 and La/Sm_n of 2 to 3 (Nicholson and Shirey, 1990; Nicholson et al., 1997; Hollings et al., 2007a). Nipigon sill suites from Hollings et al. (2007b) incorporated with analyses from this study show the Nipigon sills have $\varepsilon_{Nd(t=1100Ma)}$ values from -0.29 to -6.42, which is consistent with contamination by an older crustal source. As outlined in section 5.1, rocks of the Quetico Subprovince display strongly negative ε_{Nd} values from -16 to -23 with lower Sr_i values than rocks of the Sibley Group. Sibley Group sedimentary rocks have ε_{Nd} values of -5.20 and -5.38 with higher Sr_i values than the Quetico rocks. Rocks of the Quetico are present at depth whereas rocks of the Sibley Group are only present at shallower depths. Rocks of the Marmion Terrane, formerly the Wabigoon Subprovince, are present towards the northern part of the Embayment and display a wide range of ε_{Nd} values; -12 to -23 for felsic units and -14 to +7 for mafic units (Tomlinson et al., 2003). The positive ε_{Nd} values for the mafic units of the Wabigoon make it an unlikely candidate for the contamination of MCR-related rocks (Hollings et al., 2007b). Sedimentary rocks of the Animikie Group are also present to the south of the Nipigon Embayment but are not exposed in the immediate vicinity of the Embayment, nor are they thought to be present at depth (Hollings et al., 2007b). Furthermore, no Sr data is available for either Wabigoon or Animikie rocks making discrimination between contamination sources difficult (Hollings et al., 2007b). The most plausible contaminant sources for the intrusive rocks of the Nipigon Embayment are the Sibley Group sedimentary rocks and the metasedimentary and migmatitic rocks of the Archean Quetico Subprovince. Additionally, Hollings et al. (2007a) reported that both the Sibley Group sedimentary rocks and the Quetico Subprovince rocks fulfill the criteria for a low Ta, Nb, P and moderate Ti contamination material with elevated large-ion lithophile elements and LREE. Furthermore, it is possible to distinguish between contaminant sources as the Sibley rocks have a stronger control on Sr values whereas the Quetico rocks have a stronger control on ε_{Nd} values (Fig. 5.4 and 5.5).

The degree of crustal contamination that a magma experienced during emplacement can be assessed using the plot of Th/Yb_{pm} versus Nb/Th_{pm} (Fig. 5.1 and 5.6) with Th/Yb_{pm} controlling contamination by crustal material (e.g., Lightfoot et al., 1990; Pearce and Peate, 1995; Lightfoot and Hawkesworth, 1998; Pearce; 2008; Jowitt and Ernst, in press). Progressively elevated Th/Yb_{pm} values for a given source region suggests that the source magma has undergone progressively increased interaction with continental crust (i.e. higher Th/Yb_{pm} value indicating more crustal contamination). The plot of Th/Yb_{pm} versus Nb/Th_{pm} (Fig. 5.3) shows Nipigon sill types I, II, and III displaying progressively increased crustal contamination. The Th/Yb_{pm} values for the more contaminated Nipigon sill types trend towards the Th/Yb_{pm} values for Quetico and Sibley Group rocks, which are broadly consistent with the values for average upper

continental crust defined by Taylor and McLennan (1985). Using Th/Yb_{pm} as a proxy for crustal contamination, three distinct Nipigon sill units are proposed here. The Nipigon sill types defined by Th/Yb_{pm} values show consistent results with the Nd isotope data on the plot of $\varepsilon_{Nd(t=1100Ma)}$ versus Th/Yb_{pm} with more negative $\varepsilon_{Nd(t=1100Ma)}$ values correlating with higher Th/Yb_{pm} (Fig. 5.9). Furthermore, the plot of La/Sm_{pm} versus Th/Yb_{pm} shows a positive correlation suggesting that the contaminant has high La/Sm_{pm} values as well as higher Th/Yb_{pm} values (Fig. 5.8). Nipigon sill type I represents the least contaminated suite denoted by the lowest Th/Yb_{pm} and La/Sm_{pm} values, the highest Nb/Th_{pm} values and the least negative $\varepsilon_{Nd(t=1100Ma)}$ values. Nipigon sill type II displays moderate contamination signatures denoted by relatively moderate Th/Yb_{pm}, La/Sm_{pm}, and Nb/Th_{pm} values as well as the moderately negative ε_{Nd1100} values. Nipigon sill type III is the most contaminated of the suites denoted by elevated Th/Yb_{pm}, and La/Sm_{pm} values the lowest Nb/Th_{pm} values and the most negative $\varepsilon_{Nd(t=1100Ma)}$ values.

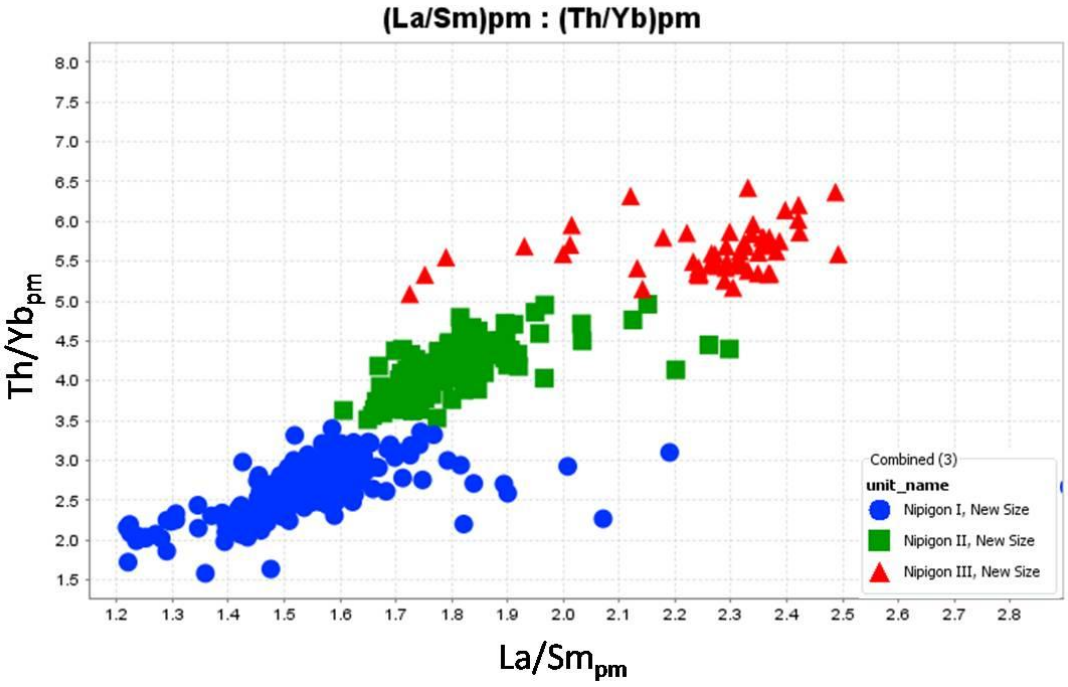

Figure 5.8: Plot of La/Sm_{pm} versus Th/Yb_{pm} showing Nipigon sill types I, II, and III. Normalizing values from Sun and McDonough (1989)

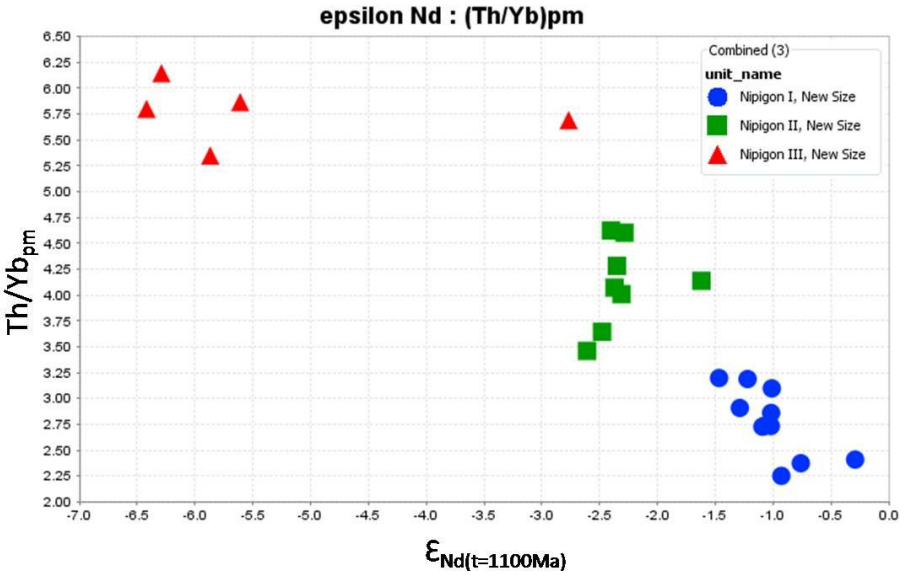

Figure 5.9: $\varepsilon_{Nd(t=1100Ma)}$ versus Th/Yb_{pm} showing Nipigon sill types I, II, and III. Normalizing values from Sun and McDonough (1989).

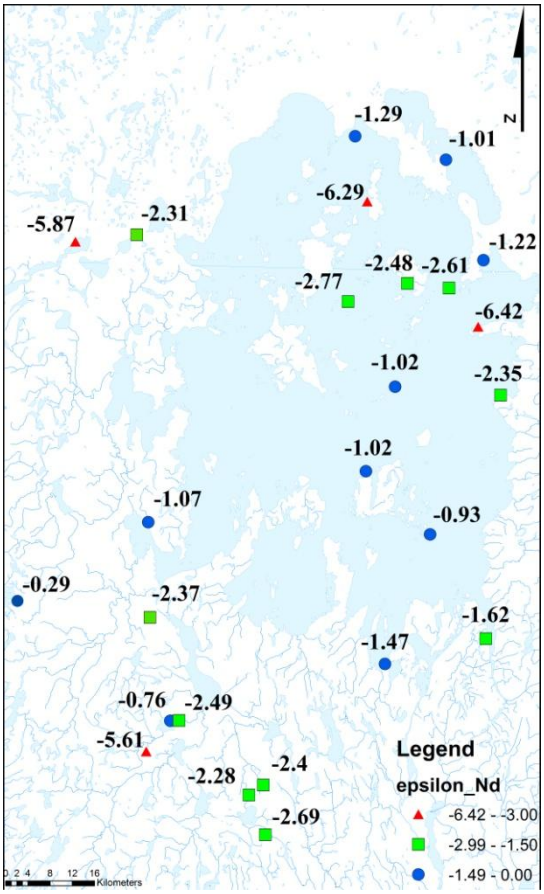

Figure 5.10: Location map showing samples with $\varepsilon_{Nd(t=1100Ma)}$ values. Nipigon sill type I (blue circles), type II (green squares) and type II (red triangles). Additional data from Hollings et al. (2007b).

When evaluating the potential source of contamination for each of the three Nipigon sill types, the isotope data as well as the trace element data must be considered. Nipigon sill type I, II and III show negative $\varepsilon_{Nd(t=1100Ma)}$ values which is consistent with contamination by a dominantly Archean crustal source with potential for contribution by the rocks of the Sibley Group. By this measure, the more negative $\varepsilon_{Nd(t=1100Ma)}$ values of the Nipigon sill type III suggest that they experienced the greatest degree of crustal contamination by Quetico country rocks, Nipigon sill type II experienced a moderate degree of crustal contamination by Quetico rocks and Nipigon sill type I underwent the least amount of crustal contamination by country rocks of all three sill types. No sign of variation is observed in the Sr isotope data with all three Nipigon sill types displaying similar ranges for $^{87}Sr/^{86}Sr_{initial}$ between 0.70403 – 0.70761 (Fig. 5.4 and 5.5). As previously mentioned, contamination by Sibley Group rocks is the dominant control on $^{87}Sr/^{86}Sr_{initial}$ values (Hollings et al., 2007a) The data presented here suggests that all three Nipigon sill types experienced a broadly similar degree of contamination by the rocks of the Sibley Group.

Analysis of trace element data of the contaminant sources displays results that are not consistent with the isotope data. The plot of Nb/Nb* versus Th/Yb_{pm} show that Archean rocks of the Quetico Subprovince appear to control the Th/Yb_{pm} values, whereas Sibley Group sedimentary rocks have a stronger control on Nb/Nb* (Fig. 5.12). For the Nipigon sills, Nb/Nb* values show consistent results with Th/Yb_{pm} values as Nb/Nb* values closer to zero correlate with higher Th/Yb_{pm} values (Fig. 5.11). Type I Nipigon sills display Nb/Nb* values closer to one denoting the weakest negative Nb anomaly of all three sill types. Type II Nipigon sills display Nb/Nb*values in between those of type I and II sills termed here to denote a moderate niobium anomaly. Type III sills display the strongest negative Nb anomaly of all three sill types shown by Nb/Nb* values closer to zero. This data suggests that type I Nipigon sills have more interaction with the Sibley group whereas type II and III Nipigon sills have more interaction with Quetico rocks at depth. A greater degree of interaction with the rocks of the Sibley Group suggests shallower level contamination as the Sibley Group unconformably overlies Archean rock within the Nipigon Embayment (Rogala et al., 2007). On the plot of Th/Yb_{pm} versus Nb/Th_{pm} (Fig. 5.3), Nipigon sill types I, II and III plot along an inferred line of mixing towards the sources of contamination (Quetico and Sibley group rocks) as well as the value for average continental crust. The plot of Th/Yb_{pm} versus Nb/Th_{pm} supports the evidence for these suites being progressively more contaminated by country rock but does not discriminate between the source of the contaminant as in the plot of Nb/Nb* versus Th/Yb_{pm}.

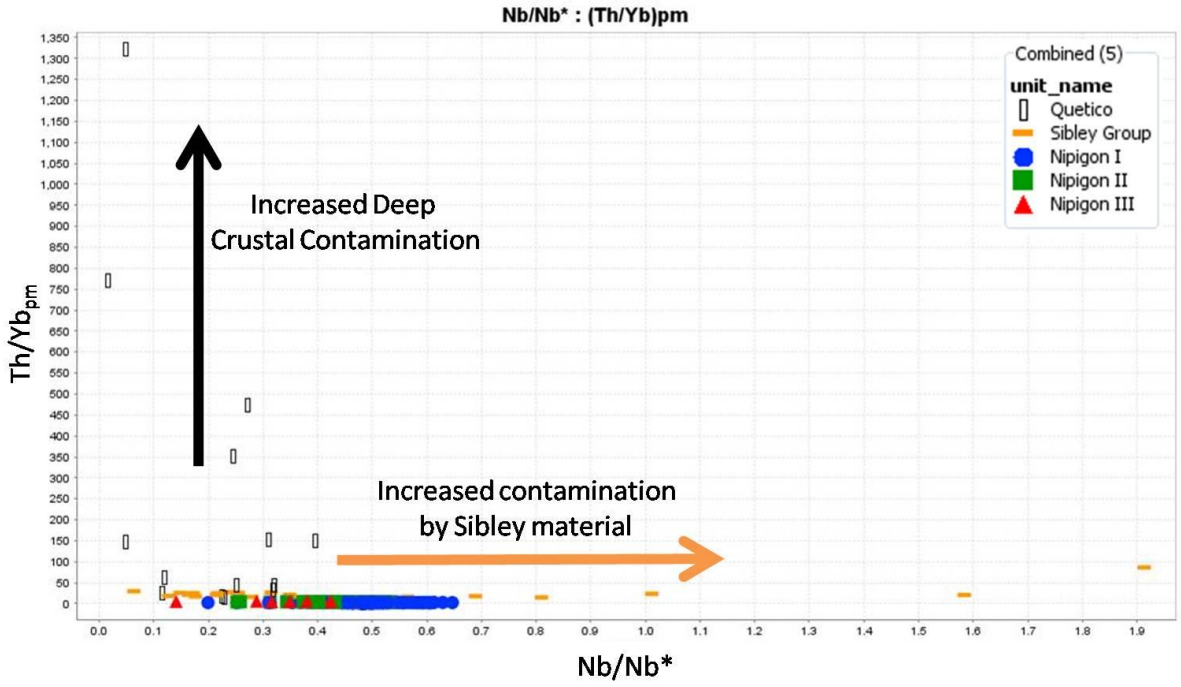

Figure 5.11: Plot of Nb/Nb* versus Th/Yb_{pm} showing Nipigon sill types I, II, and III with Quetico and Sibley Group samples. Normalizing values from Sun and McDonough (1989).

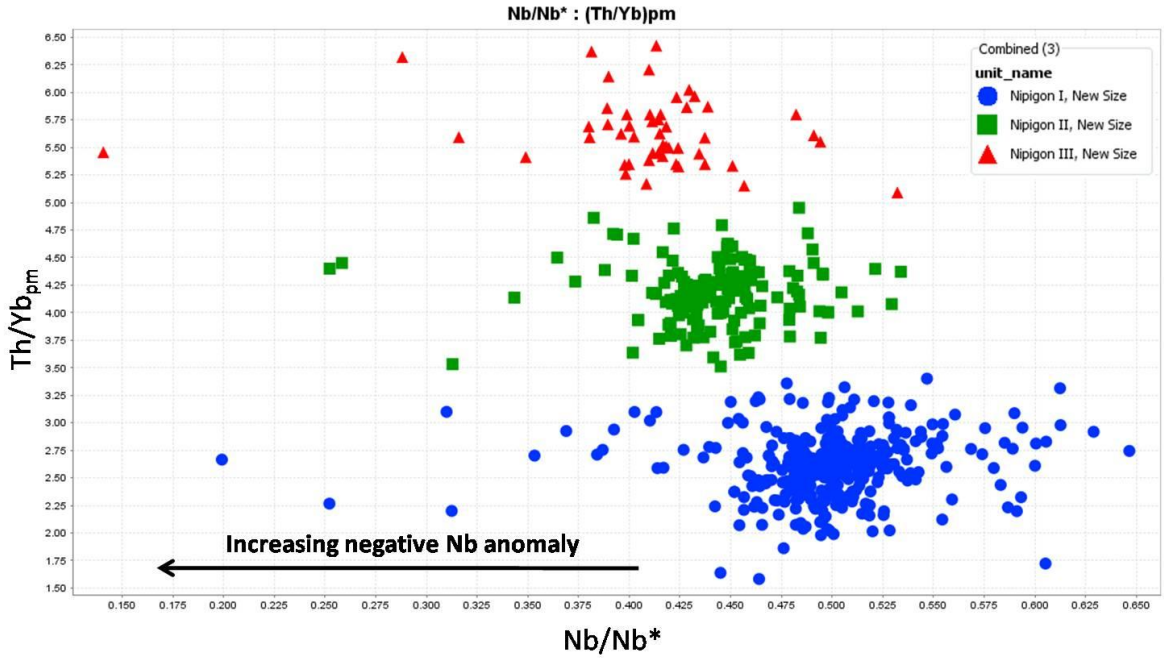

Figure 5.12: Plot of Nb/Nb* versus Th/Yb_{pm}. Normalizing values from Sun and McDonough (1989).

5.2.3 Petrogenesis and emplacement history of the Nipigon sills

Type I Nipigon sills are located peripheral to Nipigon sill types II and III and do not appear to be related to any known major structures (Fig. 5.13). Populations of more-contaminated samples (Nipigon types II and III) dominantly lie within two areas; a north-trending, linear group in the south-western Nipigon Embayment and an arcuate array in northern and eastern Lake Nipigon (Fig. 5.13). In the southwest corner of the Nipigon Embayment, Nipigon sill types II and III are proximal to the Black Sturgeon Fault which has been noted to be a major structural control on the emplacement of intrusive units in the area (e.g. Hart and MacDonald, 2007). Spatially restricted populations of more contaminated samples are present within the north and northwest portions of the Nipigon Embayment but a lack of sample density restricts interpretation relative to the less contaminated samples. These concentrations of more contaminated Nipigon sills are referred to as contamination centres or foci and are outlined in red on Figure 5.13.

As the data set did not always indicate elevation data for the spatially located samples, all Nipigon sill data was plotted against a digital elevation model (DEM) to evaluate a consistent measure of elevation and investigate any geochemical differences with stratigraphic height within the Nipigon Embayment. Figure 5.14 shows the results of elevation data generated from the DEM plotted against Th/Yb_{pm}. No discernable correlation can be observed between elevation and the dominant crustal contamination signature (Th/Yb_{pm}). This suggests that the variation observed between Nipigon sill types cannot be correlated to stratigraphic height.

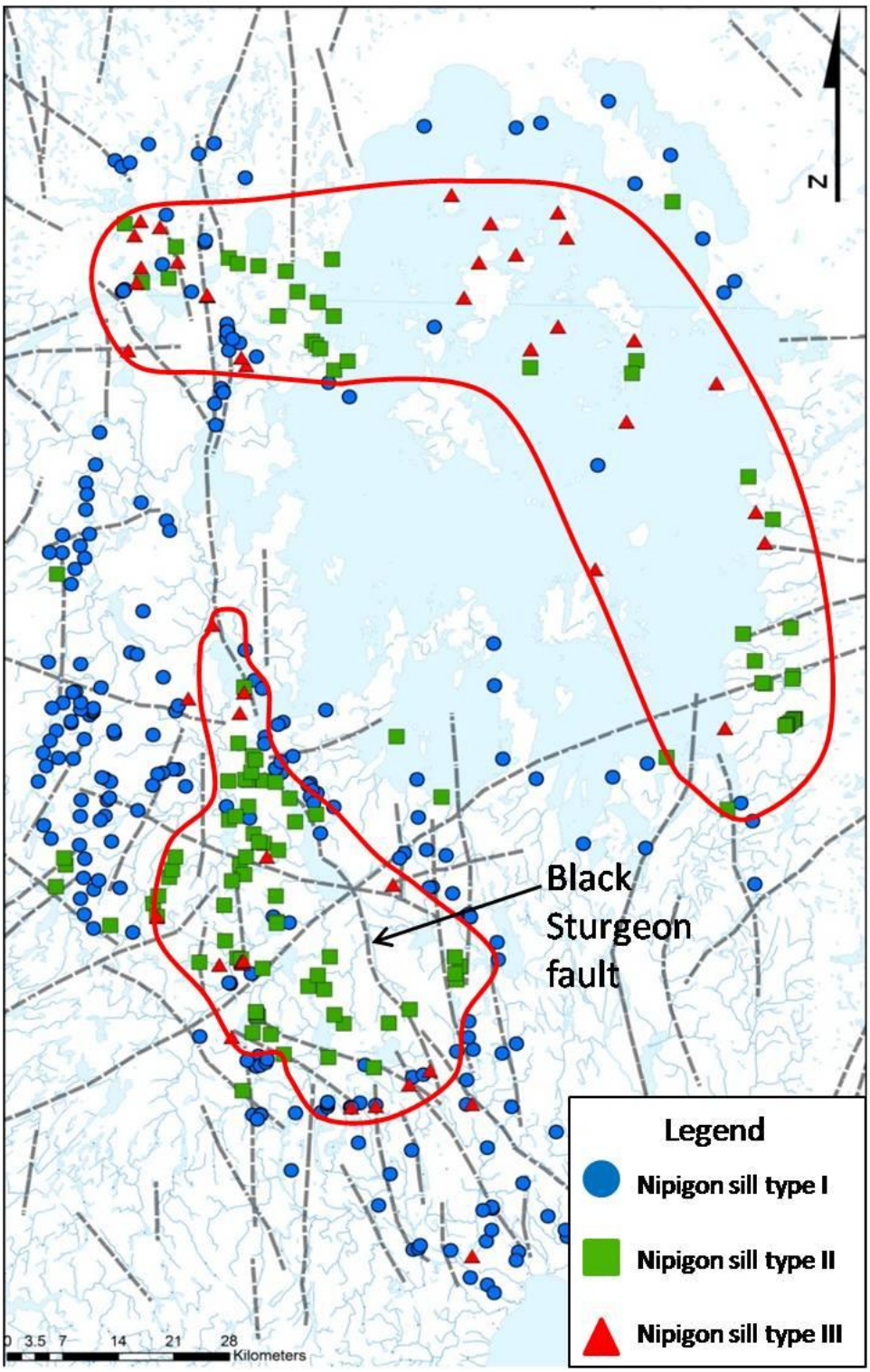

Figure 5.13: Map of the Nipigon Embayment showing Nipigon sill types I, II and III defined by Th/Yb_{pm} values (Fig. 5.1 and 5.6).Contamination centres outlined in red. Major faults after Hart and MacDonald (2007).

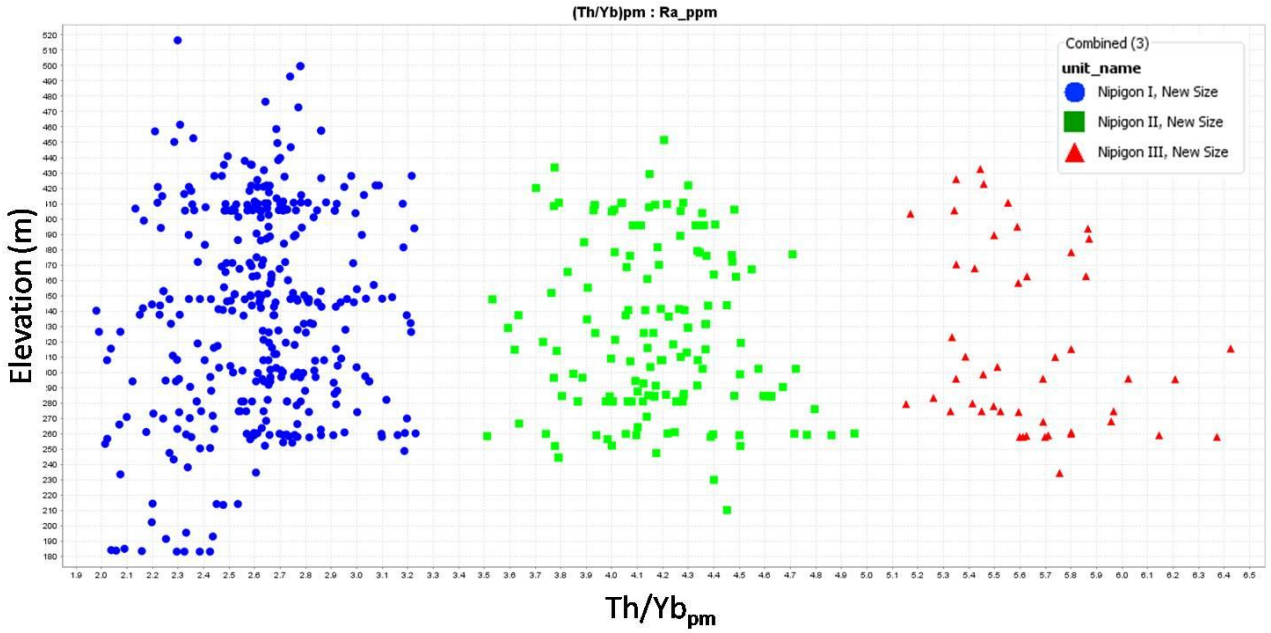

Figure 5.14: Plot of Th/Yb_{pm} versus elevation in metres showing Nipigon sill types I, II and III. Normalizing values from Sun and McDonough (1989).

The more crustally-contaminated nature of type II and III sills in conjunction with their proximity to major structures, suggests that magmas feeding these sills ascended through structures or conduits that provide more interaction with Quetico rocks at greater depths. This is supported by type II and III samples showing more negative $\varepsilon_{Nd(t=1000Ma)}$ values than type I samples, a signature that reflects interaction with older continental crust. The source magma feeding type I Nipigon sills possibly exploited the same pathways yet had less interaction with continental crust at depth as the system was armoured by previously ascended magmas. Current geochronological data shows the oldest Nipigon sill ages to be present within the contamination centre in the southwest portion of the Embayment suggesting that the more contaminated sills are older than the less contaminated sills (Fig. 5.15). The emplacement process described above is similar to that of the "flushing" model proposed for Kambalda by Lesher et al. (2001) and for the Raglan deposits in the Cape Smith fold belt (Miller et al., 2010; Jowitt, pers. comm., 2012). In this model, magma flowed over thin sedimentary rock underlain by basalt. The sediments were eroded away and contaminated the flowing basalt exposing the underlying basalt. The refractory nature of the underlying basalt inhibited any contamination of subsequently emplaced magma. Although this model varies slightly from the process inferred here, it provides an analogue for the refractory nature of basaltic material inhibiting contamination by country rock.

When considering the emplacement mechanisms of many of the ultramafic intrusions of the Nipigon Embayment (Seagull, Disraeli, Hele, Kitto), an alternative model arises. The ultramafic intrusions do not display significant negative niobium anomalies which has been argued to be the result of little crustal contamination as these magmas were emplaced relatively rapidly along lithospheric-scale faults (Hollings et al., 2007a; Hart and MacDonald, 2007). Using the model for the emplacement of the ultramafic intrusions as an analogue, the Nipigon magmas should have experienced little contamination within the conduit if the Nipigon magmas ascended through the lithosphere along major structures as in a "flushing" model. This lends to the alternative model of the less contaminated type I magmas being emplaced along faults with less crustal interaction, akin to the process for the emplacement of ultramafic units described above. The more contaminated type II and III magmas were subsequently emplaced having had a longer residency time ponding in a crustal level magma chamber where they assimilated more crustal material. This model will henceforth be referred to as the "ponding" model.

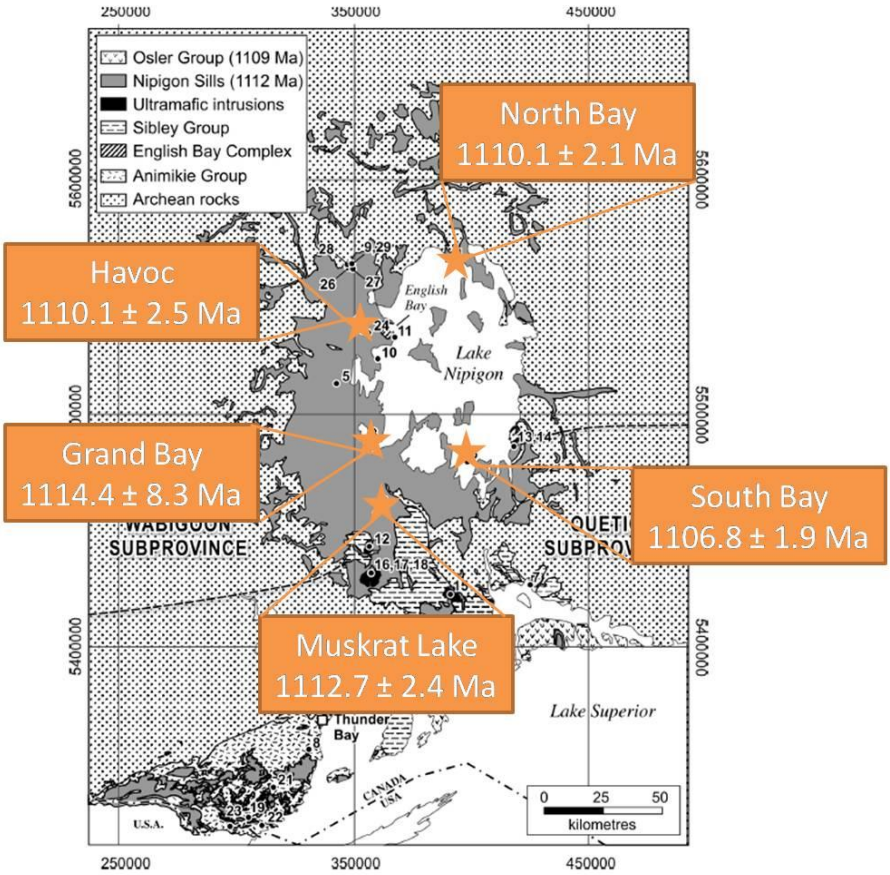

Figure 5.15: Simplified geological map showing geochronological data for the Nipigon sills. Data from Heaman et al. (2007).

The flushing model for the emplacement of the Nipigon sills is consistent with the trace element contamination data (i.e., Nb/Nb* values) with type I sills having more interaction with the Sibley Group after the emplacement of the more crustally contaminated type II and III sills. However, as previously mentioned, the Sr isotope data shows no evidence for type I sills having more interaction with the Sibley Group. To speculate that type I sills only had interaction with the Sibley Group would ignore the fact that all three Nipigon sill types have been reported to be in contact with or in proximity to Sibley Group rocks, an observation confirmed by the coherent Sr isotope data for all three sill types. Although the "ponding" model is not consistent with the current geochronology, the overlapping error of the Nipigon sill dates makes inferences into the timing of sill types challenging (Fig. 5.15). Therefore, based on the evidence presented here, most notably the Nd isotope data, it is more likely that the more contaminated signatures of type II and II sills are dominantly controlled by the Quetico rocks, as in the "ponding" model described above.

CHAPTER 6
LOGAN BASIN EMPLACEMENT SEQUENCE

6.1 Results

6.1.1 Field Observations

Dykes within the Logan Basin form prominent east to east-northeast trending ridges making outcrops abundant, particularly towards the shore of Lake Superior. Logan sills form towering mesas with steep cliff-faces throughout the study area. Field traverses were carried out in order to investigate the timing relationship between dyke units as well as their relationship with the surrounding Logan diabase sills. The dykes within the Logan basin are currently grouped into three lithological units based primarily on their orientation: the east-northeast- to northeast-trending Pigeon River dykes; the east-northeast-trending Mount Mollie dyke; and the north-northwest- to northwest-trending Cloud River dykes (Hollings et al. 2010).

Mapping undertaken in this study, following the work of Geul (1970, 1973), has confirmed the presence of two distinct Pigeon River dyke orientations. However, attempts to discern a timing relationship between dykes occupying the two orientations was difficult, as no crosscutting relationships were observed between Pigeon River dykes of different orientations. Furthermore, dykes of both trends display a subophitic to ophitic texture, making textural distinctions difficult. These observations suggest that there is no obvious way to discern the two orientations of Pigeon River dykes in the field.

Mapping along the banks of the Arrow River has also uncovered an outcrop of the recently recognized Devon volcanics (Fig. 6.1; Cundari, 2010). The unit crops out on a cliff face on the west bank of the Arrow River and displays a very fine-grained texture with abundant amygdules. This outcrop lies ~4km west of the previously mapped outline of the unit (Cundari, 2010), suggesting the Devon volcanics are more extensive than previously recognized. This is supported by trace element geochemistry and will be further discussed in section 6.2. A dyke directly underlying the new Devon volcanics outcrop extension appeared to either feed the overlying unit or be truncated by it. No direct contact could be located due to overburden and talus cover. The material within the potential feeder dyke appeared medium grained with pink colouring, starkly different from a typical Pigeon River dyke texture. Trace element geochemistry suggests that the dyke is a potential feeder for the overlying volcanic rocks and will be discussed further in section 6.2.

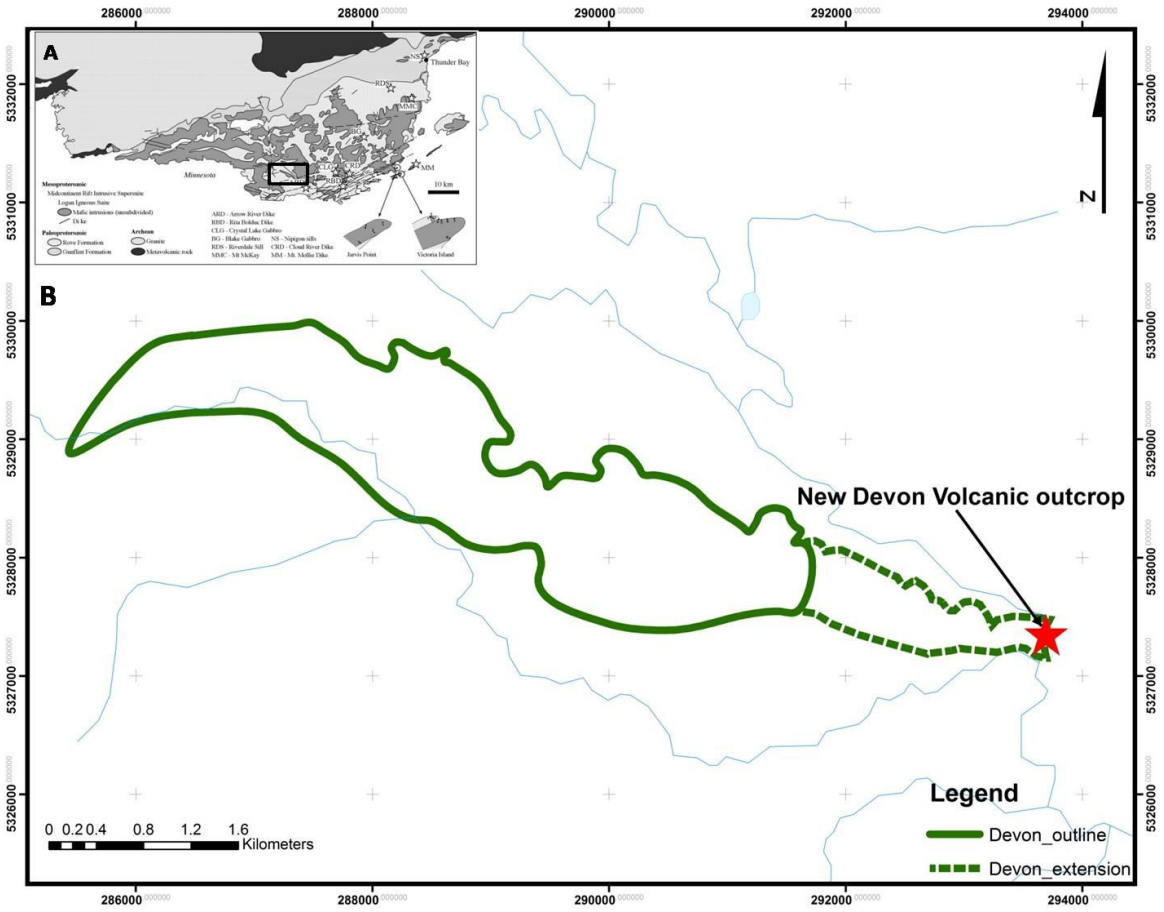

Figure 6.1: A) Map showing the location of the Devon volcanics. Modified after Hollings et al. (2007a); B) Map showing previously mapped outline of the Devon volcanic unit with new proposed extent. Modified after Cundari (2010).

The east-trending Arrow River dyke was studied to ascertain its place within the Pigeon River dyke swarm as well as to attempt to resolve the relatively young age of 1078 ± 3 Ma (Heaman et al., 2007). As the Arrow River dyke lies on a roughly parallel trend with the Pigeon River dykes, no cross cutting relationship between dykes was discovered. It can be inferred that the Arrow River dyke exhibits a cross-cutting relationship with a west dipping Logan sill as sill material of similar character was located on the north and south side of the dyke (Fig. 6.2 A). No direct contact relationship between the Arrow River dyke and the Logan sills was discovered but it can be postulated that the Arrow River dyke post-dates the Logan sills. This sequence is consistent with the current geochronology.

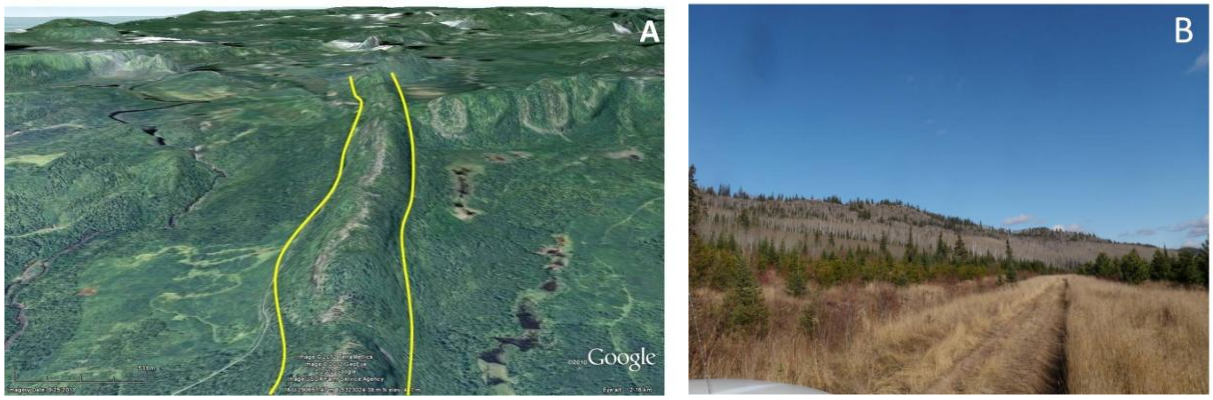

Figure 6.2: A) Satellite image showing Arrow River dyke cross-cutting a relatively steeply dipping Logan sill (image looking WSW). Topography displayed at 3x vertical exaggeration; B) Photo showing pronounced topographic high defined by the Arrow River dyke (photo looking NE). Satellite photo courtesy of Google Earth.

Reconnaissance work on Victoria Island in Lake Superior has revealed that the Mount Mollie dyke intruded and was chilled against a northeast (050°)-trending dyke of Pigeon River affinity (Fig. 6.3 A and B). The Pigeon River dyke displays a typical subophitic texture while the cross-cutting Mount Mollie dyke exhibits abundant granophyric patches set within coarse-grained gabbroic material. Ages are pending on samples from the Pigeon River dyke and the Mount Mollie dyke at the locality shown in Figure 6.3. A cross-cutting relationship between an older porphyritic diabase sill and a younger northeast trending dyke (Fig. 6.4 A and B) is also present on the southwest shore of Victoria Island.

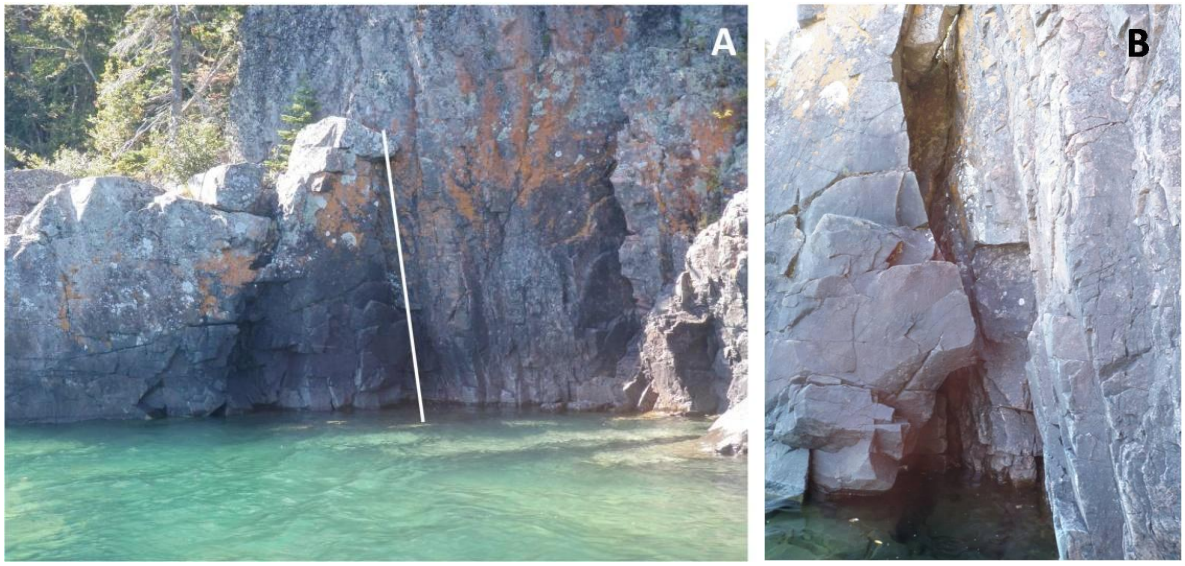

Figure 6.3: A) Photo of the Mount Mollie dyke (right; sample 110) cross-cutting a northeast (050°) trending Pigeon River dyke (left; sample 111; contact outlined in white); B) Closeup of cross-cutting relationship shown in Figure 6.3A (Pigeon River dyke (left), Mount Mollie dyke (right)).

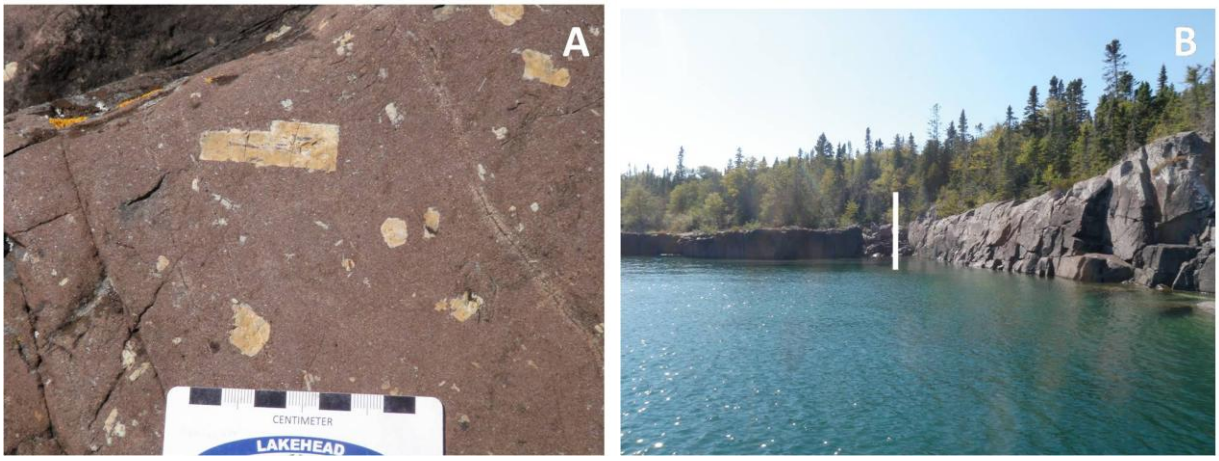

Figure 6.4: A) Photo showing tablular plagioclase phenocrysts within Logan diabase sill taken from the left side of 6.4B; B) Photo showing ENE trending Pigeon River dyke (sample 113; right) cross-cutting a Logan diabase sill (sample 112; left) (contact outlined in white).

Traverses in the Mount Mollie area (Fig. 6.5) also provided evidence for an emplacement sequence for the three main dyke units. Although no cross-cutting relationships or chilled margins were noted in this area, truncation of ridges (i.e., dykes) and mapping of textures distinct to each dyke unit suggest the following proposed emplacement sequence: Pigeon River dykes, followed by Cloud River dykes and, lastly, the Mount Mollie dyke (Fig. 6.6). Following the north to north-west trending Cloud River dyke north (Fig. 6.7 A and B), a cross-cutting relationship can be observed between an east-northeast trending Pigeon River dyke and a Cloud River dyke. Here, a clear cross-cutting relationship is observed whereby the Cloud River dyke is cross-cutting the Pigeon River dyke. This relationship is consistent with that observed on Mount Mollie.

Figure 6.5: Satellite image showing the location of the Mount Mollie area, outlined in white (looking N). Satellite photo courtesy of Google Earth.

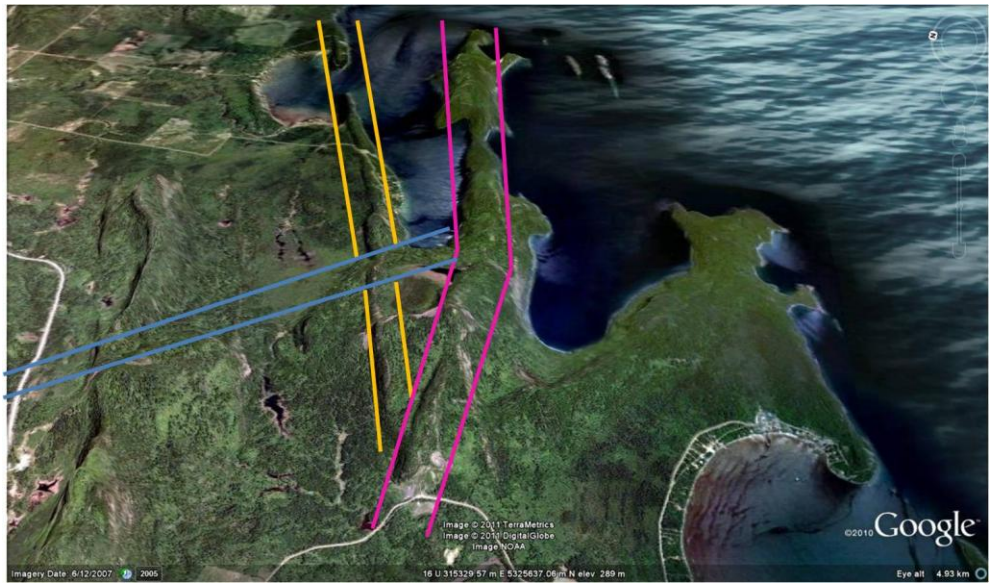

Figure 6.6: Satellite image of Mount Mollie showing cross-cutting relationships between a Pigeon River dyke (yellow), a Cloud River dyke (blue) and the Mount Mollie dyke (pink). Topography displayed at 3x vertical exaggeration. Satellite photo courtesy of Google Earth.

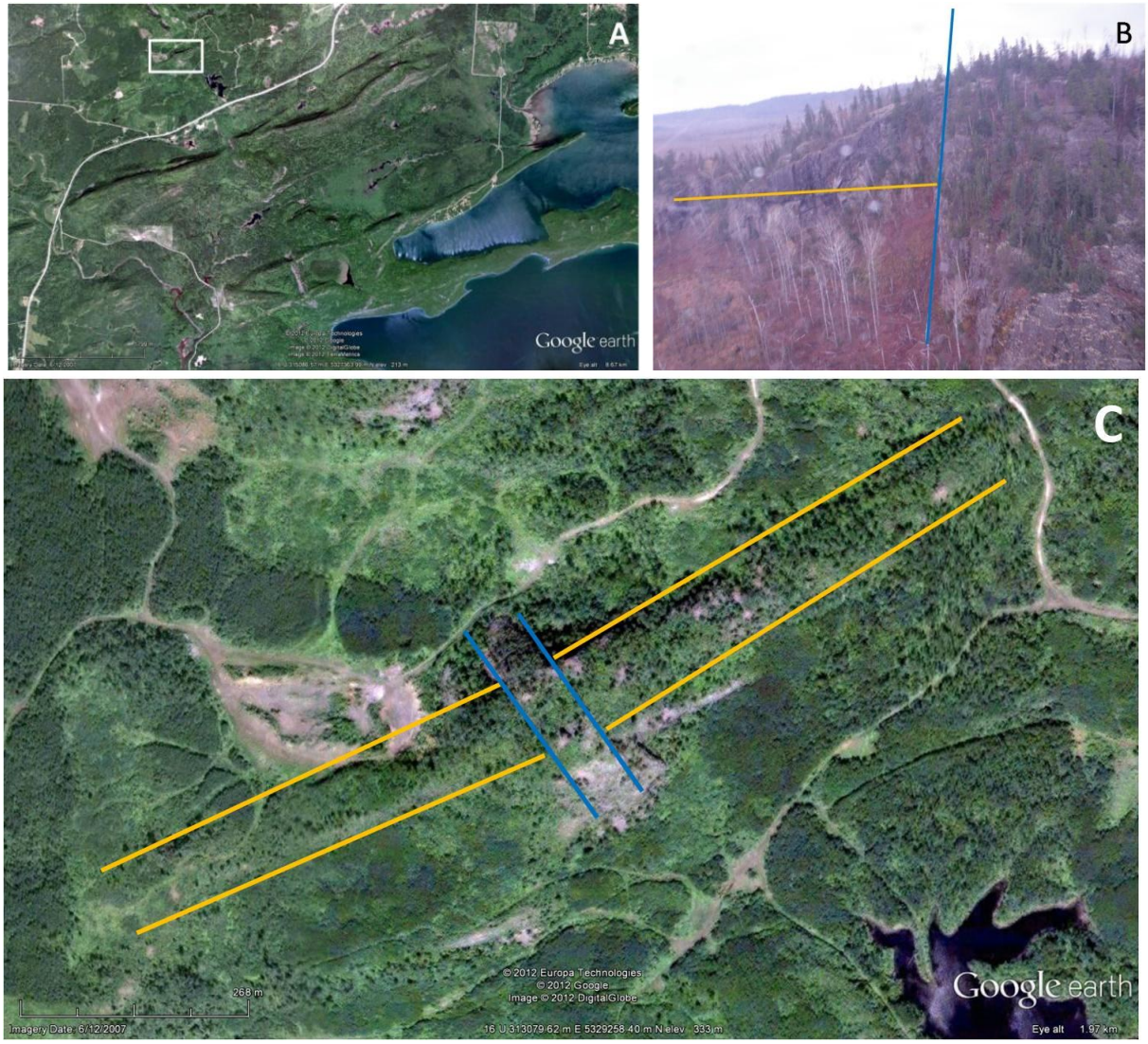

Figure 6.7: A) Satellite photo showing location of cross-cutting relationship; B) Photo from the air showing a Pigeon River dyke (yellow) being cross-cut by a Cloud River dyke (blue); C) Satellite image showing cross-cutting relationship in B. Satellite photos courtesy of Google Earth.

Based on cross-cutting relationships observed in the field, the proposed emplacement sequence for intrusive units of the Logan basin is outlined in Table 6.1. This sequence is broadly consistent with the current geochronological and paleomagnetic evidence with the exception of the Pigeon River dyke ages which will be addressed in the discussion section.

Table 6.1: Proposed emplacement sequence for MCR-related units within the Logan Basin. Ages from Hollings et al. (2010) and Heaman et al. (2007); Paleomagnetic data from Piispa et al. (2011).

Unit	Trend/Polarity	Age
Arrow River dyke?		1078.0 ± 3.0 Ma
Crystal Lake gabbro	E; N polarity	1099.6 ± 1.2 Ma
Mount Mollie dyke	E; N polarity	1109.3 ± 6.3 Ma
Cloud River dykes	NW; N polarity	1109.2 ± 4.4 Ma
Pigeon River dykes	E-NE; N polarity	1141.0 ± 20 Ma
Logan sills	N polarity	1114.7 ± 1.1 Ma
Devon Volcanics	R polarity	tbd
Riverdale sill	R polarity	tbd

6.1.2 Whole-rock geochemistry

A total of 53 samples from the Logan Basin were analyzed for major and trace element geochemistry in this study (Fig.6.9). This complements the existing database compiled from previous studies (see Chapter 2). Full geochemical data analyses for each sample analyzed for this study are presented in Appendix D. The majority of samples were taken from Pigeon River dykes (including the Arrow River dyke), the Cloud River dykes and the Mount Mollie dyke. Additional samples were taken from the Devon Volcanics, Logan sills and Nipigon sills. Currently, the most useful plot for discriminating between Midcontinent Rift-related intrusive rocks is the plot of La/Sm_n versus Gd/Yb_n (Fig. 6.10).

Logan sill samples from this study display elevated Gd/Yb_n and a tight range of La/Sm_n ratios. TiO_2 values for all Logan sills sampled in this study were comparable to the published values for the Logan sills of Hollings et al. (2007a; Fig. 6.10). A sample of very fine-grained, volcanic material taken from the west bank of the Arrow River displayed characteristics akin to those described for the Devon volcanics by Cundari (2010), as described above (Fig. 6.1). This sample showed elevated Gd/Yb_n value plotting within the field for the Devon volcanics of Cundari (2010; Fig. 6.10).

Detailed sampling of the 1078 Ma Arrow River dyke (Fig. 6.8a; Heaman et al., 2007) showed no discernable geochemical differences along the strike length of the dyke. All samples show nearly identical trace element patterns on a primitive normalized trace element diagram with the exception of sample 129 which displayed elevated Th (Fig. 6.8b). Sample 129 was taken from close to the south contact of the Arrow River dyke with Rove Formation shale. All Arrow River dyke samples plot in a tight population within the Pigeon River dyke field on the plot of La/Sm_n versus Gd/Yb_n showing no discernable differences from other Pigeon River dykes (Fig. 6.10).

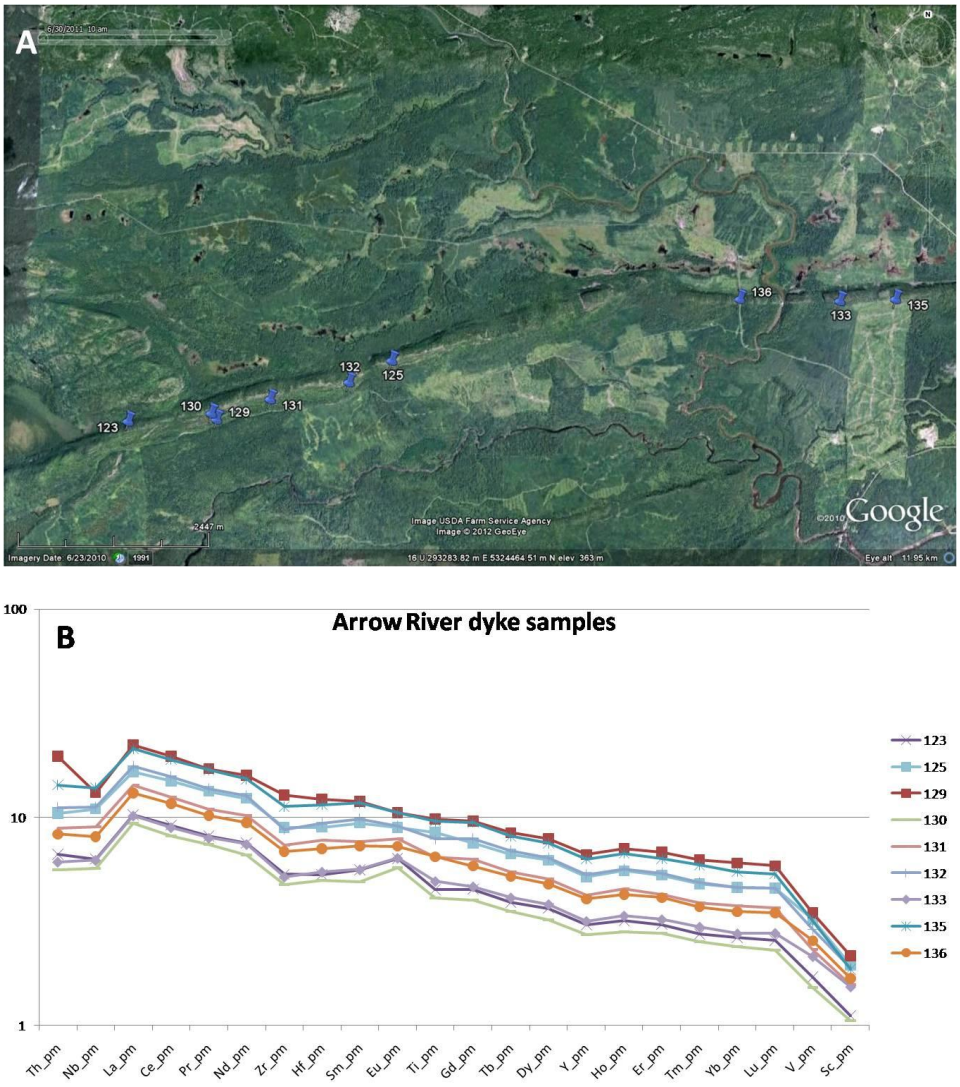

Figure 6.8: A) Satellite photo showing location of Arrow River dyke samples. B) Primitive mantle-normalized diagrams for all Arrow River dyke samples. Normalizing values from Sun and McDonough (1989).

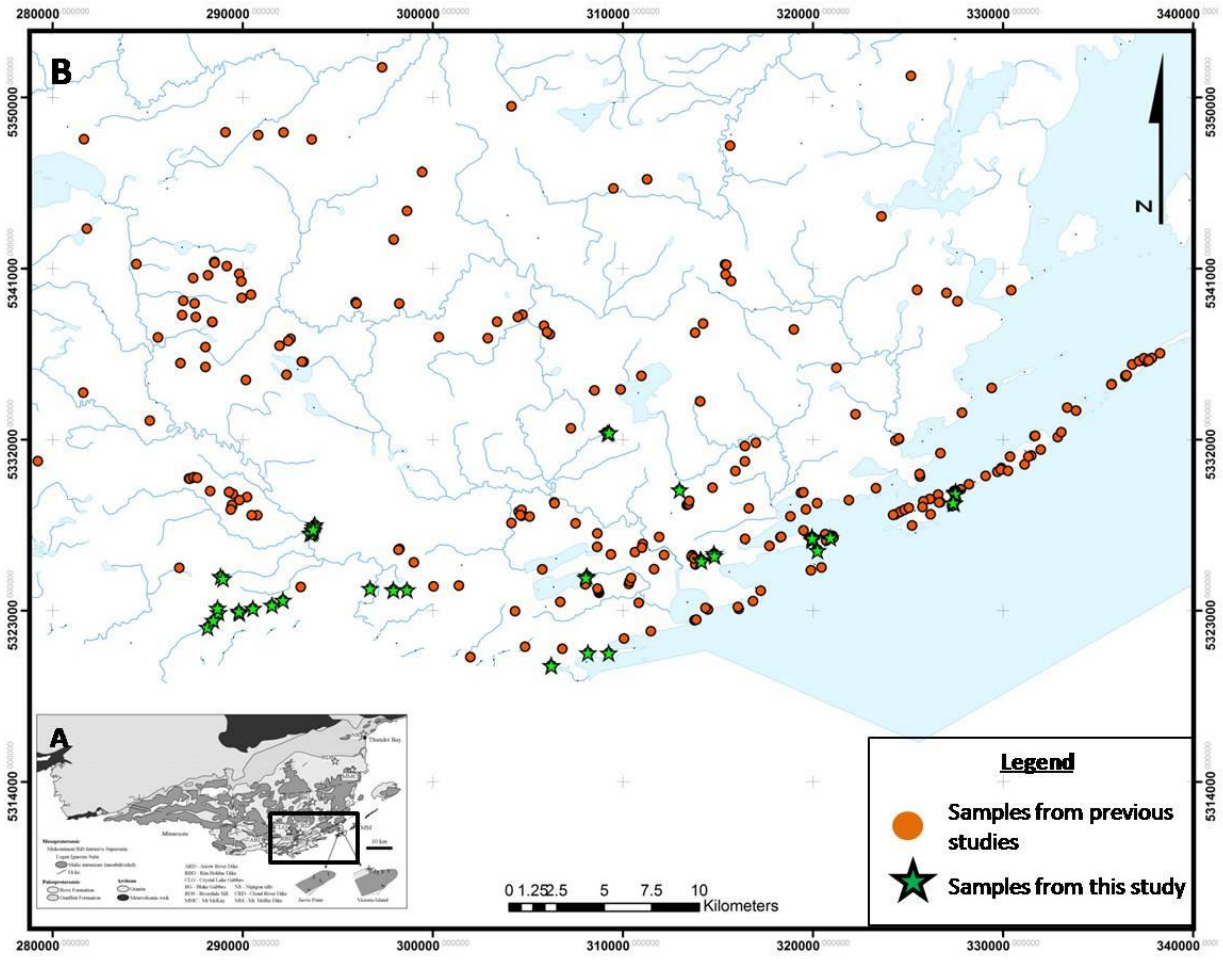

Figure 6.9: A) Map showing location of sampling area relative to the Logan Basin and the city of Thunder Bay. Modified after Hollings et al. (2007a). B) Map showing sample locations for this study and sample locations from previous studies.

All samples taken from east-northeast trending dykes plot within the field for Pigeon River dykes defined by Hollings et al. (2010). No discernable geochemical differences between Pigeon River dykes of different trends could be made as all samples taken from Pigeon River dykes plot within the Pigeon River field on the plot of La/Sm_n versus Gd/Yb_n (Fig. 6.10). Samples taken from north-northwest trending dykes all plot within or close to the field for Cloud River dykes (Fig. 6.10). The Cloud River dyke samples from this study show slight variability from the field of Hollings et al. (2010) but still form a relatively tight array. Furthermore, the Cloud River dyke field overlies the Pigeon River dyke field showing broadly similar trace element characteristics. The Mount Mollie dyke samples broadly plot within the Mount Mollie field defined by Hollings et al. (2010). One sample from this study shows a higher La/Sm_n ratio than the majority of the Mount Mollie samples and also displays the most negative

$\varepsilon_{Nd(t=1100Ma)}$ value (Fig. 6.10). The Mount Mollie dyke, the Pigeon River and Cloud River dykes all show considerable overlap in Figure 6.10 with broadly similar Gd/Yb_n values and a large spread of La/Sm_n.

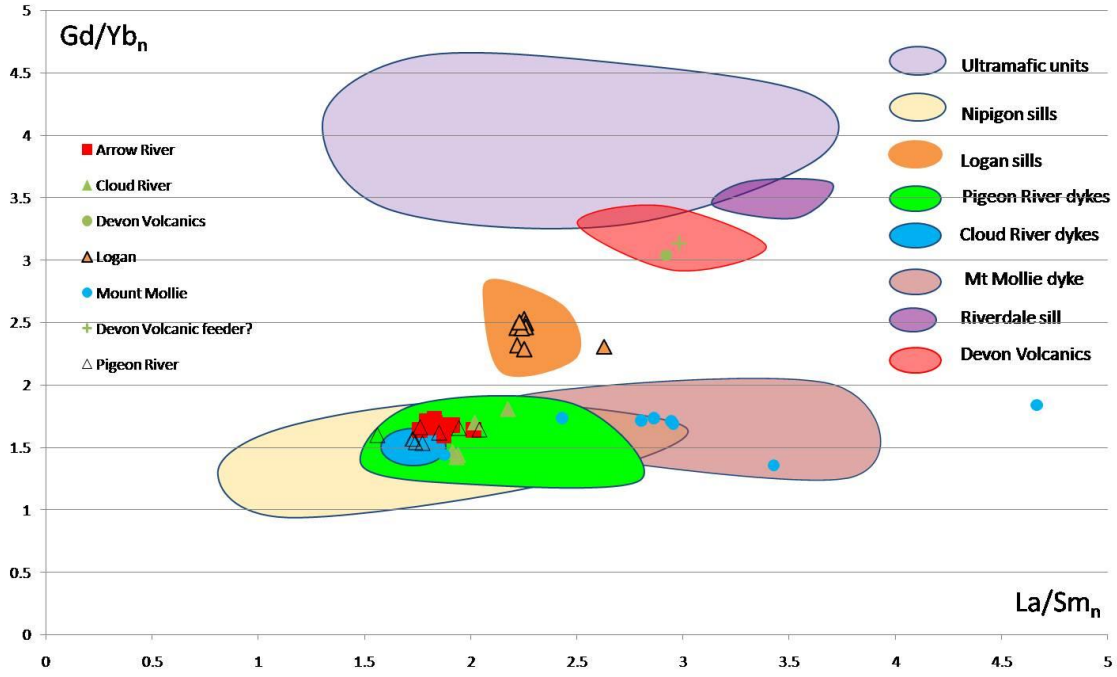

Figure 6.10: Plot of La/Sm_{pm} vs. Gd/Yb_{pm} showing samples from this study and fields for Midcontinent Rift-related mafic rocks defined by Hollings et al. (2007a) and Hollings et al. (2010). Normalizing values from Sun and McDonough (1989).

6.1.3 Isotope geochemistry

Eight samples from the Logan Basin were analyzed for Sm-Nd and Rb-Sr isotopes in this study (Table 6.2). The full data set for each sample analyzed for this study is presented in Appendix E. Four of the samples were chosen from localities where a cross cutting relationship was clearly seen (samples 110, 111, 112 and 113; Figs. 6.3 and 6.4). Two samples were chosen from newly recognized outcrops of two units cropping out on the banks of the Arrow River; one an outcrop of the Devon and the other from an east-northeast, Pigeon River style dyke. The remaining two samples were chosen from the Arrow River dyke and the Cloud River dyke. The $\varepsilon_{Nd(t=1100Ma)}$ values for the three Pigeon River dyke samples in this study show zero and positive values (Table 6.2). The range for Pigeon River dykes as defined by Hollings et al. (2011b) is 0.9 to -7.9 which makes the value of 1.5 for sample 111 the most positive $\varepsilon_{Nd(t=1100Ma)}$ recognized for a Pigeon River dyke. The sample taken for the Arrow River dyke plots within the range for the Pigeon River dykes with a value of -0.2. The Cloud River dyke sample shows an $\varepsilon_{Nd(t=11\ 00Ma)}$ value of

-4.0 which is slightly more negative than the published data for the Cloud River dykes showing $\varepsilon_{Nd(t=1100Ma)}$ values of 0.3 and -3.0 (Hollings et al., 2011b). The Mount Mollie sample shows an extremely negative $\varepsilon_{Nd(t=1100Ma)}$ value of -13.3 which is by far the most negative value for the Mount Mollie dyke and among the most negative $\varepsilon_{Nd(t=1100Ma)}$ values for Midcontinent Rift-related rocks. Additionally, the Logan sill sample taken from plagioclase phenocryst-rich material on Victoria Island shows an $\varepsilon_{Nd(t=1100Ma)}$ value of -4.2 which is the most negative value for all known Logan sill samples. This value is well outside the range of $\varepsilon_{Nd(t=1100Ma)}$ values (0.1 to -1.5) defined by Hollings et al. (2011b). The Devon volcanic sample shows an $\varepsilon_{Nd(t=1100Ma)}$ value of -2.9 which is broadly consistent with the value of -3.5 defined by Hollings et al. (2011b). Sr isotope data show the Logan sill sample and the Mount Mollie sample to display the highest $^{87}Sr/^{86}Sr_i$ ratios of all samples analysed at 0.71196 and 0.71662, respectively. The Devon Volcanics display a $^{87}Sr/^{86}Sr_i$ ratio of 0.70931. The Pigeon River dykes (including the Arrow River dyke) display a range of $^{87}Sr/^{86}Sr_i$ values from 0.68910 to 0.70498. Lastly, the Cloud River dyke displays a $^{87}Sr/^{86}Sr_i$ value of 0.70722, higher than that displayed by the Pigeon River dykes. All isotope data show a weakly negative correlation between Sr and Nd isotope data with higher $^{87}Sr/^{86}Sr_i$ values correlating with more negative $\varepsilon_{Nd(t=1100Ma)}$ values (Fig. 6.11).

Table 6.2: Isotope data for Logan Basin units analysed in this study. Comparative data (ranges and averages) from Hollings et al. (2011b).

Unit	**Sample numbers**	**$\varepsilon_{Nd(t=1100Ma)}$ values**	**$\varepsilon_{Nd(t=1100Ma)}$ range**	**$\varepsilon_{Nd(t=1100Ma)}$ average**	**$^{87}Sr/^{86}Sr_i$**
Arrow River	136	-0.2	*See Pigeon River*		0.70343
Cloud River	126	-4.0	0.3 to -3.0	-1.4 (n=2)	0.70722
Devon Volcanics	SP-RC-008	-2.9	-3.5	(n=1)	0.70931
Logan	112	-4.2	0.1 to -1.8	-0.7 (n=16)	0.71196
Mount Mollie	110	-13.3	0.9 to -3.8	-1.6 (n=3)	0.71662
Pigeon River	SP-RC-014	0.0	0.9 to -7.9	-0.86 (n=5)	0.68910
	113	0.0			0.70461
	111	1.5			0.70498

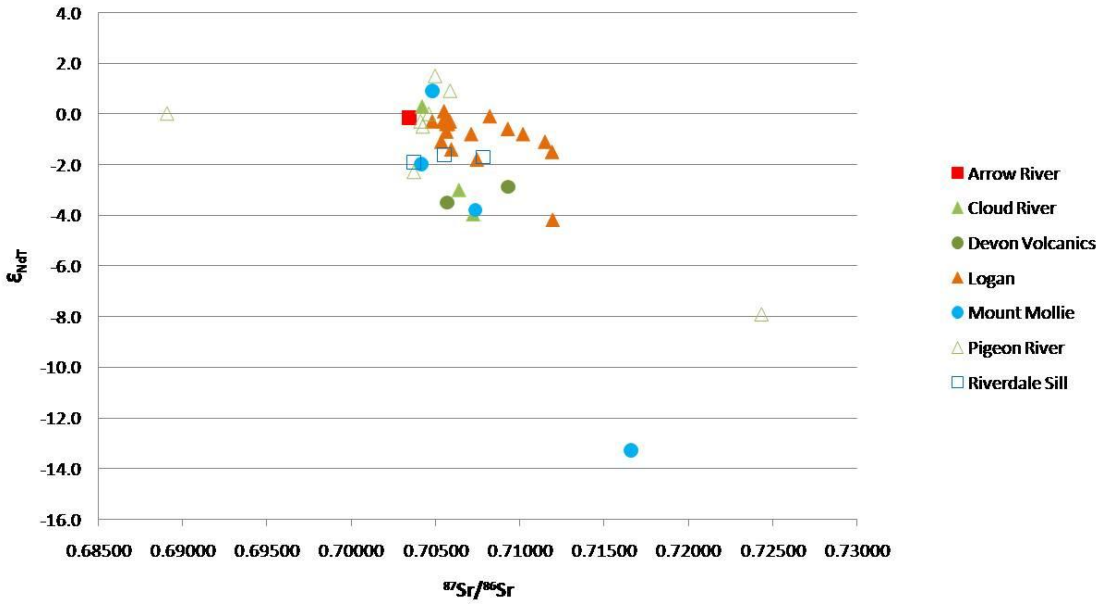

Figure 6.11: $^{87}Sr/^{86}Sr$ versus $\varepsilon_{Nd(t=1100Ma)}$ for Midcontinent rift related units in the Logan Basin. Additional data from Hollings et al. (2011b).

6.2 Discussion

6.2.1 Geochemistry, geochronology and paleomagnetism of the units of the Logan Basin

Constraining the timing of emplacement of the units present within the Logan basin allows for inferences to be made about the geodynamic and geochemical evolution of the area. Recent geochronological, geochemical and paleomagnetic data have refined our understanding of Midcontinent Rift-related rocks present within the Logan Basin (e.g., Heaman et al., 2007; Hollings et al., 2010; Hollings et al., 2011b). The expression of Midcontinent Rift-related magmatism in the Logan Basin is manifested by a variety of intrusive units (Logan sill, Riverdale sill, Pigeon River dykes, Cloud River dykes, the Mount Mollie dyke, and the Crystal Lake gabbro) as well as one volcanic unit, the Devon volcanics. The dominant dyke units are the Pigeon River dykes which generally display a N polarity with only two Pigeon River dykes located close to the U.S. border displayed R polarity (Robertson and Fahrig, 1971; Pesonen, 1978). The Pigeon River dykes analysed in Hollings et al. (2010) display nearly identical, normally polarized paleomagnetic signatures which is not consistent with the published ages of 1141 ± 20 Ma and 1078 ± 3 Ma for the Rita Bolduc dyke and the Arrow River dyke, respectively (Heaman et al., 2007). The reason for this inconsistency between the geochronological and paleomagnetic data is that one would expect a R polarity for an age of 1141 Ma and a N polarity for an age of 1078 Ma. Furthermore, all Pigeon River

dykes display broadly similar trace element signatures where one would expect some geochemical variations over a 60 m.y. time period (Hollings et al., 2010). The ages for both Pigeon River dykes are questionable as the Rita Bolduc data is discordant (4-12%) and the Arrow River data is based on a single micro-baddeleyite analysis (Hollings et al., 2010). Geochemically, the Pigeon River dykes display broadly similar trace element characteristics to those of the Nipigon sills to the north. This is best displayed on the plot of La/Sm_n versus Gd/Yb_n (Figs. 6.10 and 6.12) showing the similar LREE and HREE abundances of both units. However, the Pigeon River dykes are not thought to be the feeders to the Nipigon sills as the Pigeon River dykes lie some distance away from the Nipigon sills (Hollings et al., 2010).

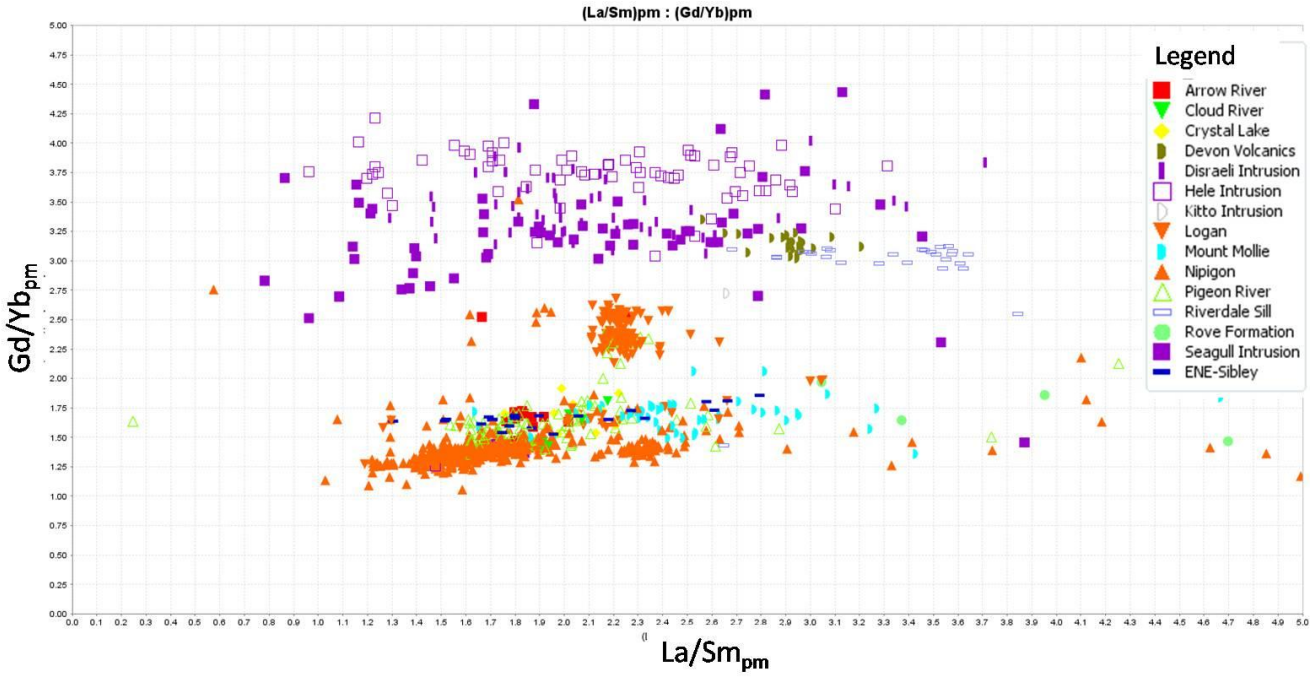

Figure 6.12: Diagram showing La/Sm_{pm} vs. Gd/Yb_{pm} ratios for Midcontinent rift-related mafic rocks. Normalizing values from Sun and McDonough (1989).

The cross-cutting relationships presented in this study have revealed new discrepancies surrounding the current geochronological data. The Pigeon River dykes have been shown in this study to cross-cut and therefore post-date the Logan sills. The 1078 ± 3 Ma age for the Arrow River dyke (a Pigeon River dyke) supports the Pigeon River dykes post-dating the 1114.7 ± 1.1 Ma Logan sills, which they cross cut. However, the 1078 Pigeon River dyke age is contradicted by the 1109.2 ± 4.2 Ma age for the Cloud River dyke and the 1109.3 ± 6.3 Ma age for the Mount Mollie dyke, both of which have been shown to cross-cut Pigeon River dykes. The 1141 ± 20 Ma age for the Rita Bolduc dyke (a Pigeon River dyke) does not

support the Pigeon River dykes cross-cutting the Logan sills but supports the Pigeon River dykes being cross-cut by the Cloud River and the Mount Mollie dykes. Further geochronology is warranted to resolve these inconsistencies. High precision, U/Pb dates are pending on the cross-cutting relationship between a Pigeon River dyke and the Mount Mollie dyke, shown in Figure 6.3.

Discrepancies have also arisen with respect to the Cloud River dyke polarity. Robertson and Fahrig (1971) first defined an R polarity for a north northwest trending Cloud River dyke. Hollings et al., (2010) reported similar data for the Cloud River dyke displaying an R polarity, however, these results are based on two samples which is too small a number for meaningful statistics. Piispa et al. (2011) defined an N polarity for the Cloud River dyke based on eight samples taken across the width of the dyke exposure directly adjacent to the sample location of Hollings et al. (2010). Based on the number of samples and the subsequent meaningfulness of the statistics, the Cloud River dyke is believed to display an N polarity as defined by Piispa et al. (2011). The N polarity for the Cloud River dyke has been confirmed by Halls (pers. comm., 2012) based on recent sampling. However, an N polarity contradicts the 1109.2 ± 4.2 Ma age defined for the Cloud River dyke as one would expect an R polarity for an age older than ~1103 Ma (Hollings et al., 2010). Geochemically, the Cloud River dykes display broadly similar trace element characteristics to the Pigeon River dykes and also to the Nipigon sills to the north (Figs. 6.10 and 6.13; Hollings et al., 2010). Refinement of the geochronology is warranted to explain the contradiction between the date for the Cloud River dyke and its paleomagnetic signature.

The Mount Mollie dyke was suggested to be associated with the Crystal Lake gabbro as the Mount Mollie dyke extends east from the Crystal Lake gabbro (Guel, 1973; Smith and Sutcliffe, 1989). Baddeleyite ages of 1109.3 ± 6.3 Ma for the Mount Mollie dyke and 1099.6 ± 1.2 Ma for the Crystal Lake gabbro suggest that the two are not co-genetic (Heaman et al., 2007; Hollings et al., 2010). Furthermore, the two units are geochemically distinct with the Mount Mollie dyke characterized by higher La/Sm_n values than the Crystal Lake gabbro, likely due to a greater amount of crustal contamination (Fig. 6.10; Hollings et al., 2010). The Mount Mollie dyke is, however, geochemically similar to the surrounding Pigeon River dykes albeit with a greater range of La/Sm_n values (Fig. 6.10; Hollings et al., 2010).

The 1114.7 ± 1.1Ma Logan sills (Heaman et al., 2007) represent the most volumetrically significant unit within the Logan Basin, as discussed in Chapter 3. The relationship between the Logan sills and the Pigeon River dykes has been somewhat ambiguous as dykes appear to both cross-cut and merge with sills (Guel, 1970, 1973; Smith and Sutcliffe; 1989; Hollings et al., 2010). Hollings et al. (2010) proposed that the Pigeon River dykes are not the feeders to the Logan sills based on trace element chemistry, with the Logan sills having elevated Gd/Yb_n ratios compared to those for the Pigeon River dykes (Figs. 6.10 and

6.12). Furthermore, Carl (2010) noted Pigeon River dykes clearly cross-cutting Logan sills on Sibley Peninsula which is consistent with field observations from this study that noted Pigeon River dykes cross-cutting Logan sills. Based on field and geochemical evidence, it can be stated with confidence that the Pigeon River dykes post-date the Logan sills which supports the 1078 Ma age for the Arrow River dyke as well as the N polarity for the majority of the Pigeon River dykes. The dominantly N polarity of the Pigeon River dykes (with the exception of the two R polarized Pigeon River dykes previously mentioned) supports the Pigeon River dykes post-dating the R polarized Logan sills which they cross-cut.

The Riverdale sill is located in the northern part of the Logan Basin, spatially and geochemically distinct from the surrounding Logan sills (Hollings et al., 2010; Puchalski, 2010). Geochemically, the Riverdale sill displays elevated Gd/Yb_n ratios, similar to the ultramafic intrusions of the Nipigon Embayment (Fig. 6.10 and 6.12; Puchalski, 2010). In addition to the geochemical similarities, the Riverdale sill displays an R polarity further suggesting it may be coeval with the ultramafic intrusions of the Nipigon Embayment (Hollings et al., 2010; Puchalski, 2010). Furthermore, the presence of a Logan type dyke cross-cutting the Riverdale sill indicates that the Riverdale sill must predate the surrounding Logan sills (Hollings et. al, 2010). No geochronological data is available for the Riverdale sill due to the absence of datable material.

The Devon volcanics comprise an extrusive body located within the southern portion of the Logan Basin in Devon Township (Fig. 6.1). Geochemically, the Devon volcanics display an elevated Gd/Yb_n denoting significant HREE fractionation, similar to that of the Riverdale sill. Furthermore, the Devon volcanics display a similar R polarity to that of the Riverdale suggesting the two units may be genetically related (Piispa, 2011). There is no field evidence to support a direct link between the Devon volcanics and the Riverdale sill as they lie ~45 km apart. As discussed in the previous section, an outcrop of volcanic rock on the west bank of the Arrow River shows the Devon volcanics to be larger than previously mapped. The new outcrop of volcanic material plots well within the field for the Devon volcanics defined by Cundari (2010) on the plot of La/Sm_n and Gd/Yb_n (Fig. 6.10). In addition to the new extension, the potential feeder dyke to the Devon volcanics has been located in the Arrow River (Section 6.1). Trace element chemistry suggests that this dyke can be interpreted to be the feeder to the overlying Devon volcanics as the dyke plots well within the field for the Devon volcanics on the plot of La/Sm_n and Gd/Yb_n (Fig. 6.10).

6.2.2 Implications for mantle source characteristics, contamination histories and the geodynamic evolution of the Logan Basin

Applying the discrimination parameters used in the re-evaluation of the Nipigon sills (see Chapter 5) to the various units in the Logan Basin provides new insights into the magmatic evolution of the Logan Basin. Evaluation of the geochemistry of units present within the Logan Basin on the plots of Th/Yb_{pm} versus Nb/Th_{pm} (Fig. 6.13) and Nb/Yb_{pm} versus Th/Yb_{pm} (Fig. 6.14) show results that suggest variable source characteristics and subsequent new relationships between units. More detailed explanations of the discrimination parameters used in this section are explained in Section 5.2. Results show that Logan Basin units were derived from potentially three different mantle sources, each progressively more depleted through time. The timing relationships defined in the previously section for units in the Logan Basin in relation to their source magmas and contamination histories are discussed in this section.

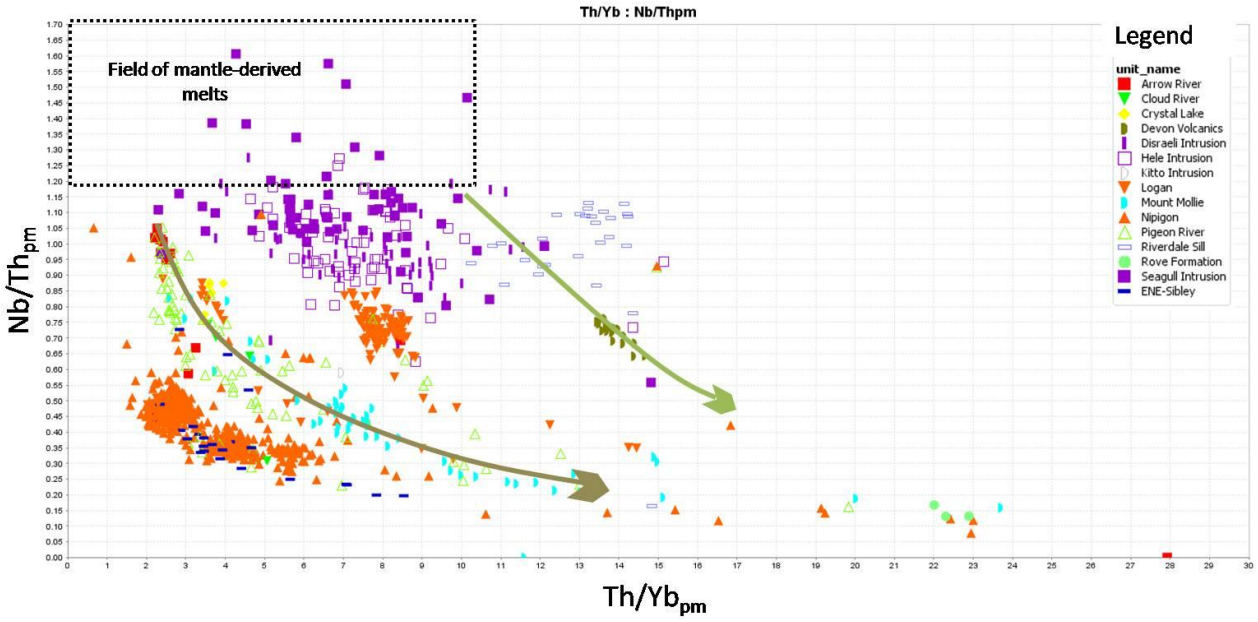

Figure 6.13: Diagram showing variations in Th/Yb_{pm} and Nb/Th_{pm} ratios for Midcontinent Rift-related mafic rocks. Arrows indicated trends suggestive of mixing between primary magmas and crustal material. Normalizing values from Sun and McDonough (1989).

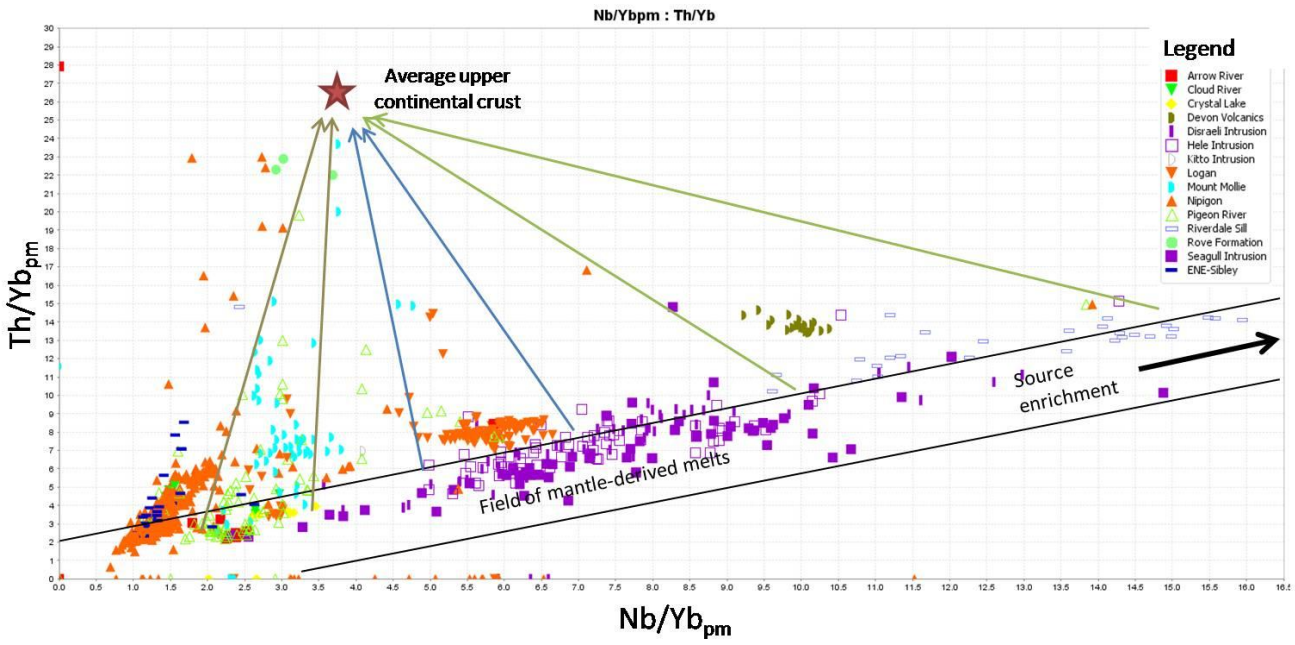

Figure 6.14: Diagram showing variations in Nb/Yb_{pm} and Th/Yb_{pm} ratios for Midcontinent Rift-related mafic rocks. Normalizing values from Sun and McDonough (1989).

The earliest magmatism present within the Logan Basin is likely the Riverdale sills and the Devon volcanics as they display R polarities as well as geochemical source characteristics (i.e. elevated Gd/Yb_n) akin to those of the early ultramafic units of the Nipigon Embayment (Hollings et al., 2010). The ultramafic units are known to be among the oldest intrusions associated with the Midcontinent Rift emplaced from 1115 to 1110 and display an elevated Gd/Yb_n signature indicative of a deep-seated mantle source (Heaman et al., 2007; Hollings et al., 2007a). Although dates are not available for the Riverdale sill and the Devon volcanics, they were likely emplaced within the same time period as the ultramafic intrusions based on geochemical and paleomagnetic evidence (Section 6.1). Further geochemical evidence suggesting that the Riverdale sill and the Devon volcanics are analogous to the ultramafic units and different from the Logan sills is displayed on the plot of Th/Yb_{pm} versus Nb/Th_{pm} (Fig. 6.13) and Nb/Yb_{pm} versus Th/Yb_{pm} (Fig. 6.14). The Riverdale sill and the Devon volcanics plot on a mixing line (DR) from the field of mantle derived melts towards values for average continental crust and the Rove Formation. The Devon volcanics and the Riverdale sills both display the highest Nb/Yb_{pm} values suggesting they were derived from the most enriched mantle source compared to all the other mafic intrusive units within the Logan Igneous suite. The Devon volcanics samples display a tight array on both Nb/Yb_{pm} versus Th/Yb_{pm} and Th/Yb_{pm} versus Nb/Th_{pm} (Figs. 6.13 and 6.14) with elevated Th/Yb_{pm} values compared to those of the Riverdale sill, likely due to the Devon Volcanic undergoing a greater degree of

crustal contamination. The more contaminated nature of the Devon Volcanics is supported by the Nd isotope data with the Devon Volcanics having $\varepsilon_{Nd(t=1100Ma)}$ values of -2.9 to -3.5 and the Riverdale sill having lower $\varepsilon_{Nd(t=1100Ma)}$ values from -1.6 to -1.9. The relationship between units present in the Logan Basin and the greater MCR area, as well as their implications for the magmatic evolution of the Midcontinent Rift will be addressed further in the next chapter.

The Logan sills represent the first volumetrically significant magmatic activity within the Logan Basin emplaced as five to six diabase sheets (Smith and Sutcliffe, 1989). Dated at 1114.7 ± 1.1 Ma, the R polarized Logan sills are among the oldest intrusive units present within the Logan Basin. If the model for the Devon volcanics and the Riverdale sill being coeval with the ultramafic units of the Nipigon Embayment is correct, it is likely that the Logan sills post-date the Devon and Riverdale. This is supported by the cross-cutting Logan dyke within the Riverdale sill quarry. However, the 1117 Ma age suggests that the Logan sills are also broadly contemporaneous with the ultramafic intrusions. Therefore, it is possible that the Logan sills, the Riverdale sills and the Devon volcanics were all emplaced within a relatively short time frame while all displaying geochemically distinct characteristics. The emplacement of these three units within a relatively short time period is supported by their similar R polarized signatures. A similar relationship was argued by Neumann (2011) for the Golden Valley Sill Complex in the Karoo Basin which showed chemically distinct sills forming from different batches of magma within a spatially restricted area. This serves as an analogue for the emplacement history and geochemical signatures of the Logan sills, the Riverdale sill and the Devon volcanics within the Logan Basin.

Geochemically, the Logan sills plot on a mixing line directly between the ultramafic intrusions and the values for average continental crust on the plots of Th/Yb_{pm} versus Nb/Th_{pm} (Fig. 6.13) and Nb/Yb_{pm} versus Th/Yb_{pm} (Fig. 6.14). The plot of Nb/Yb_{pm} versus Th/Yb_{pm} (Fig. 6.14) shows the Logan sills have similar Nb/Yb_{pm} values to the ultramafic units of the Nipigon Embayment yet higher Th/Yb_{pm} values. This suggests that the Logan sills and the ultramafic intrusions may be derived from the same source with the Logan sills experiencing a greater degree of crustal contamination than the ultramafic units, as indicated by their higher Th/Yb_{pm} contents. The average value of -0.7 for the Logan sills from previous studies, in addition to the $\varepsilon_{Nd(t=1100Ma)}$ value of -4.2 from this study, supports the contaminated nature of the Logan sills. However, variable $\varepsilon_{Nd(t=1100Ma)}$ values ranging from -0.2 to -4.0 for the Seagull intrusion (representing the ultramafic intrusions) were reported by Heggie (2005) whereby the most negative values were present towards the base of the intrusion and attributed to contamination during transport to shallow crustal levels. The negative $\varepsilon_{Nd(t=1100Ma)}$ for the ultramafic intrusions in comparison to the Logan sills does not support the Logan sills being more contaminated than the ultramafic intrusions. The discrepancy between higher Th/Yb_{pm} values and the $\varepsilon_{Nd(t=1100Ma)}$ data may be due to inadequate sample density in the

Logan sills or perhaps due to variations in the contaminant. The Logan sills display similar source characteristics to the Jackfish, McIntyre and Inspiration sills within the Nipigon Embayment based on Nb/Yb_{pm} ratios which will be discussed further in the final chapter. Thus, the geochemical evidence presented here may support a genetic relationship between the Logan sills and the ultramafic intrusions which is further supported by the geochronological data.

Evaluating the plot of Nb/Yb_{pm} versus Th/Yb_{pm} (Fig. 6.14) with the emplacement sequence proposed in this study, a model for the progression of magmatism from a more enriched mantle source to a more depleted mantle source through time can be postulated. This supports the Logan sills post-dating the Riverdale sill and the Devon volcanics. Evidence supporting this includes the fact that the Logan sills display lower Gd/Yb_n ratios than the Riverdale sill and Devon volcanics suggesting melting occurred at a relatively shallower depth. Also, the Logan sills display lower Nb/Yb_{pm} ratios than the Devon volcanics and Riverdale sill plotting on a different mixing line than (Fig. 6.14). This suggests the Logan sills were derived from a different, more depleted mantle source than the Riverdale sill and the Devon Volcanics. Based on the evidence presented above for the Riverdale sill, the Devon Volcanics and the Logan sills being emplaced in a relatively short time period in conjunction with the model for the progression of geochemically distinct source characteristics through time, it is likely that a significant change in the source region occurred during this period. This change must have been from a deeper, more enriched mantle source (Riverdale and Devon) to a shallower, more depleted mantle source (Logan) in a short time period as to satisfy the geochronological and paleomagnetic data summarized in this study.

Subsequent to the emplacement of the Logan sills, the Pigeon River dykes were emplaced. This is supported by field evidence presented in this study noting Pigeon River dykes cross-cutting Logan sills. It is further confirmed by reports of Pigeon River dykes cross-cutting sills or appearing to terminate at the base of sills (e.g. Guel, 1970; 1973; Smith and Sutcliffe, 1989; Hollings et al., 2010). As noted above, the Pigeon River dykes are geochemically similar to the Nipigon sills to the north yet are not likely to be feeders to the Nipigon sills as they lie some distance away. Carl (2010) suggested that the Pigeon River style, east-northeast trending dykes on Sibley Peninsula (here referred to as the Sibley dykes) are geochemically similar to and thus belong to the Pigeon River suite. Re-evaluation of the dyke data from the Pigeon River dykes in the Logan Basin and the Sibley dykes in relation to the Nipigon sills have shown geochemical differences between the Pigeon River dykes and the Sibley dykes. On the plots of Nb/Yb_{pm} versus Th/Yb_{pm} and Th/Yb_{pm} versus Nb/Th_{pm} (Fig. 6.13 and 6.14) the Pigeon River dykes form arrays separate to those of the Nipigon sills, with the Sibley dykes dominantly plotting within the Nipigon field. This suggests that the Sibley dykes are more likely to have been the feeders to the Nipigon sills than the Pigeon River dykes in the Logan Basin as they display very similar geochemical signatures, most

notably, similar Nb/Yb_{pm} and Nb/Th_{pm} values. Furthermore, it is more likely that the Sibley dykes represent feeders to the Nipigon sills as they lie in closer proximity to the Nipigon sills than the Pigeon River dykes. The implications for the timing of magmatism between the Nipigon Embayment and the Logan Basin will be further discussed in the final chapter.

The Cloud River dykes have been clearly shown in this study to cross-cut Pigeon River dykes at a perpendicular orientation with the Mount Mollie dyke truncating both Pigeon River dykes and Cloud River dykes. Although this is not consistent with the geochronological data, the field evidence supports this timing relationship. The variable orientation between the three dyke sets, as well as textural differences between them, allows for inferences into the geodynamic controls on the emplacement, as well as the source of the dykes. The Pigeon River dykes were emplaced at a roughly rift-axis parallel orientation likely due to magma exploiting normal faulting as extension progressed. Along with normal faulting, it is likely that accommodation or transverse faults propagated perpendicular to the orientation of the normal faults. The Cloud River dykes may represent magma exploiting accommodation or transverse faults. This process is best exemplified at the Mid-Atlantic ridge whereby east-west spreading is accompanied by transverse faults striking parallel to the direction of spreading (Winter, 2001). The Cloud River dykes contain abundant plagioclase phenocrysts characteristically different to that of the Pigeon River dykes. The similar geochemical source characteristic of the Cloud River and Pigeon River dykes, suggests that both magmas were derived from the same source or staging chamber. However, the Cloud River dyke magma may have experienced slightly longer residency time in the staging chamber than the Pigeon River dyke magma as it cross-cuts the Pigeon River dykes. The time spent by the Cloud River dyke magma in a staging chamber, may have been enough time for plagioclase phenocryst formation in the chamber. As the transverse fault propagated, it tapped the plagioclase phenocryst rich magma resulting in the emplacement of the Cloud River dyke cross-cutting the Pigeon River dykes. Similar evidence is reported in the Matachewan dyke swarm where the presence of plagioclase megacrysts in dykes has been interpreted to indicate that these melts existed for some time in chambers with lower pressures below 10kbar (Phinney and Halls, 2001). The longer residency time of the Cloud River dyke is supported by the Nd isotope data as two of the three available samples display $\varepsilon_{Nd(t=1100Ma)}$ values of -3.0 and -4.0 which are more negative than the majority of the Pigeon River dyke samples indicative of a greater degree of crustal contamination.

This process may further explain the geochemical and textural character of the Mount Mollie dyke as it displays a similar source characteristic to the Pigeon River and Cloud River dykes which suggests that all three dyke units were derived from the same source (i.e. same depth as noted by similar Gd/Yb_{pm} ratios; Figs. 6.10 and 6.12). Also, the Mount Mollie dyke has been shown to post-date both the Pigeon River and

Cloud River dykes. It is possible that the Mount Mollie dyke was sourced from the same magma chamber as the Pigeon River and Cloud River dykes yet had a longer residency time to fractionate out a felsic component, which is manifested by the composite nature of the Mount Mollie dyke containing abundant granophyre. The longer residency time of the Mount Mollie dyke is supported by the more contaminated geochemical signature, as the Mount Mollie dyke displays the highest Th/Yb_{pm} ratios of the three dykes as well as the broadest range of La/Sm_{pm} values. Furthermore, the Mount Mollie dyke displays a wide range of $\varepsilon_{Nd(t=1100Ma)}$ from 0.9 to -13.3 suggesting both primary source characteristics as well as a complex crustal contamination history. This supports the petrogenetic model of the dyke having spent longer residency time in a magma chamber than the Pigeon River and Cloud River. Also, an $\varepsilon_{Nd(t=1100Ma)}$ value of -13.3 is the most negative of any previously reported in the study area further supporting the Mount Mollie dykes contaminated nature. The Sr data for dyke sets in the Logan Basin does not show any correlation to the emplacement sequence. Elevated $^{87}Sr/^{86}Sr_i$ values are interpreted to be a result of shallow level contamination by Animikie Rove Formation sedimentary rocks (Hollings et al., 2011b). $^{87}Sr/^{86}Sr_i$ values for the Pigeon River dykes, the Cloud River dykes and the Mount Mollie dyke (Fig. 6.11), show considerable overlap and broad ranges suggesting that individual dykes underwent variable shallow level contamination during emplacement.

The similar source characteristics of all three dykes sets supports the model of them being tapped from the same magma chamber each experiencing more crustal contamination through time (i.e. similar Gd/Yb_{pm}; Fig. 6.12 and Nb/Yb_{pm} values; Fig. 6.14). The average $\varepsilon_{Nd(t=1100Ma)}$ values for each of the three dyke sets is consistent with the progressively more contaminated nature of the dykes through time; Pigeon River = -0.86, Cloud River -1.4 and Mount Mollie = -1.6 (Table 6.2), supporting the timing relationship determined in this study. The data presented here begins to explain the magmatic evolution of dykes within the Logan Basin in light of the cross-cutting relationship, the variable textures between units, the similar geochemical signature of the three units as well as the variable crustal contamination signatures present. Further work is warranted on this topic to further solidify this theory, most notably, refinement of the geochronology on the dyke sets and work towards a better understanding of the composite nature of the Mount Mollie dyke.

The timing relationship established in this study has improved our understanding of the geochemical relationships between units in the Logan Basin. However, the new emplacement sequence has contradicted the current ages for the Pigeon River dykes as well as the paleomagnetic data. Based on the validity of the data of Heaman et al. (2007) noted in section 6.2.1, neither the 1141 Ma nor the 1078 Ma age for Pigeon River dykes is correct. Theoretically, the Pigeon River dykes should fall between 1117 Ma (Logan sill) and 1109 Ma based on the cross-cutting relationship outlined here. This age bracket

contradicts the dominantly normal paleomagnetic signature for the Pigeon River dykes but is consistent with the R polarity for two Pigeon River dykes towards the southeast corner of the Logan Basin. However, the R and N polarities for the Pigeon River dykes, in conjunction with the broad spread in ages suggests that magmatism was long lived and not necessarily a single pulse event as suggested by Hollings et al. (2010).

CHAPTER 7

RE-EVALUATION OF MIDCONTINENT RIFT-RELATED GEOCHEMISTRY AND IMPLICATIONS FOR THE MAGMATIC EVOLUTION OF THE SYSTEM

Criteria for the discrimination of mafic rocks has been introduced in this study along with a previously unrecognized emplacement sequence to provide an improved understanding of the relationship between intrusive units associated with the 1.1 Ga Midcontinent Rift. Detailed descriptions of these parameters are summarized in Chapter 5 and have been referred to throughout this study. This section serves as a summary to relate the intrusive units of the Nipigon Embayment to one another and also to the units present within the Logan Basin as well as to provide a concise summary of the study.

The plot of Th/Yb_{pm} versus Nb/Th_{pm} (Fig. 7.1) can be inferred as a mixing model between the field of mantle-derived melts and the source of contamination. Separate trends scattering away from the field of mantle-derived melt compositions towards lower Nb/Th_{pm} and higher Th/Yb_{pm} values suggests the presence of separate, distinct magma types which have undergone separate crustal contamination histories (Jowitt and Ernst, in press). The plot of Nb/Yb_{pm} versus Th/Yb_{pm} (Fig. 7.2) also delineates distinct primary source compositions as distinct ranges of Nb/Yb_{pm} values which underwent their own crustal contamination history as indicated by higher Th/Yb_{pm} values. The results derived from the aforementioned plots are supported on the plot of La/Sm_{pm} versus Gd/Yb_{pm} which denotes depth of melting (Gd/Yb_{pm}) as well as partial melting and contamination histories (La/Sm_{pm}). Many workers (Nicholson et al., 1997; Hollings et al., 2007a) suggest that the compositions of the ultramafic units are the best indicators for the primary magma formed from a mantle plume. This is displayed by the elevated Gd/Yb_{pm} ratios of the ultramafic intrusions denoting a deep-seated mantle source. The positions of the ultramafic units on the plot of Nb/Yb_{pm} versus Th/Yb_{pm} (Fig. 7.2) as well as Th/Yb_{pm} versus Nb/Th_{pm} (Fig. 7.1) support this as the ultramafic intrusions plot within or towards the field of mantle-derived melts. Based on these criteria, three distinct distributions can be observed on this plot for Midcontinent Rift-related rocks, each indicative of a separate primary magma type which underwent its own crustal contamination history; the Nipigon sill trend, the Jackfish, McIntyre, Inspiration and Logan trend and the Devon Volcanics and the Riverdale sill trend. The distributions or mixing lines are denoted by coloured arrows in Figures 7.1 and 7.2; red indicates the Nipigon trend, blue indicates the Jackfish sill, McIntyre sill, Inspiration sill and Logan sills (JMIL), and green indicates the Devon volcanics and Riverdale sill trend (DR).

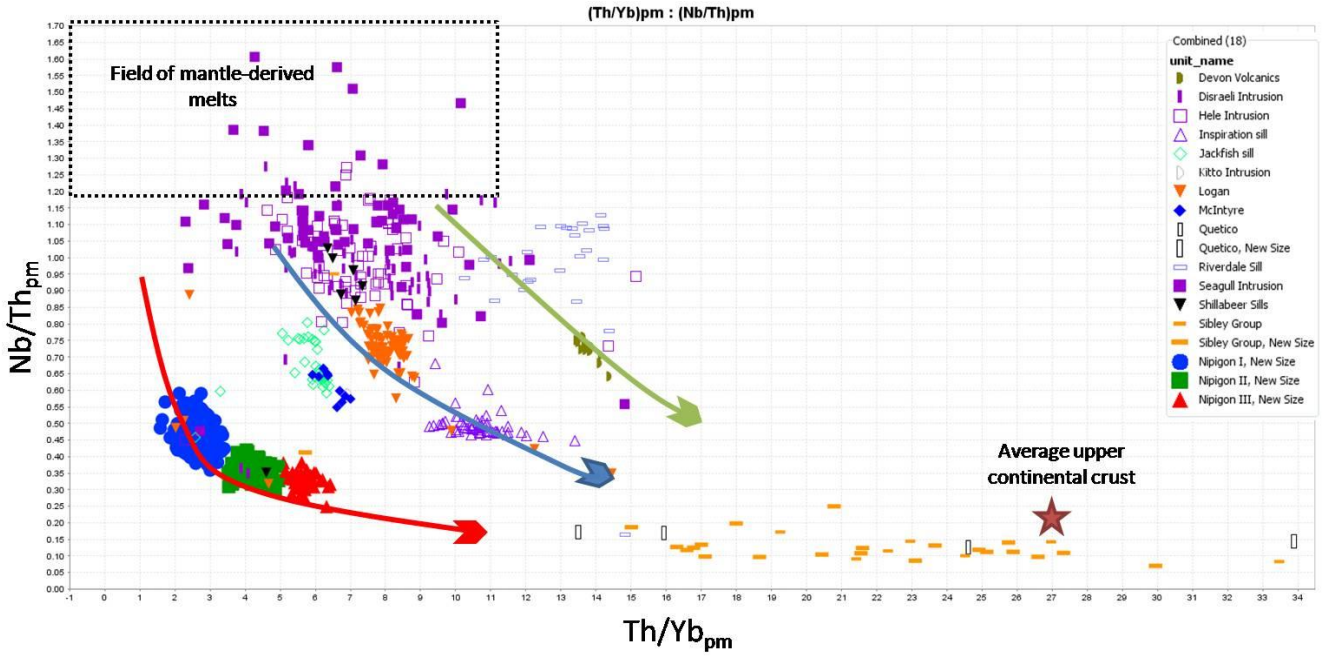

Figure 7.1: Diagram showing variations in Th/Yb_{pm} and Nb/Th_{pm} ratios for Midcontinent rift-related mafic rocks. Arrows indicated trends suggestive of mixing between primary magmas and crustal material. Red arrow indicate Nipigon trend, blue arrow indicate JMIL trend and green arrows indicate DR trend. Normalizing values from Sun and McDonough (1989).

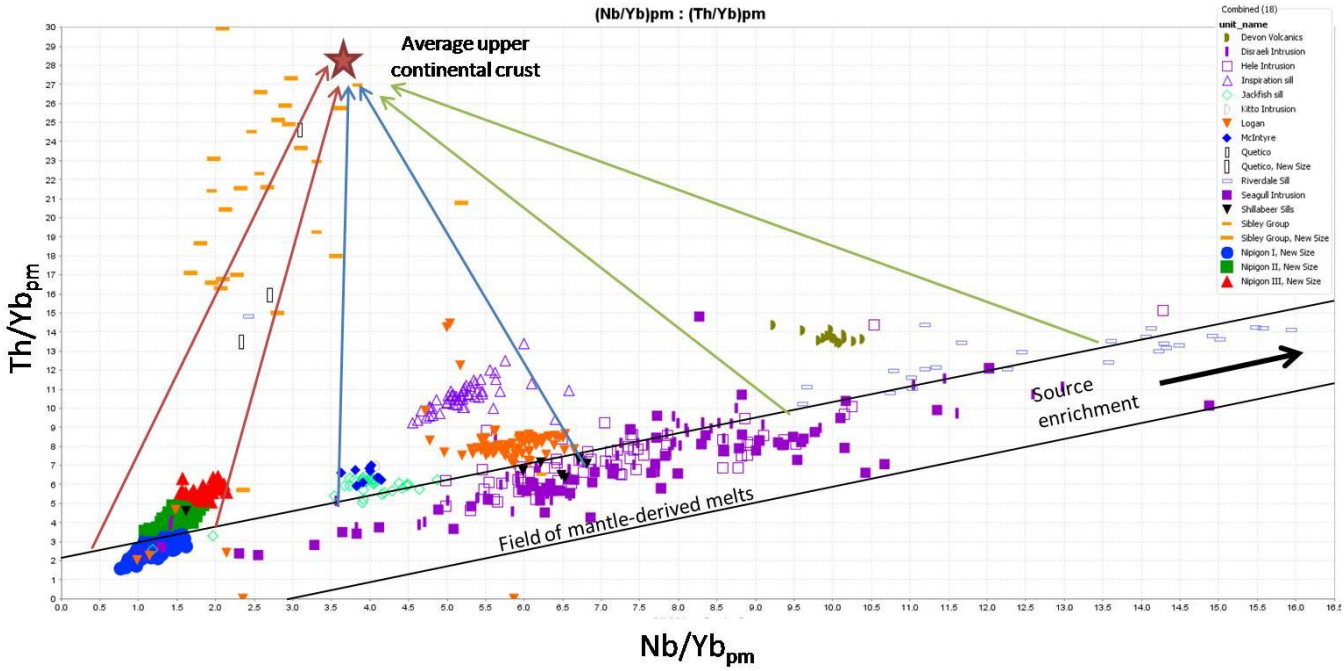

Figure 7.2: Diagram showing variations in Nb/Yb_{pm} and Th/Yb_{pm}ratios for Midcontinent rift-related mafic rocks. Red arrow indicate Nipigon trend, blue arrow indicate JMIL trend and green arrows indicate DR trend. Normalizing values from Sun and McDonough (1989).

The first trend is that of the Nipigon sills which lies on a separate mixing line to the other Midcontinent Rift-related unit trends (JMIL and DR).The Nipigon trend (red arrows; Figs. 7.1 and 7.2) is characterized by lower Nb/Th_{pm} and lower Nb/Yb_{pm} values than the other units present in the Nipigon Embayment. This suggests it was derived from a different primary magma source which underwent its own crustal contamination history with the more contaminated sill types trending away from the field of mantle-derived melts and towards crustal compositions. The distinction between the source of the Nipigon sills and the source of the other intrusive units is supported by Nipigon sills displaying lower Gd/Yb_{pm} ratios (Fig. 7.3) suggesting that melting occurred at a shallower depth compared to the other intrusive units (excluding the Inspiration sill). The data presented here implies that the Nipigon sills were in fact formed from a different starting magma composition which underwent its own crustal contamination history separate to that of the Jackfish, McIntyre, Inspiration and Logan sills as well as the Devon volcanics and the Riverdale sill.

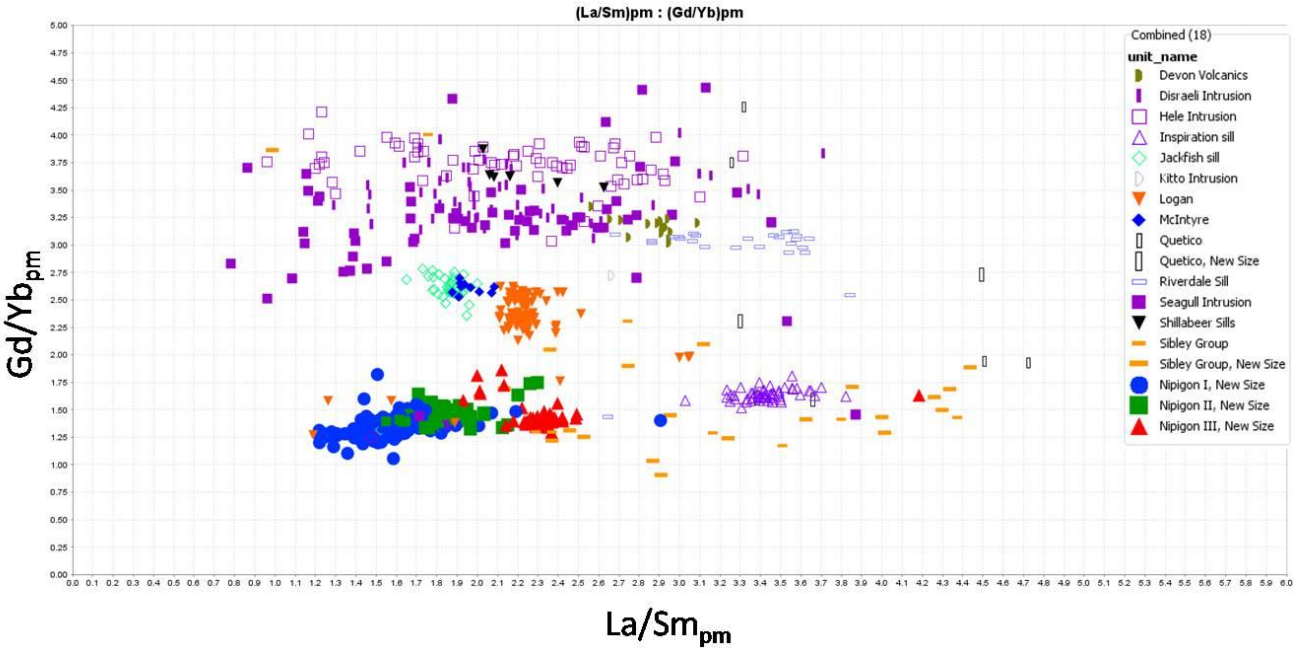

Figure 7.3: Diagram showing La/Sm_{pm} vs. Gd/Yb_{pm}ratios for Midcontinent rift-related mafic rocks. Normalizing values from Sun and McDonough (1989).

The second trend present on this diagram comprises the Jackfish sill, the McIntyre sill, the Logan sills and the Inspiration sill (JMIL). The JMIL trend (blue arrows; Figs. 7.1 and 7.2) is characterized by Nb/Th_{pm} and Nb/Yb_{pm} values in between that of the Nipigon sill trend and the Devon volcanics and Riverdale sill trend. It is possible that the JMIL trend may have had a primary magma composition similar to the compositions of the ultramafic intrusions of the Nipigon Embayment as the JMIL mixing line trends directly from the ultramafic units (Fig. 7.1 and 7.2). The JMIL trend suggests that the Jackfish, McIntyre, Logan and Inspiration sills were derived from a source different to that of the Nipigon sills, possibly similar to that of the composition of the ultramafic intrusions. Hollings et al. (2007a) suggested that the Nipigon sills and the Jackfish, McIntyre, Inspiration and Logan were derived from the same source, different to that of the ultramafic intrusions. In contrast, the data presented here supports the Nipigon sills being derived from a different source than the ultramafic intrusions but suggests the Jackfish, McIntyre, Inspiration and Logan to be derived from a source similar to that of the present composition of the ultramafic intrusions.

The spread in Th/Yb_{pm} suggests the Logan sills underwent a greater degree of crustal contamination than the Jackfish and McIntyre sills. Also, the higher Th/Yb_{pm} values for the Inspiration sill suggest that it was derived from the same source but underwent a greater degree of crustal contamination. The more contaminated nature of the Inspiration sill compared to the Jackfish and McIntyre sills is supported by isotope data from Hollings et al. (2007b). The Inspiration sill displays $\varepsilon_{Nd(t=1000Ma)}$ values from -6.1 to -6.6 whereas the Jackfish and McIntyre sills display $\varepsilon_{Nd(t=1000Ma)}$ values from -0.5 to -1.1 and -2.3 to -3.2, respectively. The mixing trend present of the Th/Yb_{pm} versus Nb/Th_{pm} plot is also supported on the plot of La/Sm_{pm} versus Gd/Yb_{pm} (Fig. 7.3). The Jackfish, McIntyre, and Logan sills all display similar Gd/Yb_{pm} ratios from 2.0 to 2.8 suggesting they were derived at broadly the same depth of melting. The Inspiration sill, however, displays a lower Gd/Yb_{pm} ratio suggesting it was derived from a shallower depth. The more contaminated nature of the Inspiration sill may imply a longer residency time in the crust whereby melting might have occurred at a slightly shallower depth and had time to assimilate more crustal material. This data also presents a spatial problem as the Logan sills are located >100 km away from the Nipigon Embayment. It is hard to envisage units derived from the same parent magma tapping the same source over such a long distance. The slightly greater degree of crustal contamination of the Logan sills compared to that of the Jackfish and McIntyre sills may provide reasoning for this discrepancy. As the Logan sills were emplaced a large distance away, their source magmas may have spent more time in a crustal level magma chamber which migrated south-westward and assimilated more crustal material. This

may be supported by the isotope data from Hollings et al. (2011b) who reported $\varepsilon_{Nd(t=1000Ma)}$ values from 0.1 to -3.0 for Logan sills as well as a -4.2 for a Logan sill sample in this study.

The third trend is that of the Devon volcanics and the Riverdale sill (DR), both located within the Logan Basin south of Thunder Bay, which lie on a separate mixing line to the other two MCR-related trends (Nipigon and JMIL). The DR trend (green arrows: Figs. 7.1 and 7.2) is characterized by higher Nb/Th_{pm} and higher Nb/Yb_{pm} values than the other units present in the Nipigon Embayment. This suggests both units on this trend were derived from a different, more enriched primary magma source which underwent its own crustal contamination history. As the DR mixing line trends towards the compositions of the ultramafic intrusions, it is possible the Devon volcanics and the Riverdale sill were derived from a similar source. The elevated Th/Yb_{pm} values and lower Nb/Th_{pm} values suggest variability in contamination between the two units with the more contaminated Devon volcanics trending away from the field of mantle-derived melts and towards crustal compositions.

The identification of different magma source characteristics within the Nipigon Embayment provides insight into the magmatic evolution of the area as well as the Midcontinent Rift system as a whole. The data presented here show that distinct batches of source material were present throughout the evolution of the MCR. Each of these three source magmas underwent variable contamination histories as well as potentially different degrees of partial melting to produce the mafic intrusive units currently preserved. Similar results were reported by Neumann (2011) for the Golden Valley Sill Complex in the Karoo Basin whereby most geochemically distinct units were emplaced in spatially restricted areas. Furthermore, they implied the mechanism of emplacement to be a combination of two models; 1) the sills are fed by chemically distinct batches of magma through separate feeders; and 2) sill complexes are generated from a single magma batch which suggests multiple sills forming an interconnected network of chemically distinct sills. This serves as an analogue for the Logan Igneous Suite as geochemically distinct sill suites are located in relatively close proximity to each other comprising an interconnected network of sills. The relationship between spatially restricted yet geochemically distinct units is prevalent in many of the ultramafic intrusions which are cross-cut by Nipigon sills. Furthermore, this implies that the evolution of intrusive units within the Logan Igneous Suite was complex involving heterogeneous source characteristics and variable crustal contamination histories.

CONCLUSIONS

8.1 The progression of magmatism of the Logan Igneous Suite

The majority of this study is focussed on defining the emplacement sequence of units and relating it to the geochemical source and contamination characteristics so as to better understand the magmatic evolution of the Midcontinent Rift. New geochemical parameters have revealed previously unrecognized relationships between units as well as allowing for inferences into the timing and geochemical evolution of the MCR. The progression of magmatism for both the Logan basin and the Nipigon Embayment suggest that source characteristics became more depleted through time. Evidence towards the link between the Logan Basin and the Nipigon Basin has also been put forth by relationship between the Riverdale sill, the Devon volcanics and the Logan sills with the mafic and ultramafic units of the Nipigon Embayment (excluding the Nipigon sills). Furthermore, the spatial link between the two magmatically endowed areas is potentially bridged by the dykes of Sibley Peninsula which may be potential feeders to Nipigon sills.

8.2 The Coubran Lake basalts

The Coubran Lake basalts present within the Coldwell Complex have provided a link to the spatial gap in Midcontinent Rift-related volcanism along the northeast shore of Lake Superior. Physical features including proximity to surrounding syenites as well as alteration features have confirmed the notion that the Coubran Lake basalts represent a pre-existing roof pendent into which the Coldwell Complex intruded. Geochemical evidence has linked the Coubran Lake basalt to the Two Duck Lake gabbro suggesting the basalts may represent the volcanic expression of the TDLG. Trace element and Nd isotopes have suggested the Coubran Lake basalts are comparable to a basalt type I composition linking the unit to the Lower Siemens Creek volcanics, the basal units in the Ely's Peak and Grand Portage areas of the North Shore Volcanics, and as the lower suite of the Osler Group. The geochemical data presented here is consistent with the paleomagnetic data suggesting the basalts were erupted early in Midcontinent Rift history.

8.3 Closing remarks

The summary of the geochemical and spatial re-evaluation of the rocks of the Logan Basin and the Nipigon Embayment is outlined in section 8.1. The new relationships between units present within the Logan Basin and Nipigon Embayment have provided new insights into the magmatic evolution of the Midcontinent Rift. The emplacement sequence defined for the Logan Basin has been supported by geochemical data but is not wholly consistent with the existing geochronological data. One main focus of

this study was to return to the field and establish sound field relationships to which the geochemical constraints can be applied. It is clear that in light of the established emplacement sequence, further work is required to refine the dating and paleomagnetic polarities of the Midcontinent rift-related rocks of the Logan Basin (Piispa, in progress).

The geochemical and petrogenetic model for the Nipigon sills has suggested that the emplacement mechanisms by which the sills were emplaced are more complex than previously thought. The sampling gaps present throughout the Embayment may provide insight into the distribution of the contamination centres, the stratigraphic relationships between sill types and the emplacement mechanisms governing the geochemical differences between units. Also, the structures beneath the Nipigon Embayment may serve as the answer to some of the geochemical issues brought about in this and previous studies. Also, further geochronology would aid in evaluating the timing between the three Nipigon sill types defined in this study.

References Cited

Addison, W.D., Brumpton, G.R., Vallini, D.A., McNaughton, N.J., Davis, D.W., Kissin, S.A., Fralick, P.W. and Hammond, A.L., 2005. Discovery of distal ejecta from the 1850 Ma Sudbury impact event; Geology 33: 193-196.

Amurawaiye, O., 2001. The Paleoproterozoic Rove Formation of northwestern Ontario: A turbidite-dominated shelf sequence; unpublished H.B.Sc thesis, Lakehead University, Thunder Bay, Ontario, 44p.

Annells, R.N., 1973. Proterozoic flood basalts of eastern Lake Superior: the Keweenawan volcanic rocks of the Mamainse Point area, Ontario. Geological Survey of Canada, Paper 72-10.

Bell., R., 1870. Report on the geology of the northwest side of Lake Superior, and of the Nipigon district. In: Reports on Ontario 1865-1886, Geological and Natural History Survey of Canada, reprinted from Geological Survey of Canda, Reports of Progress 1866-1869, pp. 313-364.

Beskar, S., 2001. The Blake gabbro: A taxitic-textured gabbro sill south of Thunder Bay, Ontario; 47th Institute on Lake Superior Geology, Annual Meeting, Madison, Wisconsin, May 9-12, 2001, Proceedings Volume 47, Part 1, p.1.

Blackburn, C.E., Johns, G.W., Ayer, J., and Davis, D.W., 1991. Wabigoon Subprovince. In: Geology of Ontario, Ontario Geological Survey, Special Volume 4, Part I. P. 303-381.

Burnham, O.M., Hechler, J.H., Semenyna, L., and Schweyer, J., 2002. Mineralogical controls on the determination of trace elements following mixed acid dissolution. In*:* Summary of Field Work and Other Activities 2002. Ontario Geological Survey Open File Report 6100, 36-1 to 36-12.

Burnham, O.M., and Schweyer, J., 2004. Trace Element Analysis of Geological Samples by ICP-MS at the Geoscience Laboratories: Revised Capabilities Due to Improvements to Instrumentation. In: Summary of Field Work and Other Activities 2004. Ontario Geological Survey Open File Report 6145, 54-1 to 54-20.

Card, K.D., and Ciesielski, A., 1986. Subdivisions of the Superior Province of the Canadian Shield, Geoscience Canada, 13: 5-13.

Carl, C. 2011. Geochemistry and petrology of intrusive rocks of the Sibley Peninsula. Unpublished honours thesis. Lakehead University.

Carter, M.W., McIlwaine, W.H., Wisbey, P.A., 1973. Nipigon-Schreiber sheet, Thunder Bay District. Ontario Geological Survey, Geological Compilation Series, Map 2232, scale 1 inch = 4 miles.

Cheadle, B.A., 1986. Alluvia-playa sedimentation in the lower Keewenawan Sibley Group, Thunder Bay district, Ontario, Canadian Journal of Earth Science. V. 23, p527-542.

Coates, M.E., 1972. Geology of the Black Sturgeon River area, District of Thunder Bay. Ontario Department of Mines and Northern Affairs, Geoscience Report 98, 41 p.

Cogulu, E.H. 1990. Mineralogical and petrological studies of the Crystal Lake intrusion, Thunder Bay, Ontario; Geological Survey of Canada, Open File 2277, 15 p. plus figures and tables.

Cundari, R., 2010. Geology and Geochemistry of the Devon Volcanics south of Thunder Bay, Ontario. Unpublished HBSc thesis, Lakehead University. 68 p.

Currie, K.L. 1980. A contribution to the petrology of the Coldwell alkaline complex, northern Ontario; Geological Survey of Canada, Bulletin 287, 42 p.

Davis, D.W. and Sutcliffe, R.M., 1985. U-Pb ages from the Nipigon plate and northern Lake Superior; Geological Society of America Bulletin, v.96, p.1572-1579.

Davis, D.W., Sutcliffe, R.H., and Trowell, N.F., 1988. Geochronological constraints on the tectonic evolution of a late Archean greenston belt, Wabigoon subprovince, northwest Ontario, Precambrian Research, 39: 171-191.

Davis, D.W., Pezzuto, F., and Ojakangas, R.W. 1990. The age and provenance of metasedimentary rocks in the Quetico subprovince, Ontario, from single zircon analyses: Implications for Archean sedimentation and tectonics in the Superior Province; Earth and Planetary Science Letters, v. 99, p. 195-205.

Davis, D.W., and Green, J.C., 1997. Geochronology of the North American Midcontinent rift in western Lake Superior and implications for its geodynamic evolution. Canadian Journal of Earth Sciences, 34: 476-488.

Ernst, R.E., Buchan, K.L., Heaman, L.M., Hart, T.R. and Morgan, J. 2006. Multidisciplinary study of north- to north-northeast-trending dikes in the region west of the Nipigon Embayment: Lake Nipigon Region Geoscience Initiative; Ontario Geological Survey, Miscellaneous Release—Data 194.

Flank, S., 2011. The geology, petrology and geochemistry of the Mesoproterozoic Hele sill, Nipigon Ontario. Unpublished H.B.Sc. thesis, Lakehead University, Thunder Bay, ON. 83 p.

Foley, D. 2011. Petrology and Cu-Ni-PGE Mineralization of the Bovine Igneous Complex, Baraga County, Northern Michigan. Unpublished M.Sc. thesis. University of Minnesota Duluth. 109 p.

Fralick, P.W. and Barrett, T.J., 1995. Depositional controls on iron formtion association in Canada. In: Sedimentary facies analysis. Edited by A.G. Plint. International Association of Sedimentologists, Special Publication No. 22, p. 35-39.

Fralick, P., Davis, D.W., and Kissin, S.A., 2002. The age of the Gunflint Formation, Ontario, Canada: single zircon U-Pb age determinations from reworked volcanic ash. Canadian Journal of Earth Sciences 39: 1085-1091.

Fralick, P., Purdon, R.H., and Davis, D.W., 2006a. Neoarchean trans-subprovince sediment transport in western Superior Province; Canadian Journal of Earth Sciences, v. 43, p. 1055-1070.

Fralick, P.W., Hollings, P., Kissin, S.A., Heggie, G.J., Metsaranta, R., Richardson, A.J., Rogala, B. and Somarin, A.K., 2006b. Stratigraphic, geochemical and isotopic data from Lakehead University researchers: Lake Nipigon Region Geoscience Initiative; Ontario Geological Survey, Miscellaneous Release—Data 190.

Franklin, J.M., McIlwaine, W., Poulsen, K., and Wanless, R. 1980 Straigraphy oand depositional setting of the Sibley Group, Thunder Bay District, Ontario, Canada.Canadian Journal of Earth Sciences, v. 17, p. 633-650.

Fujimaki, H., Tatsumoto, M. and Aoki, K., 1984. Partition coefficients of Hf, Zr and REE between phenocrysts and groundmasses. Proceedings of the fourteenth lunar an planetary science conference, Part 2. Journal of Geophysical Research, 89. Suppl. B662-B672.

Giguere, J.F. 1975. Geology of the St. Ignace Island and adjacent islands, District of Thunder Bay. Ontario Ministry of Natural Resources, Geological Report 118.

Goldner, B.D., 2011. Igneous Petrology of the Ni-Cu-PGE Mineralized Tamarack Intrusion, Aitkin and Carlton Counties, Minnesota. Unpublished M.Sc. thesis, University of Minnesota-Duluth, Duluth, MN. 156 p.

Goodwin, A.M., 1960, Gunflint Iron Formation of the Whitefish Lake area: Ontario Department of Mine, v. 69, Part 7, p. 41-63.

Good, D.J., 1993. Genesis of Copper - Precious Metal Sulfide Deposits in the Port Coldwell Alkalic Complex, Ontario. Ph.D. thesis, McMaster University, Hamilton. Ontario Geological Survey, Open File Report 5839.

Green, J.C., 1982. Geology of the Keweenawan extrusive rocks. In Geology and tectonics of the Lake Superior basin. Edited by R.J. Wold and W.J. Hinze. Geological Society of America. Memoir 156, pp. 47-55.

Green, J.C., 1983. Geologic and geochemical evidence for the nature and development of the Middle Proterozoic (Keweenawan) midcontinent rift of North America. Tectonophysics. 94: 413-437.

Green, J.C., Bornhorst, T.J., Chandler, V.W., Mudrey, M.G. Jr., Myers, P.E., Pesonen, L.J. and Wilband, J.T., 1987. Keeweenawan dikes of the Lake Superior region: evidence for evolution of the middle Proterozoic Midcontinent Rift of North America. In: Halls, H.C., Fahrig, W.F. (Eds.), Geological Association of Canada, Special Paper 34, p. 289-302.

Guel, J.J.C., 1970. Geology of Devon and Pardee Townships and the Stuart Location; Ontario Department of Mines, Geological Report 87, 52 p.

Guel, J.J.C., 1973. Geology of Crooks Township, Jarvis and Prince Locations, and Offshore Islands, District of Thunder Bay; Ontario Department of Mines, Geological Report 102, 46 p.

Halls, H.C., and Pesonen, L.J., 1982. Paleomagnetism of Keweenawan rocks. In: Geology and tectonics of the Lake Superior Basin. Geological Society of America, Memoir 156, p. 173 -201.

Hart, T.R., 2002. Proterozoic volcanic and intrusive whole rock geochemical data associated with the Keweenawan Midcontinent Rift, Lake Superior area, Ontario; Ontario Geological Survey, Miscellaneous Release-Data 114.

Hart, T.R., 2005a. Southern Black Sturgeon River–Seagull Lake area, Nipigon Embayment, northwestern Ontario: lithogeochemical, assay and compilation data; Ontario Geological Survey, Miscellaneous Release—Data 147.

Hart, T.R., 2005b. Precambrian geology of the Southern Black Sturgeon River and Seagull Lake area, Nipigon Embayment, northwestern Ontario; Ontario Geological Survey, Open File Report 6165, 64 p.

Hart, T.R., and MacDonald, C.A., 2003. Lake Nipigon Region Geoscience Initiative. Proterozoic and Archean geology of the south-central and north areas of the western Nipigon Embayment; In: Summary of Field Work and Other Activities 2003, Ontario Geological Survey, Open File Report 6120, p.44-1 to 44-15.

Hart, T.R. and MacDonald, C.A., 2007. Proterozoic and Archean Geology of the Nipigon Embayement: implications for emplacement of the Mesoproterozoic Nipigon diabase sills and mafic to ultramafic intrusions. Canadian Journal of Earth Sciences 44: 1021-1040.

Hart, T.R., Jolette, C. and terMeer, M., 2002. Phoenix bedrock mapping project: whole rock lithogeochemical and assay data, mineral deposit information, and diamond drill hole compilation of the Kitto, Eva, Summers, Dorothea, and Sandra townships, Beardmore area, northwestern Ontario; Ontario Geological Survey, Miscellaneous Release—Data 105.

Hart, T.R. and Magyarosi, Z., 2004a. Northern Black Sturgeon River–Disraeli Lake area, Nipigon Embayment, northwestern Ontario: lithogeochemical, assay and compilation data; Ontario Geological Survey, Miscellaneous Release—Data 133.

Hart, T.R. and Magyarosi, Z., 2004b. Precambrian geology of the northern Black Sturgeon River and Disraeli Lake area, Nipigon Embayment, northwestern Ontario; Ontario Geological Survey, Open File Report 6138, 56 p.

Hart, T.R. and Préfontaine, S., 2004a. Precambrian geology of the Black Sturgeon Lake area, Ontario Geological Survey, Preliminary Map P.3538, scale 1:50 000.

Hart, T.R. and Préfontaine, S., 2004b. Precambrian geology of the Disraeli Lake area; Ontario Geological Survey, Preliminary Map P.3539, scale 1:50 000.

Hart, T.R. and Tolson, A., 2005. Southern Black Sturgeon River–Seagull Lake area geological cross-sections, Nipigon Embayment, northwestern Ontario; Ontario Geological Survey, Preliminary Map P.3563, scale 1:50 000.

Hart, T.R., Whaley, A.G. and Pace, A. 2005. Precambrian geology of the Southern Black Sturgeon River–Seagull Lake–Disraeli Lake area, Nipigon Embayment, northwestern Ontario; Ontario Geological Survey, Preliminary Map P.3562, scale 1:50 000.

Heaman, L.M., Easton, M., Hart, T.R., Hollings, P., Macdonald, C.A. and Smyk, M., 2007. Further refinement to the timing of Mesoproterozoic magmatism, Lake Nipigon region, Ontario. Canadian Journal of earth Sciences 44: 1055-1086.

Heaman, L.M. and Easton, R.M., 2006. Preliminary U/Pb geochronology results: Lake Nipigon Region Geoscience Initiative. Ontario Geological Survey, Miscellaneous Release-Data 191, 79p.

Heaman, L.M. and Machado, N., 1992. Timing and origin of midcontinent rift alkaline magmatism, North America: evidence from the Coldwell Complex; Contributions to Mineralogy and Petrology, v. 110, p. 289-303.

Heggie, G.J., 2005. Whole rock geochemistry, mineral chemistry. Petrology and Pt, Pd mineralization of the Seagull Intrusion, northwestern Ontario. M.Sc. thesis, Lakehead University, Thunder Bay, ON.

Heggie, G., MacTavish, A., Johnson, J., Weston, R. And Leon, M.A. 2012. Structural control on the emplacement of the TBN-Igneous Complex. 58th Institute on Lake Superior Geology, Annual Meeting, Thunder Bay, Ontario, Part 1- Proceedings and Abstracts, v. 58, part 1, p. 37-38.

Henry, P., Stevenson, R.K., and Gariepy, C. 1998. Late Archean mantle composition and crustal growth in the Western Superior Province of Canada; neodymium and lead isotopic evidence from the Wawa, Quetico, and Wabigoon subprovinces. Geochimica et Cosmochimica Acta, 62: 143–157

Hemming, S.R., McLennan, S.M. And Hanson, G.N., 1995. Geochemical and Nd/Pb isotopic evidence for the provenance of the Early Proterozoic Virginia Formation, Minnesota. Implications for tectonic setting of the Animikie Basin. Journal of Geology 103: 147-168.

Hill, D. 1998. Crustal contamination and chalcophile depletion of the Osler Group of the Keeweenawan igneous province and the potential for a Ni-Cu ore deposit; unpublished BSc thesis, University of Toronto, Toronto, Ontario, 1998, 43 p.

Hoffman, P.F. 1989. Precambrian geology and tectonic history of North America; In: The Geology of North America: An Overview, The Geology of North America, Volume A, Geological Society of America, p.447-512.

Hollings, P., Fralick, P., Kissin, S., 2004. Geochemistry and geodynamic implications of the Mesoproterozoic English Bay Granite-Rhyolite complex, northwester Ontario Canada. Canadian Journal of Earth Sciences 41, 1329-1338.

Hollings, P., Hart, T., Richardson, A. and MacDonald, C.A., 2007a. Geochemistry of the mid-Proterozoic intrusive rocks of the Nipigon Embayement, northwestern Ontario. Canadian Journal of Earth Sciences 44: 1087-1110.

Hollings, P., Richardson, A., Creaser, R. and Franklin, J., 2007b. Radiogenic isotope characteristics of the mid-Proterozoic intrusive rocks of the Nipigon Embayement, northwestern Ontario. Canadian Journal of Earth Science 44: 1111-1129.

Hollings, P., Fralick., P. and Cousens, B., 2007c. Early history of the Midcontinent Rift inferred from geochemistry and sedimentology of the Mesoproterozoic Osler Group, northwestern Ontario. Canadian Journal of Earth Sciences 44: 389-412.

Hollings, P.N., Smyk, M.C., Hart, T., 2007d. Geochemistry of Midcontinent Rift-related mafic dikes and sills near Thunder Bay: New insights into geographic distribution and the geochemical affinities of Nipigon and Logan sills and Pigeon River and other dikes. 53rd Institute on Lake Superior Geology, Annual Meeting, Proceedings volume 53, Part 1. Lutsen, Minnesota, May 2007, pp. 40–41.

Hollings, P., Smyk, M., Heaman, L.M., and Halls, H., 2010. The geochemistry, geochronology, and paleomagnetism of dikes and sills associated with the Mesoproterozoic Midcontinent Rift near Thunder Bay, Ontario, Canada. Precambrian Research. Precambrian Research, v. 183, iss. 3, p.553-571.

Hollings, P., Cundari, R., Pulchalski, R. and Smyk, M.C., 2011a. Geochemistry of Midcontinent Rift-related mafic intrusions, Thunder Bay area; Ontario Geological Survey, Miscellaneous Release—Data 261 – Revised.

Hollings, P., Smyk, M., and Cousens, B., 2011b. The radiogenic isotope characteristics of dikes and sills associated with the Mesoproterozoic Midcontinent Rift near Thunder Bay, Ontario, Canada. Precambrian Research. In press.

Irvine, T. N. and Baragar, W. R . A. 1971. A guide to the chemical classification of the common volcanic rocks. Canandian Journal of Earth Sciences 8, p. 523-548.

Jenner, G.A. 1996. Trace element geochemistry of igneous rocks; geochemical nomenclature and analytical geochemistry. In: Trace element geochemistry of Volcanic Rocks: applications for massive sulphide exploration, vol. 12. Geological Association of Canada, Short Course Notes, p. 51-77

Jones, N. W. 1984. Petrology of some Logan diabase sills, Cook County, Minnesota; Minnesota Geological Survey, Report of Investigation 29, 40p.

Jowitt, S.M. and Ernst, R.E. (in press). Lithogeochemistry of the 130-80 Ma High Arctic LIP (HALIP) event and implications for Ni-Cu-PGE prospectivity. Lithos.

Kerr, H.L. 1910. Nepheline syenites of Port Coldwell; Ontario Department of Mines, Annual Report for 1910, Vol. XIX, pt. 1, p.194-232, accompanied by map 19b.

Kissin, S.A., and Fralick, P.W., 1994. Early Proterozoic volcanics of the Animikie Group, Ontario and Michigan, and their tectonic significance. Proceedings of the Institute on Lake Superior Geology 40: 18-19.

Kissin, S.A., Heggie, G.J. and Somarin, A.K., 2006. Sulphide saturation mechanisms in gabbroic intrusions in the Nipigon Embayment: Lake Nipigon Region Geoscience Initiative; Ontario Geological Survey, Open File Report 6176, 17p.

Klewin, K. And Berg, J., 1990. Geochemistry of the Mamainse Point volcanics, Ontario, and implications for the Keweenawan paleomagnetic record. Canadian Journal of Earth Sciences 27: 1194-1199.

Klewin, K.W., and Shirey, S.B., 1992. The igneous petrology and magmatic evolution of the Midcontinent rift system. Tectono-physics 213: 33-40.

Kulakov, E.K., Smirnov, A.V., and Diehl, J.F., 2012. Paleomagnetism of the Geordie Lake and Silver Mountain basalts. 58th Institute on Lake Superior Geology, Annual Meeting, Thunder Bay, Ontario, Part 1- Proceedings and Abstracts, v. 58, part 1, p. 37-38.

Kuno, H., 1969. Andesites in time and space. In: Proc. of the Andesite Conference (A.R. McBirny, Ed.), State of Oregon, Dep. Geol. Miner. Ind. Bull. 65, pp. 13-20.

Kuzmich, B., 2012. Geochemistry and petrology of the Dog Lake Granite Chain, Quetico Basin, Northwestern Ontario. Unpublished honours thesis. Lakehead University, Thunder Bay, ON. 136 p.

Laarman, J.E., 2007. Geochemistry and PGE mineralization of the Kitto intrusion: A product of Mesoproterozoic plume magmatism through fault bounded Archean crust, east Nipigon Embayment, northern Ontario. M.Sc. thesis, Lakehead University, Thunder Bay, ON. 276 p.

Laberge, G.L., 1992, The Early Proterozoic Emporer volcanic Complex: implications for the geology of the eastern Gogebic District, northern Michigan: Program and Abstracts, Institute on Lake Superior Geology, 38th Annual Meeting, p. 53-55.

Le Maitre, R.W., Bateman, P., Dudek, A., Keller, J., Lameyre, J., Le Bas, M.J., Sabine, P.A., Schmid, R., Soresen, H., Streckeisen, A., Woolley, A.R. and Zanettin, B., 1989. A Classification of Igneous Rocks and Glossary of Terms: Recommendations of the International Union of Geological Sciences Subcommission on the Systematics of Igneous Rocks. Oxford: Blackwell Scientific.

Lesher, M.C., Burnham, O.M., Keays, R.R., Barnes, S.J., and Hulbert, L., 2001. Trace-element geochemistry and petrogenesis of barren and ore-associated komatiites. Canadian Mineralogist, 39. P. 673-696.

Lightfoot, P.C., Hawkesworth, C.J., 1998. Origin of Deccan Trap Lavas: Evidence from combined trace element and Sr-, Nd-, and Pb isotope studies. Earth and Planetary Science Letters, v. 91, p. 89-104.

Lightfoot, P.C., Hawkesworth C.J., Devey C.W., Rogers N.W., Van Calsteren P.W.C., 1990. Source and differentiation of Deccan Trap Lavas: Implications of geochemical and mineral chemical variations. Journal of Petrology, v. 31, p. 1165-1200.

Lightfoot, P., Sutcliffe, R., and Doherty, W., 1991. Crustal contamination identified in Keweenawan Osler Group tholeiites, Ontario: a trace element perspective. Journal of Geology, 99: 739–760.

Lightfoot, P.C., 1995. Mineral potential of the Keweenawan Midcontinent Rift, Thunder Bay region, Ontario; In Summary of Field Work and Other Activities 1995, Ontario Geological Survey, Miscellaneous Paper 164, p.94-99.

Lightfoot, P.C., Sage, R.P., Doherty, W., Naldrett, A.J. and Sutcliffe, R.H., 1999. Mineral potential of Proterozoic Keweenawan intrusions: implications of major and trace element geochemical data from bimodal mafic and felsic volcanic sequences of Mamainse Point and the Black Bay Peninsula, Ontario; Ontario Geological Survey, Open File Report 5998, 91p.

Lightfoot, P.C., Doherty, W. and Sutcliffe, R.H., 1989. Precise determination of trace element abundances in basalts from the Black Bay Peninsula and Mamainse Point sections of the Keweenawan volcanic pile using inductively coupled plasma mass spectrometry; In Summary of Field Work and Other Activities 1989, Ontario Geological Survey, Miscellaneous Paper 146, p.265-274.

Listerud, W.H., and Meineke, D.G., 1977, Mineral resources of a portion of the Duluth Complex and adjacent rocks in St. Louis and Lake Counties, northeastern Minnesota: Hibbing, Minn., Minnesota Department of Natural Resources, Division of Minerals Report 93, 74p.

MacDonald, C.A., 2004. Precambrian geology of the south Armstrong–Gull Bay area, Nipigon Embayment, northwestern Ontario; Ontario Geological Survey, Open File Report 6136, 42p.

MacDonald, C.A. and Tremblay, E., 2004. Geological and lithogeochemical data from the northwest Nipigon Embayment, Lake Nipigon Region Geoscience Initiative (LNRGI); Ontario Geological Survey, Miscellaneous Release—Data 132.

MacDonald, C.A. and Tremblay, E., 2005. Geological and lithogeochemical data from the western Nipigon Embayment, 2003-2004, Lake Nipigon Region Geoscience Initiative (LNRGI); Ontario Geological Survey, Miscellaneous Release—Data 146.

MacDonald, C.A., Tremblay, E., and Easton, R.M., 2004a. Lake Nipigon Region Geoscience Initiative: Preliminary results of mapping in the west-central Nipigon Embayment; In Summary of Field Work and Other Activities 2004, Ontario Geological Survey, Open File Report 6145, p.49-1 to 49-18.

MacDonald, C.A., ter Meer, M., Lepage, L., Préfontaine, S. and Tremblay, E., 2004b. Precambrian geology of the Waweig–Wabinosh lakes area, western Nipigon Embayment, northwestern Ontario; Ontario Geological Survey, Preliminary Map P.3536, scale 1:50 000.

MacDonald, C.A., ter Meer, M., Lepage, L., Préfontaine, S. and Tremblay, E., 2004c. Precambrian geology of the English Bay–Havoc Lake area, western Nipigon Embayment, northwestern Ontario; Ontario Geological Survey, Preliminary Map P.3537, scale 1:50 000.

MacDonald, C.A., Tremblay, E. and Easton, R.M., 2005a. Precambrian geology of the west-central map area, Nipigon Embayment, northwestern Ontario, Lake Nipigon Region Geoscience Initiative; Ontario Geological Survey, Open File Report 6164, 49 p.

Macdonald, C.A., Tremblay, E. and ter Meer, M., 2005b. Precambrian geology of the Kabitotikwia Lake area, west-central Nipigon Embayment, northwestern Ontario; Ontario Geological Survey, Preliminary Map P.3559.

Macdonald, C.A., Tremblay, E. and ter Meer, M., 2005c. Precambrian geology of the Cheeseman–Black Sturgeon lakes area, west-central Nipigon Embayment, northwestern Ontario; Ontario Geological Survey, Preliminary Map P3560.

Macdonald, C.A., Tremblay, E., ter Meer, M., Hart, T.R. and Easton, R.M., 2005d. Precambrian geology of the Max–Muskrat lakes area, west-central Nipigon Embayment, northwestern Ontario; Ontario Geological Survey, Preliminary Map P.3561.

Magma Metals Ltd. Thunder Bay North Polymetallic Project, Ontario, Canada. 2011. NI 43-101 Technical Report on Preliminary Assessment. March 17, 2011.

Magnus, S.J., 2010. An investigation of the assimilation hypothesis in the Navilus sill, Thunder Bay, Ontario. Unpublished honours thesis. Lakehead University. 68p.

Marathon PGM Corporation, 2010. NI 43-101 Technical Report of the Updated Feasibility for the Marathon PGM-Cu Project, Marathon, Ontario, Canada. January 8, 2010.

Maric, M. And Fralick, P.W., 2005. Sedimentology of the Rove and Virginia Formations and their tectonic significance. Institute on Lake Superior Geology 51: 41-42.

McIlwaine, W.H. And Wallace, H., 1976. Geology of the Black Bay Peninsula Area, District of Thunder Bay. Accompanied by Map 2304, scale 1 inch to 1 mile: Ontario Div. Mines, v. GR133, 54p.

Miller, J.D., Jr., Green, J.C., Severson, M.J., Chandler, V.W., Hauck, S.A., Peterson, D.M., and Wahl, T.E. 2002. Geology and mineral potential of the Duluth Complex and related rocks of northeastern Minnesota. Minnesota Geological Survey, Report of Investigations 58.

Miller, J.D., Jr., and Vervoot, J.D., 1996. The latent magmatic stage of the Midcontinent rift: a period of magmatic underplating and melting of the lower crust: Institue on Lake Superior Geology, 42nd Annual Meeting, Cable, Wis., Proceedings, v. 42, Program and Abstracts, pt. 1, p. 33-35.

Miller, J.D., Smyk, M.C. and Hollings, P.N., eds. 2010. Cu-Ni-PGE deposits in mafic intrusions of the Lake Superior region: A field trip for the 11th International Platinum Symposium; Ontario Geological Survey, Open File Report 6254, 166p.

Mitchell, R.H. and Platt, R.G., 1977. Field guide to aspects of the geology of the Coldwell alkaline complex; 23rd Annual Meeting, Institute of Lake Superior Geology. 34 p.

Mitchell, R.H. and Platt, R.G., 1978. Mafic mineralogy of ferroaugite syenite from the Coldwell alkaline complex, Ontario Canada. Journal of Petrology 19: 627-651.

Mitchell, R.H. and Platt, R.G., 1982. Mineralogy and petrology of nepheline syenites from the Coldwell alkaline complex, Ontario, Canada; Journal of Petrology, v. 23, p. 186-214.

Morey, G.B. and Southwick, D.L., 1995. Allostratigraphic relationships of early Proterozoic iron-formations in the Lake Superior Region. Economic Geology 90: 1983-1993.

Naldrett, A.J., 1992. A model for the Ni-Cu-PGE ores of the Noril'sk region and its application to other areas of flood basalt; Economic Geology, 87: 1945-1962

Nicholson, S.W., Shirey, S., Schulz, K., and Green, J., 1997. Rift-wide correlation of 1.1 Ga Midcontinent rift system basalts: implications for multiple mantle sources during rift development. Canadian Journal of Earth Sciences 34: 504-520.

Nicholson, S.W. and Shirey, S.B., 1990. Midcontinent Rift volcanism in the Lake Superior Region: Sr, Nd and Pb isotopic evidence for a mantle plume origin. Journal of Geophysical Research 95: 10851-10868.

North, J., 2000. Nature and distribution of Logan diabase sills and gabbro channels in the Keweenawan rift near Thunder Bay, Ontario: Brief comparison to Noril'sk: Abstract, 46th Institute on Lake Superior Geology, Annual Meeting, Thunder Bay, Ontario, Proceedings v. 46, Part 1.

Neumann, E-R, Svensen, H., Galerne, C.Y., and Planke, S., 2011. Multistage evolution of dolerites in the Karoo Large Igneous Province, Central South Africa. Journal of Petrology 52. 959-984.

Paces, J.B., 1988. Magmatic processes, evolution and mantle source characteristics contributing to the petrogenesis of Midcontinent rift basalts: Portage Lake basalts, Keweenaw Peninsula, Michigan. Ph.D. thesis, Michigan Technological University, Houghton, Michigan.

Palmer, H., 1970. Paleomagnetism and correlation of some Middle Keweenawan rocks, Lake Superior. Canadian Journal of Earth Sciences 7: 1410-1436

Pan, Y., Fleet, M.E., and Longstaffe, F.J., 1999. Melt-related metasomatism in mafic granulites of the Quetico Subprovince, Ontario: constraints from O–Sr–Nd isotopic and fluid inclusion data. Canadian Journal of Earth Sciences, 36: 1449–1462

Pearce, J.A. and Peate, D.W. 1995. Tectonic implications of the compositions of volcanis arc magmas. Annual Review Earth Planetary Sciences. 23: 251-285.

Pearce J.A. 2008. Geochemical fingerprinting of oceanic basalts with applications to ophiolite classification and the search for Archean oceanic crust. Lithos 100. Iss. 1-4, p. 14-48.

Percival, J.A., 2003. Orogenic framework for the Superior Province: Dissection of the ~~"~~Kenoran Orogeny" Geological Survey of Canada, Western Superior NATMAP working group, Online Abstract. http://www.lithoprobe.ca/Contributed%20Abstracts/Oral%20Presentation/Percival-abstract.pdf.

Pervical, J.A., Sanborn-Barrie, M., Skulski, T., Stott, G.M., Helmstaedt, H., and White, D.J., 2006. Tectonic evolution of the western Superior Province from NARMAP and Lithoprobe studies. Canadian Journal of Earth Sciences, 43: 1085-1117.

Percival, J., 2007. Geology and Metallogeny of the Superior Province, Canada. In Goodfellow, w., ed., Mineral Deposits of Canada: A Synthesis of Major Deposit Types, District Metallogeny, the Evolution of Geological Provinces, and Exploration Methods: Geological Association of Canada, Mineral Deposits Division, Special Publication No. 5, p. 903-928.

Pesonen, L.J., 1978. Paleomagnetic, paleointensity and paleosecular variation studies on Keweenawan igneous and baked contact rocks. Unpublished PhD thesis. University of Toronto, 346 p.

Phinney, W.C. and Halls, H.C., 2001. Petrogenesis of the early proterozoic Matachewan syke swarm, Canada, and implications for magma emplacement and subsequent deformation. Canadian Journal of Earth Sciences, 38: 1541-1563.

Piispa, E., Smirnov, A., and Pesonen, L., 2011. Paleomagnetism of Midcontinent Rift rocks from the northern shore of Lake Superior, Ontario, Canada: Preliminary results. 57th Institute on Lake Superior Geology, Annual Meeting, Ashland, Wisconsin, May 18-21, 2011, Proceedings Volume 57, Part 1, p.65.

Puchalski, R., 2010. The petrography and geochemistry of the Riverdale sill. H.B.Sc. thesis, Lakehead University, Thunder Bay, ON. 65 p.

Pufahl, P. And Fralick, P., 2000. Depositional environments of the Paleoproterozoic Gunflint Formation; 46th Institute on Lake Superior Geology, v. 46, pt.2, Proceedings with abstracts.

Puskas, F.P., 1967. The geology of the Port Coldwell area, Thunder Bay, Ontario; Ontario Department of Mines, Open File Report 5104.

Pye, E.G., Fenwick, K.G., 1965. Atikokan-Lakehead sheet, Kenora, Rainy River and Thunder Bay districts. Ontario Department of Mines, Geological Compilation Series, Map 2065, scale 1 inch = 4 miles.

Richard, P., Shimizu, N., Allegre, C.J. 1976. $^{143}Nd/^{146}Nd$, a natural tracer: an application to oceanic basalts. Earth and Planetary Science Letters, 31, 269-278.

Richardson, A.J., Hollings, P. and Franklin, J.M., 2005. Geochemistry and radiogenic isotope characteristics of the sills of the Nipigon Embayment: Lake Nipigon Region Geoscience Initiative; Ontario Geological Survey, Open File Report 6175, 88p.

Rio Tinto, Conceptual Estimate, Rio Tinto press release, 2008. http://www.riotinto.com/documents/ReportsPublications/Nickel-Copper_exploration_target_at_Tamarack.pdf

Robertson, W.A. and Fahrig, W., 1971. The great Logan Paleomagnetic Loop – the polar wandering path from Canadian shield rocks during the Neohelikian era. Canadian Jornal of Earth Sciences. 8, 1355-1372.

Rogala, B., Fralick, P.W. and Metsaranta, R., 2005. Stratigraphy and sedimentology of the Mesoproterozoic Sibley Group and related igneous intrusions, northwestern Ontario: Lake Nipigon Region Geoscience Initiative; Ontario Geological Survey, Open File Report 6174, 128p.

Rogala, B., Fralick, P.W., Heaman, L.M., and Metsaranta, R., 2007. Lithostratigraphy and chemostratigraphy of the Mesoproterozoic Sibley Group, northwestern Ontario, Canada. Canadian Journal of Earth Science 44, 1131-1149.

Rollinson, H., 1993. Using geochemical data: evaluation, presentation, interpretation. Pearson, Prentice Hall. 352p.

Rossell, D., 2008, Geology of the Keweenawan BIC Intrusion. Institute on Lake Superior Geology field Trip Guide Book, 54, pp. 181-193.

Sage, R.P., 1991. Alkalic rock, carbonatite and kimberlite complexex on Ontario, Superior Province In: Geology of Ontario, Ontario Geological Survey, Special Volume 4, Part I. P.683-709.

Schulz, K.J. and Cannon, W.F., 2007. The Penokean orogeny in the Lake Superior region. Precambrian Research 157, 4-25.

Shirey, S., Klewin, K., Berg, J., and Carlson, R., 1994. Temporal changes in the sources of flood basalts: Isotopic and trace element evidence for the 1100 Ma old Keweenawan Mamainse Point Formation, Ontario, Canada. Geochim. Cosmochim. Acta 58, 4475-4490.

Simard, M., 2008. Synthèse du nord-est de la Province du Supérieur; Ministère des Resources naturelles et de la Faune, Québec, MM 2008-02, 196p.

Sims, P.K., Van Schmus, W.R., Schulz, K.J., and Peterman, Z.E., 1989. Tectono-stratigraphic evolution of the Early Proterozoic Wisconsin magmatic terranes of the Penokean Orogen: Canadian Journal of Earth Sciences 26: 2145-2158.

Smith, A.R. And Sutcliffe, R.H., 1987. Keweenawan intrusive rocks of the Thunder Bay. In: Summary of Field Work 1987, Ontario Geological Survey, Miscellaneous Paper 137: 248-255.

Smith, A.R. And Sutcliffe, R.H., 1989. Precambrian geology of Keweenawan intrusive rocks in the Crystal Lake-Pigeon River area: Ontario Geological Survey, Map P. 3139, scale 1:50 000.

Smyk, M. and Hollings, P., 2007. Midcontinent rift-related mafic intrusion north of the international border. Proceedings of the Institute on Lake Superior Geology 53: 53-80.

Smyk, M.C. and Hollings, P., 2009. Mesoproterozoic Midcontinent Rift-related mafic intrusions near Thunder Bay; Update; In: Summary of Field Work and Other Activities 2009, Ontario Geological Survey, Open File Report 6240, p.11-1 to 11-5.

Smyk, M.C., Hollings, P.N., and Cundari, R.C., 2011. The Pillar Lake Volcanics: new insights into an enigmatic mesoproterozoic volcanic suite near Armstrong, Ontario. 57th Institute on Lake Superior Geology, Annual Meeting, Ashland, Wisconsin, May 9-12, 2011, Proceedings Volume 57, Part 1, p.75-76.

Stott, G. N., Corkery, M.T., Percival, J.A., Simard, M. and Goutier, J., 2010. A revised terrane subdivision of the Superior Province. In: Summary of Field Work and Other Activities, 2010, Ontario Geological Survey, Open File Report 6260, p. 20-1 to 20-10.

Sun, S.S., and McDonough, W.F., 1989. Chemical and isotopic systematics of oceanic basalts: implications for mantle composition and processes. In: Magmatism in the ocean basins. Geological Society, Special Publication No.42, 313-345.

Sutcliffe, R.H., 1981. Geology of the Wabigoon–Quetico Subprovince boundary in the Lake Nipigon area, District of Thunder Bay. In*:* Summary of field work. Ontario Geological Survey, Miscellaneous Paper 100, p. 26–29.

Sutcliffe, R.H., 1982. Precambrian geology of the Wabigoon–Quetico Subprovince Boundary, Grand Bay sheet, Thunder Bay District. Ontario Geological Survey, Preliminary Map P.2528, scale 1:50 000.

Sutcliffe, R.H., 1986. Proterozoic rift related igneous rocks at Lake Nipigon, Ontario. Unpublished Ph.D. thesis, The University of Western Ontario, London, Ontario, 325 p.

Sutcliffe, R.H., 1991. Proterozoic geology of the Lake Superior area. In*:* Geology of Ontario. Edited by P.C. Thurston, H.R. Williams, R.H. Sutcliffe, and G.M. Stott. Ontario Geological Survey, Special Vol. 4, Part 1, pp. 405–484.

Sutcliffe, R.H., and Greenwood, R.C., 1982. Geology of the Lake Nipigon area; In Wood, J., White, O.L., Barlow, R.B., Colvine, A.C. (Editors), Summary of Field work 1982, Ontario Geological Survey, Miscellaneous Paper 106, p. 19-23.

Sutcliffe, R.H., and Greenwood, R.C., 1985a*.* Geological series, Precambrian geology, Lake Nipigon area, Kelvin Island sheet, District of Thunder Bay. Ontario Geological Survey, Preliminary Map P.2838, scale 1:50 000.

Sutcliffe, R.H., and Greenwood, R.C., 1985b. The geology of Eva and Kitto townships ultramafic intrusion; Fig. 1, scale 1 : 50 000. In: Precambrian geology of the Lake Nipigon area, Livingstone Point sheet, District of Thunder Bay. Ontario Geological Survey, Preliminary Map P.2839, scale 1:50 000.

Sutcliffe, R.H., and Greenwood, R.C., 1985c. Geological series, Precambrian geology, Lake Nipigon area, Castle Lake – Pikitigushi Lake sheet, District of Thunder Bay. Ontario Geological Survey, Preliminary Map P.2836, scale 1:50 000.

Sutcliffe, R.H. and Smith, A.R., 1988. Geology of the St. Ignace Island volcanic-plutonic complex; In: Summary of Field Work and Other Activities 1988, Ontario Geological Survey, Miscellaneous Paper 141, p.368-371.

Susumu, U., Lipman, P.W., and Obata, S., 2000. Subaqueous lava flow lobes, observed on ROV KAIKO dives off Hawaii. Geology 28: 503-506.

Swanson-Hysell, N.L., Maloof, A.C., Weiss, B.J. and Evans, D.A.D., 2009. No asymmetry in geomagnetic reversals recorded by 1.1-billion-year-old Keweenawa basalts. Letters to Nature geosciences. V. 2, p 713-717.

Swanson-Hysell, N.L., Burgess, S.D., Maloof, A.C., and Bowring, S.A., 2012. Temporal context of the Mamainse Point succession: a record of magmatic activity and fast plate motion across the ~~l~~latent stage" of Midcontinent Rift development. 58th Institute on Lake Superior Geology, Annual Meeting, Thunder Bay, Ontario, Part 1- Proceedings and Abstracts, v. 58, part 1, p. 84-85.

Tanton T.L., 1931. Pigeon River area, Thunder Bay District; Geological Survey of Canada, Sheet 1, Map 354A, scale 1:63360.

Tanton T.L., 1936a. Pigeon River area, Thunder Bay District. Geological Survey of Canada, Sheet 1, Map 354A, scale 1:63,360.

Tanton T.L., 1936b. Pigeon River area, Thunder Bay District. Geological Survey of Canada, Sheet 2, Map 355A, scale 1:63,360.

Taylor, S.R. and McLennan, S.M., 1985. The Continental Crust: Its Composition and Evolution. Blackwell Scientific, London, U.K.

Thurston, P.C., 1991. Archean Geology of Ontario: Introduction, in Geology of Ontario, Ontario Geological Survey, Special volume 4, Part, 73-98.

Tomlinson, K.Y., Bowins, R., and Heshler, J., 1998. Refinement of Hafnium (Hf) and Zirconium (Zr) analysis by improvement in the sample digestion procedure. Ontario Geological Survey, Miscellaneous Paper 169:189–192.

Tomlinson, K.Y., Davis, D.W., Stone, D., and Hart, T.R., 2003. U–Pb age and Nd isotopic evidence for crustal recycling and Archean terrane development in the south-central Wabigoon Subprovince, Canada. Contributions to Mineralogy and Petrology, 144: 684–702.

Tomlinson, K.Y. Stott, G.M., Percival, J.A., and Stone, D., 2004. Basement terrane correlations and crustal recycling in the western Superior Province: ND isotopic character of granitoid and felsic volcanic rocks in the Wabigoon subprovince, N. Ontario, Canada. Precambrain Research, 132: 245-274.

Ueng, W.C., Fox, T.P., Larue, D.K., and Wilband, J.T., 1988. Geochemistry and petrogenesis of the early Proterozoic Hemlock volcanic rocks and the Kiernan sills, southern Lake Superior region. Canadian Journal of Earth Sciences 25: 528-546.

Van Schmus, W.R., 1992. Tectonic setting of the Midcontinent Rift system. Tectonophysics 213: 1-15.

Vervoort, J.D., and Green, J.C. 1997. Origin of evolved magmas in the Midcontinent Rift system, northeast Minnesota: Nd-isotope evidence for melting of Archean crust. Canadian Journal of Earth Sciences, **34**: 521–535.

Walker, E.C., Sutcliffe, R.H., Shaw, C.S.J., Shore, G.T., and Penczak, R.C., 1993. Precambrian geology of the Coldwell Alkalic Complex; Ontario Geological Survey, Open File Report 5868, 30p.

Ware, A., 2007. Michigan Basin Geological Society. Abstract. The Geology of the Eagle Nickel Copper Deposit. http://www.mbgs.org/newsletters/2007/01-07.pdf.

White, D.J., Musacchio, G., Helmstaedt, H.H., Harrap, RM., Thurston, P.C., van der Velden, A. and Hall, K., 2003. Images of a lower-crustal ocean slab: Direct evidence for tectonic accretion in the Archean western Superior Province. Geology, 31: 997-1000.

Weiblen, P.W., Mathez, E.A. and Morey, G.B., 1972. Logan intrusions; In: Sims, P.K. and Morey, G.B. eds., Geology of Minnesota: A centennial volume; Minnesota Geological Survey, p.394-410.

Williams, H.R., Stott, G.M., Heather, K.B., Muir, T.L. and Sage, R.P., 1991. Wawa Subprovince. In: Geology of Ontario, Ontario Geological Survey, Special Volume 4, Part I. P. 485-539.

Williams, H.R., 1990. Quetico Subprovince. In: Geology of Ontario, Ontario Geological Survey, Special Volume 4, Part I. p. 383-409.

Winchester, J.A., and Floyd, P.A., 1977. Geochemical discrimination of different magma series and their differentiation products using immobile elements: Chemical Geology, v. 20, p. 325-343.

Winter, J.D. 2001. An introduction to igneous and metamorphic petrology. Prentice Hall. 697 p.

Appendix A

Field descriptions for the Coubran Lake basalts

sample	zone	description	UTM E	UTM N
CL-RC-01	16	N/E end of the flow, pipe vesicles trending N-S. Possible at the top of the flow as the overlying material appears massive.	538053	5410732
CL-RC-02	16	~1m above previous sample, odd accretionary vein-like features. Likely overlying flow from GL-RC-001.	538035	5410727
CL-RC-03	16	~1m above previous, very small amygdules denoting mid-flow.	538017	5410728
CL-RC-04	16	Dense population of amygdules; sample taken from just above as amygdaloidal material was difficult to sample. Sample represents „highest" point within the trenched area.	537984	5410728
CL-RC-05	16	Odd feeder dyke/accretionary vein feature. Sample taken from above material. Samples 1-5 appear to be emplaced up the hillcrest each generally higher (~1m) than the previous. Individual flows are not possible to distinguish for that section. From sample 6 onwards, we trend down topography and theoretically down section although the unit appears to be draped over a hill (denoted by the slope of flow toes). Again, distinction between individual flows may be difficult to ascertain but systematic samples should provide a proper characterization.	537964	5410731
CL-RC-06	16	Appears to be the most massive section within the unit. Sample taken adjacent to paleomag drillhole. Material is slightly darker and contains a slightly coarser plagioclase phase.	537933	5410730
CL-RC-07	16	Syenite dyke, ~2m wide trending at 110/60N	537921	5410728
CL-RC-08	16	~1m below previous sample on ledge; semi-massive with small- medium amygdules resistant to weathering; pipe-like amygdules also present	537907	5410727
CL-RC-09	16	Amygdaloidal chill directly overlying ropy flow top (pic 16). Sample taken from overlying chilled flow.	537885	5410733
CL-RC-10	16	Sample taken from ropy flow top underlying sample GL-RC-009. (chips from a 1x1m area adjacent to feeder)	537882	5410730
CL-RC-11	16	Sample taken from midway between flow-tops (~4ft below previous sample). NOTE: Amygdules appear to change up-section from dominantly calcite to actinolite/tourmaline	537877	5410730
CL-RC-12	16	Ropy flow top ~2m below previous. Sequential presence of flow tops indicate that this flow in particular is ~2m thick and is likely the case for the entire unit. (See strat section in field manual)	537871	5410734
CL-RC-13	16	Flow-top ~1m below previous flow-top	537851	5410726
CL-RC-14	16	Down stratigraphy ~1.5m from previous flow-top; relatively massive material with small amygdules (mid – flow?)	537813	5410731
CL-RC-15	16	~1.5m below previous smaple with hard-large, semi-abundant amygdules infilled with feldspar and calcite	537785	5410730
CL-RC-16	16	~1m lower in the sequence; sparse small amygdules. NOTE: after ropy flow top are present, the unit is dominated by massive flows and "uninteresting" with variable amounts and sizes of amygdules. Here, the flows become impossible to distinguish. Sampling becomes more systematic for the next 3 samples.	537757	5410729
CL-RC-17	16	Massive flow ~1.5m below previous, hard to break. Guessing this flow is ~2m thick with the sample taken from the middle .	537731	5410730
CL-RC-18	16	Highly amygdaloidal flow (densest population within unit). Appears infilling changed down sample from actinolite/tourmaline below to calcite/feldspar above. This variation is likely seen within individual flow as obsevered here but also may be present through stratigraphy.	537715	5410725
CL-RC-19	16	Lowest sequence on trail out; highly amygdaloidal flow ~2-3ft from syenite dyke.	537680	5410726

Appendix B

Whole-rock geochemical data for the Coubran Lake basalts

sample	CL-RC-01	CL-RC-02	CL-RC-03	CL-RC-04	CL-RC-05	CL-RC-06	CL-RC-08
Raw							
SiO2	49.45	48.66	50.37	49.38	48.69	49.05	48.65
TiO2	0.85	0.85	0.85	0.85	0.83	0.90	0.88
Al2O3	14.63	15.05	14.73	14.33	14.87	15.02	14.72
Fe2O3	11.31	10.71	10.76	10.22	10.27	9.96	10.96
FeO	10.18	9.64	9.68	9.20	9.24	8.96	9.86
MnO	0.43	0.41	0.32	0.35	0.42	0.43	0.51
MgO	6.61	6.80	6.45	7.18	6.32	5.45	5.86
CaO	9.04	11.24	11.23	11.97	11.49	10.76	9.81
Na2O	3.40	2.31	2.26	2.21	3.01	3.71	3.85
K2O	1.30	1.02	1.15	1.05	1.07	1.24	0.99
P2O5	0.18	0.19	0.19	0.20	0.19	0.20	0.20
Na2O+K2O	4.70	3.33	3.41	3.26	4.08	4.95	4.84
LOI	2.54	3.34	1.74	2.29	2.64	3.27	3.65
Total	99.73	100.56	100.04	100.03	99.80	99.99	100.08
Ti	4837.00	4779.00	4958.00	4953.00	4759.00	5182.00	5275.60
P	708.00	724.00	771.00	785.00	747.00	796.00	<15
Cr	100.00	107.00	99.00	110.00	95.00	89.00	96.00
Co	79.73	45.74	46.15	51.46	47.74	35.58	44.24
Ni	111.70	90.10	97.10	115.00	96.90	69.20	78.70
Rb	51.60	37.27	93.64	46.09	35.33	72.77	39.85
Sr	400.70	411.00	458.60	419.50	443.20	366.30	590.50
Cs	4.70	2.70	5.53	2.89	6.54	6.64	42.43
Ba	382.70	351.80	349.50	305.70	322.70	381.40	316.60
Sc	32.20	33.00	35.00	35.40	32.40	31.70	33.80
V	222.80	218.70	238.30	241.50	233.40	228.20	222.70
Ta	0.92	0.93	0.94	0.91	0.87	0.96	0.94
Nb	21.93	24.16	20.98	20.09	18.78	20.71	21.33
Zr	92.00	93.00	98.00	96.00	92.00	100.00	97.00
Hf	2.20	2.22	2.31	2.26	2.20	2.35	2.29
Th	4.51	4.56	4.45	4.32	3.97	4.64	4.41
U	0.97	1.16	0.88	0.78	0.81	1.02	1.34
Y	19.12	20.56	17.01	15.80	16.32	16.80	17.08
La	36.33	46.31	24.57	12.61	21.71	37.63	34.59
Ce	79.38	87.50	47.08	30.47	33.81	67.06	67.10
Pr	9.65	9.72	5.49	4.17	4.03	7.35	6.97
Nd	37.88	36.98	22.46	18.36	17.64	27.59	25.61
Sm	6.80	6.64	4.63	4.09	4.14	5.10	4.95
Eu	2.05	1.87	1.25	1.34	1.22	1.55	1.64
Gd	5.14	5.23	3.93	3.62	3.69	4.17	4.17
Tb	0.69	0.72	0.57	0.52	0.54	0.59	0.59
Dy	3.97	4.18	3.37	3.12	3.21	3.40	3.43
Ho	0.75	0.80	0.66	0.60	0.62	0.65	0.66
Er	2.07	2.20	1.81	1.66	1.75	1.80	1.79
Tm	0.29	0.30	0.25	0.23	0.24	0.25	0.25
Yb	1.80	1.92	1.60	1.49	1.56	1.58	1.61
Lu	0.27	0.28	0.23	0.22	0.23	0.23	0.23
Cu	13.60	12.10	233.20	62.20	176.60	4.00	22.80
Zn	159.00	142.00	487.00	241.00	378.00	176.00	615.00
Mo	0.46	0.65	1.59	1.95	15.73	0.58	1.12
Tl	0.20	0.15	0.28	0.12	0.09	0.27	0.30
Pb	5.80	4.10	15.90	5.60	20.60	6.60	105.00
Sn	2.17	1.42	0.42	0.51	0.73	0.64	1.19
Au	0.40	0.37	4.01	0.49	0.98	0.22	0.66
Ir	0.23	0.30	0.20	0.23	0.22	0.19	0.21
Pd	8.61	7.12	8.56	7.97	22.60	7.58	4.18
Pt	10.30	10.00	10.60	10.10	10.00	9.01	10.30
Rh	0.47	0.53	0.53	0.49	0.50	0.46	0.50
Ru	0.12	0.12	0.12	0.15	0.12	0.09	0.13

sample	CL-RC-09	CL-RC-10	CL-RC-11	CL-RC-12	CL-RC-13	CL-RC-14	CL-RC-15
Raw							
SiO2	47.81	49.37	48.29	49.25	49.59	51.24	49.03
TiO2	0.96	0.87	0.81	0.86	0.90	0.77	0.83
Al2O3	16.71	14.88	13.74	14.87	15.60	13.94	15.05
Fe2O3	11.59	12.31	16.21	10.69	11.70	14.85	11.76
FeO	10.43	11.08	14.59	9.62	10.53	13.36	10.58
MnO	0.31	0.24	0.18	0.25	0.22	0.31	0.30
MgO	5.64	5.72	5.59	6.04	5.96	4.70	6.38
CaO	8.32	9.29	6.21	10.30	7.99	7.27	9.97
Na2O	3.70	3.30	3.00	3.46	4.03	3.76	3.33
K2O	1.62	1.18	1.98	0.90	1.01	1.56	1.13
P2O5	0.24	0.23	0.18	0.19	0.19	0.17	0.19
Na2O+K2O	5.32	4.48	4.98	4.36	5.04	5.32	4.46
LOI	3.14	3.07	3.24	2.93	2.30	1.91	2.32
Total	100.03	100.46	99.41	99.74	99.48	100.49	100.27
Ti	5260.00	4794.00	4531.00	4753.00	4926.00	4323.00	4538.00
P	859.00	819.00	734.00	733.00	670.00	647.00	728.00
Cr	110.00	99.00	96.00	102.00	103.00	89.00	107.00
Co	60.74	49.91	46.23	63.78	40.14	100.67	46.93
Ni	103.30	81.80	86.10	75.70	91.50	79.60	88.30
Rb	113.79	89.66	195.16	41.40	73.50	100.17	74.67
Sr	449.40	446.00	390.60	448.30	420.50	434.90	498.10
Cs	10.38	9.11	17.72	5.30	5.92	7.57	7.14
Ba	276.60	277.00	303.90	199.50	218.60	579.10	337.10
Sc	31.30	33.00	33.10	33.20	33.10	31.30	34.50
V	244.00	214.80	213.00	216.60	214.00	209.30	217.10
Ta	1.04	0.92	0.90	0.92	0.98	0.85	0.87
Nb	21.81	20.01	19.61	20.11	22.25	19.32	18.36
Zr	112.00	98.00	91.00	98.00	102.00	87.00	91.00
Hf	2.66	2.33	2.18	2.37	2.44	2.06	2.18
Th	4.05	4.59	3.31	4.49	4.46	3.88	4.29
U	1.05	1.37	0.69	0.89	0.98	0.80	0.84
Y	22.38	17.96	13.50	19.72	20.37	14.85	16.85
La	25.62	27.25	15.76	24.40	25.68	17.21	31.41
Ce	54.56	63.44	31.21	52.29	56.88	37.12	61.91
Pr	7.32	7.35	3.85	6.60	7.62	4.75	7.05
Nd	31.25	27.80	16.01	27.32	30.73	19.51	27.07
Sm	6.75	5.33	3.47	5.56	5.90	4.11	5.02
Eu	1.45	1.59	0.86	1.55	1.57	1.07	1.55
Gd	5.67	4.42	3.04	4.73	4.80	3.54	4.09
Tb	0.80	0.63	0.45	0.67	0.70	0.51	0.58
Dy	4.66	3.68	2.67	3.93	4.14	3.05	3.34
Ho	0.88	0.70	0.52	0.76	0.79	0.59	0.65
Er	2.42	1.93	1.43	2.10	2.15	1.62	1.77
Tm	0.33	0.27	0.20	0.29	0.30	0.22	0.25
Yb	2.04	1.70	1.28	1.85	1.88	1.40	1.57
Lu	0.29	0.25	0.19	0.27	0.27	0.21	0.23
Cu	324.50	465.20	15.30	91.60	471.30	374.90	18.20
Zn	487.00	243.00	144.00	135.00	335.00	360.00	157.00
Mo	5.81	13.88	0.95	0.67	1.72	1.21	1.35
Tl	0.47	0.30	0.37	0.23	0.22	0.24	0.20
Pb	40.60	19.10	7.70	14.90	9.30	32.20	4.40
Sn	0.82	0.84	0.77	0.90	0.94	1.03	0.95
Au	13.20	9.67	0.40	1.09	36.00	4.51	0.50
Ir	0.26	0.23	0.21	0.23	0.23	0.21	0.24
Pd	14.50	15.00	4.42	20.80	9.71	23.50	8.31
Pt	11.10	8.97	8.60	9.73	9.73	7.65	9.89
Rh	0.59	0.53	0.48	0.52	0.52	0.47	0.51
Ru	0.15	0.13	0.13	0.14	0.13	0.12	0.13

sample	CL-RC-16	CL-RC-17	CL-RC-18	CL-RC-19
Raw				
SiO2	49.74	48.68	49.72	49.16
TiO2	0.87	0.82	0.90	0.91
Al2O3	15.12	15.22	13.87	13.76
Fe2O3	10.85	12.36	11.09	13.08
FeO	9.76	11.12	9.98	11.77
MnO	0.28	0.30	0.38	0.57
MgO	5.86	5.95	6.67	5.93
CaO	10.61	7.95	8.46	8.57
Na2O	2.96	3.68	3.61	2.91
K2O	0.86	2.04	1.78	2.58
P2O5	0.19	0.17	0.20	0.25
Na2O+K2O	3.82	5.72	5.39	5.49
LOI	2.71	2.68	3.19	2.35
Total	100.05	99.85	99.87	100.07
Ti	4684.00	4448.00	4905.00	5031.00
P	749.00	677.00	755.00	952.00
Cr	102.00	102.00	102.00	62.00
Co	33.99	42.32	47.05	60.56
Ni	63.10	81.30	91.30	80.10
Rb	64.88	138.13	114.64	153.03
Sr	466.60	462.20	527.40	600.20
Cs	6.04	14.19	13.28	10.26
Ba	257.60	561.90	687.80	1066.00
Sc	33.70	33.50	37.30	33.20
V	232.10	206.50	249.50	249.70
Ta	0.88	0.85	0.97	1.16
Nb	16.57	19.37	22.18	28.57
Zr	95.00	90.00	99.00	111.00
Hf	2.26	2.13	2.36	2.59
Th	4.12	3.94	6.06	30.33
U	0.94	0.99	1.42	1.78
Y	17.49	17.46	24.16	50.53
La	22.83	25.97	108.03	208.88
Ce	42.02	54.69	160.37	348.28
Pr	4.94	6.60	16.13	32.76
Nd	20.08	25.72	58.09	103.95
Sm	4.44	5.10	9.37	14.47
Eu	1.38	1.72	2.20	2.54
Gd	3.98	4.28	6.79	9.79
Tb	0.58	0.60	0.91	1.34
Dy	3.50	3.52	5.04	7.51
Ho	0.67	0.66	0.95	1.42
Er	1.84	1.85	2.60	3.92
Tm	0.26	0.26	0.35	0.54
Yb	1.63	1.58	2.23	3.27
Lu	0.24	0.23	0.32	0.44
Cu	10.70	25.80	387.20	209.20
Zn	107.00	155.00	350.00	612.00
Mo	1.35	1.28	0.51	9.22
Tl	0.16	0.41	0.36	0.65
Pb	4.30	5.10	23.70	162.00
Sn	0.80	1.44	1.82	3.79
Au	0.70	0.54	5.17	4.81
Ir	0.20	0.26	0.14	0.10
Pd	6.93	5.32	7.56	11.10
Pt	9.43	10.30	8.63	7.24
Rh	0.45	0.49	0.45	0.40
Ru	0.11	0.13	0.10	

Appendix C

Field descriptions for samples from the Logan Basin

sample	zone	description	UTM_E	UTM_N
SP-RC-001	16	outcrop of E bank of Wrrow river at bend cloe to highway and Native retreat. Blocky and fractured at 120 (Perpendicular to dike trend?) rubbly weathering surface and possibly more so towards centre of ~40m exposure. Texture is ophitic/oikycrystic w/~45-55% plagioclase, cpx and tr diss. pyrite (anhedral)	293795	5327524
SP-RC-002	16	on NE corener of map, SE edge of dried creek/NE fault scar? (060). No columnar jointing presentmapped as 2c (unclassified diabase) with a 3d (dike unclassified) directly on road. Texture looks like sill but both are sampled for geochem	309188	5332340
SP-RC-003	16	Close to previous (SP-RC-003) possibly on trend but tough to determine which is 2c and 3d from map. Outcrop directly on road.	309281	5332376
SP-RC-004	16	inferred contact between dyke and Rove (several pictures taken; 1&2=contact, 3=seds). Textural difference noted between units with platy (Sed) breakage to S and igneous xtalline textures to the N. Contact inferrend to be ~090 but somewhat difficult at it is heavily weathered and lying within riverbed.~1% sulphide. Possibly two dykes or an off-chute. more than likely sampled from extension of SP-RC-001	293729	5327416
SP-RC-005	16	S of 001&004 dyke. Outcrop adjacent to small stream. Rubbly, looks like it was previously visited. Along E-W trending ridge at ~090. texturally distinct from N dyke ie. more crystalline, coarser and more interstitial? (no sulphides, maybe trace).	293663	5327096
SP-RC-006	16	~120m at 070 from previous (005). Traced out and mapped dyke alonf what appears to be on trend with previous ridge blending into topo high. Outcrop weathers slightly more rubbly denoting possible middle of unit? Definitely same dyke unit as previous but may be more well formed pyroxene.	293557	5327068
SP-RC-007	16	Low-lying, heavily fractures outcrop ~5m wide directly in river bed. Rove appears upstream at same elevation suggesting this unit is x-cutting. Contaminated with ~2-3% kspar? From seds? Unit may be underlying above sill (acutally flow!!) and could not be traced out beyond river bed. possibly feeding above unit?? blebby rounded sulphide, like a small off-chute (contamination?) as unit appears small and grain size varies from FG-MCG. Feeder to overlying Devon Volcanics?	293717	5327201

SP-RC-008	16	W side of arrow river atop large cliff face. Underlying rove formation in contact with what appears to be volcanic rock. Contact is chilled and grainsize remains fine 2m above contact on outcrop top. Amygdules present here are infilled with qtz, qtz/calc, pyrite. looks VOLCANIC, turtle shell cracking texture and "radial" fresh breakage surfaces lends itself to this being a new extension of the Devon Volcanics.	293709	5327277
SP-RC-009	16	Logan sill, West side of the Logan basin north of the arrow river dyke. Columnar jointed	288847	5324806
SP-RC-010	16	Logan sill, West side of the Logan basin north of the arrow river dyke. Columnar jointed. Same sill as previous, ~250m SE.	288976	5324690
SP-RC-011	16	Small offchute sill in Centennial Park, taken on the west bank of the Current River	335105	5367391
SP-RC-012	16	Pigeon River Dyke, falls	306233	5320117
SP-RC-013	16	late stage injection within Pigeon River dyke	306248	5320108
SP-RC-014	16	Pigeon River Dyke, Finger Point	309255	5320780
SP-RC-015	16	Pigeon River Dyke, Finger Point	308174	5320791
SP-RC-016	16	Silver Harbour, late stage bleb within Nipigon sill	354403	5374985
SP-RC-017	16	Nipigon sill, Silver Harbour	354403	5374985
SP-RC-018	16	Late-stage dyke within Nipigon sill	354403	5374985
100	16	Cloud River dyke on McKeller Point	319948	5326714
101	16	Megacrystic Mount Mollie on McKeller Point	319953	5326886
102	16	Mount Mollie Granophyre on McKeller Point	319973	5326836
103	16	FG contaminated gabbro, likely Mount mollie	319964	5326814
104	16	No Sample	320656	5326651
105	16	NE end of Victoria Island, 050-trending dyke on ridge jutting out to Lk Superior. Likely Pigeon River. (SEE DIAGRAM IN	327503	5329255
106	16	FG diabase with granopyric patch, ~05-1cm. Inferred Mt. Mollie contact material in contact with NE dyke (sample 105).	327512	5329254
107	16	Chilled Mt. Mollie gabrro with pink weathered surfaces. On E-W trend with 106, likely chilled material in inferred contact with NE dyke (105) of rove shale (present on shore ~20m NNE)	327502	5329247
108	16	Likely hornfelsed rove shale on W wide of ravine (we used to walk up) P9080017	327490	5329245
109	16	on E side of ravine opposite 108. part of NE ridge jutting out to Lk Superior (likely akin to 105).	327490	5329245
110	16	Granophyric Mt Mollie on SE corner of Victoria Island. X-cutting 050 trending dyke (see photos), granophyric breccia?	327497	5329176
111	16	SE corner of Victoria Island, 050- dyke being x-cut by Mt Mollie (ie. 110). See photos. Should be geochemically coherant with 105 and possibly 109.	327486	5329167
112	16	Porphyritic diabsae sills on SW corner of Vic Island. Being x-cut by NE trending PR dyke	327428	5328665
113	16	NE trending dyke (050) x-cutting por diabase sill (112).	327374	5328690
114	16	Porphyriritc db dyke (possible feed to sills to the sill on McKeller point).	314148	5325633

115	16	Porpyritic Diabase. NNW ridge. Possible feeder to sills lying to the SSE. Being x-cut by ENE PRD. On same ridge as 115.	314091	5325705
116	16	NE trending subophitic-ophitic diabase dyke. No contact with NNW (114/115) observed but texture distinctions truncate the NNW dyke.	314144	5325612
117	16	NNW trending dyke, plag-phyric defining NNW ridge on MT. Mollie	314796	5326012
118	16	Headed S from prv NNW dyke and hit MT Mollie dyke, texturally coarser grained with a slight pink weathered surface	314829	5325878
119	16	E facing cliff face. CR dyke? Texturally unsure what is happening here. Looks to be of intergranular qtz diabase.	308119	5324827
120	16	Dyke on N side of Lenore Lake road. 4-5% py. Intergranular qtz diabase?	308061	5324734
121	16	McKeller Point, E-W Mt. Mollie, contaminated mafic db with granophyric patches and open space filling (qtz, kspar and radial white pectolite?)	320913	5326849
122	16	NW dyke, likely close to DB-59. intergranular texture.	320244	5326170
123	16	Arrow river dyke ~250m south of oddly dipping Logan sill (125). Outcrop on N side of dyke.	288736	5322911
124	16	Logan sill. Being cut by arrow river dyke which lies to the south. Sill dipping oddly at 30 to the west (inferred).	288688	5323137
125	16	Arrow River dyke. Landed on top of ARD.	292116	5323556
126	16	Cloud river dyke. Extends NW from Mount Mollie. Clearly cross-cutting a PRD. Measured from ridge to ridge at 330.	312991	5329365
127	16	Logan sill. Being cut by arrow river dyke which lies to the north. Likely same sill as 124.	288156	5322127
128	16	Arrow River dyke	288467	5322497
129	16	Arrow River dyke	289834	5322882
130	16	Arrow River dyke	289799	5322974
131	16	Arrow River dyke	290543	5323122
132	16	Arrow River dyke	291547	5323293
133	16	Arrow River dyke	297931	5324107
134	16	Arrow River dyke	297944	5324078
135	16	Arrow River dyke	298652	5324106
136	16	Arrow River dyke	296712	5324170

Appendix D

Whole-rock geochemical data for samples from the Logan Basin

sample	SP-RC-001	SP-RC-002	SP-RC-003	SP-RC-004	SP-RC-005	SP-RC-006	SP-RC-007	SP-RC-008	SP-RC-009
Raw									
SiO2	48.64	50.50	49.01	49.42	48.07	47.76	57.19	55.61	50.12
TiO2	1.32	3.64	3.65	3.82	1.62	1.53	1.92	2.27	3.74
Al2O3	17.08	12.90	12.67	12.74	15.70	16.53	13.71	13.62	12.69
Fe2O3	11.31	16.21	16.84	16.18	13.45	12.87	10.66	11.48	16.05
FeO	10.18	14.59	15.15	14.56	12.10	11.58	9.59	10.33	14.44
MnO	0.16	0.20	0.19	0.19	0.18	0.17	0.18	0.14	0.18
MgO	7.72	3.40	4.06	4.33	7.54	7.82	2.67	3.35	3.95
CaO	10.72	7.66	7.48	6.44	10.20	9.94	3.60	3.21	7.28
Na2O	2.37	3.25	3.02	2.75	2.44	2.40	4.22	3.52	2.78
K2O	0.42	1.38	0.98	2.09	0.64	0.58	2.25	2.86	1.16
P2O5	0.14	0.46	0.42	0.46	0.18	0.17	0.72	0.65	0.45
LOI	0.51	1.02	1.74	1.96	0.48	1.06	3.22	3.53	2.00
Total	100.39	100.61	100.06	100.37	100.50	100.84	100.33	100.25	100.38
Ti	7919.00	21921.00	22219.00	22904.00	9790.00	9069.00	11410.00	13437.00	22346.00
P	610.96	2007.44	1832.88	2007.44	785.52	741.88	3142.08	2836.60	1963.80
Cr	190.00	6.00	22.00	28.00	218.00	186.00	5.00	5.00	14.00
Co	55.81	44.56	53.32	52.30	59.63	61.22	22.96	28.22	51.34
Ni	196.00	32.00	70.00	66.00	164.00	191.00	5.00	4.00	56.00
Rb	9.97	45.00	40.76	71.82	16.55	13.70	48.43	63.23	38.85
Sr	297.60	503.60	428.30	445.60	348.80	322.40	409.00	349.70	457.90
Cs	1.14	4.34	4.62	1.02	1.61	2.05	0.56	0.78	3.02
Ba	151.30	372.70	306.20	841.00	184.40	179.80	714.50	909.30	344.80
Sc	27.60	29.80	27.70	28.20	32.30	28.00	15.20	16.80	28.90
V	217.50	362.90	>370	>370	243.60	222.90	75.00	113.20	>370
Ta	0.47	1.84	1.72	1.90	0.53	0.50	3.03	2.97	1.81
Nb	7.34	27.23	25.89	28.19	8.37	7.82	46.57	46.05	27.44
Zr	90.00	264.00	242.00	263.00	111.00	103.00	406.00	381.00	258.00
Hf	2.60	7.24	6.67	7.16	3.10	2.88	10.38	10.05	6.82
Th	1.15	4.58	4.16	4.38	1.20	1.10	8.04	7.49	4.38
U	0.28	1.40	1.28	1.37	0.31	0.28	2.13	1.96	1.38
Y	20.34	38.93	36.86	38.39	23.93	22.14	41.92	39.56	37.06
La	11.60	34.86	33.08	36.43	13.21	12.27	72.69	65.98	35.41
Ce	25.56	80.46	75.54	83.22	29.73	27.74	161.34	146.14	80.25
Pr	3.41	10.46	9.89	11.05	4.02	3.71	20.22	18.50	10.57
Nd	15.13	46.25	43.43	47.90	18.00	16.85	82.93	76.17	45.73
Sm	3.67	10.16	9.49	10.56	4.39	4.05	15.74	14.61	10.12
Eu	1.34	3.13	3.00	3.40	1.53	1.44	4.47	4.18	3.12
Gd	3.87	9.51	8.74	9.66	4.59	4.24	12.54	11.67	9.27
Tb	0.63	1.39	1.30	1.40	0.73	0.67	1.68	1.58	1.32
Dy	3.89	8.14	7.58	8.11	4.62	4.26	9.10	8.66	7.71
Ho	0.78	1.53	1.41	1.50	0.91	0.85	1.62	1.57	1.43
Er	2.27	4.09	3.82	3.94	2.62	2.41	4.24	4.00	3.78
Tm	0.31	0.55	0.51	0.52	0.36	0.34	0.55	0.53	0.51
Yb	1.95	3.39	3.17	3.19	2.30	2.12	3.31	3.18	3.11
Lu	0.29	0.49	0.46	0.46	0.34	0.31	0.47	0.45	0.45
Cu	102.30	264.90	251.10	270.50	147.20	140.30	9.60	9.10	259.40
Cu(ppb)	########	264900.00	251100.00	270500.00	147200.00	140300.00	9600.00	9100.00	259400.00
Zn									
Mo	1.05	1.86	1.77	2.01	0.79	1.05	2.59	2.40	1.72
Ag									
Tl	0.04	0.25	0.29	0.52	0.16	0.31	0.48	0.55	0.28
Pb	2.50	6.70	6.50	4.90	2.40	2.30	9.20	7.20	6.10
Sn	0.95	2.61	2.50	2.45	1.13	1.20	2.99	2.91	2.49
Sb	0.04	0.21	0.31	0.93	0.05	0.04	0.20	0.59	0.50
Au									
Ir									
Pd									
Pt									
Rh									
Ru									

sample	SP-RC-010	SP-RC-011	SP-RC-012	SP-RC-013	SP-RC-014	SP-RC-015	SP-RC-016	SP-RC-017
Raw								
SiO2	50.18	90.84	47.89	46.44	46.89	46.48	64.75	48.86
TiO2	3.72	0.01	1.42	0.86	1.53	0.81	0.51	0.71
Al2O3	12.72	0.93	16.02	18.46	16.09	18.68	11.97	14.91
Fe2O3	15.90	5.20	13.53	10.89	13.46	11.35	5.31	12.26
FeO	14.31	4.68	12.17	9.80	12.11	10.21	4.78	11.03
MnO	0.19	0.14	0.18	0.14	0.20	0.15	0.09	0.18
MgO	3.98	0.33	8.06	8.44	6.88	9.46	2.66	8.02
CaO	7.39	0.53	10.82	10.54	10.12	10.60	3.59	9.07
Na2O	2.77	<0.01	2.36	2.06	2.28	2.05	3.50	1.61
K2O	1.10	0.06	0.28	0.23	0.58	0.18	2.19	2.08
P2O5	0.45	0.02	0.14	0.09	0.16	0.09	0.11	0.06
LOI	2.27	2.48	-0.07	1.63	1.59	0.43	5.60	2.67
Total	100.67	100.45	100.64	99.78	99.78	100.26	100.28	100.43
Ti	22934.00	51.00	8180.00	4928.00	8669.00	4654.00	3039.00	3957.00
P	1963.80	82.00	562.00	358.00	633.00	334.00	389.00	245.00
Cr	19.00	97.00	179.00	124.00	188.00	113.00	98.00	155.00
Co	51.03	2.35	61.35	65.77	56.69	65.87	16.99	56.45
Ni	56.00	3.00	146.00	222.00	137.00	273.00	71.00	117.00
Rb	35.09	2.07	5.09	5.59	15.87	3.78	43.32	83.65
Sr	465.10	4.50	254.10	273.20	240.70	269.90	107.20	320.30
Cs	2.22	0.34	0.94	3.41	3.89	1.99	0.46	2.61
Ba	369.80	27.30	115.90	81.90	161.80	75.30	316.00	95.70
Sc	30.00	<1.1	31.80	20.10	31.20	19.70	13.90	35.60
V	>370	4.80	245.90	150.00	234.00	142.80	186.10	228.80
Ta	1.83	<0.023	0.39	0.24	0.43	0.22	0.76	0.12
Nb	27.04	1.06	6.16	3.85	6.51	3.66	12.15	1.98
Zr	258.00	14.00	82.00	51.00	100.00	49.00	173.00	41.00
Hf	6.88	0.27	2.26	1.42	2.84	1.31	4.64	1.14
Th	4.39	0.30	0.75	0.51	1.21	0.46	10.18	0.70
U	1.37	0.09	0.22	0.18	0.38	0.13	10.19	0.36
Y	37.17	1.67	19.17	11.98	23.16	11.68	27.77	14.49
La	35.23	1.32	9.38	6.41	10.70	5.94	36.54	4.18
Ce	80.24	3.12	21.66	14.44	24.80	13.44	76.18	9.50
Pr	10.59	0.27	2.98	1.96	3.34	1.83	8.95	1.32
Nd	45.98	1.08	13.42	8.79	15.14	8.26	34.04	6.32
Sm	10.16	0.21	3.44	2.20	3.90	2.07	6.32	1.88
Eu	3.19	0.07	1.30	0.95	1.44	0.92	0.93	0.72
Gd	9.34	0.23	3.78	2.37	4.32	2.22	5.16	2.34
Tb	1.37	0.03	0.60	0.37	0.70	0.36	0.79	0.40
Dy	7.77	0.20	3.80	2.33	4.37	2.22	4.89	2.66
Ho	1.46	0.04	0.76	0.47	0.90	0.45	1.01	0.56
Er	3.88	0.11	2.10	1.34	2.56	1.26	3.03	1.63
Tm	0.52	0.02	0.29	0.18	0.36	0.18	0.45	0.23
Yb	3.15	0.10	1.88	1.16	2.33	1.14	3.07	1.50
Lu	0.45	0.01	0.28	0.17	0.34	0.17	0.48	0.22
Cu	262.40	7.70	127.20	84.60	190.60	114.30	294.90	102.80
Cu(ppb)	262400.00							
Zn		11.00	105.00	81.00	170.00	84.00	233.00	88.00
Mo	1.69	4.04	1.27	0.45	0.57	0.39	18.90	0.35
Ag								
Tl	0.22							
Pb	7.50							
Sn	2.31							
Sb	0.64							
Au								
Ir								
Pd		0.12	<0.12	3.11	2.14	8.30	2.88	9.68
Pt		0.17	<0.17	3.39	2.30	7.52	3.61	5.15
Rh		0.02	0.04	0.17	0.12	0.43	0.17	0.31
Ru		0.08	0.12	0.16	0.16	0.25	0.20	0.28

sample	SP-RC-018	100	101	102	103	105	106	107
Raw								
SiO2	58.03	48.62	49.93	60.75	64.94	46.95	54.93	56.67
TiO2	0.50	3.86	1.61	1.45	0.75	1.33	1.18	0.95
Al2O3	10.90	11.32	15.60	12.73	15.29	15.35	15.13	19.04
Fe2O3	12.14	18.46	14.68	11.64	7.29	11.64	9.97	9.16
FeO	10.92	16.61	13.21	10.47	6.56	10.47	8.97	8.24
MnO	0.15	0.25	0.13	0.15	0.04	0.17	0.18	0.08
MgO	4.17	3.83	3.66	1.01	2.24	8.20	5.45	3.37
CaO	1.54	7.20	7.61	3.52	0.60	10.35	7.17	1.12
Na2O	0.81	2.38	2.66	3.24	2.24	1.64	2.34	1.47
K2O	2.37	2.53	1.20	4.57	3.43	1.35	1.28	4.62
P2O5	0.08	0.53	0.25	0.44	0.14	0.14	0.16	0.14
LOI	8.83	1.19	2.93	1.20	3.25	2.28	2.43	3.40
Total	99.52	100.17	100.26	100.69	100.20	99.40	100.21	100.02
Ti	2850.00	>16400	9269.00	8090.00	4326.00	7200.00	6465.00	5603.00
P	314.00	2147.00	924.00	1600.00	533.00	482.00	575.00	511.00
Cr	154.00	4.00	186.00	13.00	168.00	263.00	136.00	205.00
Co	22.09	44.81	91.28	11.12	17.12	53.41	39.87	26.23
Ni	95.00	22.00	244.00	8.00	67.00	209.00	119.00	91.00
Rb	54.18	103.79	39.11	174.34	113.54	51.65	59.96	77.52
Sr	46.60	595.50	250.20	198.00	91.30	440.80	276.10	136.80
Cs	2.44	1.90	2.83	3.87	2.58	4.18	3.71	7.47
Ba	421.30	690.20	321.90	1167.10	490.00	588.90	606.20	750.60
Sc	17.50	38.60	25.70	28.70	12.90	31.50	24.10	12.80
V	329.30	263.20	207.70	43.50	120.30	235.80	180.90	169.50
Ta	0.61	1.48	0.82	1.52	0.68	0.40	0.57	0.86
Nb	8.86	22.25	12.84	24.29	9.62	5.95	8.28	12.23
Zr	138.00	294.00	171.00	354.00	155.00	88.00	132.00	150.00
Hf	3.67	7.99	4.69	10.23	4.34	2.43	3.63	4.24
Th	8.10	4.13	3.96	11.00	7.23	0.83	4.62	7.75
U	6.69	1.07	1.78	5.09	3.47	0.24	1.29	3.78
Y	14.45	54.09	31.30	65.88	15.09	20.36	21.99	18.06
La	21.89	37.61	24.33	61.15	20.31	8.37	21.56	25.63
Ce	48.30	84.47	53.57	129.17	46.70	19.84	45.33	54.65
Pr	5.42	11.07	6.89	16.32	5.84	2.82	5.58	6.94
Nd	20.27	48.16	28.75	66.35	23.19	12.97	22.52	26.33
Sm	3.77	11.17	6.46	14.08	4.58	3.47	4.73	4.83
Eu	0.39	3.15	2.02	2.28	0.96	1.19	1.44	0.95
Gd	2.98	11.33	6.33	13.22	3.70	3.88	4.47	3.69
Tb	0.45	1.74	0.98	2.04	0.54	0.62	0.68	0.55
Dy	2.78	10.75	6.05	12.53	3.27	3.94	4.25	3.55
Ho	0.56	2.11	1.21	2.50	0.63	0.80	0.84	0.71
Er	1.66	5.98	3.40	7.02	1.80	2.24	2.42	2.14
Tm	0.25	0.83	0.48	1.00	0.27	0.32	0.34	0.33
Yb	1.71	5.19	3.03	6.39	1.77	2.01	2.17	2.25
Lu	0.26	0.76	0.45	0.95	0.26	0.29	0.32	0.34
Cu	393.20	240.20	609.20	38.70	25.00	128.90	139.80	28.00
Cu(ppb)								
Zn	123.00	191.00	131.00	204.00	107.00	151.00	111.00	90.00
Mo	27.49	1.53	5.83	2.51	1.61	0.43	1.27	0.77
Ag								
Tl								
Pb								
Sn								
Sb								
Au								
Ir								
Pd	10.40	0.15	<0.12	12.50	0.14	0.98	7.71	5.43
Pt	6.60	0.33	0.23	6.88	0.26	0.82	5.67	4.14
Rh	0.57	0.06	0.05	0.60	0.08	0.11	0.32	0.25
Ru	0.40	<0.08	<0.08	0.45	<0.08	0.13	0.25	0.15

sample	108	109	110	111	112	113	115	116
Raw								
SiO2	47.38	47.62	66.45	48.57	54.31	47.95	48.81	48.74
TiO2	1.42	1.29	0.51	1.26	2.39	1.39	0.94	1.68
Al2O3	16.67	15.91	13.95	15.94	13.33	16.40	16.04	15.51
Fe2O3	12.21	11.65	5.06	11.11	14.20	12.88	12.82	14.08
FeO	10.99	10.48	4.55	10.00	12.78	11.59	11.54	12.67
MnO	0.18	0.18	0.05	0.19	0.21	0.18	0.20	0.19
MgO	6.63	8.55	2.72	8.21	2.29	7.07	7.31	7.09
CaO	10.77	10.55	1.09	10.13	4.47	9.85	8.44	10.03
Na2O	2.04	1.83	3.75	1.82	4.18	2.30	1.85	2.46
K2O	0.67	0.63	3.92	0.76	2.22	0.45	1.94	0.50
P2O5	0.14	0.13	0.08	0.13	0.65	0.15	0.10	0.18
LOI	2.04	1.76	2.12	2.10	1.86	1.85	2.10	0.22
Total	100.16	100.11	99.71	100.23	100.11	100.46	100.55	100.68
Ti	8088.00	7129.00	3186.00	7171.00	13945.00	7838.00	5582.00	9672.00
P	539.00	466.00	290.00	489.00	2444.00	564.00	388.00	684.00
Cr	302.00	265.00	86.00	268.00	8.00	134.00	82.00	127.00
Co	57.14	54.07	16.45	53.41	29.36	59.49	58.81	59.03
Ni	209.00	225.00	53.00	216.00	17.00	152.00	181.00	132.00
Rb	31.32	27.31	136.60	31.55	70.66	16.68	64.24	14.94
Sr	231.00	246.10	325.70	219.80	369.00	244.60	465.60	258.70
Cs	4.33	5.85	2.28	6.28	1.99	3.72	3.06	2.87
Ba	327.00	347.40	1026.30	362.90	1002.00	230.80	>1740	147.00
Sc	33.20	30.40	11.70	30.10	23.50	29.80	30.30	34.30
V	244.40	225.60	90.00	225.90	127.00	236.40	243.90	274.20
Ta	0.42	0.37	0.59	0.39	1.89	0.39	0.25	0.48
Nb	6.43	5.85	6.98	6.31	28.93	6.13	3.88	7.27
Zr	95.00	85.00	117.00	91.00	337.00	89.00	69.00	103.00
Hf	2.56	2.31	3.36	2.47	8.89	2.51	1.93	3.04
Th	0.86	0.87	11.51	0.90	6.80	0.96	1.45	1.19
U	0.26	0.24	3.44	0.29	1.71	0.28	0.44	0.36
Y	22.56	19.25	13.29	20.00	50.02	20.54	18.55	24.49
La	10.96	8.31	26.83	8.70	55.20	9.45	8.28	11.34
Ce	24.05	19.56	51.66	20.20	120.76	21.98	17.70	26.44
Pr	3.32	2.73	5.82	2.80	15.49	3.02	2.37	3.63
Nd	15.09	12.51	20.85	12.61	65.05	13.63	10.63	16.55
Sm	3.85	3.22	3.72	3.25	13.56	3.54	2.77	4.22
Eu	1.58	1.17	0.87	1.17	3.84	1.28	0.93	1.51
Gd	4.31	3.63	2.90	3.71	12.18	3.86	3.22	4.70
Tb	0.69	0.59	0.42	0.60	1.75	0.62	0.54	0.75
Dy	4.32	3.74	2.52	3.85	10.31	3.99	3.53	4.82
Ho	0.87	0.76	0.48	0.76	1.94	0.79	0.72	0.97
Er	2.48	2.11	1.37	2.18	5.29	2.25	2.07	2.78
Tm	0.35	0.30	0.20	0.31	0.71	0.32	0.29	0.39
Yb	2.18	1.90	1.31	1.96	4.37	2.04	1.88	2.52
Lu	0.32	0.28	0.20	0.29	0.64	0.30	0.27	0.37
Cu	210.70	135.00	105.90	136.30	156.50	139.50	161.00	181.10
Cu(ppb)								
Zn	158.00	105.00	68.00	105.00	189.00	98.00	112.00	110.00
Mo	0.54	0.43	2.35	0.54	1.50	0.50	0.44	0.65
Ag								
Tl								
Pb								
Sn								
Sb								
Au								
Ir								
Pd	1.68	9.02	8.06	3.08	7.58	2.71	5.20	25.50
Pt	1.25	5.87	5.66	1.70	5.42	1.08	4.64	7.31
Rh	0.15	0.38	0.35	0.14	0.32	0.09	0.26	0.88
Ru	0.12	0.26	0.24	0.09	0.19	<0.08	0.20	0.47

sample	117	118	119	120	121	122	123	124
Raw								
SiO2	49.59	48.06	48.31	48.00	58.93	48.85	46.10	49.55
TiO2	1.29	0.94	1.68	1.51	1.20	2.32	0.96	3.72
Al2O3	15.05	15.69	16.48	14.61	14.67	15.81	18.90	12.11
Fe2O3	14.06	13.17	13.81	15.26	10.51	13.74	10.85	16.19
FeO	12.65	11.85	12.43	13.73	9.46	12.36	9.76	14.57
MnO	0.21	0.18	0.19	0.21	0.10	0.19	0.14	0.19
MgO	6.20	6.69	6.77	7.05	2.00	4.71	8.37	3.74
CaO	10.01	10.21	10.47	8.02	1.80	10.02	10.67	7.18
Na2O	2.42	2.07	2.46	2.45	1.97	2.83	2.10	3.00
K2O	0.79	1.05	0.45	0.79	4.42	0.94	0.32	1.53
P2O5	0.12	0.08	0.17	0.16	0.27	0.26	0.11	0.45
LOI	1.05	1.61	0.12	1.87	3.17	1.25	0.71	1.32
Total	100.79	99.76	100.90	99.93	99.04	100.92	99.24	98.99
Ti	7464.00	5253.00	9662.00	8622.00	6984.00	12437.00	5361.00	20788.00
P	468.00	316.00	666.00	503.00	971.00	901.00	119.00	35.00
Cr	94.00	131.00	120.00	152.00	96.00	164.00	126.00	9.00
Co	54.40	56.19	54.48	99.74	20.04	42.14	60.66	46.79
Ni	102.00	128.00	115.00	637.00	57.00	55.00	228.00	39.00
Rb	34.34	41.88	11.24	23.01	169.15	32.94	6.79	51.14
Sr	232.50	268.10	232.40	394.30	209.70	319.10	311.70	512.80
Cs	2.11	3.51	1.29	1.85	5.33	3.87	2.09	3.33
Ba	190.80	573.90	127.70	119.20	1436.00	936.40	98.60	403.70
Sc	37.40	38.40	33.30	32.00	25.90	38.10	19.10	30.10
V	318.30	278.80	265.80	306.40	121.20	307.70	142.40	333.60
Ta	0.32	0.21	0.46	0.41	1.18	0.79	0.28	1.88
Nb	4.93	3.29	7.06	6.39	17.80	12.20	4.45	27.11
Zr	81.00	53.00	100.00	93.00	260.00	161.00	59.00	259.00
Hf	2.42	1.57	2.86	2.56	7.40	4.42	1.62	6.98
Th	1.84	1.15	1.03	0.94	10.17	1.96	0.56	4.63
U	0.53	0.34	0.30	0.29	7.27	0.51	0.14	1.40
Y	22.86	17.11	24.46	21.95	45.04	33.28	13.71	37.87
La	9.94	7.20	10.51	9.73	46.30	19.55	6.99	36.77
Ce	21.72	15.42	24.47	22.44	97.32	44.49	16.11	84.02
Pr	2.84	2.06	3.43	3.09	12.19	5.96	2.22	11.10
Nd	12.76	9.23	15.54	14.11	48.78	25.95	10.09	47.81
Sm	3.31	2.48	4.02	3.58	10.13	6.26	2.46	10.51
Eu	1.20	1.10	1.48	1.43	1.96	1.96	1.05	3.21
Gd	3.98	2.96	4.59	4.02	9.24	6.55	2.66	9.71
Tb	0.66	0.49	0.74	0.65	1.42	1.05	0.42	1.40
Dy	4.26	3.19	4.70	4.18	8.75	6.54	2.67	7.98
Ho	0.87	0.65	0.95	0.85	1.72	1.30	0.52	1.50
Er	2.53	1.88	2.72	2.41	4.95	3.65	1.45	3.93
Tm	0.36	0.26	0.39	0.35	0.70	0.51	0.20	0.52
Yb	2.29	1.70	2.44	2.22	4.53	3.19	1.30	3.22
Lu	0.33	0.25	0.36	0.33	0.68	0.47	0.19	0.45
Cu	166.20	115.10	171.00	952.00	142.70	205.60	85.60	240.70
Cu(ppb)								
Zn	117.00	117.00	108.00	122.00	205.00	112.00	83.00	143.00
Mo	0.49	0.45	0.55	0.61	9.03	0.87	0.66	1.60
Ag								
Tl							0.05	0.23
Pb							1.20	4.80
Sn							0.61	2.47
Sb							<0.04	0.29
Au							1.61	3.77
Ir							0.48	0.04
Pd	9.13	15.50	12.10	4.47	30.60	1.93	5.05	4.93
Pt	6.20	6.63	5.17	4.97	20.40	1.27	4.64	2.15
Rh	0.34	0.55	0.60	0.23	1.22	0.10	0.29	0.11
Ru	0.21	0.31	0.42	0.11	0.95	0.12	0.53	<0.08

sample	125	126	127	128	129	130	131	132
Raw								
SiO2	46.93	48.86	50.70	49.51	47.32	46.57	46.92	47.66
TiO2	1.83	1.13	3.67	3.75	2.06	0.87	1.37	1.66
Al2O3	15.13	15.05	12.30	12.09	14.45	18.46	17.03	16.03
Fe2O3	14.60	13.17	15.60	16.11	14.57	11.54	13.19	13.73
FeO	13.14	11.85	14.04	14.50	13.11	10.38	11.87	12.35
MnO	0.19	0.19	0.15	0.19	0.19	0.15	0.17	0.18
MgO	7.39	6.34	4.22	3.80	6.22	8.69	7.82	7.00
CaO	10.25	10.17	6.31	7.06	9.11	10.25	10.09	10.42
Na2O	2.45	2.25	3.64	3.13	2.33	2.28	2.37	2.52
K2O	0.34	0.93	0.66	1.51	0.49	0.26	0.53	0.41
P2O5	0.19	0.12	0.44	0.47	0.23	0.10	0.15	0.19
LOI	-0.27	1.51	2.20	1.10	1.79	0.15	0.02	0.03
Total	99.02	99.72	99.90	98.72	98.76	99.32	99.65	99.82
Ti	10223.00	6486.00	20801.00	21196.00	11589.00	4935.00	7762.00	9465.00
P	159.00	134.00	46.00	30.00	103.00	104.00	128.00	156.00
Cr	155.00	122.00	16.00	6.00	88.00	103.00	118.00	154.00
Co	60.98	54.06	47.50	44.87	58.15	64.44	62.18	57.35
Ni	137.00	110.00	55.00	31.00	116.00	208.00	167.00	129.00
Rb	6.03	37.79	21.04	49.92	17.59	5.02	10.51	8.40
Sr	256.80	257.00	331.70	521.90	235.80	303.50	332.30	292.60
Cs	0.49	3.40	1.02	1.55	4.64	1.07	0.82	1.20
Ba	142.50	150.50	237.60	426.40	160.40	91.90	134.40	147.00
Sc	33.80	37.10	29.30	31.50	36.60	18.20	27.10	32.70
V	272.80	283.90	356.40	332.50	285.90	127.50	194.80	243.60
Ta	0.50	0.31	1.78	1.92	0.61	0.25	0.41	0.50
Nb	7.84	4.76	26.15	28.16	9.17	4.05	6.42	8.00
Zr	100.00	84.00	254.00	274.00	140.00	53.00	82.00	98.00
Hf	2.77	2.34	6.68	7.24	3.69	1.53	2.39	2.90
Th	0.89	1.86	4.40	4.85	1.63	0.48	0.75	0.95
U	0.23	0.55	1.38	1.52	0.48	0.12	0.20	0.24
Y	23.49	22.68	36.29	39.44	29.54	12.41	19.18	24.06
La	11.38	9.97	34.28	38.06	14.99	6.42	9.80	12.08
Ce	26.52	21.65	78.20	86.28	34.19	14.39	22.19	27.86
Pr	3.69	2.90	10.39	11.44	4.63	2.04	3.03	3.79
Nd	16.73	12.60	45.26	49.23	21.11	8.88	13.78	17.16
Sm	4.17	3.37	10.01	10.93	5.17	2.17	3.39	4.35
Eu	1.50	1.17	3.05	3.35	1.73	0.96	1.32	1.52
Gd	4.49	3.95	9.12	10.15	5.60	2.39	3.74	4.70
Tb	0.72	0.65	1.32	1.44	0.89	0.38	0.59	0.75
Dy	4.59	4.25	7.68	8.40	5.69	2.37	3.73	4.70
Ho	0.91	0.87	1.42	1.54	1.14	0.46	0.74	0.92
Er	2.53	2.44	3.78	4.12	3.19	1.33	2.04	2.59
Tm	0.35	0.35	0.50	0.55	0.45	0.19	0.29	0.36
Yb	2.27	2.23	3.07	3.33	2.92	1.18	1.85	2.27
Lu	0.34	0.33	0.43	0.47	0.42	0.17	0.27	0.34
Cu	138.40	150.10	152.60	266.50	208.40	86.10	123.50	149.60
Cu(ppb)								
Zn	120.00	108.00	101.00	132.00	158.00	82.00	102.00	112.00
Mo	0.59	0.54	1.65	1.69	0.77	0.38	0.53	0.63
Ag								
Tl	0.02	0.19	0.12	0.19	0.24	0.04	0.09	0.13
Pb	2.10	2.10	6.50	7.70	3.60	1.00	1.40	1.60
Sn	1.04	0.85	3.43	2.48	1.27	0.52	0.78	1.02
Sb	0.05	0.13	1.30	0.43	0.36	<0.04	<0.04	<0.04
Au	1.84	3.72	6.37	3.32	3.06	1.20	1.95	2.35
Ir	0.17	0.10	0.04	0.04	0.09	0.18	0.39	0.15
Pd	3.93	15.90	6.06	6.24	6.85	4.06	6.10	7.13
Pt	4.74	8.55	1.96	2.35	5.61	3.22	5.23	6.07
Rh	0.31	0.74	0.19	0.16	0.34	0.26	0.36	0.35
Ru	0.23	0.47	<0.08	<0.08	0.22	0.27	0.32	0.21

sample	133	134	135	136	137
Raw					
SiO2	46.97	43.42	46.71	47.01	48.97
TiO2	1.05	0.30	2.02	1.37	1.09
Al2O3	17.08	18.29	15.43	16.42	14.13
Fe2O3	12.72	14.10	14.95	13.40	11.47
FeO	11.45	12.69	13.45	12.06	10.32
MnO	0.17	0.12	0.20	0.18	0.18
MgO	8.41	8.80	6.73	8.09	7.33
CaO	10.56	9.40	9.79	10.42	11.69
Na2O	2.39	1.66	2.53	2.40	2.39
K2O	0.25	0.38	0.51	0.27	0.82
P2O5	0.11	0.03	0.23	0.14	0.10
LOI	-0.22	2.85	0.10	-0.31	0.66
Total	99.48	99.34	99.19	99.39	98.84
Ti	5940.00	1584.00	11519.00	7820.00	6066.00
P	184.00	165.00	107.00	175.00	235.00
Cr	186.00	167.00	93.00	183.00	232.00
Co	63.69	129.49	58.17	64.12	51.04
Ni	180.00	478.00	127.00	163.00	56.00
Rb	4.24	15.78	12.61	4.80	25.79
Sr	277.20	318.70	288.50	270.80	382.90
Cs	0.37	3.78	0.97	0.38	1.74
Ba	104.40	80.70	185.20	116.30	333.20
Sc	26.50	13.40	32.20	29.20	50.50
V	179.90	85.20	268.20	215.30	296.70
Ta	0.28	0.06	0.63	0.37	0.42
Nb	4.44	0.99	9.89	5.78	6.81
Zr	58.00	16.00	126.00	77.00	55.00
Hf	1.69	0.42	3.55	2.19	1.64
Th	0.52	0.20	1.22	0.71	0.90
U	0.13	0.08	0.29	0.18	0.18
Y	14.42	3.92	28.72	18.51	15.54
La	6.99	2.19	14.71	9.03	9.86
Ce	15.88	4.62	33.62	20.71	21.23
Pr	2.20	0.64	4.66	2.82	2.86
Nd	10.05	2.93	20.65	12.81	12.67
Sm	2.49	0.70	5.20	3.24	3.07
Eu	1.07	0.57	1.76	1.22	1.22
Gd	2.77	0.75	5.64	3.49	3.15
Tb	0.44	0.12	0.88	0.56	0.49
Dy	2.81	0.77	5.55	3.53	3.01
Ho	0.55	0.15	1.10	0.70	0.60
Er	1.55	0.43	3.05	1.98	1.68
Tm	0.22	0.06	0.44	0.28	0.24
Yb	1.36	0.38	2.70	1.74	1.52
Lu	0.21	0.05	0.40	0.26	0.22
Cu	84.80	496.20	168.70	124.30	31.90
Cu(ppb)					
Zn	92.00	90.00	127.00	110.00	85.00
Mo	0.35	8.26	0.62	0.49	0.58
Ag					
Tl	0.02	0.34	0.04	0.04	0.14
Pb	1.10	15.00	2.10	1.30	2.00
Sn	0.60	0.66	1.56	0.76	1.03
Sb	<0.04	0.84	0.04	<0.04	<0.04
Au	1.02	9.93	1.61	1.77	0.29
Ir	0.16	0.61	0.20	0.17	<0.01
Pd	4.10	20.20	5.70	7.65	<0.12
Pt	3.26	12.82	6.42	4.43	<0.17
Rh	0.26	0.77	0.37	0.36	0.02
Ru	0.23	0.83	0.24	0.25	<0.08

Appendix E

Rb-Sr and Sm-Nd isotope geochemistry results

Sample Name	SP-RC-001	SP-RC-008	SP-RC-014	110	111	112	113	126
AGE	1100	1100	1100	1100	1100	1100	1100	1100
Nd (ppm)	15.01	84.21	13.68	19.27	13.94	60.53	14.69	12.50
143Nd/144Nd (current)	0.512171	0.511920	0.512353	0.511312	0.512431	0.511922	0.512339	0.512241
Sm (ppm)	3.68	16.41	3.56	3.41	3.63	12.71	3.77	3.51
147Sm/144Nd	0.1482	0.1178	0.1571	0.1070	0.1575	0.1270	0.1554	0.1698
143Nd/144Nd initial	0.511101	0.511070	0.511218	0.510539	0.511294	0.511005	0.511217	0.511015
+/- (2 sigma)	0.000041	0.000033	0.000044	0.000031	0.000044	0.000036	0.000043	0.000047
Eps Nd (CHUR)T=1100	-2.29	-2.89	0.01	-13.27	1.48	-4.17	-0.01	-3.97
87Sr/86Sr (current)	0.705254	0.717550	0.708204	0.735772	0.711523	0.720690	0.707716	0.713920
87Sr/86Sr initial	0.703728	0.709306	0.689099	0.716616	0.704982	0.711956	0.704610	0.707218
Eps Sr	4.52	83.82	-203.46	187.73	22.35	121.50	17.05	54.13

Sample Name	136	GL-RC-01	GL-RC-04	GL-RC-09	GL-RC-13	GL-RC-17	GL-RC-19	03CAM020
AGE	1100	1100	1100	1100	1100	1100	1100	1100
Nd (ppm)	12.94	36.56	17.45	30.91	29.02	24.19	95.12	15.27
143Nd/144Nd (current)	0.512322	0.511958	0.512139	0.512119	0.512020	0.512020	0.511799	0.512009
Sm (ppm)	3.30	6.49	3.86	6.69	5.57	4.72	13.18	3.82
147Sm/144Nd	0.1541	0.1073	0.1337	0.1309	0.1160	0.1181	0.0838	0.1512
143Nd/144Nd initial	0.511210	0.511183	0.511173	0.511174	0.511182	0.511168	0.511194	0.510918
+/- (2 sigma)	0.000043	0.000031	0.000038	0.000037	0.000033	0.000034	0.000025	0.000042
Eps Nd (CHUR)T=1100	-0.15	-0.68	-0.87	-0.86	-0.70	-0.97	-0.47	-5.87
87Sr/86Sr (current)	0.704241	0.710289	0.709075	0.715398	0.711831	0.717183	0.716460	0.710523
87Sr/86Sr initial	0.703434	0.704422	0.704070	0.703856	0.703866	0.703558	0.704836	0.705750
Eps Sr	0.33	14.38	9.37	6.33	6.48	2.09	20.27	33.26

Sample Name	03CAM254	04CAM065	04CAM024	03TRH111
AGE	1100	1100	1100	1100
Nd (ppm)	11.93	8.93	9.21	15.44
143Nd/144Nd (current)	0.512321	0.512441	0.512298	0.512012
Sm (ppm)	3.34	2.53	2.54	3.82
147Sm/144Nd	0.1691	0.1715	0.1664	0.1498
143Nd/144Nd initial	0.511100	0.511203	0.511097	0.510931
+/- (2 sigma)	0.000047	0.000048	0.000046	0.000042
Eps Nd (CHUR)T=1100	-2.31	-0.29	-2.37	-5.61
87Sr/86Sr (current)	0.708656	0.706532	0.707603	0.713717
87Sr/86Sr initial	0.705298	0.704484	0.704844	0.707614
Eps Sr	26.84	15.26	20.38	59.76